Mass spectrometric analysis of short-lived intermediates and ancient fossils

Dissertation

Anne Schnell

Bonn 2021

Mass spectrometric analysis of short-lived intermediates and ancient fossils

Dissertation

zur Erlangung des Doktorgrades (Dr. rer. Nat.) der

Mathematisch-Naturwissenschaftlichen Fakultät

der Rheinischen Friedrich-Wilhelms-Universität Bonn

vorgelegt von

Anne Schnell

geboren in Troisdorf

Bonn 2021

Angefertigt mit der Genehmigung der Mathematisch-Naturwissenschaftlichen Fakultät der Rheinischen Friedrich-Wilhelms-Universität Bonn

1. Gutachterin	PD Dr. Marianne Engeser
2. Gutachter	Prof. Dr. Andreas Gansäuer
Tag der Promotion:	21.05.2021
Erscheinungsjahr:	2021

Acknowledgments

My thanks go out to all the people who have supported me during my time as PhD student.

A special thanks goes out to PD Dr. Marianne Engeser, who has welcomed me in her research group and was always willing to give advice and support.

Also, I want to thank Prof. Dr. Andreas Gansäuer for his input and agreeing to be the second examiner.

Further thanks are for Prof. Dr. Martin Sander of the paleontology department, who was always available for fruitful discussions about our cooperation and kindly agreed to be the fourth examiner.

I would like to thank Prof. Dr. Thomas Bredow for agreeing to be the third examiner.

Moreover, I am grateful for the great cooperation with Dr. Moritz Liesegang, the interesting discussions we had and the things we could learn from each other about our respective fields.

Especially, I would like to thank everybody from the Engeser group and beyond for the great atmosphere, all the fun we had and great Friday lunches. Above all I would like to mention in alphabetical order: Alexander Willms, Aron Janusko, Christina Braun, Julius Nimzyk, Kim Schuppener, Leonard Maurer, Marius Herbst and Wiebke Rautenberg.

I thank the staff of the mass spectrometry department especially K. Peters-Pflaumbaum and C. Sondag for coordinating measuring time and help with the instruments. Furthermore, my thanks go to the staff of NMR department.

Further, my thanks go out to the pharmacy and biology department from the university of Bonn and the group of Prof. U. Karst at the university of Münster for giving me measuring time at their instruments.

Last but not least I want to thank my parents, Annegret Schnell and Thomas Jurké, and friends, Jana Richter, Laura Schäkel, Muriel Hagenaars and Pia Fürtjes, for their constant support.

Publications, talks and conference posters

Publication

A part of this thesis has already been published in an international, peer-reviewed journal:

> A. Schnell, J. A. Willms, S. Nozinovic, M. Engeser, "Mechanistic studies of an L-proline-catalyzed pyridazine formation involving a Diels-Alder reaction with inverse electron demand", *Beilstein J. Org. Chem.* **2019**, *15*, 30–43. DOI: 10.3762/bjoc.15.3.

Talks

Parts of this thesis have been presented in a talk:

"*Studies of L-proline-catalyzed Diels-Alder reactions of unsaturated aldehydes with ESI-MS*"

A. Schnell, ***BIGS Summer School****, Bonn*, 10.09.-12.09.2019

"*Studies of L-proline-catalyzed Diels-Alder reactions of unsaturated aldehydes with ESI-MS*"

A. Schnell, ***DGMS Young Scientists****, Hünfeld*, 23.09.-25.09.2019

Posters

Parts of this thesis have been presented as a poster:

"Studies of a L-proline catalyzed inverse electron demand Diels-Alder reaction by ESI MS"

A. Schnell, J. A. Willms, M. Engeser, ***European Mass Spectrometry Conference****, Saarbrücken*, 11.03.-15.03.2018

"Studies of a L-proline catalyzed inverse electron demand Diels-Alder reaction by ESI MS"

A. Schnell, J. A. Willms, M. Engeser, ***International Mass Spectrometry Conference****, Florence*, 26.08.-31.08.2018

"Studies of L-proline-catalyzed Diels-Alder reactions of unsaturated aldehydes with ESI-MS"

A. Schnell, M. Engeser, ***Jahrestagung der Deutschen Gesellschaft für Massenspektrometrie****, Rostock,* 10.03.-13.3.2019

"MALDI-TOF analysis of fossilized wood"

A. Schnell, M. Liesegang, M. Engeser, ***Jahrestagung der Deutschen Gesellschaft für Massenspektrometrie***, Münster, 01.03.-04.03.2020

Abstract

The first part of this thesis focuses on mechanistic studies of two L-proline catalyzed reactions with electrospray ionization mass spectrometry. The second part describes mass spectrometric analyses of fossils, dinosaur egg shells and silicified wood.

For the first L-proline catalyzed reaction of α,β-unsaturated aldehydes, a catalytic cycle with two intermediates was postulated. I studied the reaction by taking samples directly out of the reaction solution and feeding them into the mass spectrometer. Apart from the two postulated intermediates I found two additional species which fit into the mechanistic scenario. With the aid of MS^n experiments, it was possible to investigate the intermediates and additional species in the gas phase and confirm their structure. The MS^2 experiment of the second intermediate was riveting, as it was possible to induce it to go backwards and forwards in the catalytic cycle, thereby mimicking its behavior in the gas phase. With the aid of a charge-tagged L-proline derived catalyst, I could study the intermediates in their unprotonated form and observed the same behavior for the second intermediate. By taking samples out of the reaction solution at regular intervals, insight into the temporal progress of the reaction was gained. The rate determining step of the reaction is the liberation of the catalyst and product from the second intermediate. The reaction was studied with *trans*-2-hexenal and *trans*-2-pentenal; their results are in accordance with each other.

The second L-proline catalyzed reaction of acetone with a tetrazine has a postulated catalytic cycle with three intermediates. In experiments with L-proline without a charge-tag, the first and the third intermediate could be detected. A charge-tagged tetrazine was synthesized, however only small amounts of the third intermediate could be detected with it. When the charge-tagged L-proline derived catalyst was used, I was able to detect the so far elusive second intermediate in addition to the first and third intermediate. In an MS^2 experiment, the second intermediate could be induced to go backwards and forwards in the catalytic cycle, thereby mimicking its behavior in the gas phase. Through this first experimental evidence of the second intermediate, I could confirm that the reaction proceeds in a stepwise manner via the second intermediate and not in a concerted step from the first to the third intermediate.

In the third project I studied dinosaur egg shells with HPLC-ESI MS. In preliminary work to the project, the color pigments biliverdin (BV) and protoporphyrin (PP) were detected in three different egg shells from Oviraptorosauria. The goal was to reproduce the results from the preliminary work, optimize the method and expand the methodology to a wider range of samples. The coloring of egg shells is of interest as it is an indicator of different ecological factors like nesting behavior. I tried to reproduce the preliminary work by extracting the same oviraptorid egg shells with the published EDTA extraction

method, but was not able to detect either BV or PP. With a more effective extraction method based on hydrochloric acid (HCl) I was still not able to detect BV or PP in the oviraptor egg shells. In measurements at more sensitive instruments, PP was detected with the EDTA extraction method, but in lower concentrations than published in the preliminary work and not in all oviraptor egg shells. When testing the different extraction methods in spiking experiments the EDTA method proved to be unsuitable for the extraction of BV, while PP was acceptable. The HCl extraction method showed a better performance, however for low concentrations of PP, impossibly high extraction ratios were found. Due to this, solvent tests were performed as to see if the solvent effects the detectability of BV and PP. A solvent mimicking the sample solution after HCl extraction showed a highly improved detectability of PP over other solvents, whereas BV was undetectable in it. This does not fit to the results of the spiking experiments, where BV was well detected with the HCl extraction method. To investigate this discrepancy in the next steps of the project the effects of the solvents should be tested again. Further, the oviraptorid egg shells should be extracted with the HCl extraction method and measured at the highly sensitive Qtrap instrument, which should be promising.

In the last project I analyzed with MALDI MS a specimen of 150 million years old silicified wood, which has differently colored domains. The goal for the analysis was to find an explanation for the coloration and if organic compounds can still be detected. The sample preparation needed to be adapted to a fossilized specimen. Thus, a fine powder of the specimen's different domains was generated by drilling into it with a diamond drill. The sample powder was then suspended in a matrix solution and prepared on the MALDI target. Through this preparation, reasonable MALDI spectra could be obtained. In the dark domain I detected amorphous carbon, which is in agreement with findings of Raman measurements of the sample. As amorphous carbon is black this brings an explanation for the darker coloring of the dark domain. Fascinatingly I was further able to detect organic compounds, like lignin, cellobiose and coniferin, which are basic building blocks of wood.

This work has shown that mass spectrometry is a useful tool for different scientific problems like studying reaction mechanisms to find elusive intermediates or detecting compounds in millions of year-old fossils.

Table of contents

1 Fundamentals

1.1 Electrospray ionization mass spectrometry

Electrospray ionization (ESI) is an ionization method for liquid solutions.[1] The work of *Dole* et al.[2] is the foundation on which *Fenn* and colleagues[3,4] build to develop the method in combination with mass spectrometry (MS). For his pioneering work, *Fenn* was honored with the Nobel Prize in Chemistry in 2002.[5,6] ESI is applicable to a large variety of compounds with a broad range of molecular weights, starting at small inorganic analytes going up to large polymers and proteins. [1,6–8] Thus, it is one of the most commonly used ionization methods in mass spectrometry.[1,7,8]

1.1.1 Basic principle

The setup of an early ESI ion source is depicted in Figure 1.1.1.[4] Between a needle and a counter electrode a 2-4 kV voltage is applied under ambient pressure.[1,7,9] The sample solution is pumped through that needle and experiences the electric field, generating the electrospray.[1,4,7,9] With the aid of heated drying and nebulizing gas streams, the solvent is evaporated, and the remaining matter is led through the transfer capillary guided by the electric field. After the transfer capillary, the first pumping stage is reached. Upon exit of the transfer capillary, a mayor part of the expanding gas is pumped off, while only a minor part enters the high vacuum via the skimmer.[1,4] Through electrostatic lenses the newly generated ions are focused and transferred to the mass detector.[1,4]

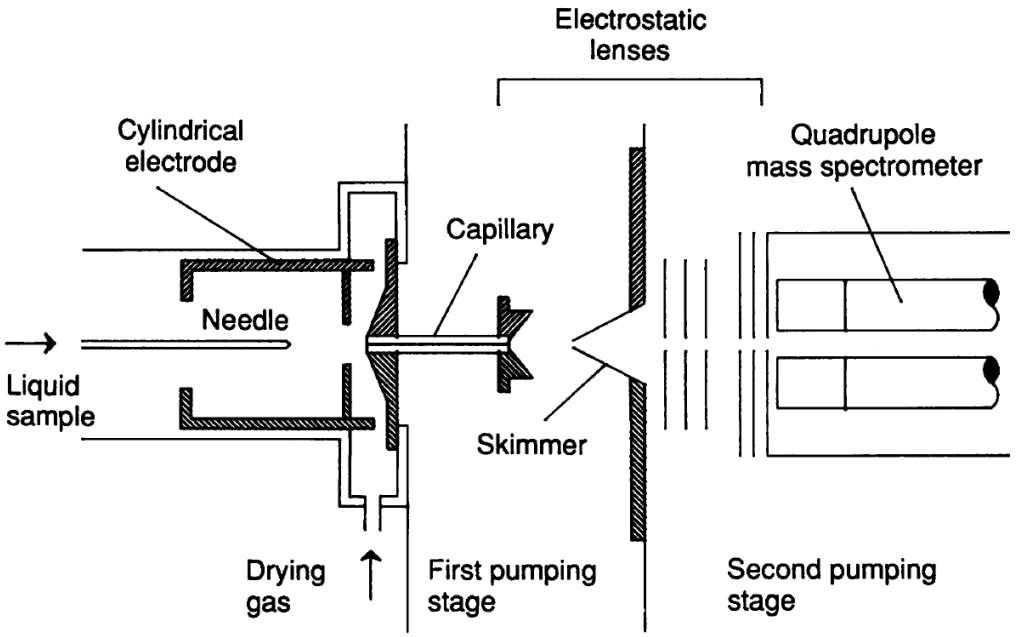

Figure 1.1.1 Setup of an early ESI ion source reproduced from *Fenn* et al.[4]. Reprinted with permission from AAAS (© American Association for the Advancement of Science, 1989)

1.1.2 Ion formation in ESI

When the sample solution passes through the needle, it experiences the highest electric field ($E \approx 10^6$ V m^{-1}) at the needle tip.[7] This causes the solution to form a meniscus, the so-called *Taylor cone* (Figure 1.1.2).[10] When the electric field is sufficiently high, a fine jet is formed from the *Taylor cone's* tip.[7] On the jet's surface lies an excess of positive ions, which break the jet up into small charged droplets due to their repulsion.[7]

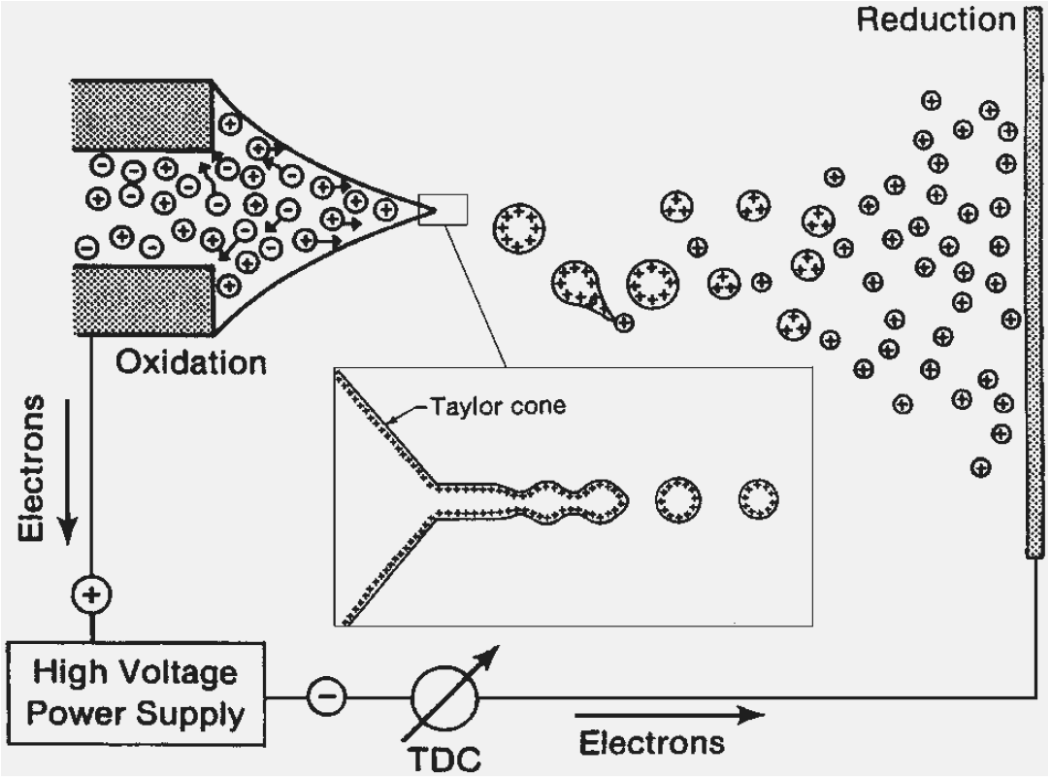

Figure 1.1.2 Schematic depiction of the Taylor cone formation, with the ejection of a jet and formation of small charged droplets. Reproduced by permission from Springer Nature: Mass Spectrometry a Textbook by J. H. Gross © 2005.[1]

These charged droplets shrink by evaporating solvent at a constant charge until their radius is small enough to reach the *Rayleigh limit*.[7,8,11,12] At the *Rayleigh limit*, the electrostatic repulsion is high enough to overcome the droplet's surface tension. At this point, the droplets discharge a series of small droplets out of the elongated tail in an uneven fission.[13] In this process, the new microdroplets retain only about 1-2 % of the mass but about 10-15 % of the precursor droplet's charge.[11,13] This process was captured in a flash shadowgraph by *Gomez* et al. (Figure 1.1.3).[14] The microdroplets and the parent droplets undergo evaporation and uneven fission repeatedly until ion generating droplets are reached.[7,13]

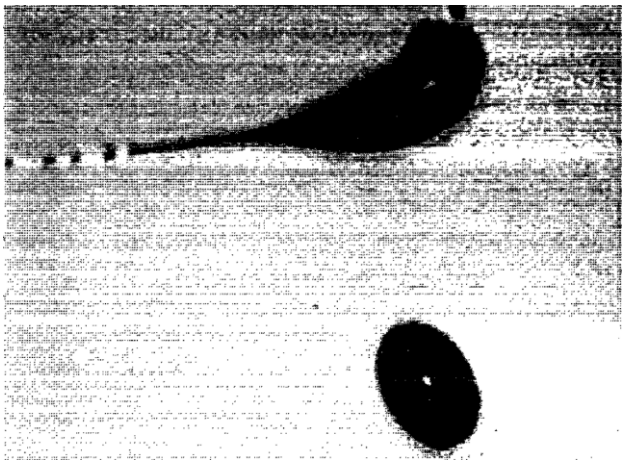

Figure 1.1.3 Flash shadowgraph of a flying microdroplet setting free offspring droplets captured by *Gomez et al.*[14]. Reproduced from *Gomez et al.*[14] with the permission of © AIP Publishing.

For the final ion generating step different mechanisms have been proposed.[1] The older charge residue model (CRM) was proposed by *Dole* et al.[2], the ESI-pioneer (Figure 1.1.4 a)). Therein, they suggest, that highly charged droplets break down further and further until only one analyte ion is left.[2] The ion evaporation model (IEM), which is the second proposed mechanism, was published by *Thomson and Iribarne*[15,16] (Figure 1.1.4 b)). The IEM states, when the electric field is strong enough in small droplets, ions can evaporate directly from the surface.[15,16] The CRM likely applies for large molecules, e.g. native proteins,[6–8] and the IEM for small molecules. [1,8]

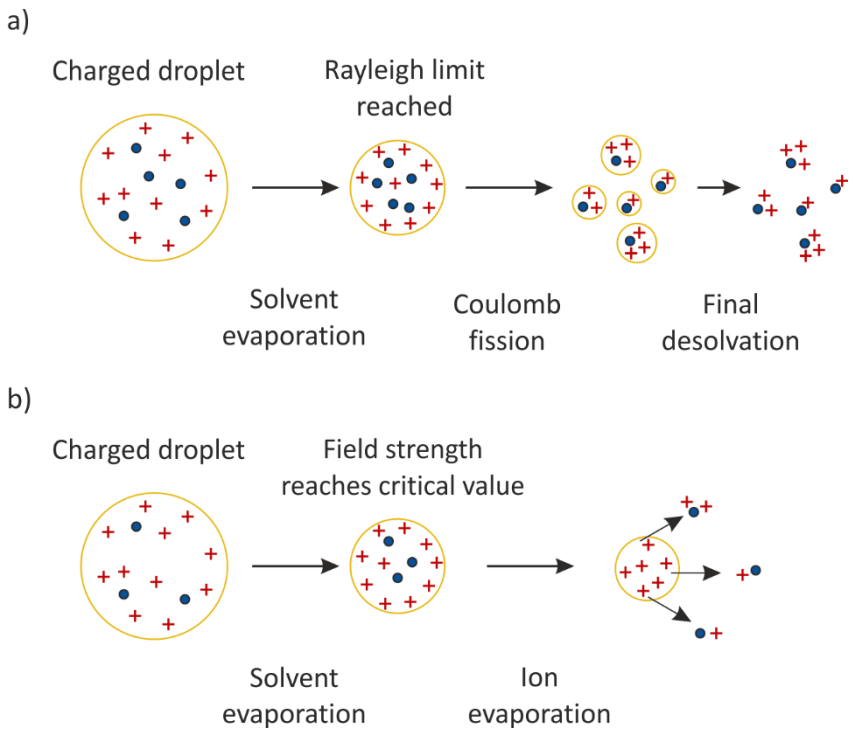

Figure 1.1.4 Schematic depiction of a) charge residue model (CRM) and b) ion evaporation model (IEM).

1.2 Tandem mass spectrometry

Tandem mass spectrometry, or MS/MS, describes the mass-selection of a precursor ion (MS^1) and analysis of the product ion(s) (MS^2).[1] The product ions can be formed through intentional fragmentation of the precursor ion or gas phase reactions. Tandem MS can be accomplished through different instrumental setups, which can be separated into two classes: *tandem-in-space* and *tandem-in-time*.[1]

The *tandem-in-space* setup is used in beam transmitting devices. For example, a quadrupole analyzer can be followed by a *time-of-flight* (*TOF*) analyzer. Thereby, the quadrupole analyzer performs the precursor ion's selection (MS^1), whereas the *TOF* analyzer performs the detection of the product ions (MS^2).[1] This is the case in the micrOTOF-Q instrument used in this work.

Whereas ion trap mass spectrometers, like the ion trap part of the Orbitrap XL instrument used in this work, have the *tandem-in-time* setup.[1] Here the precursor ion's selection (MS^1) and product ion analysis (MS^2) occur in the same place.[1] Therefore not only MS^2 experiments can be performed, but MS^3 and higher MS^n experiments can be accomplished as well.[1]

For the dissociation of the precursor ions different methods can be used: e.g. collision-induced dissociation (CID), electron transfer dissociation (ETD), or infrared multiphoton dissociation (IRMPD).[1]

1.3 High performance liquid chromatography coupled with ESI MS

Many samples of interest present themselves as a complex mixture of compounds.[1,17] Analyzing such a mixture directly i.e. without prior separation can be difficult.[1,17] To separate components from these complex mixtures, chromatographic techniques have been developed.[1,17] When coupling a chromatographic technique to a mass spectrometer, an additional dimension of analysis emerges[1], and easier and better identification of compounds can be accomplished.[17]

Gas chromatography (GC) was the first separation technique to be coupled to mass spectrometry (GC-MS).[1,17] In order to couple liquid chromatography to mass spectrometry, suitable ionization methods like ESI (see chapter 1.1) needed to be established.[1] Incidentally, the need for these suitable ionization methods inspired their invention.[1]

1.3.1 Basic principle

Samples for HPLC measurements need to be soluble in organic solvents. A schematic of an HPLC MS setup can be seen in Figure 1.3.1. The beginning is the mobile phase, for which different solvents are degassed and then mixed in every possible composition in the pump compartment. The pump

generates a high pressure, which is necessary to pass over the column. Via an autosampler, a defined sample volume is injected, and the sample flushed onto the column with the solvent mixture created by the pump. On the column the separation occurs, and the different compounds elute from the column over time and flow into an UV detector followed by the mass spectrometer.

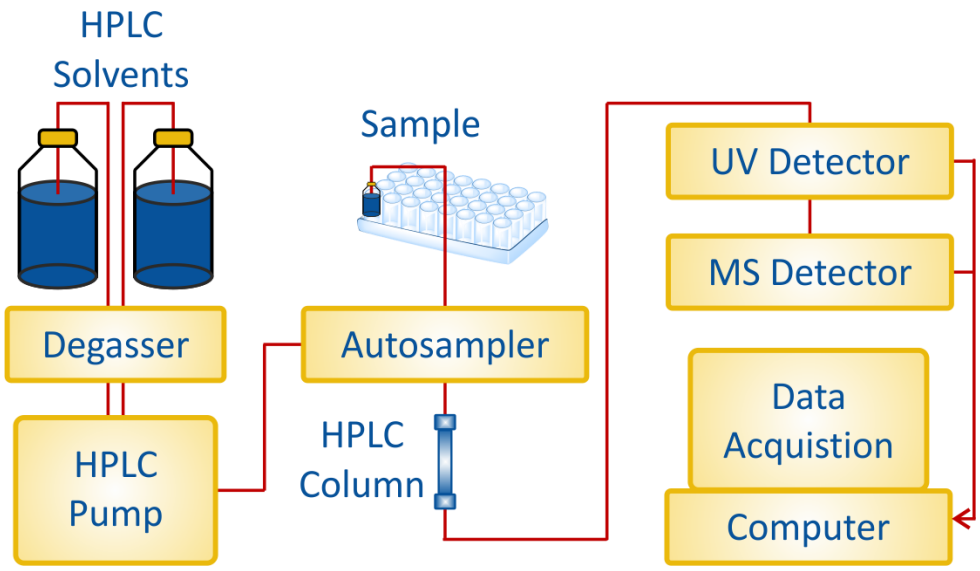

Figure 1.3.1 Schematic setup of an HPLC MS system.

Data of HPLC-ESI MS measurements are obtained in the form of chromatograms.[1] In chromatograms different units are plotted against the time or retention time (x-axis, see Figure 1.3.2).[1] Depending on the marking on the y-axis, different chromatograms are common. In a *total ion current chromatogram* (TICC) the total ion count of the MS spectrum is marked on the y-axis, which gives an overview of the measurement.[1,17,18] When the interest lies upon a specific target compound, an *extracted ion chromatogram* (EIC) is useful.[17,18] In an EIC one peak assigned to the compound of interest is chosen and its intensity is plotted on the y-axis.[17,18] Thus, it becomes apparent when the compound elutes from the column, which is the compound's characteristic retention time.[17] The MS spectra for every retention time can be imagined in an additional dimension, the z-axis (see Figure 1.3.2).

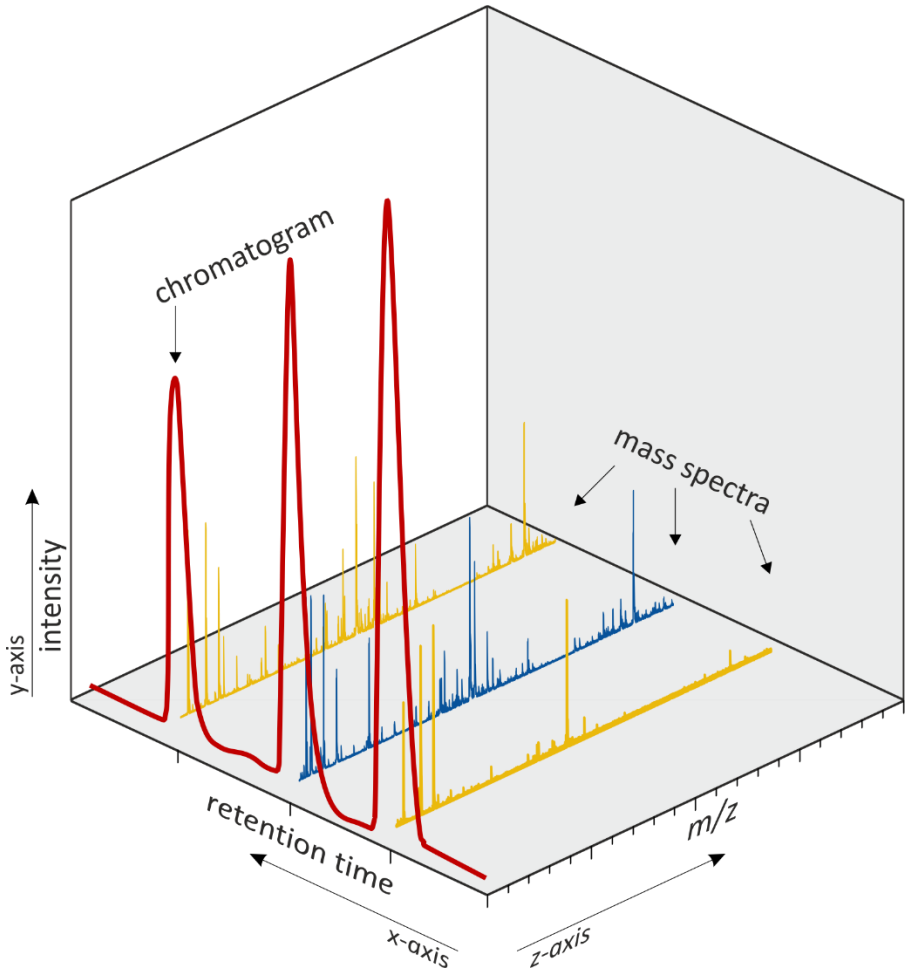

Figure 1.3.2 Three-dimensional depiction of a chromatogram with mass spectra.

1.3.2 Quantification

Often the analytical task for HPLC-ESI MS measurements is not only the identification of compounds within a complex mixture, but also the quantification of these compounds. This is not easily achieved, since the ionization efficiency is dependent on the specific compound.[1] A calibration procedure is needed, to gauge the relationship between observed signal intensities and the concentration of the target compound in the sample.[1,19]

Different quantification methods are established: External standardization, internal standardization, and isotope dilution, which is a special case of internal standardization.[1]

1.3.2.1 External standardization

Solutions of different concentrations of the pure target compound are made up e.g. by a serial dilution.[1,17] These solutions are measured with the same procedure as the sample, ideally starting from the lowest concentration to higher concentrations to avoid memory effects.[1]

A calibration curve can be generated by plotting the target compound area against the concentration (Figure 1.3.3).[1] The target compound area is gained through integration underneath the chromatogram peak of the EIC (Figure 1.3.4).[1] The calibration curve (Figure 1.3.3) ideally has a linear range in which the area of the target compound is directly proportional to the concentration.[1] The linear range is limited on the lower concentration end by chemical background noise and memory (leads to overestimation) or adsorption (leads to underestimation).[1,17] On the higher concentration end the limit occurs due to the saturation of the detector or ion source.[1,17]

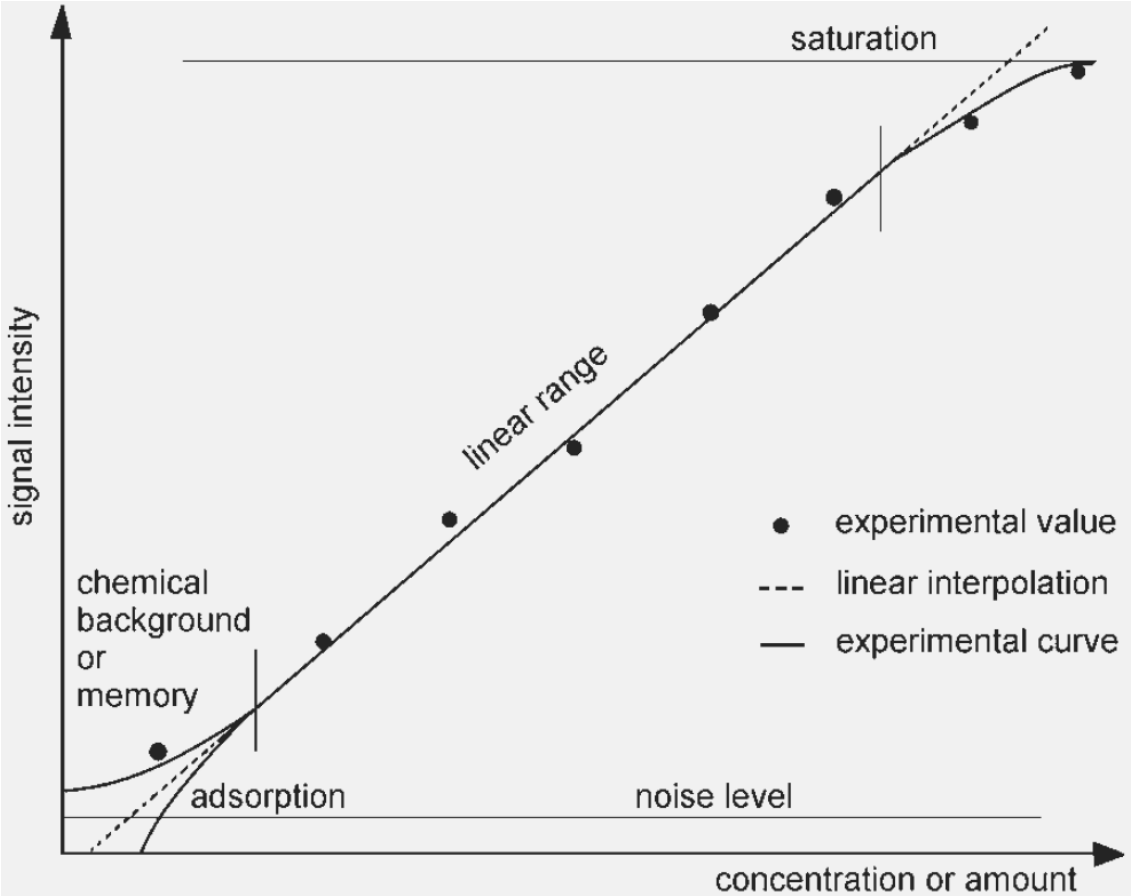

Figure 1.3.3 Exemplary calibration curve of HPLC quantification. Reproduced with permission from Springer Nature: Mass Spectrometry a Textbook by J. H. Gross © 2005.[1]

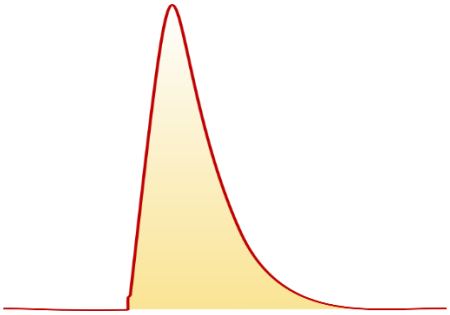

Figure 1.3.4 Area underneath a chromatogram peak, gained through integration.

When the linear range has been established linear regression can be performed which gives Equation 1.3.1:

$$area = concentration * slope \quad \textbf{Equation 1.3.1}$$

The concentration of the sample can then easily be quantified with integration of the target compounds EIC with Equation 1.3.2:

$$concentration = \frac{area}{slope} \quad \textbf{Equation 1.3.2}$$

Through this external quantification procedure, the concentration of the target compound in the sample can be determined.

1.3.2.2 Internal standardization

Internal standardization means the addition of a known amount of an additional compound into the sample.[1,17] This way, an internal reference point is generated.[1,17]

Typically, standard compounds are used which have similar ionization efficiencies and retention times as the target compound.[1] These can be homologues or isotopomers to the target compound.[1] When isotopomers are used, the procedure is called isotope dilution.[1] Isotopomers are isotopic isomers i.e. molecules with the same structure only isotopically labeled in known positions.[1] E.g. isotopomers could be ^{13}C-labeled or deuterated (^{2}H-labeled). Due to the isotopic label, the *m/z* value is shifted compared to the target compound, so that a separate EIC can be obtained.[1] Retention times of isotopomers differ only slightly compared to their unlabeled isotopomers, e.g. deuterated isotopomers have shorter retention times.[1] The standard compounds should be added as early as possible and before clean up procedures to ensure the same possible loss of target and standard compound.[1,17] With the internal standard as reference, the concentration of the target compound can be determined.[1,17]

In a different procedure, the sample is measured and then aliquots of the target compound are successively added.[17] The sample is measured after every additional aliquot.[17] From this series of measurements, the concentration of the unknown sample can be extrapolated.[17]

1.3.2.3 Matrix Effect

Often the solutions used for the calibration are made in pure solvents.[17] Signal intensities that are gathered from these solutions are then used to quantify the unknown samples.[17] By this, the matrix's effect, i.e. the surroundings of the target compound, is neglected in the unknown sample.[17] The samples surroundings can significantly affect the signal intensity of the target compound, e.g. due to suppression effects.[17,20] An attempt to overcome the matrix effect is to generate a solvent, which

resembles the sample without the target compound and prepare the calibration solutions in that solvent.[17]

1.3.3 Tandem MS in HPLC analysis

The principle of tandem MS has been discussed in chapter 1.2. It is an established tool in HPLC-MS analysis.[1] In non-tandem HPLC-MS analysis, the whole MS spectrum over the chosen *m/z* range is acquired.[1] With selected reaction monitoring (SRM) (Figure 1.3.5), a precursor ion is selected (MS analyzer 1) and fragmented. The product ion of specified *m/z* value is selected (MS analyzer 2) and recorded (MS analyzer 3).[1,18] This enhances the selectivity for detecting target compounds because they are identified by their precursor ions *m/z* value and their characteristic product ion(s).[1,21–24] This sets the target compounds apart from the unspecific matrix compounds in complex mixtures, as two conditions need to be met for the analysis and not only one: the precursor ions *m/z* value and the product ions *m/z* value.[1,21–24] The detection limits are also improved due to the enhanced selectivity and because the chemical background noise is eliminated through the precursor selection.[1,25] Multiple reaction monitoring (MRM) is the expansion of SRM to multiple precursor ions and their product ions.[18] With MRM, multiple target compounds can be selected and analyzed specific to their characteristic fragmentation pathways.[1]

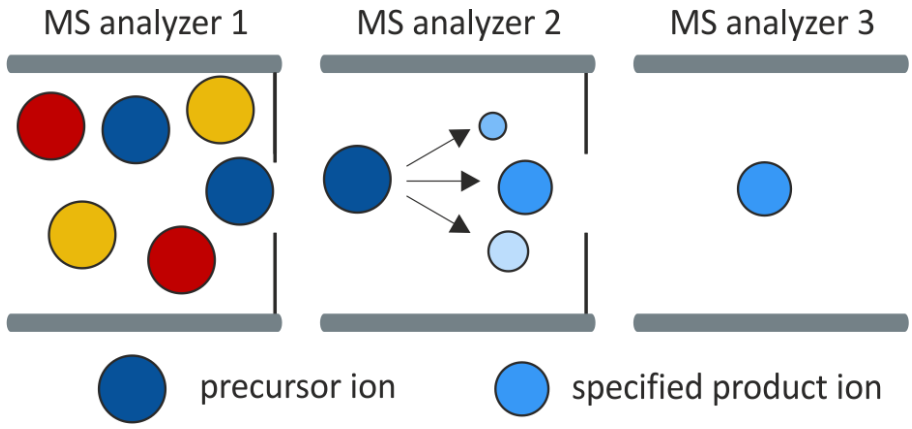

Figure 1.3.5 Schematic depiction of selected reaction monitoring (SRM) with three MS analysis stages.

1.4 Matrix-Assisted Laser Desorption/Ionization Mass Spectrometry

Laser desorption/ionization (LDI) was developed in the 1960s,[1,26,27] which was limited to molecules in the lower mass ranges[26,27,28]. However, with the development of *Matrix-Assisted Laser Desorption/Ionization* (MALDI) by *Karas* and *Hillenkamp*[29–32] molecules with masses up to 100 000 Da could be detected[1,30,33]. The new feature of MALDI in comparison to LDI is the admixing of an organic matrix to the analyte (Figure 1.4.1).[1,34] MALDI has become an essential analytical tool in life sciences,[35] for the analysis of peptides, proteins, DNA, and other large organic molecules like polymers[36].[1,34]

1.4.1 Basic principle

The most commonly used lasers in MALDI are UV nitrogen lasers (337 nm), with emitting pulses of 3-10 ns duration.[1] The sample is deposited on a target as a crystalline mixture of analyte and a surplus of matrix.[1,34] Stainless steel targets are reusable, but one time use plastic targets are also available. Short pulses of the laser are focused on the sample to achieve a sudden ablation from the sample layer.[1] This is caused by the matrix absorbing the laser beam's energy and transferring it to the analyte. The analyte molecules are then carried away with the excited matrix molecules into an expanding plume (Figure 1.4.1 b)).[29,34]

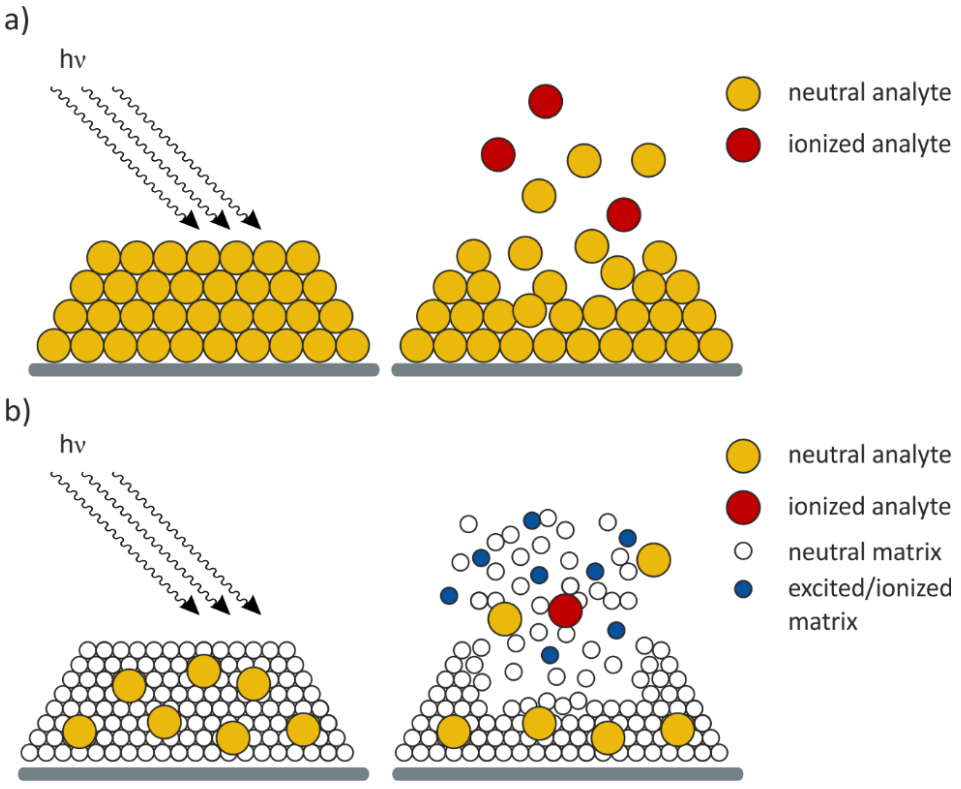

Figure 1.4.1 a) Laser desorption/ionization (LDI) b) matrix-assisted laser desorption/ionization (MALDI).

1.4.2 Ion formation

The mechanism of ion formation in MALDI is highly complex and still an issue of ongoing research.[1,34,37–39] Two different models describing the ionization process have been suggested: The older two-step model and the newer "lucky survivor" model.[34]

In the two-step model, the first step is the photoionization of the matrix molecules by the laser beam, while the analytes are assumed to be neutral molecules in the matrix crystals.[31,40] The second step occurs in the plume, where the matrix ions transfer their charge to the analyte molecules via chemical reactions.[34,37] Thus, a secondary ionization of analyte molecules occurs.[34,37]

The newer "lucky survivor" model was proposed by *Karas* et al.[38] in 2000 based on the findings from *Krüger* et al.[41].[34] They found out that the analyte molecules must retain at least some of their solvation shell within the matrix's crystal lattice, including their counterions.[34,41] Because they observed that pH-indicator molecules maintained their color and charge state in the matrix's crystal lattice.[41] *Karas* et al.[38] then proposed that the crystal lattice breaks up during the desorption process. Only some of the resulting small clusters contain one analyte ion.[34] Due to an additional or missing counterion, some of these clusters are charged.[34,38] In the plume clusters become smaller by evaporation of neutral molecules, like matrix, solvent, or counter ions as free acids or bases.[34,38] These neutral molecules, can only be evaporated because they transferred their charge in a proton-transfer neutralization to the analyte beforehand.[34,38] Only if the initial cluster was charged, a charged analyte is generated, which makes it the "lucky survivor" of the neutralization process. [34,38]

In 2011 *Jaskolla* and *Karas*[42] demonstrated that the combination of the two-step and "lucky survivor" model describe the MALDI ion formation. However, which of the two is the paramount model is dependent on the individual type of analyte, matrix, and experimental parameters.[42]

1.4.3 Matrix

Typical matrices in UV-MALDI can be seen in Figure 1.4.2.[1] They all have an aromatic core in common. The aromatic core is necessary because with it the matrix molecules absorb the light in the wavelength range of the UV laser.[1,34] This way, the matrix can transfer the absorbed energy to the sample.[29,34] The functionalization with ligands of the core ring determines the exact absorption maximum.[1,34] Which matrix to choose or switch to for optimization for a specific measurement or analyte is mostly based on empirical methods.[34]

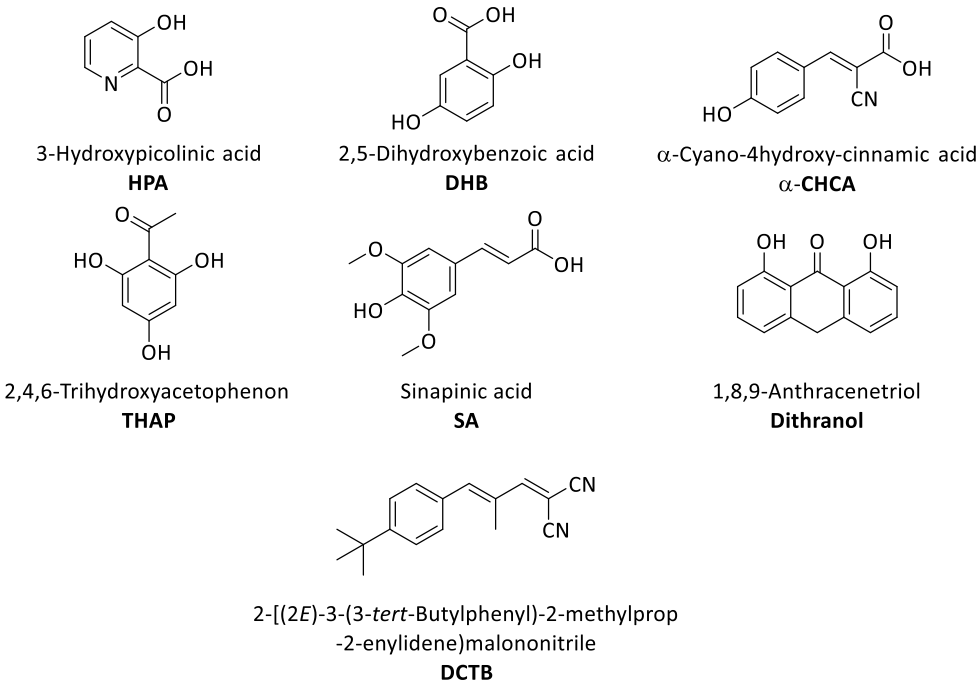

Figure 1.4.2 Common MALDI matrices.[1]

1.4.4 Sample preparation

The most commonly used sample preparation is the *dried droplet* technique: 0.5-2 µL of a mixture of analyte and matrix solution are deposited onto the stainless-steel MALDI target.[1] The solvent is evaporated under ambient conditions or with the aid of a flow of cold air.[34] The molar ratio of matrix to analyte is usually between 500:1 and 5000:1 to achieve reduced ion fragmentation and adequate signal-to-noise ratio.[1]

When analytes are poorly soluble or insoluble, it is possible to utilize a solvent-free sample preparation.[1] Here the analyte and matrix are ground together to generate a fine powder, which is spread onto the target[43] or pressed and afterwards fixed onto the target with double-sided adhesive tape[44].

1.5 References

[1] J. H. Gross, *Mass Spectrometry*. *A Textbook*, Springer Berlin Heidelberg, Berlin, Heidelberg, **2004**.

[2] M. Dole, L. L. Mack, R. L. Hines, R. C. Mobley, L. D. Ferguson, M. B. Alice, *J. Chem. Phys.* **1968**, *49*, 2240.

[3] a) C. M. Whitehouse, R. N. Dreyer, M. Yamashita, J. B. Fenn, *Anal. Chem.* **1985**, *57*, 675; b) M. Yamashita, J. B. Fenn, *J. Phys. Chem.* **1984**, *88*, 4451; c) M. Yamashita, J. B. Fenn, *J. Phys. Chem.* **1984**, *88*, 4671.

[4] J. B. Fenn, M. Mann, C. K. Meng, S. F. Wong, C. M. Whitehouse, *Science* **1989**, *246*, 64.

[5] Nobelprize.org The Nobel Prize in Chemistry 2002, The Royal Swedish Academy, https://www.nobelprize.org/prizes/chemistry/2002/summary/, (accessed 27/11/2020), "Nobelprize 2002 Fenn".

[6] J. B. Fenn, *Angew. Chem. Int. Ed.* **2003**, *42*, 3871.

[7] P. Kebarle, U. H. Verkerk, *Mass Spectrom. Rev.* **2009**, *28*, 898.

[8] L. Konermann, E. Ahadi, A. D. Rodriguez, S. Vahidi, *Anal. Chem.* **2013**, *85*, 2.

[9] G. J. van Berkel, V. Kertesz, *Anal. Chem.* **2007**, *79*, 5510.

[10] G. I. Taylor, *Proc. R. Soc. Lond. A* **1964**, *280*, 383.

[11] P. Kebarle, L. Tang, *Anal. Chem.* **1993**, *65*, 972A-986A.

[12] Lord Rayleigh, *Philos. Mag.* **1882**, *14*, 184.

[13] R. B. Cole, *Org. Mass Spectrom.* **2000**, *35*, 763.

[14] A. Gomez, K. Tang, *Phys. Fluids* **1994**, *6*, 404.

[15] B. A. Thomson, J. V. Iribarne, *J. Chem. Phys.* **1979**, *71*, 4451.

[16] J. V. Iribarne, *J. Chem. Phys.* **1976**, *64*, 2287.

[17] R. E. Ardrey, *Liquid chromatography-mass spectrometry*, Wiley, N.Y., **2003**.

[18] K. K. Murray, R. K. Boyd, M. N. Eberlin, G. J. Langley, L. Li, Y. Naito, *Pure Appl. Chem.* **2013**, *85*, 1515.

[19] H.-J. Hübschmann, *Handbook of GC/MS*. *Fundamentals and applications*, Wiley-VCH, Weinheim, **2015**.

[20] a) B. K. Choi, D. M. Hercules, A. I. Gusev, *Fresenius J Anal Chem* **2001**, *369*, 370; b) B. K. Choi, D. M. Hercules, A. I. Gusev, *J. Chromatogr. A* **2001**, *907*, 337.

[21] R. Dams, C. M. Murphy, W. E. Lambert, M. A. Huestis, *Rapid Commun. Mass Spectrom.* **2003**, *17*, 1665.

[22] X.-S. Miao, C. D. Metcalfe, *Anal. Chem.* **2003**, *75*, 3731.

[23] Y. Tondeur, P. W. Albro, J. R. Hass, D. J. Harvan, J. L. Schroeder, *Anal. Chem.* **1984**, *56*, 1344.

[24] J. V. Johnson, R. A. Yost, K. F. Faull, *Anal. Chem.* **1984**, *56*, 1655.

[25] E. de Hoffmann, *Org. Mass Spectrom.* **1996**, *31*, 129.

[26] N. C. Fenner, N. R. Daly, *Rev. Sci. Instrum.* **1966**, *37*, 1068.

[27] F. J. Vastola, R. O. Mumma, A. J. Pirone, *Org. Mass Spectrom.* **1970**, *3*, 101.

[28] a) R. M. Jones, J. H. Lamb, C. K. Lim, *Rapid Commun. Mass Spectrom.* **1995**, *9*, 921; b) R. E. Honig, J. R. Woolston, *Appl. Phys. Lett.* **1963**, *2*, 138.

[29] M. Karas, D. Bachmann, F. Hillenkamp, *Anal. Chem.* **1985**, *57*, 2935.

[30] M. Karas, F. Hillenkamp, *Anal. Chem.* **1988**, *60*, 2299.

[31] M. Karas, D. Bachmann, U. Bahr, F. Hillenkamp, *Int. J. Mass Spectrom.* **1987**, *78*, 53.

[32] F. Hillenkamp, M. Karas, R. C. Beavis, B. T. Chait, *Anal. Chem.* **1991**, *63*, 1193A-1203A.

[33] M. Karas, U. Bahr, A. Ingendoh, F. Hillenkamp, *Angew. Chem. Int. Ed.* **1989**, *28*, 760.

[34] F. Hillenkamp, J. Peter-Katalinić (Eds.) *MALDI MS*. *A practical guide to instrumentation, methods and applications*, Wiley - VCH, Weinheim, **2009**.

[35] a) R. J. Cotter, *Time-of-flight mass spectrometry*. *Instrumentation and applications in biological research*, American Chemical Society, Washington, **1997**; b) G. Siuzdak, *The Expanding Role of Mass Spectrometry in Biotechnology*, McC Press, United States of America, **2003**.

[36] a) G. Montaudo, R. Lattimer, *Mass spectrometry of polymers*, CRC Press, Boca Raton, Fla., **2002**; b) L. Li, *MALDI mass spectrometry for synthetic polymers analysis*, Wiley, Chichester, **2010**.

[37] R. Zenobi, R. Knochenmuss, *Mass Spectrom. Rev.* **1998**, *17*, 337.

[38] M. Karas, M. Glückmann, J. Schäfer, *J. Mass Spectrom.* **2000**, *35*, 1.

[39] M. Glückmann, A. Pfenninger, R. Krüger, M. Thierolf, M. Karasa, V. Horneffer, F. Hillenkamp, K. Strupat, *Int. J. Mass Spectrom.* **2001**, *210-211*, 121.

[40] H. Ehring, M. Karas, F. Hillenkamp, *Org. Mass Spectrom.* **1992**, *27*, 472.

[41] R. Krüger, A. Pfenninger, I. Fournier, M. Gluckmann, M. Karas, *Anal. Chem.* **2001**, *73*, 5812.

[42] T. W. Jaskolla, M. Karas, *J. Am. Soc. Mass Spectrom.* **2011**, *22*, 976.

[43] a) S. Trimpin, A. Rouhanipour, R. Az, H. J. Räder, K. Müllen, *Rapid Commun. Mass Spectrom.* **2001**, *15*, 1364; b) S. Trimpin, A. C. Grimsdale, H. J. Räder, K. Müllen, *Anal. Chem.* **2002**, *74*, 3777; c) J. K. Pruns, J.-P. Vietzke, M. Strassner, C. Rapp, U. Hintze, W. A. König, *Rapid Commun. Mass Spectrom.* **2002**, *16*, 208.

[44] R. Skelton, F. Dubois, R. Zenobi, *Anal. Chem.* **2000**, *72*, 1707.

2 Introduction

2.1 Organocatalysis

Organocatalysis describes the use of a small, metal-free, organic molecule as a catalyst in a chemical reaction.[1,2] Although the concept of using purely organic molecules for catalytic purposes had been known for more than a century, its breakthrough occurred only two decades ago (Figure 2.1.1).[2,3] Since then, organocatalysis has made its mark as its own branch in the field of enantioselective catalysis, being able to compete with metal- and enzyme- catalysis.[1,2,4] Especially as organocatalysts are cheap, non-toxic, and tolerant towards oxygen and moisture.[1,2,4]

The underlying principle of organocatalysis can be separated into covalent and non-covalent catalysis. Examples for covalent catalysis are enamine, iminium, and singly occupied molecular orbital (SOMO) catalysis.[3] Hydrogen bonding, counterion, and phase transfer catalysis are examples of non-covalent catalysis.[3,5] An extensive repertoire of stereoselective organocatalysts has been developed to optimize selectivity and yield of a large variety of different reactions.[6] L-proline was one of the first organocatalysts used[7] and will be introduced in detail in chapter 3.1.2.

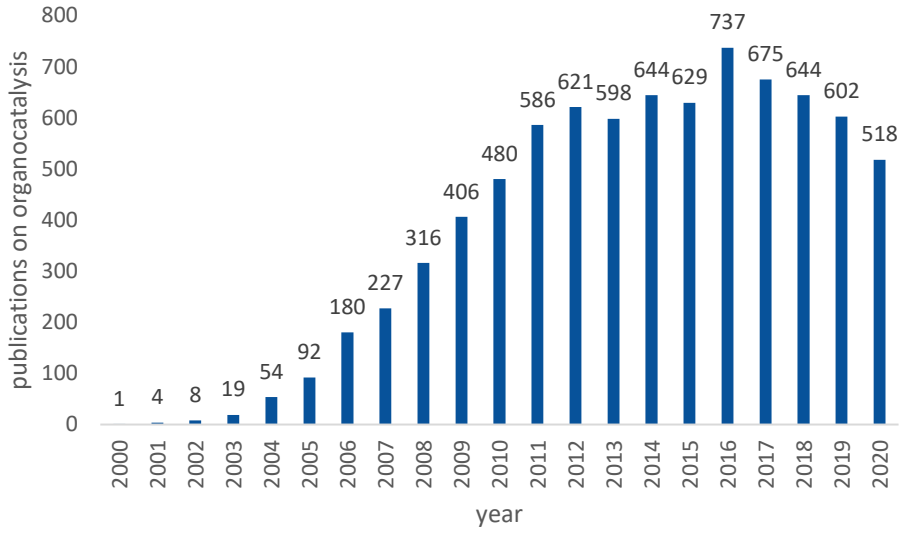

Figure 2.1.1 Number of publications on organocatalysis from 2000 – 2020.[8]

2.2 Studying reaction mechanisms with ESI MS

ESI MS is a well-suited mass spectrometric method for studying reaction mechanisms.[9] No or only minimal fragmentation of the species of interest occurs during the ionization process, as ESI can be a soft ionization method.[9] Furthermore, short-lived transient intermediates can be studied[10] because it is a fast analytical method.[9,10]

Different on-line monitoring setups have been developed for the analysis of fast reactions: one example is the continuous flow version from *Metzger* and coworkers.[11,12] A pressurized sample infusion setup (PSI) for sensitive reactions was developed by *McIndoe* and coworkers.[13] ESI MS has been used for the study of numerous types of reactions like organometallic reactions[10,12,14–18], organic reactions like aldol[19–21], the Baylis-Hillman[22,23,24], or Diels-Alder reactions[25,26].

A beneficial feature of ESI MS is that it generates sharp, distinct signals for each ionized species, and signal superposition occurs rarely.[10] This is extremely useful, because reaction mixtures are typically a "soup of reactants"[10], and thus can be analyzed without prior separation.[10,18] This is in contrast to other analysis methods such as NMR-, IR- or UV-spectroscopy, where signals of different species can overlap and thus not easily be assigned.[27]

A downside to MS is the blindness towards differentiating between isomers, as they have the same exact mass and therefore generate the same signal.[9] Although, with more elaborate and sophisticated setups, isomers can be distinguished from one another, e.g. with ion mobility MS[28], tandem MS[9], action IR spectroscopy[29] or the coupling to liquid or gas chromatography[9]. Also, there is no direct correlation between the signal intensities of a species in ESI MS and its concentration in solution; the analyte's ESI response has to be considered.[9,30] Different analytes have different ESI responses due to differences in their chargeability and surface activities; also the applied electrospray conditions have an impact.[30,31] When a severe discrepancy in the ESI response between analytes occurs, one analyte with a high ESI response might suppress another analyte with a low ESI response.[20,32] This phenomenon can be circumvented with charge-tagging.

2.2.1 Charge-tagging

The technique of charge-tagging has been widely applied in studies of reaction mechanisms using ESI MS.[10,13,15,16,18,21,26,33,34,35] Charge-tagging proceeds by incorporating covalently linked charge-tags into analytes, typically using moieties like alkylated amines or phosphines for cations[10,18] and sulfonates for anions[36,37]. The charge-tag can either be placed within the substrate[14,35,38] or the catalyst[21,37,39,40]; examples are given in Figure 2.2.1.

Due to the charge-tag's inherent charge, all species containing the charge-tag have a similarly high ESI response.[10,14] When the catalyst is charge-tagged, only species, which are part of the reaction, contain the charge-tag. Thus, only species of interest have an enhanced ESI response and are easier detected than species, which are not part of the reaction. This has coined the phrase a charge-tag facilitates "fishing"[18,26,34,35] for transient intermediates that otherwise would have been elusive.

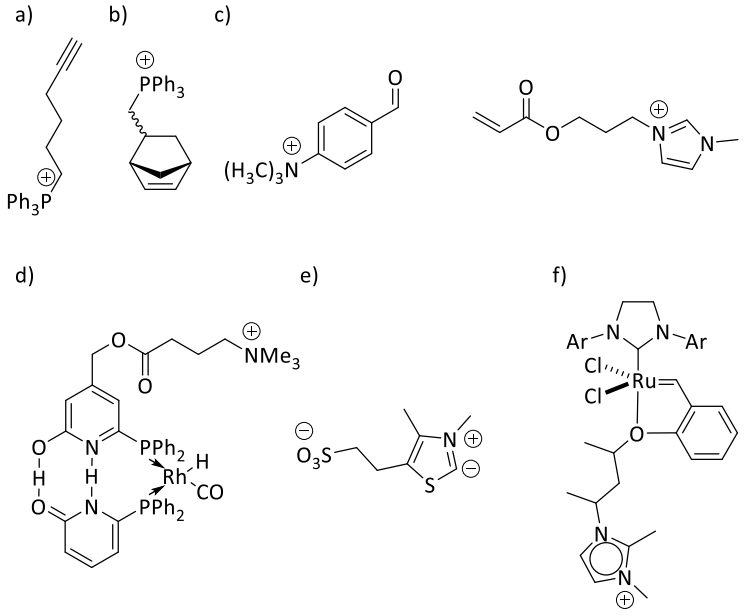

Figure 2.2.1 Charge-tagged substrates (a-c)) and charge-tagged catalysts (d-f)): a) alkyne with phosphonium moiety for the study of alkyne reduction with *Wilkinsons* catalyst by *McIndoe* and coworkers[14], b) norbornene with phosphonium moiety for the study of *ring-opening metathesis polymerization* (*ROMP*) by *Adlhart* et al.[35], c) aldehyde with ammonium moiety and acrylate with imidazolium moiety for the study of the *Baylis-Hillman* reaction by *Eberlin* and coworkers[23,24], d) rhodium catalyst with ligand carrying an ammonium moiety for the study of Rh-catalyzed hydroformylation of terminal alkenes by *Beilerlein* et al.[39], e) thiazolium salt with sulfonate moiety for the study of a benzoin condensation by *Zeng* et al.[37], f) Hoveyda-type catalyst with imidazolium moiety from *Limberger* et al.[41].

2.3 Mass spectrometric analysis of fossilized specimens

Mass spectrometry (MS) is a highly sensitive method that can detect trace amounts of chemical compounds.[9] Further, MS can be coupled to separation techniques like HPLC or GC.[9] This is helpful in the analysis of fossilized specimens because they are by nature a complex mixture of inorganic matter and trace amounts of organic matter. By separation prior to analysis, the detection of specific compounds is simplified.[9] The high sensitivity of MS is also useful as compounds of interest might have decomposed or are degraded over time, thus only leaving small amounts of organic compounds.

MS analysis of fossilized specimens becomes easier when the paleontological question includes specific compounds. Projects are simplified when MS analysis is utilized as a search tool for specific compounds of significance and not the general question of “What is in the specimen?” is posed. When specific compounds are of interest, the analytical method can be tailored to the compounds.[9] For example, not all compounds are suitable for ESI MS analysis, as they might not have a high enough ESI response.[31] Further, fossilized specimens are usually solid and thereby need to be prepared for analysis. ESI MS requires a liquid sample; thus, extraction of the specimen is an option, but the extraction method should be tailored to the specific compounds too. This can be accomplished by variation of the polarity of the extracting solvent and testing the standard compound’s solubility. For MALDI a soluble sample is beneficial, but also solid samples can be analyzed.[9,42] Fossilized samples are precious and often not available in abundance, but MS analysis is a destructive analytical method. Thus, initial experiments with reference material or standard compounds should be performed first to spare the fossilized sample.

2.4 References

[1] P. I. Dalko, L. Moisan, *Angew. Chem. Int. Ed.* **2001**, *40*, 3726.

[2] B. List, *Chem. Rev.* **2007**, *107*, 5413.

[3] D. W. C. MacMillan, *Nature* **2008**, *455*, 304.

[4] S. Bertelsen, K. A. Jørgensen, *Chem. Soc. Rev.* **2009**, *38*, 2178.

[5] T. Hashimoto, K. Maruoka, *Chem. Rev.* **2007**, *107*, 5656.

[6] B. List, *Asymmetric organocatalysis*, Springer, Berlin, **2010**.

[7] a) Z. G. Hajos, D. R. Parrish, *J. Org. Chem.* **1974**, *39*, 1615; b) U. Eder, G. Sauer, R. Wiechert, *Angew. Chem. Int. Ed.* **1971**, *10*, 496; c) B. List, R. A. Lerner, C. F. Barbas, *J. Am. Chem. Soc.* **2000**, *122*, 2395.

[8] Web of Science search on "Organocatalysis" 22.12.2020, *www.webofknowledge.com*.

[9] J. H. Gross, *Mass Spectrometry*. *A Textbook*, Springer Berlin Heidelberg, Berlin, Heidelberg, **2004**.

[10] L. P. E. Yunker, R. L. Stoddard, J. S. McIndoe, *J. Mass Spectrom.* **2014**, *49*, 1.

[11] L. S. Santos, L. Knaack, J. O. Metzger, *Int. J. Mass Spectrom.* **2005**, *246*, 84.

[12] L. S. Santos, J. O. Metzger, *Angew. Chem. Int. Ed.* **2006**, *45*, 977.

[13] K. L. Vikse, M. P. Woods, J. S. McIndoe, *Organometallics* **2010**, *29*, 6615.

[14] J. Luo, A. G. Oliver, J. S. McIndoe, *Dalton Trans.* **2013**, *42*, 11312.

[15] K. L. Vikse, Z. Ahmadi, C. C. Manning, D. A. Harrington, J. S. McIndoe, *Angew. Chem. Int. Ed.* **2011**, *50*, 8304.

[16] L. P. E. Yunker, Z. Ahmadi, J. R. Logan, W. Wu, T. Li, A. Martindale, A. G. Oliver, J. S. McIndoe, *Organometallics* **2018**, *37*, 4297.

[17] G. T. Thomas, E. Janusson, H. S. Zijlstra, J. S. McIndoe, *Chem. Commun.* **2019**, *55*, 11727.

[18] D. Schröder, *Acc. Chem. Res.* **2012**, *45*, 1521.

[19] G. Guillena, M. d. C. Hita, C. Nájera, S. F. Viózquez, *J. Org. Chem.* **2008**, *73*, 5933.

[20] C. Marquez, J. O. Metzger, *Chem. Commun.* **2006**, 1539.

[21] J. A. Willms, R. Beel, M. L. Schmidt, C. Mundt, M. Engeser, *Beilstein J. Org. Chem.* **2014**, *10*, 2027.

[22] a) L. S. Santos, C. H. Pavam, W. P. Almeida, F. Coelho, M. N. Eberlin, *Angew. Chem. Int. Ed.* **2004**, *43*, 4430; b) G. W. Amarante, M. Benassi, H. M. S. Milagre, A. A. C. Braga, F. Maseras, M. N. Eberlin, F. Coelho, *Chem. Eur. J.* **2009**, *15*, 12460; c) G. W. Amarante, M. Benassi, R. N. Pascoal, M. N. Eberlin, F. Coelho, *Tetrahedron* **2010**, *66*, 4370; d) T. Regiani, V. G. Santos, M. N. Godoi, B. G. Vaz, M. N. Eberlin, F. Coelho, *Chem. Commun.* **2011**, *47*, 6593.

[23] T. S. Rodrigues, V. H. C. Silva, P. M. Lalli, H. C. B. de Oliveira, W. A. da Silva, F. Coelho, M. N. Eberlin, B. A. D. Neto, *J. Org. Chem.* **2014**, *79*, 5239.

[24] R. Galaverna, N. S. Camilo, M. N. Godoi, F. Coelho, M. N. Eberlin, *J. Org. Chem.* **2016**, *81*, 1089.

[25] a) S. Fürmeier, J. O. Metzger, *J. Am. Chem. Soc.* **2004**, *126*, 14485; b) A. Teichert, A. Pfaltz, *Angew. Chem. Int. Ed.* **2008**, *47*, 3360; c) F. A. M. G. van Geenen, M. C. R. Franssen, H. Zuilhof, M. W. F. Nielen, *Anal. Chem.* **2018**, *90*, 10409; d) G. Scotti, S. M. E. Nilsson, M. Haapala, P. Pöhö, G. Boije af Gennäs, J. Yli-Kauhaluoma, T. Kotiaho, *React. Chem. Eng.* **2017**, *2*, 299.

[26] A. Schnell, J. A. Willms, S. Nozinovic, M. Engeser, *Beilstein J. Org. Chem.* **2019**, *15*, 30.

[27] M. Hesse, H. Meier, B. Zeeh, *Spectroscopic methods in organic chemistry*, Thieme, Stuttgart, **2008**.

[28] a) D. J. Harvey, Y. Watanabe, J. D. Allen, P. Rudd, K. Pagel, M. Crispin, W. B. Struwe, *J. Am. Soc. Mass Spectrom.* **2018**, *29*, 1250; b) K. Pagel, D. J. Harvey, *Anal. Chem.* **2013**, *85*, 5138; c) J. Hofmann, K. Pagel, *Angew. Chem. Int. Ed.* **2017**, *56*, 8342.

[29] a) M. Lettow, M. Grabarics, E. Mucha, D. A. Thomas, Ł. Polewski, J. Freyse, J. Rademann, G. Meijer, G. von Helden, K. Pagel, *Anal. Bioanal. Chem.* **2020**, *412*, 533; b) A. P. Cismesia, L. S. Bailey, M. R. Bell, L. F. Tesler, N. C. Polfer, *J. Am. Soc. Mass Spectrom.* **2016**, *27*, 757.

[30] N. B. Cech, C. G. Enke, *Mass Spectrom. Rev.* **2001**, *20*, 362.

[31] P. Liigand, J. Liigand, K. Kaupmees, A. Kruve, *Anal. Chim. Acta* **2020**.

[32] R. B. Cole, *Electrospray ionization mass spectrometry*. *Fundamentals, instrumentation, and applications*, Wiley, New York, NY, **1997**.

[33] a) A. E. Crotti, D. Previdi, P. M. Donate, J. Scott McIndoe, *Inorg. Chim. Acta* **2020**, *508*, 119654; b) Z. Ahmadi, L. P. E. Yunker, A. G. Oliver, J. S. McIndoe, *Dalton Trans.* **2015**, *44*, 20367; c) J. A. Willms, J. Vidic, J. Barthelmes, V. Steinmetz, T. Bredow, P. Maître, M. Engeser, *Phys. Chem. Chem. Phys.* **2019**, *21*, 2578.

[34] C. Iacobucci, S. Reale, F. de Angelis, *Angew. Chem. Int. Ed.* **2016**, *55*, 2980.

[35] C. Adlhart, P. Chen, *Helv. Chim. Acta* **2000**, *83*, 2192.

[36] a) J.-M. Basset, D. Bouchu, G. Godard, I. Karamé, E. Kuntz, F. Lefebvre, N. Legagneux, C. Lucas, D. Michelet, J. B. Tommasino, *Organometallics* **2008**, *27*, 4300; b) P. Kumar, I. Cisarova, *J. Organomet. Chem.* **2013**, *735*, 32.

[37] H. Zeng, K. Wang, Y. Tian, Y. Niu, L. Greene, Z. Hu, J. K. Lee, *Int. J. Mass Spectrom.* **2014**, *369*, 92.

[38] M. A. Schade, J. E. Fleckenstein, P. Knochel, K. Koszinowski, *J. Org. Chem.* **2010**, *75*, 6848.

[39] C. H. Beierlein, B. Breit, R. A. Paz Schmidt, D. A. Plattner, *Organometallics* **2010**, *29*, 2521.

[40] D. E. Polyansky, J. T. Muckerman, J. Rochford, R. Zong, R. P. Thummel, E. Fujita, *J. Am. Chem. Soc.* **2011**, *133*, 14649.

[41] J. Limberger, B. C. Leal, A. L. Monteiro, J. Dupont, *Chem. Sci.* **2015**, *6*, 77.

[42] F. Hillenkamp, J. Peter-Katalinić (Eds.) *MALDI MS*. *A practical guide to instrumentation, methods and applications*, Wiley - VCH, Weinheim, **2009**.

3 ESI MS studies of L-proline catalyzed Diels-Alder reactions

3.1 Introduction

3.1.1 The Diels-Alder reaction

The *Diels-Alder (D-A)* reaction is named in honor of *Otto Diels* and *Kurt Alder*, the authors of the seminal publications in the 1920s[1].[2] The *D-A* reaction is the most distinguished reaction for the formation of six-membered rings and one of the most widely used synthetic tools for C,C-bond formation.[2,3]

A conjugated diene and a dienophile react in a [4+2]-cycloaddition forming a cyclohexene derivative (Figure 3.1.1).[2,4] Depending on the electronic structure of the diene and dienophile, the reaction is classified as a *normal electron-demand D-A* or an *inverse electron-demand D-A* reaction.[2] In a *normal electron-demand D-A* reaction, the diene is electron rich with electron-donating groups, and the dienophile electron poor with electron-withdrawing groups (Figure 3.1.1).[2] As the name suggests, in an *inverse electron-demand D-A* reaction the situation is reversed: The diene is electron poor with electron-withdrawing groups, and the dienophile electron rich with electron-donating groups (Figure 3.1.1).[2] The *D-A* reaction can also take place when heteroatoms are included and is then called a *hetero-D-A* reaction.[2,5] Furthermore, the reaction works in reverse; when an unsaturated six-membered ring breaks up into a diene and dienophile, it is called a *retro-D-A* reaction.[2,6]

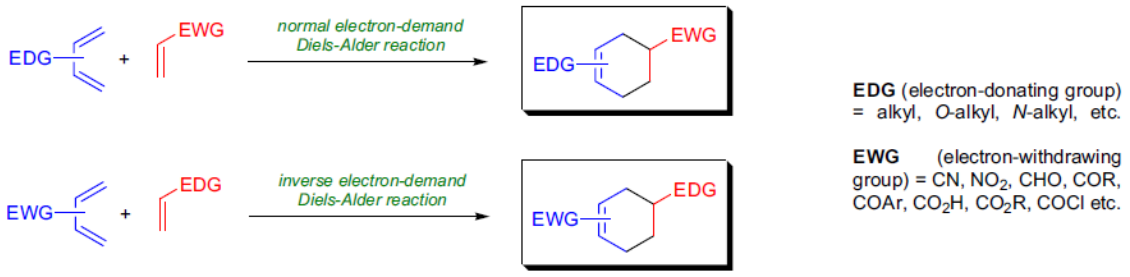

Figure 3.1.1 *Diels-Alder* reaction with *normal electron-demand* and *inverse electron-demand.* Reprinted with permission from ©Elsevier Inc.[2]

In the general case of a *D-A* reaction, the mechanism is a concerted, pericyclic reaction via an aromatic transition state (Figure 3.1.2).[2,4]

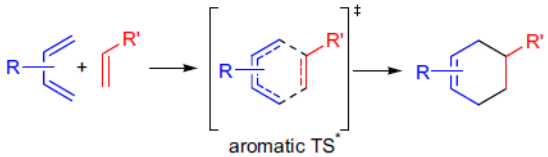

Figure 3.1.2 Schematic *Diels-Alder* reaction with diene (blue) and dienophile (red) via an aromatic transition state. Reprinted with permission from ©Elsevier Inc.[2]

The reaction occurs due to orbital interactions from the 4π electron system of the diene and the 2π electron system of the dienophile; thus, it is also a [4+2] cycloaddition.[2,4] In a *D-A* reaction with *normal electron demand*, the HOMO (highest occupied molecular orbital) of the diene interacts with the LUMO (lowest unoccupied molecular orbital) of the dienophile (Figure 3.1.3). In a *D-A* with *inverse electron demand*, the HOMO of the dienophile interacts with the LUMO of the diene.[4,7] Two new σ-bonds are formed, which is the driving force of the reaction.[2,4]

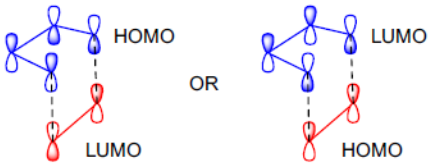

Figure 3.1.3 HOMO LUMO interaction of *D-A* reaction with *normal electron-demand* (left) and *inverse electron-demand* (right). Reprinted with permission from ©Elsevier Inc.[2]

The *D-A* reaction is of immense synthetic value as it allows to define up to four stereogenic centers in one step.[2,4] The stereochemistry is predictable, as the substrates' stereoinformations are transferred to the product (Figure 3.1.4).[2,4] Further, the reaction is highly regioselective.[2,4] Regioselectivity can be seen in the preferred formation of the *"ortho"* and *"para"* products instead of the *"meta"* product (Figure 3.1.4).[2,4] The dienophile's stereochemical information is transferred to the product; i.e. when the two substituents of the dienophile are arranged in a *cis* (*Z*) configuration, these two substituents will be in a *cis* configuration in the product; equally *trans* (*E*) configuration in the substrate translates into *trans* configuration in the product (Figure 3.1.4).[2,4] Not only the dienophiles stereochemical information is transferred but also the diene's.[2,4] Further, the *endo* product is preferred over the *exo* product in irreversible *D-A* reactions (see Figure 3.1.4).[2,4]

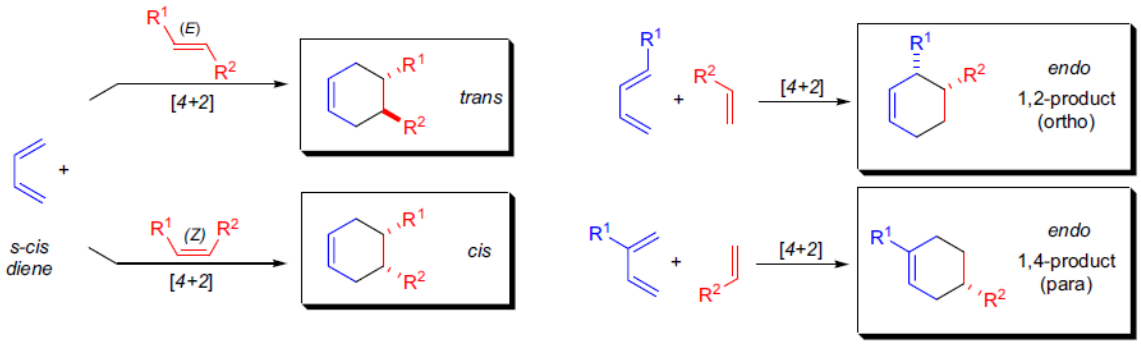

Figure 3.1.4 Schematic depiction of selectivities of the *D-A* reaction. Reprinted with permission from ©Elsevier Inc.[2]

3.1.2 Proline catalysis

Proline is a non-essential proteinogenic amino acid; both enantiomers (Figure 3.1.5) are readily available and inexpensive.[8,9]

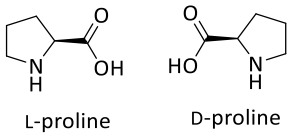

Figure 3.1.5 L- und D-proline.

Among the proteinogenic amino acids, proline is an exception by containing a secondary amine moiety instead of a primary amine moiety.[8,9] This results in a higher pK_a value and higher nucleophilicity for proline than the other proteinogenic amino acids[8,9] and enables proline to react faster with carbonyl compounds[10].

One of the first proline catalyzed reactions was the *Hajos-Parrish-Eder-Sauer-Wiechert*-reaction (Figure 3.1.6), which was discovered by two independent research groups in the 1970s.[11,12]

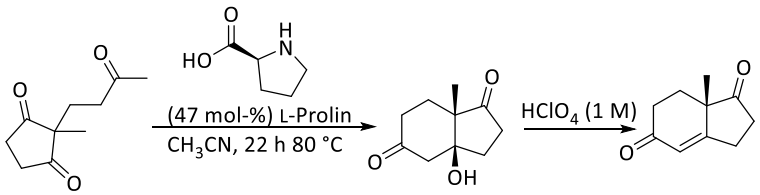

Figure 3.1.6 *Hajos-Parrish-Eder-Sauer-Wiechert*-reaction[11,12]: an L-proline catalyzed intramolecular *Robinson annulation* to the *Wieland-Miescher* ketone, which is a useful building block in steroid synthesis.

However, it took till the turn of the millennia for the groundbreaking publication from *List* et al.[13] to spike the communities' interest in proline catalysis. They published an asymmetric aldol reaction catalyzed by L-proline and proposed an enamine mechanism for the reaction.[13]

3.1.2.1 Enamine catalysis

Enamine catalysis has been a prominent topic of interest in the scientific community since the publication from *List* et al.[13]. Various reactions utilizing enamine catalysis have been published ranging from reaction types like aldol[14,15,16], Diels-Alder[15–17], Mannich[15,18], Michael[15,16,19], domino, one-pot and tandem reactions[20]. However, the mechanism is still an ongoing discussion in the scientific community, especially the role of the different isomers possible (iminium ion, enamine, and oxazolidinone (Figure 3.1.7)), when proline reacts with a carbonyl compound.

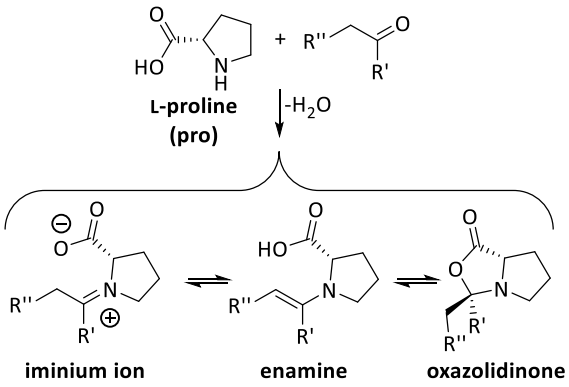

Figure 3.1.7 L-proline condensation with carbonyl compound and three possible isomers: iminium ion, enamine and oxazolidinone.

However, general agreement has been reached, that the key intermediate structure is the enamine or its deprotonated carboxylate form.[13,21,22–28] Although, the role of the oxazolidinone structure in the mechanism is still under discussion. [22–27,29,30]

For L-proline catalyzed *Diels-Alder* reactions (see chapter 3.1.1), the key reactive intermediate must be the enamine form, as the double bond moiety is a prerequisite for the reaction[2]. As the amine moiety is an electron-donating group (EDG), the enamine is an electron rich dienophile, thus being a useful reaction partner in a *Diels-Alder* reaction with *inverse electron demand* (Figure 3.1.8).[7]

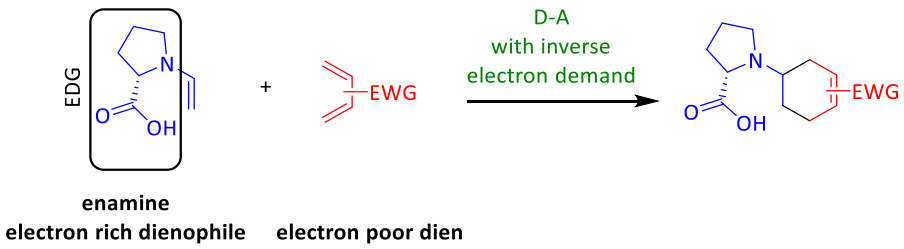

Figure 3.1.8 *Diels-Alder* reaction with *invers electron demand* with an enamine as electron rich dienophile and an electron poor diene, with electron withdrawing group (EWG).

Figure 3.1.9 shows the frontier molecular orbital model of the reaction in which the HOMO of the enamine is raised in comparison to the carbonyl compound. Thus, the HOMO LUMO gap between the diene and dienophile (enamine) is shortened, facilitating the reaction.

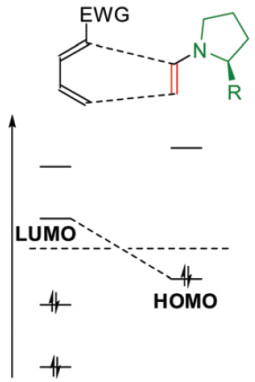

Figure 3.1.9 Frontier molecular orbital model for an enamine and an electron poor diene in a *D-A* reaction with *inverse electron demand*. Adapted with permission from the *Royal Chemical Society*[7].

3.1.2.2 Dienamine catalysis

When L-proline is mixed with a carbonyl compound, which is unsaturated at the α,β position, analogous to the enamine formation, a dienamine is formed by the shift of the initial double bond (Figure 3.1.10).

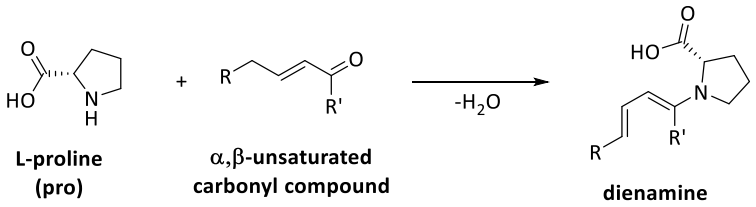

Figure 3.1.10 Dienamine formation from α,β-unsaturated carbonyl compound and L-proline.

Dienamine catalysis has been utilized in numerous ways, in different Michael-Additions[31,32], vinylogous aldol reactions [33,34] and various cycloadditions: [2+2] [7,35], [3+2] [7,36] and [4+2] [7,37,38,39] (Figure 3.1.11).

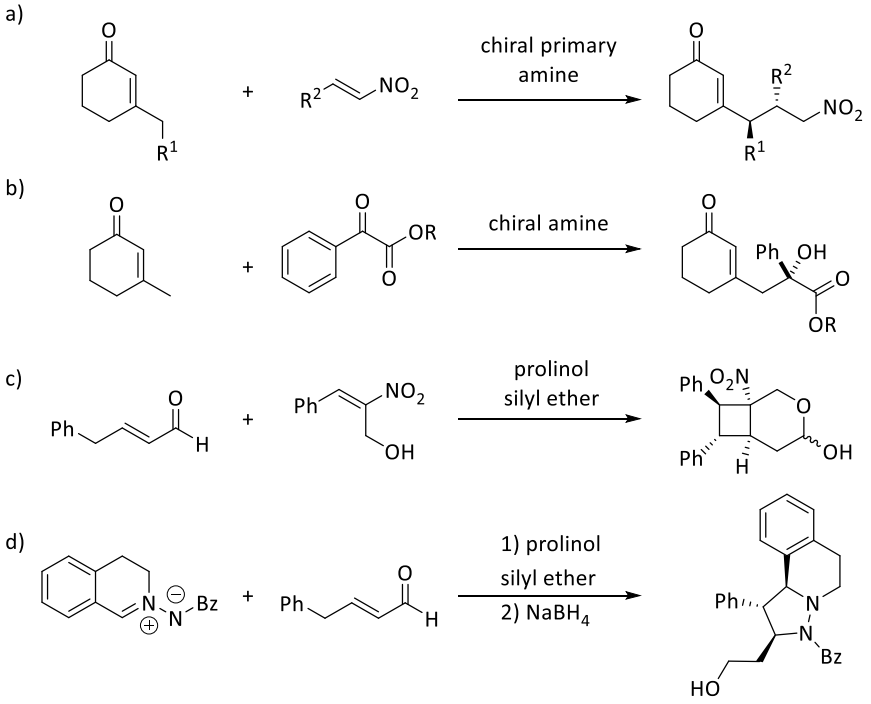

Figure 3.1.11 Dienamine catalysis in a a) direct vinylogous Michael addition by *Bencivenni* et al.[32] b) direct vinylogous aldolization by *Bastida* et al.[33] c) one-step synthesis of cyclobutanes via [2+2] cycloaddition by *Talavera* et al.[35] d) [3+2] cycloaddition by *Li* et al.[36].

A [4+2] cycloaddition then is a *Diels-Alder* reaction with *normal electron demand*, where the dienamine reacts as electron rich diene with an electron poor dienophile (Figure 3.1.12).[7]

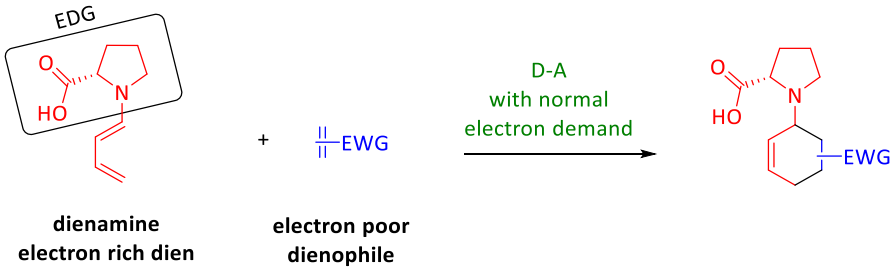

Figure 3.1.12 *Diels-Alder* reaction with *normal electron demand* with a dienamine as electron rich diene and an electron poor dienophile.

Figure 3.1.13 shows the frontier molecular orbital model for the reaction in which the HOMO of the dienamine is raised in comparison to the α,β-unsaturated carbonyl compound. Thus, the HOMO LUMO gap between the diene (dienamine) and dienophile is shortened, facilitating the reaction.

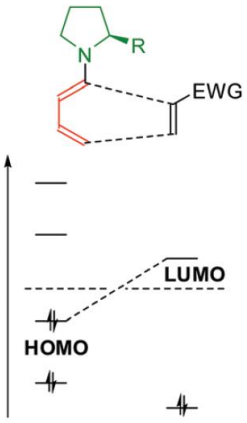

Figure 3.1.13 Frontier molecular orbital model for a dienamine and an electron poor dienophile in a *D-A* reaction with *normal electron demand*. Adapted with permission from the *Royal Chemical Society*[7].

Extensive research has been done on the stereochemistry and enantioselectivity of dienamines by *Gschwind* and coworkers[40,41] and *Jørgensen* and coworkers.[38,39]

For example, *Gschwind* and coworkers[40,41] encountered the so-called "Z/E dilemma". A dienamine can form two isomers with its second double bond, the *E*-isomer and the *Z*-isomer. The "Z/E dilemma" means that the ratio of the two isomers does not correlate to the *ee* (enantiomeric excess) in a γ-functionalization, based on the model of shielding (Figure 3.1.14). However, with NMR and theoretical studies they found three aspects that influence and explain the *ee*: the *Z*-dienamine is kinetically, and the *E*-dienamine thermodynamically preferred. [40,41] Further, the *Z*-dienamine has a lower activation barrier for an electrophilic attack.[40,41]

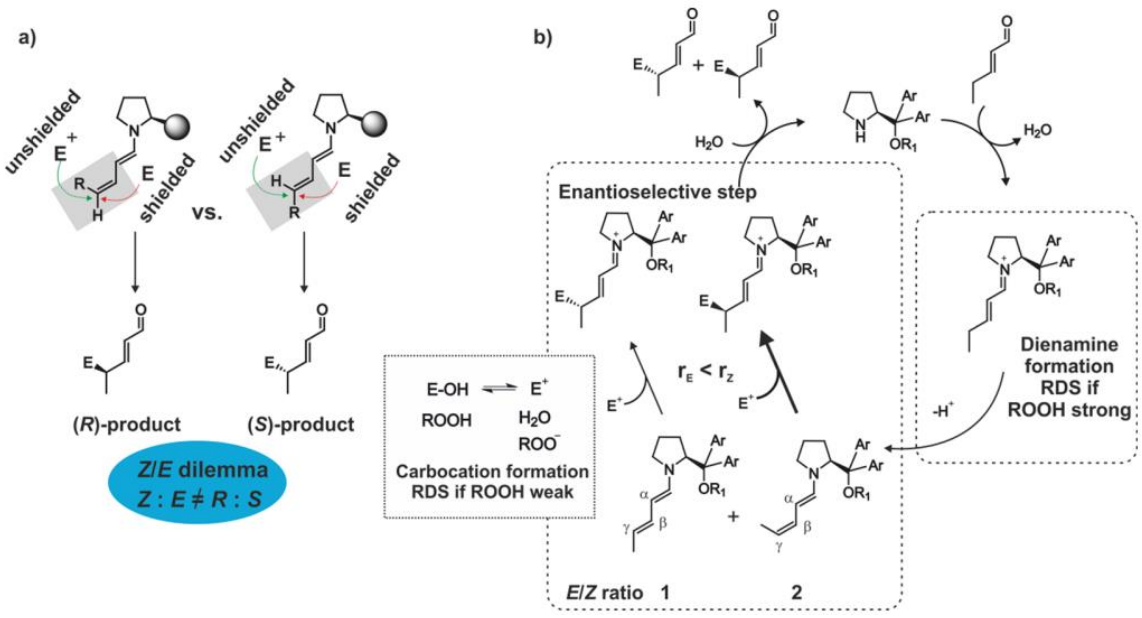

Figure 3.1.14 a) "Z/E dilemma" ratio of Z:E does not correlate to ratio of R:S product, b) catalytic cycle for γ-functionalization with electrophilic attack. Reprinted with permission from ACS (https://pubs.acs.org/doi/10.1021/acs.accounts.7b00320).[41]

3.1.3 The charge-tagged proline derived catalyst

In our research group, a charge-tagged L-proline derived catalyst has been synthesized[27] and successfully applied to the study of aldol reactions[27,30].

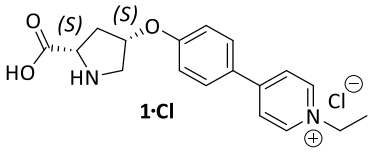

Figure 3.1.15 Proline derived charge-tagged catalyst **1·Cl**.[27]

The advantages of charge-tagging in reaction mechanism studies with ESI MS have already been discussed in chapter 2.2.1. In this charge-tagged catalyst (**1·Cl**) a pyridinium moiety is bound to the proline structure via a phenyl linker. The phenyl linker is included to place the charged pyridinium moiety at a distance to the catalytic active center, which is the proline structure's nitrogen. Through the linkers rigidity it cannot fold back, so the charge is held in place. This reduces the impact of the charge-tag on the chemical environment of the catalytic active center.

The charge-tag not only enhances the ESI response[28,42] for intermediates, but also facilitates the analysis of intermediates with unperturbed catalytic active centers. Untagged intermediates are often detected as their $[M+H]^+$ ions, and usually the nitrogen of the proline is the most basic position of the intermediate. Thus, the proton is likely added in the middle of the catalytic active center, which is highly undesirable as it changes chemical properties and reactivity. But when utilizing the charge-tagged catalyst (**1·Cl**), the addition of a proton to the intermediates is not necessary, as they are already charged.

3.1.4 References

[1] a) O. Diels, K. Alder, *Ann.* **1926**, *450*, 237; b) O. Diels, K. Alder, *Ann.* **1928**, *460*, 98; c) O. Diels, K. Alder, *Ber. dtsch. Chem. Ges.* **1929**, *62*, 2081; d) O. Diels, K. Alder, *Ber. dtsch. Chem. Ges.* **1929**, *62*, 2087.

[2] Kürti L., Czakó B., *Strategic Applications of Named Reactions in Organic Synthesis*, Elsevier Academic Press, Burlington, San Diego, London, **2004**.

[3] R. Brückner, M. Harmata, *Organic Mechanisms*, Springer Berlin Heidelberg, Berlin, Heidelberg, **2010**.

[4] J. Clayden, N. Greeves, S. G. Warren, *Organic chemistry*, Oxford University Press, Oxford, New York, **2012**.

[5] L. F. Tietze, G. Kettschau, *Hetero Diels-Alder reactions in organic chemistry, Stereoselective heterocyclic synthesis I*, Springer, Berlin, Heidelberg, **1997**.

[6] H. Kwart, K. King, *Chem. Rev.* **1968**, *68*, 415.

[7] L. Klier, F. Tur, P. H. Poulsen, K. A. Jørgensen, *Chem. Soc. Rev.* **2017**, *46*, 1080.

[8] P. I. Dalko, L. Moisan, *Angew. Chem. Int. Ed.* **2004**, *43*, 5138.

[9] P. I. Dalko, L. Moisan, *Angew. Chem. Int. Ed.* **2001**, *40*, 3726.

[10] P. W. Hickmott, *Tetrahedron* **1982**, *38*, 1975.

[11] Z. G. Hajos, D. R. Parrish, *J. Org. Chem.* **1974**, *39*, 1615.

[12] U. Eder, G. Sauer, R. Wiechert, *Angew. Chem. Int. Ed.* **1971**, *10*, 496.

[13] B. List, R. A. Lerner, C. F. Barbas, *J. Am. Chem. Soc.* **2000**, *122*, 2395.

[14] a) G. Guillena, C. Nájera, D. J. Ramón, *Tetrahedron Asymmetry* **2007**, *18*, 2249; b) V. Bisai, A. Bisai, V. K. Singh, *Tetrahedron* **2012**, *68*, 4541.

[15] W. Notz, F. Tanaka, C. F. Barbas, *Acc. Chem. Res.* **2004**, *37*, 580.

[16] S. Mukherjee, J. W. Yang, S. Hoffmann, B. List, *Chem. Rev.* **2007**, *107*, 5471.

[17] H. Xie, L. Zu, H. R. Oueis, H. Li, J. Wang, W. Wang, *Org. Lett.* **2008**, *10*, 1923.

[18] a) J. M. M. Verkade, L. J. C. van Hemert, P. J. L. M. Quaedflieg, F. P. J. T. Rutjes, *Chem. Soc. Rev.* **2008**, *37*, 29; b) B. List, *J. Am. Chem. Soc.* **2000**, *122*, 9336.

[19] a) J. Vicario, D. Badía, L. Carrillo, *Synthesis* **2007**, *2007*, 2065; b) N. Mase, K. Watanabe, H. Yoda, K. Takabe, F. Tanaka, C. F. Barbas, *J. Am. Chem. Soc.* **2006**, *128*, 4966.

[20] a) D. Enders, C. Grondal, M. R. M. Hüttl, *Angew. Chem. Int. Ed.* **2007**, *46*, 1570; b) G. Guillena, D. J. Ramón, M. Yus, *Tetrahedron Asymmetry* **2007**, *18*, 693; c) A. Walji, D. MacMillan, *Synlett* **2007**, *2007*, 1477; d) H.-C. Guo, J.-A. Ma, *Angew. Chem. Int. Ed.* **2006**, *45*, 354; e) X. Yu, W. Wang, *Org. Biomol. Chem.* **2008**, *6*, 2037; f) S. Bertelsen, K. A. Jørgensen, *Chem. Soc. Rev.* **2009**, *38*, 2178.

[21] a) S. Bahmanyar, K. N. Houk, H. J. Martin, B. List, *J. Am. Chem. Soc.* **2003**, *125*, 2475; b) B. List, L. Hoang, H. J. Martin, *Proc. Natl. Acad. Sci. USA* **2004**, *101*, 5839; c) C. Allemann, R. Gordillo, F. R. Clemente, P. H.-Y. Cheong, K. N. Houk, *Acc. Chem. Res.* **2004**, *37*, 558; d) H. Iwamura, D. H. Wells, S. P. Mathew, M. Klussmann, A. Armstrong, D. G. Blackmond, *J. Am. Chem. Soc.* **2004**, *126*, 16312; e) J. E. Hein, J. Burés, Y. Lam, M. Hughes, K. N. Houk, A. Armstrong, D. G. Blackmond, *Org. Lett.* **2011**, *13*, 5644; f) J. Burés, A. Armstrong, D. G. Blackmond, *Chem. Sci.* **2012**, *3*, 1273; g) M. Orlandi, M. Ceotto, M. Benaglia, *Chem. Sci.* **2016**, *7*, 5421; h) D. Sánchez, H. Carneros, A. Castro-Alvarez, E. Llàcer, F. Planas, J. Vilarrasa, *Tetrahedron Lett.* **2016**, *57*, 5254.

[22] D. Seebach, A. K. Beck, D. M. Badine, M. Limbach, A. Eschenmoser, A. M. Treasurywala, R. Hobi, W. Prikoszovich, B. Linder, *Helv. Chim. Acta* **2007**, *90*, 425.

[23] M. B. Schmid, K. Zeitler, R. M. Gschwind, *Angew. Chem. Int. Ed.* **2010**, *49*, 4997.

[24] A. K. Sharma, R. B. Sunoj, *Angew. Chem. Int. Ed.* **2010**, *49*, 6373.

[25] D. A. Bock, C. W. Lehmann, B. List, *Proc. Natl. Acad. Sci. USA* **2010**, *107*, 20636.

[26] T. Kanzian, S. Lakhdar, H. Mayr, *Angew. Chem. Int. Ed.* **2010**, *49*, 9526.

[27] J. A. Willms, R. Beel, M. L. Schmidt, C. Mundt, M. Engeser, *Beilstein J. Org. Chem.* **2014**, *10*, 2027.

[28] A. Schnell, J. A. Willms, S. Nozinovic, M. Engeser, *Beilstein J. Org. Chem.* **2019**, *15*, 30.

[29] a) M. H. Haindl, J. Hioe, R. M. Gschwind, *J. Am. Chem. Soc.* **2015**, *137*, 12835; b) M. A. Ashley, J. S. Hirschi, J. A. Izzo, M. J. Vetticatt, *J. Am. Chem. Soc.* **2016**, *138*, 1756; c) D. G. Blackmond, A. Moran, M. Hughes, A. Armstrong, *J. Am. Chem. Soc.* **2010**, *132*, 7598; d) N. Zotova, A. Franzke, A. Armstrong, D. G. Blackmond, *J. Am. Chem. Soc.* **2007**, *129*, 15100.

[30] J. A. Willms, J. Vidic, J. Barthelmes, V. Steinmetz, T. Bredow, P. Maître, M. Engeser, *Phys. Chem. Chem. Phys.* **2018**.

[31] a) B. Han, Y.-C. Xiao, Z.-Q. He, Y.-C. Chen, *Org. Lett.* **2009**, *11*, 4660; b) G. Zhan, Q. He, X. Yuan, Y.-C. Chen, *Org. Lett.* **2014**, *16*, 6000; c) V. Marcos, J. Alemán, *Chem. Soc. Rev.* **2016**, *45*, 6812.

[32] G. Bencivenni, P. Galzerano, A. Mazzanti, G. Bartoli, P. Melchiorre, *Proc. Natl. Acad. Sci. USA* **2010**, *107*, 20642.

[33] D. Bastida, Y. Liu, X. Tian, E. Escudero-Adán, P. Melchiorre, *Org. Lett.* **2013**, *15*, 220.

[34] C. Cassani, P. Melchiorre, *Organic letters* **2012**, *14*, 5590.

[35] G. Talavera, E. Reyes, J. L. Vicario, L. Carrillo, *Angew. Chem. Int. Ed.* **2012**, *51*, 4104.

[36] W. Li, J. Wei, Q. Jia, Z. Du, K. Zhang, J. Wang, *Chem. Eur. J.* **2014**, *20*, 6592.

[37] a) J. Peña, R. F. Moro, I. S. Marcos, F. Sanz, D. Díez, *Tetrahedron* **2014**, *70*, 4386; b) B.-C. Hong, M.-F. Wu, H.-C. Tseng, G.-F. Huang, C.-F. Su, J.-H. Liao, *J. Org. Chem.* **2007**, *72*, 8459; c) S. Bertelsen, M. Marigo, S. Brandes, P. Dinér, K. A. Jørgensen, *J. Am. Chem. Soc.* **2006**, *128*, 12973.

[38] T. K. Johansen, C. Villegas Gómez, J. R. Bak, R. L. Davis, K. A. Jørgensen, *Chem. Eur. J.* **2013**, *19*, 16518.

[39] Ł. Albrecht, G. Dickmeiss, F. Cruz Acosta, C. Rodríguez-Escrich, R. L. Davis, K. A. Jørgensen, *J. Am. Chem. Soc.* **2012**, *134*, 2543.

[40] A. Seegerer, J. Hioe, M. M. Hammer, F. Morana, P. J. W. Fuchs, R. M. Gschwind, *J. Am. Chem. Soc.* **2016**, *138*, 9864.

[41] P. Renzi, J. Hioe, R. M. Gschwind, *Acc. Chem. Res.* **2017**, *50*, 2936.

[42] a) D. Schröder, *Acc. Chem. Res.* **2012**, *45*, 1521; b) C. Adlhart, P. Chen, *Helv. Chim. Acta* **2000**, *83*, 2192; c) C. Iacobucci, S. Reale, F. de Angelis, *Angew. Chem. Int. Ed.* **2016**, *55*, 2980.

3.2 Mechanistic studies of L-proline-catalyzed Diels-Alder reaction of α,β-unsaturated aldehydes

3.2.1 The reaction

In 2015 *Griesbeck* et al. [1] published the L-proline catalyzed reaction of *trans*-2-hexenal **2** to a cyclohexadienal **3** in methanol (Figure 3.2.1).

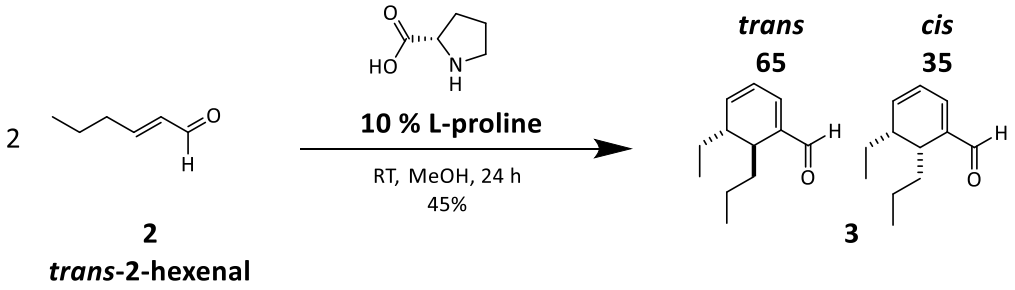

Figure 3.2.1 L-proline catalyzed reaction of *trans*-2-hexenal **2** published by *Griesbeck* et al.[1].

They postulated a catalytic cycle depicted in Figure 3.2.2.[1] The first step is the condensation of L-proline with the *trans*-2-hexenal **2** to form the first intermediate **I** the dienamine.[1] The first intermediate **I** then undergoes a [4+2]-cycloaddition with another *trans*-2-hexenal **2** forming the second intermediate **II**.[1] In the last step, the second intermediate **II** eliminates L-proline and forms product **3**.[1]

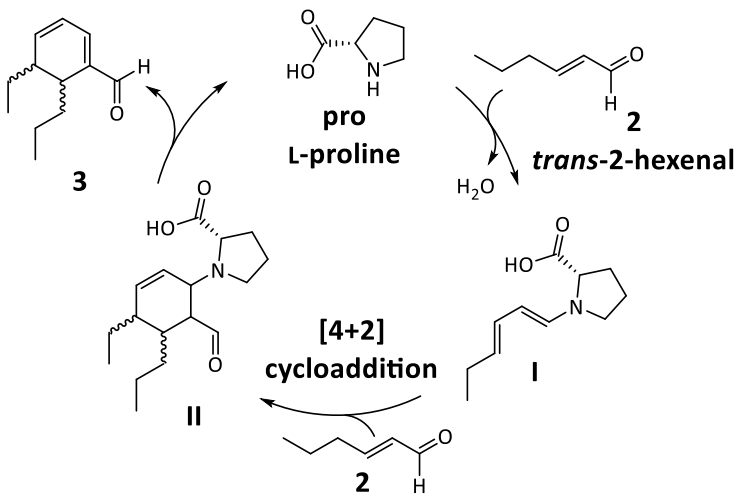

Figure 3.2.2 Catalytic cycle postulated by *Griesbeck* et al.[1].

However, *Bench* et al.[2] postulated a different mechanism (Figure 3.2.3) for a related reaction of retinal and citral; they used L-proline too but with 1.5 eq. as a chiral auxiliary. They stated that two catalyst molecules are necessary for the reaction because the iminium ion **4** and the dienamine **5** form the ring (Figure 3.2.3).[2] Further, they postulated that the ring formation can proceed either in a *Diels-Alder* reaction or an imine addition.[2] They concluded the imine addition mechanism is likely.[2] In ^{1}H-NMR experiments, and ESI MS experiments they detected the iminium ion **4** and the intermediate **8**[2], but

not the equivalent to the second intermediate **II** from the *Griesbeck*[1] mechanism. However, in ESI MS experiments the iminium ion **4** and the dienamine **5** cannot be told apart as they are isomeric structures. *Hong* et al.[3] too concluded that the reaction proceeds via an addition rather than a *Diels-Alder* reaction, albeit they postulated a mechanism where either one or two catalyst molecules participate.

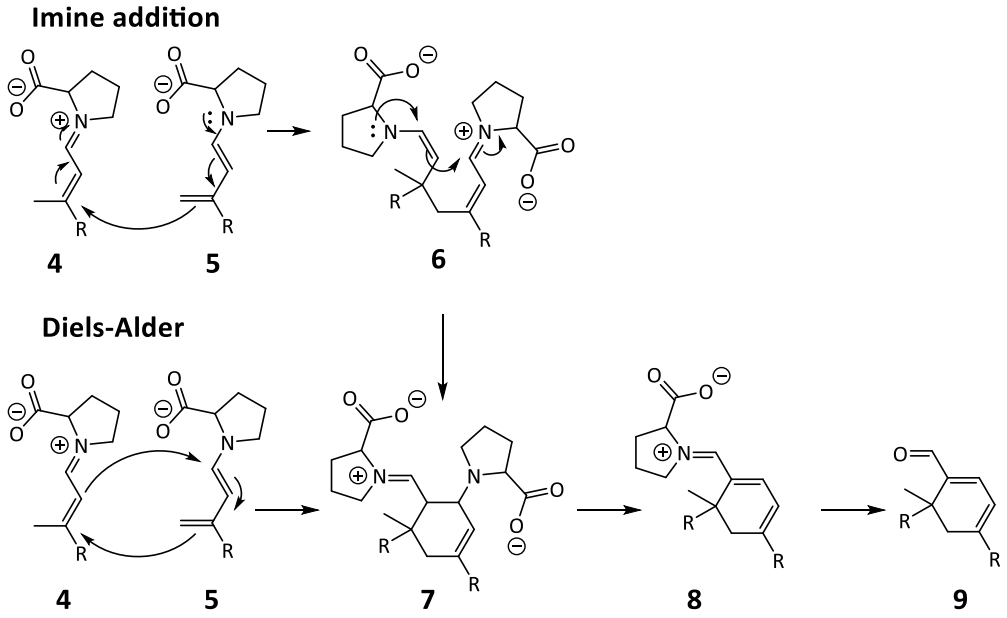

Figure 3.2.3 Mechanism postulated by *Bench* et al. [2] for the reaction with retinal and citral.

Jørgensen and coworkers[4] examined the reaction of *trans*-2-pentenal **10** with the TMS-protected diarylprolinol-catalyst **11** and diethyl azodicarboxylate (DEAD) (Figure 3.2.4). When studying the catalyst and *trans*-2-pentenal **10** with ^{1}H-NMR, they only observed the dienamine **14** and not the iminium species **13** (Figure 3.2.4). This is in accordance with the findings of *Lagiewka* and *Albrecht*.[5] *Jørgensen* and coworkers[4] conducted computational studies for the reaction of the dienamine **14** with DEAD and concluded that the ring formation occurs through a [4+2]-cycloaddition and not an addition.

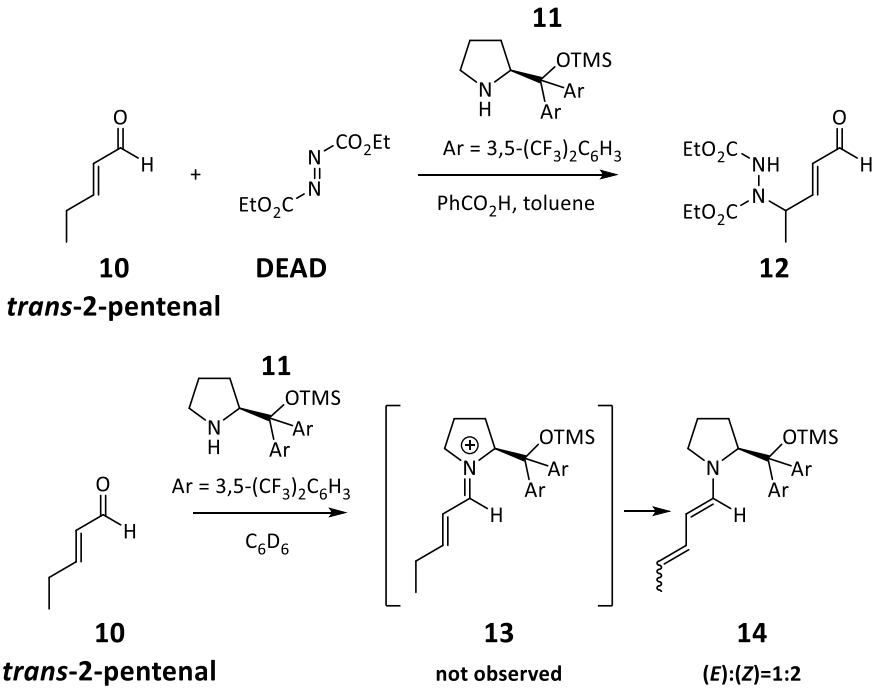

Figure 3.2.4 *Jørgensen's*[4] reaction of *trans*-2-pentenal **10** with the TMS-protected diarylprolinol-catalyst **11** and diethyl azodicarboxylate (DEAD).

Figueiredo et al. [6] studied intramolecular reactions of α,β-unsaturated aldehydes. They conclude that for α,β-unsaturated aldehydes, the reaction occurs through a [4+2]-cycloaddition, but when an α,β-unsaturated ketone is part of the reaction, it occurs through an addition.

I was intrigued by the different postulated mechanisms; thus I set out to explored the L-proline catalyzed reaction published by *Griesbeck* et al.[1].

3.2.2 Results

I performed my studies with *trans*-2-hexenal **2** as published by *Griesbeck* et al.[1] but also with the homologous *trans*-2-pentenal **10** as substrate. First, I will present the results of the experiments with *trans*-2-hexenal **2** followed by the results of *trans*-2-pentenal **10**.

3.2.2.1 Experiments with trans-2-hexenal

For the reaction, L-proline and *trans*-2-hexenal **2** are mixed in methanol. By taking samples out of the reaction solution and directly analyzing them with ESI MS, I could look into the ongoing reaction. Figure 3.2.5 shows spectra after four hours reaction time: a) ESI MS spectrum recorded on the Orbitrap XL, b) ESI MS spectrum recorded on the micrOTOF-Q and c) an APCI spectrum recorded on the micrOTOF-Q (APCI: atmospheric pressure chemical ionization). I detected the first intermediate **I** (*m/z* 196, 218, 152) and second intermediate **II** (*m/z* 294) from the catalytic cycle postulated by *Griesbeck* et al.[1]. Only in the APCI spectrum Figure 3.2.5c) it was possible to detect product **3** (*m/z* 179, 211), as it has a low ESI response. In the ionization process fragmentation can already occur leading to signals after the loss of CO_2 or H_2CO_2 like *m/z* 152, 232, 250, 262, 280 and 303.

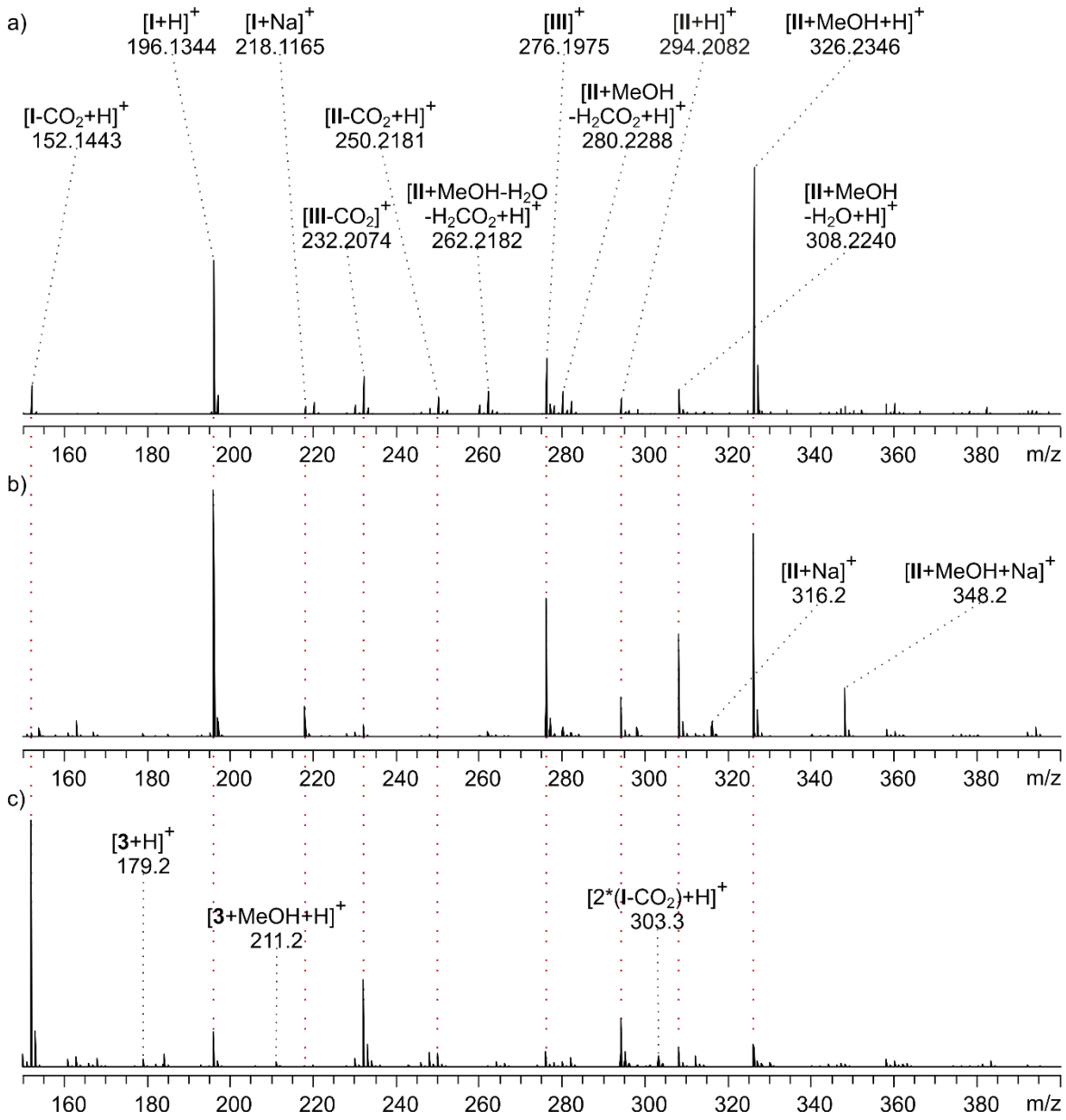

Figure 3.2.5 Spectra after four hours reaction time recorded with a) ESI(+) Orbitrap XL, b) ESI (+) micrOTOF-Q, c) APCI(+) micrOTOF-Q.

Additionally, I detected several other species, which cannot be explained by the catalytic cycle published by *Griesbeck* et al. [1] (Figure 3.2.2). The signal *m/z* 326 fits the acetal [**II**+MeOH+H]$^+$ formed through the reaction of methanol with the aldehyde moiety of the second intermediate (Figure 3.2.6).

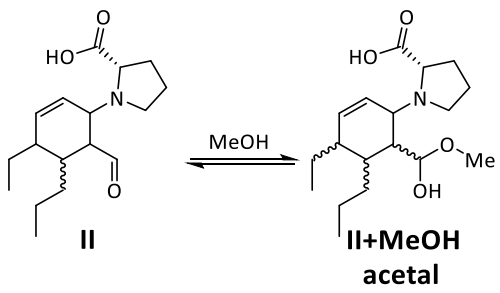

Figure 3.2.6 Methanol acetal of the second intermediate.

Through an MS^2 experiment of *m/z* 326 the structure was confirmed (Figure 3.2.7). I observed the loss of H_2O and MeOH at a collision energy of 20 eV. Another explanation for *m/z* 326 would be a solvent adduct of the second intermediate, but then the loss of H_2O could not occur, and the loss of MeOH would occur at much lower collision energies. Thus, I assigned *m/z* 326 to the methanol acetal of the second intermediate [**II**+MeOH+H]$^+$. It could be only a resting state of the second intermediate, however the formation of [**3**+MeOH+H]$^+$ through the loss of proline indicates a possible additional pathway towards the acetal of the product (Figure 3.2.10).

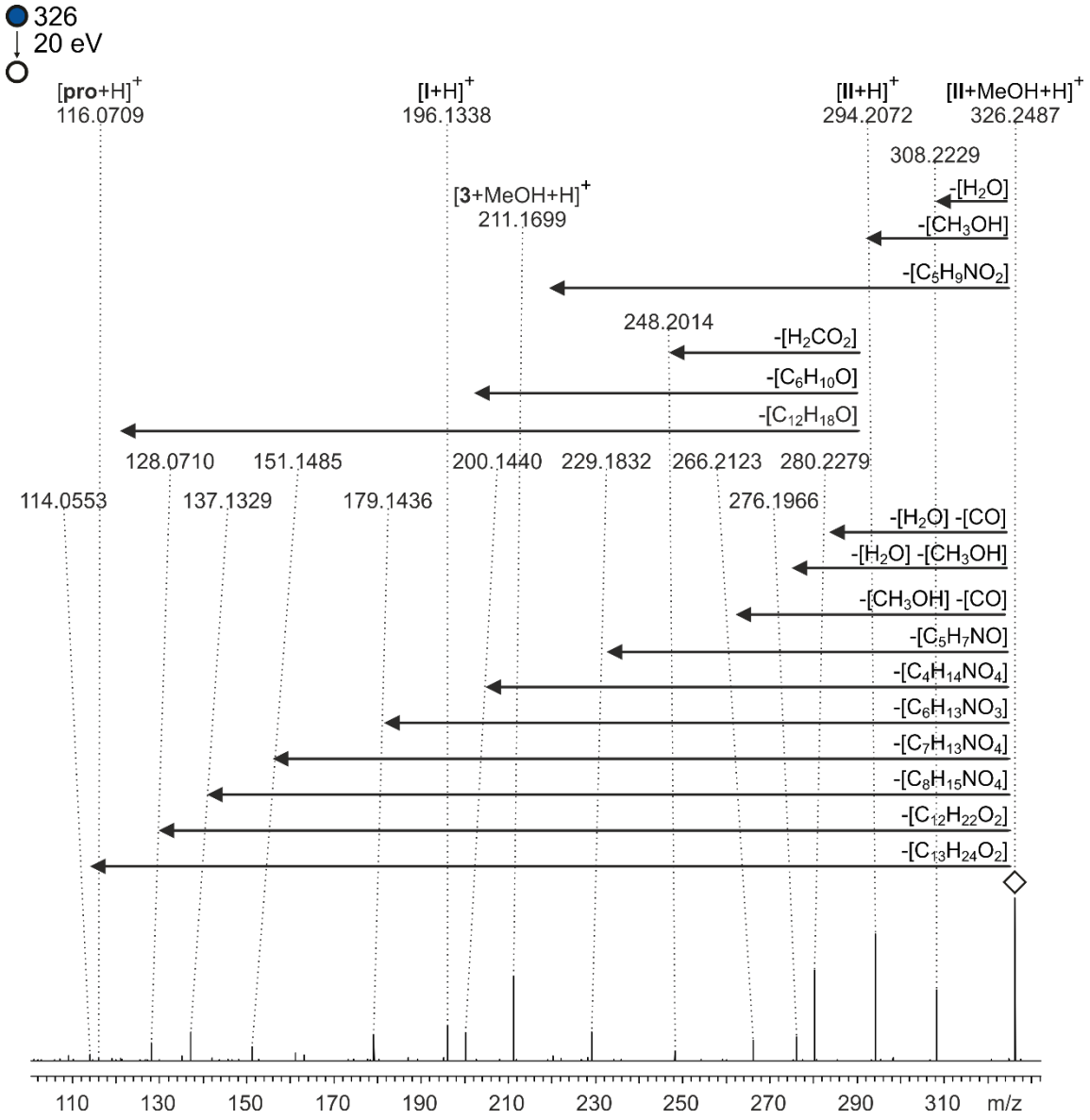

Figure 3.2.7 Orbitrap XL spectrum ESI(+) MS^2 of [II+MeOH+H]$^+$ *m/z* 326 20 eV.

The APCI spectrum shows the product [**3**+H]$^+$ *m/z* 179 and the product with methanol [**3**+MeOH+H]$^+$ *m/z* 211, which indicates the acetal of the product which can be added to the catalytic cycle.

In the spectra shown in Figure 3.2.5, I also saw species **III** (*m/z* 276, 232) (Figure 3.2.8), which fits to the intermediate **8** postulated by *Bench* et al.[2] (Figure 3.2.3).

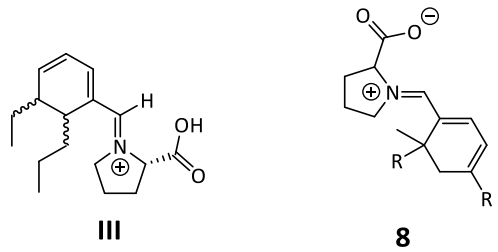

Figure 3.2.8 Species **III** and intermediate **8** postulated by *Bench* et al.[2]

Through the MS^2 experiment of $[\mathbf{III}]^+$ *m/z* 276 (Figure 3.2.9a)) and the MS^3 experiment of the fragment $[\mathbf{III}\text{-}CO_2]^+$ *m/z* 232 (Figure 3.2.9b)) I could confirm the structure of species **III**.

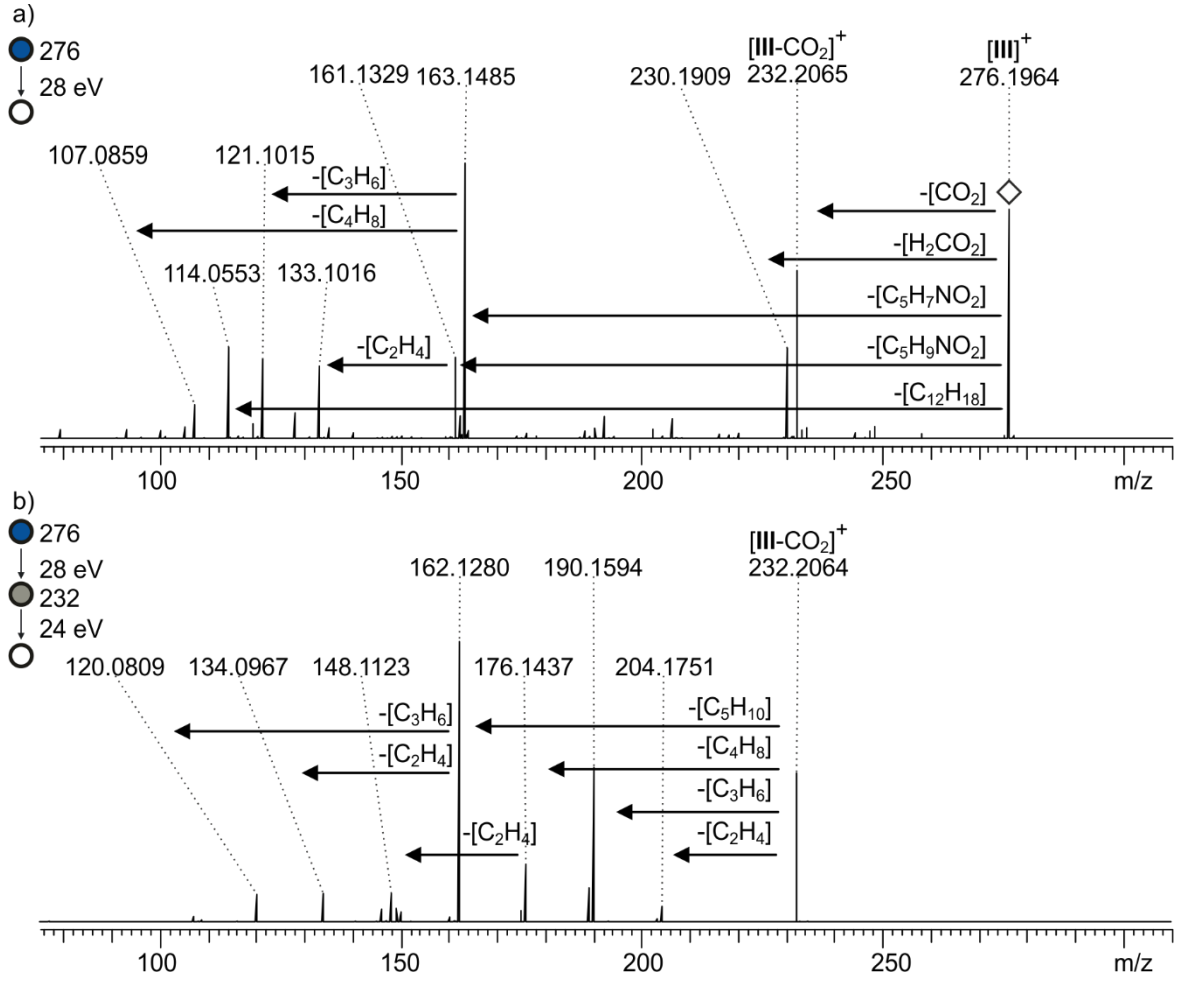

Figure 3.2.9 Orbitrap XL spectra ESI(+) a) MS^2 of $[\mathbf{III}]^+$ *m/z* 276 28 eV, b) $MS^3$of $[\mathbf{III}]^+$ *m/z* 276 28 eV, $[\mathbf{III}\text{-}CO_2]^+$ 232 *m/z* 24 eV.

Bench et al.[2] did not detect the second intermediate **II**, which I observed. With the second intermediate **II** in evidence species **III** only fits into the catalytic cycle as an off-cycle species formed by the condensation of L-proline and the product **3** (Figure 3.2.10). Thus, I add three additional species, the acetal **II**+MeOH, **III**, and the acetal of the product **3**+MeOH to a revised catalytic cycle (Figure 3.2.10).

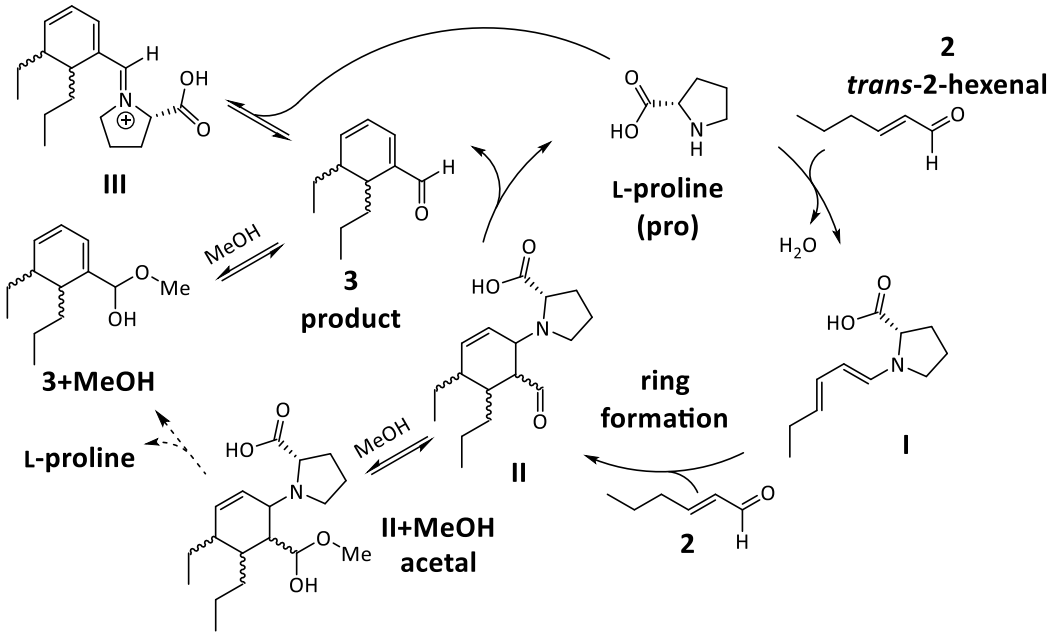

Figure 3.2.10 Revised catalytic cycle of the L-proline catalyzed reaction of *trans*-2-hexenal **2**.

Bench et al.[2] postulated that two catalyst molecules are needed for the ring formation via intermediate **7** (Figure 3.2.3), which they did not detect with ^{1}H-NMR or ESI MS. In the reaction with *trans*-2-hexenal **2** intermediate **7** is equivalent to **IV** (Figure 3.2.11), which I did not detect ([**IV**+H]$^{+}$ *m/z* 391, see Figure 3.2.5).

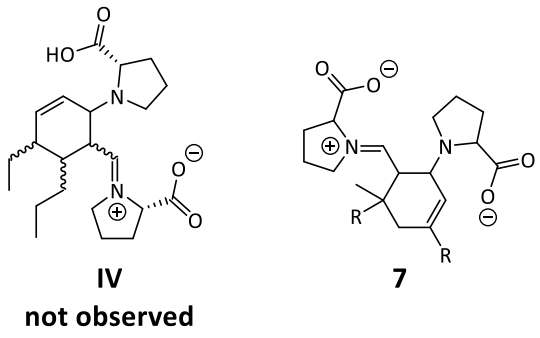

Figure 3.2.11 Not observed species **IV** which is the analog to Bench's[2] intermediate **7**.

As I did not observe **IV**, but did observe **II** I conclude, that the ring formation does not include two catalyst molecules as *Bench* et al.[2] claim, but only one. Namely, the ring formation proceeds between **I** with one catalyst molecule included and **2**. I cannot give further insight into the ring formation step, whether it proceeds via an addition or a [4+2] cycloaddition in a *Diels-Alder* reaction. However, computational studies by *Jørgensen* and coworkers[4] favor a cycloaddition rather than an addition for the reaction of DEAD with their dienamine **14** (Figure 3.2.4), which might implicate a cycloaddition here too. Further, electronically **2** fits well to an electron poor dienophile while **I** is an electron rich diene, which are the two components needed for a [4+2]-cycloaddition in a *Diels-Alder* reaction with *normal electron-demand*.

To take a closer look at the intermediates, I performed MS^n experiments. Figure 3.2.12 shows the MS^2 experiment of the second intermediate [**II**+H]$^+$ (*m/z* 294), which exhibits a riveting behavior. It is induced to go one step forward in the catalytic cycle to the catalyst proline ([**pro**+H]$^+$ *m/z* 116) and one step backward to the first intermediate ([**I**+H]$^+$ *m/z* 196). Thereby, I was able to mimic the catalytic steps in the gas phase providing evidence for the catalytic cycle (Figure 3.2.10). However only the protonated intermediates can be observed here, neutral species might not exhibit the same behavior.

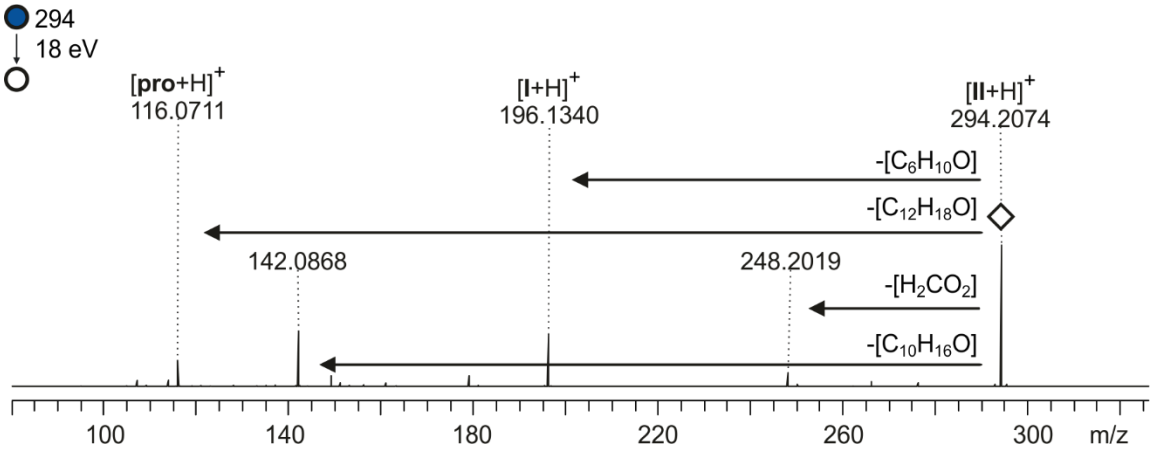

Figure 3.2.12 Orbitrap XL spectrum ESI(+) MS^2 of [**II**+H]$^+$ *m/z* 294 18 eV.

Now I can compare the MS^3 experiment of the first intermediate [**I**+H]$^+$ generated from the second intermediate [**II**+H]$^+$ with the MS^2 experiment of the first intermediate [**I**+H]$^+$ (Figure 3.2.13). Both exhibit the same fragmentation pathways, showing that the second intermediate **II** indeed forms the first intermediate **I**, when induced to go backward in the catalytic cycle and not an isomer of the first intermediate.

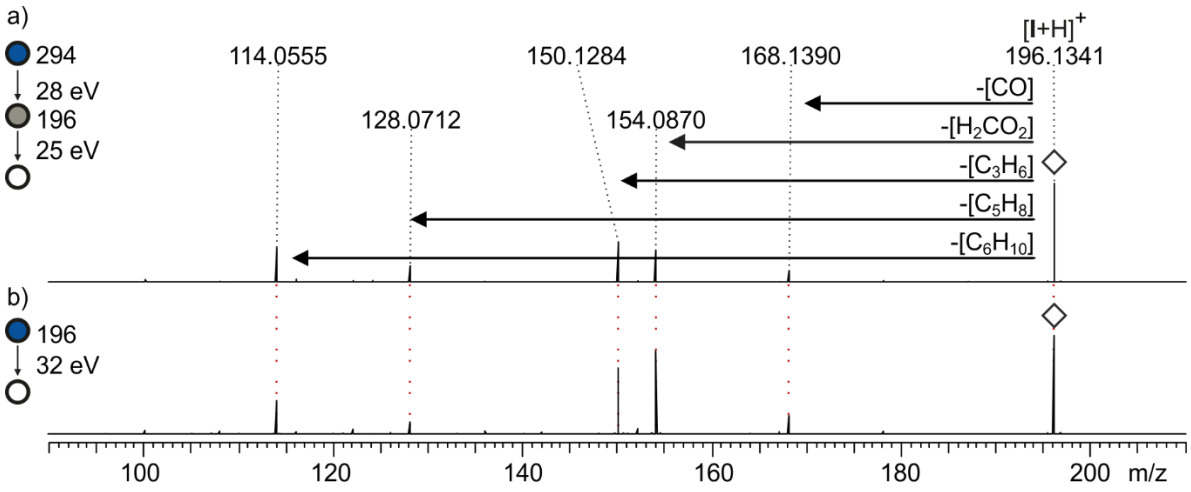

Figure 3.2.13 Orbitrap XL spectra ESI(+) a) MS^3 of [**II**+H]$^+$ *m/z* 294 28 eV, [**I**+H]$^+$ *m/z* 196 25 eV b) MS^2 of [**I**+H]$^+$ *m/z* 196 32 eV.

In the setup so far, it was only possible for me to look at the intermediates in their protonated form. As the nitrogen of the catalytic active center is the most basic position of the intermediates **I** and **II** the ionizing proton would most likely be located there. When I conducted the reaction with the

charge-tagged proline derived catalyst **1·Cl**, the intermediates $\mathbf{I}_{ct}$ and $\mathbf{II}_{ct}$ were inherently charged (Figure 3.2.14). Thus, they did not need to be protonated during the ionization process. In the spectrum of the ongoing reaction after four hours the charge-tagged intermediates are detected as $[\mathbf{I}_{ct}]^+$ (*m/z* 393) and $[\mathbf{II}_{ct}]^+$ (*m/z* 491) (Figure 3.2.15). As the charge is located at a distance to the catalytic active center, it is unperturbed in the study of the charge-tagged intermediates.

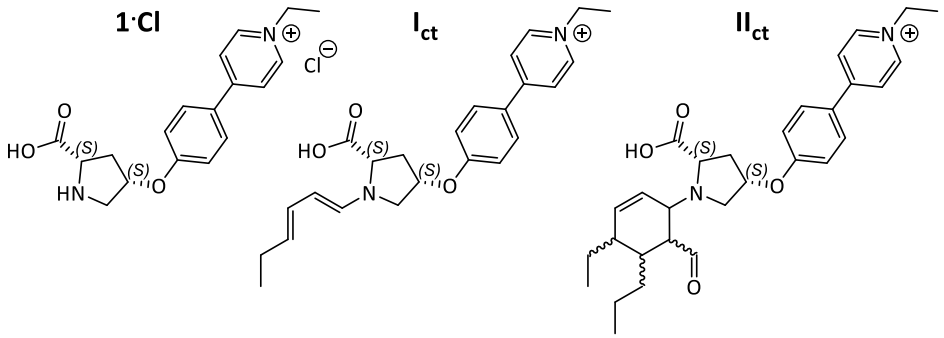

Figure 3.2.14 Charge-tagged catalyst **1·Cl** and charge-tagged intermediates $\mathbf{I}_{ct}$ and $\mathbf{II}_{ct}$.

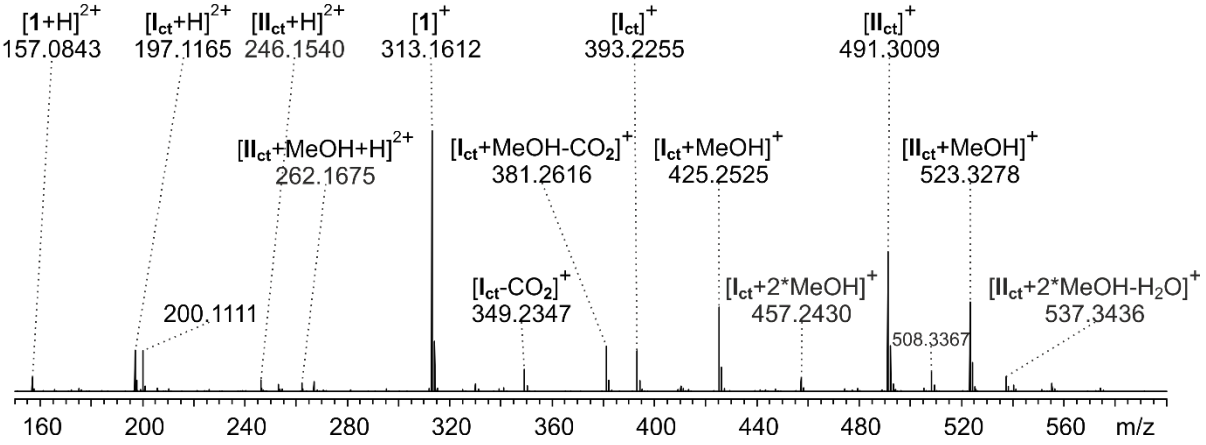

Figure 3.2.15 Orbitrap XL spectrum ESI(+) of the charge-tagged reaction of **1·Cl** and *trans*-2-hexenal **2** after 4 hours reaction time. *m/z* 200 is a known fragment of $[\mathbf{1}]^+$. The signal *m/z* 508 could not be assigned.

The intermediates are also present as doubly charged species (*m/z* 197, 246), after the loss of CO_2 (*m/z* 349, 381), and in conjunction with methanol (*m/z* 262, 381, 425, 457, 523, 537). In the experiment without the charge-tag the methanol acetal of the second intermediate was detected ($[\mathbf{II}+MeOH+H]^+$), with the charge-tag the signal for $[\mathbf{II}_{ct}+MeOH]^+$ (*m/z* 523) (Figure 3.2.16) is also present. In the MS^2 experiment of $[\mathbf{II}_{ct}+MeOH]^+$ (*m/z* 523) only the loss of methanol and not of water is observed (Figure 3.2.17). However, still 19 eV of collision energy are needed for the fragmentation, which indicates the acetal structure and not just a solvent adduct.

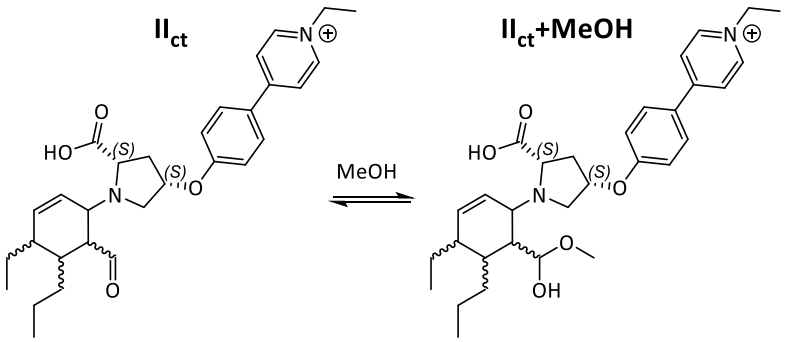

Figure 3.2.16 Charge-tagged second intermediate $\mathbf{II}_{ct}$ and methanol acetal of the charge-tagged second intermediate $\mathbf{II}_{ct}$+MeOH.

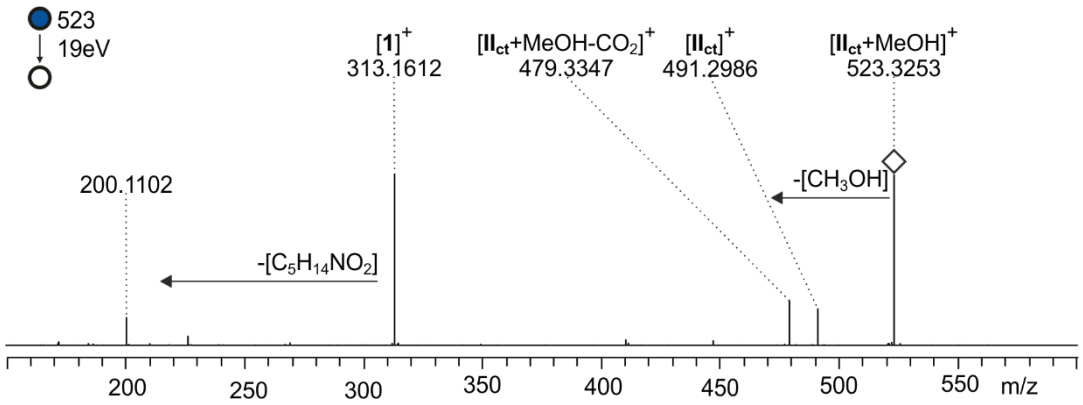

Figure 3.2.17 Orbitrap XL spectrum ESI(+) MS^2 of $[\mathbf{II}_{ct}+MeOH]^+$ *m/z* 523 19 eV.

The charge-tagged first intermediate also shows a signal for $[\mathbf{I}_{ct}+MeOH]^+$ (*m/z* 425) and a signal with two methanol molecules ($[\mathbf{I}_{ct}+2*MeOH]^+$ (*m/z* 457)), which can be interpreted as solvent adducts, as $\mathbf{I}_{ct}$ has no free aldehyde moiety for the formation of an acetal. For the second intermediate a species with two methanol molecules exists too, although with the loss of H_2O ($[\mathbf{II}_{ct}+2*MeOH-H_2O]^+$ (*m/z* 537)). This hints at the acetal structure for $\mathbf{II}_{ct}$+MeOH, which lost a water molecule and formed a solvent adduct with a further methanol.

In the MS^2 experiment of the charge-tagged second intermediate $[\mathbf{II}_{ct}]^+$ (Figure 3.2.18), I observed similar behavior as without the charge-tag. $[\mathbf{II}_{ct}]^+$ easily loses CO_2 and then forms the first intermediate without CO_2 $[\mathbf{I}_{ct}\text{-}CO_2]^+$. Additionally, $[\mathbf{II}_{ct}]^+$ forms the first intermediate $[\mathbf{I}_{ct}]^+$, although not with high intensity and $[\mathbf{II}_{ct}]^+$ forms the catalyst $[\mathbf{1}]^+$. So again, I can induce the second intermediate to mimic the steps of the catalytic cycle by going forward to the catalyst $[\mathbf{1}]^+$ and backward to the first intermediate ($[\mathbf{I}_{ct}]^+$ or $[\mathbf{I}_{ct}\text{-}CO_2]^+$). This gives further evidence to the catalytic cycle (Figure 3.2.10). In this case, no additional proton is present, thus the behavior might reflect the behavior of a neutral molecule in solution.

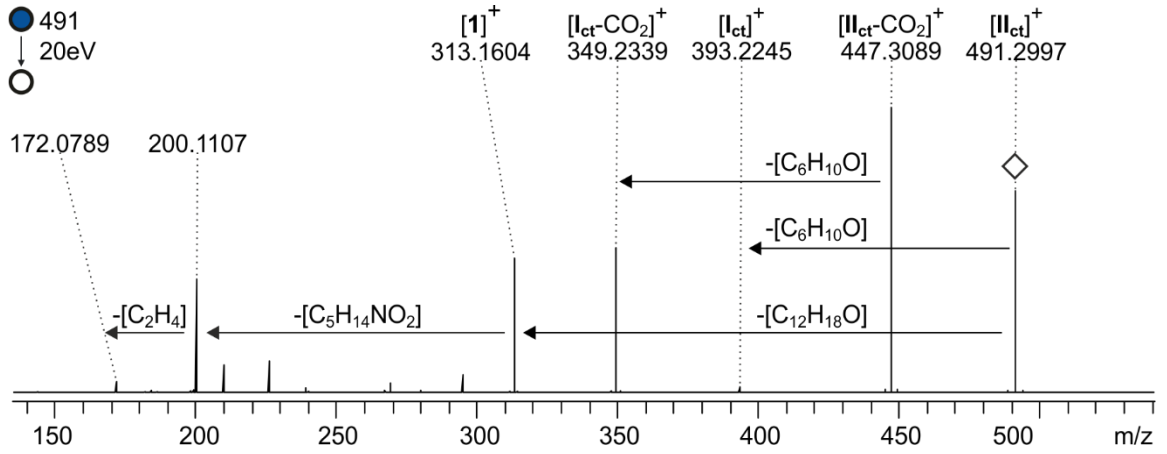

Figure 3.2.18 Orbitrap XL spectrum ESI(+) MS^2 of $[\mathbf{II_{ct}}]^+$ *m/z* 491 20 eV.

The MS^3 experiment of the second intermediate after the loss of CO_2 $[\mathbf{II_{ct}}\text{-}CO_2]^+$ (*m/z* 447) shows that $[\mathbf{II_{ct}}\text{-}CO_2]^+$ too is induced to go backwards in the catalytic cycle to form $[\mathbf{I_{ct}}\text{-}CO_2]^+$ (Figure 3.2.19).

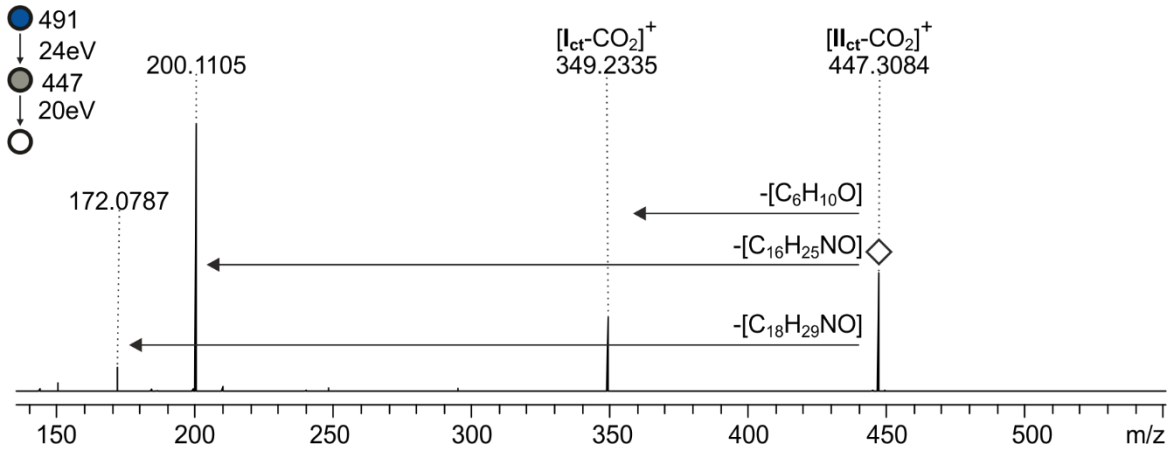

Figure 3.2.19 Orbitrap XL spectrum ESI(+) MS^3 of $[\mathbf{II_{ct}}]^+$ *m/z* 491 24 eV, $[\mathbf{II_{ct}}\text{-}CO_2]^+$ *m/z* 447 20 eV.

In the MS^2 experiment of the charge-tagged first intermediate $[\mathbf{I_{ct}}]^+$, I only observed the loss of CO_2 and the formation of the known fragment *m/z* 200 (Figure 3.2.20).

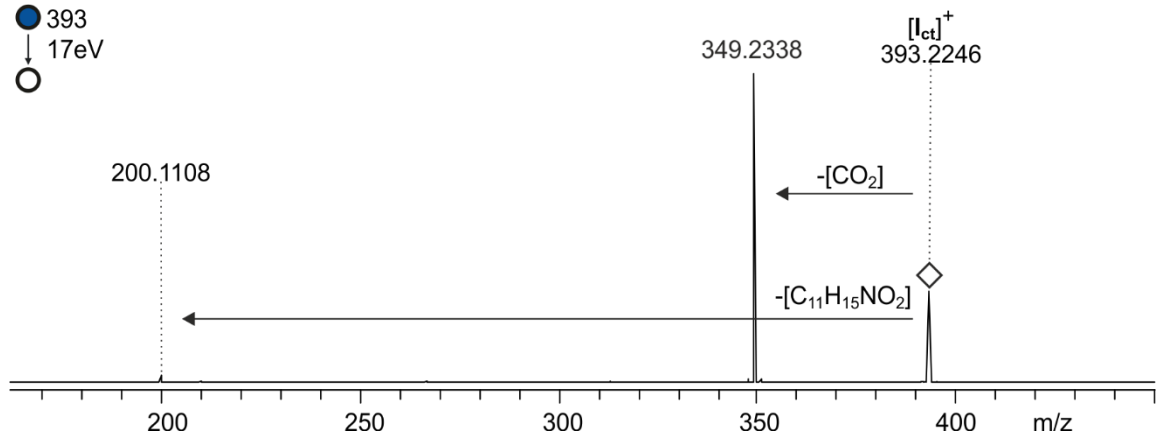

Figure 3.2.20 Orbitrap XL spectrum ESI(+) MS^2 of $[\mathbf{I_{ct}}]^+$ *m/z* 393 17 eV.

So far, I have looked at the untagged reaction only in a qualitative way, but when looking at it in a quantitative way, I can observe the reaction's temporal progress. To this end, I took samples out of the reaction mixture via an autosampler (set to 20 °C) in regular intervals and measured ESI spectra on the micrOTOF-Q. The absolute signal intensities of peaks pertaining to the same species were added and plotted against the reaction time (Figure 3.2.21). *Trans*-2-hexenal **2** is not detectable with ESI nor APCI and product **3** just with very small intensities with APCI (Figure 3.2.5 c)). Therefore, I can only plot the first intermediate **I** (*m/z* 196, 218), the second intermediate **II** (*m/z* 294), the acetal of the second intermediate **II+MeOH** (*m/z* 326), and species **III** (*m/z* 276). The first intermediate **I** starts with high intensity and slowly decays, whereas the second intermediate **II** starts at very low intensities, rises quickly in the first fifteen minutes and then stays steady. The methanol acetal of the second intermediate **II+MeOH** rises quickly in the first hour and then stays steady, but rises to intensities four times higher than the second intermediate **II**. This shows that the resting state **II+MeOH** is favored in the equilibrium between it and the second intermediate **II**. Species **III** behaves similarly to **II+MeOH**, namely rising quickly in the first hour and then staying steady but reaching approximately half the intensity of **II+MeOH**.

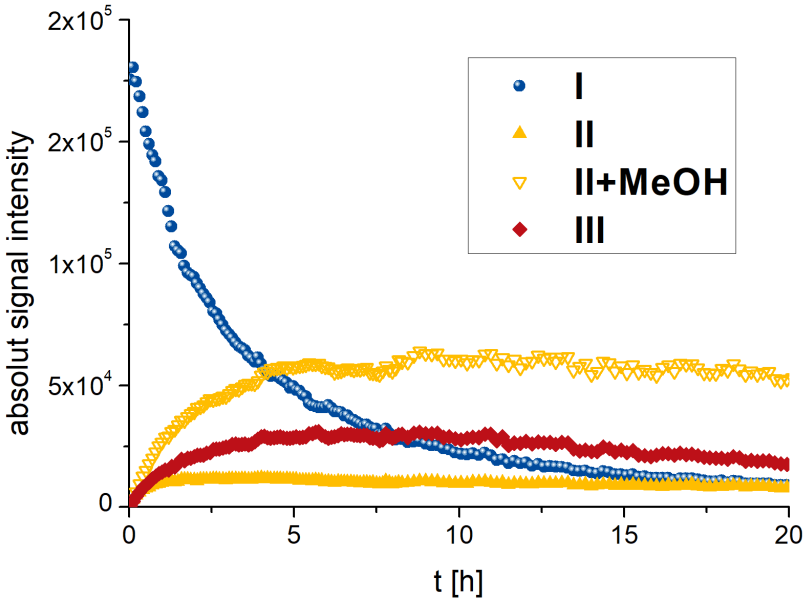

Figure 3.2.21 Temporal progress of the L-proline catalyzed reaction with *trans*-2-hexenal **2** based on micrOTOF-Q spectra. The H and Na-adduct signals were added for plotting. **I** (*m/z* 196, 218), **II** (*m/z* 294,316), **II**+MeOH (*m/z* 326, 348), **III** (only *m/z* 276).

Because the first intermediate **I** decays while the second intermediate **II** and the acetal of the second intermediate **II+MeOH** steady over time, I conclude that the ring formation is faster than the liberation of the catalyst and product, making the last step the rate-determining step of the reaction. In tests to speed the reaction up, I added acetic acid and pyridine in separate experiments to the reaction mixture, but no changes were observed (see Figure 6.1.1 p. 125 and Figure 6.1.2 p. 125).

3.2.2.2 Experiments with trans-2-pentenal

The reaction was also studied with *trans*-2-pentenal **10** as the substrate (Figure 3.2.22).

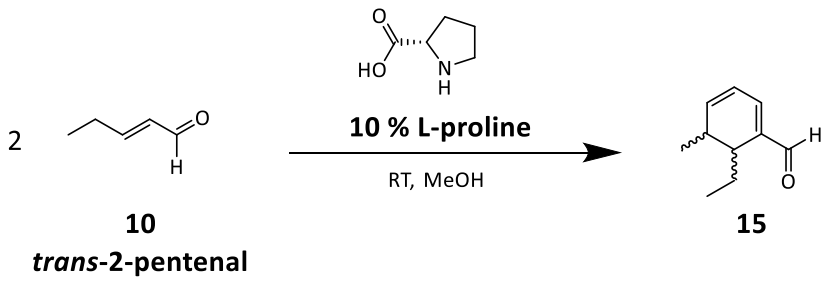

Figure 3.2.22 L-proline catalyzed reaction of *trans*-2-pentenal **10**.

In Figure 3.2.23 the overview spectra of the reaction with *trans*-2-hexenal **2** a) and *trans*-2-pentenal **10** b) can be compared. For all species found for the reaction with *trans*-2-hexenal **2** the corresponding species are found for the reaction with *trans*-2-pentenal **10** and are marked with the suffix **P**.

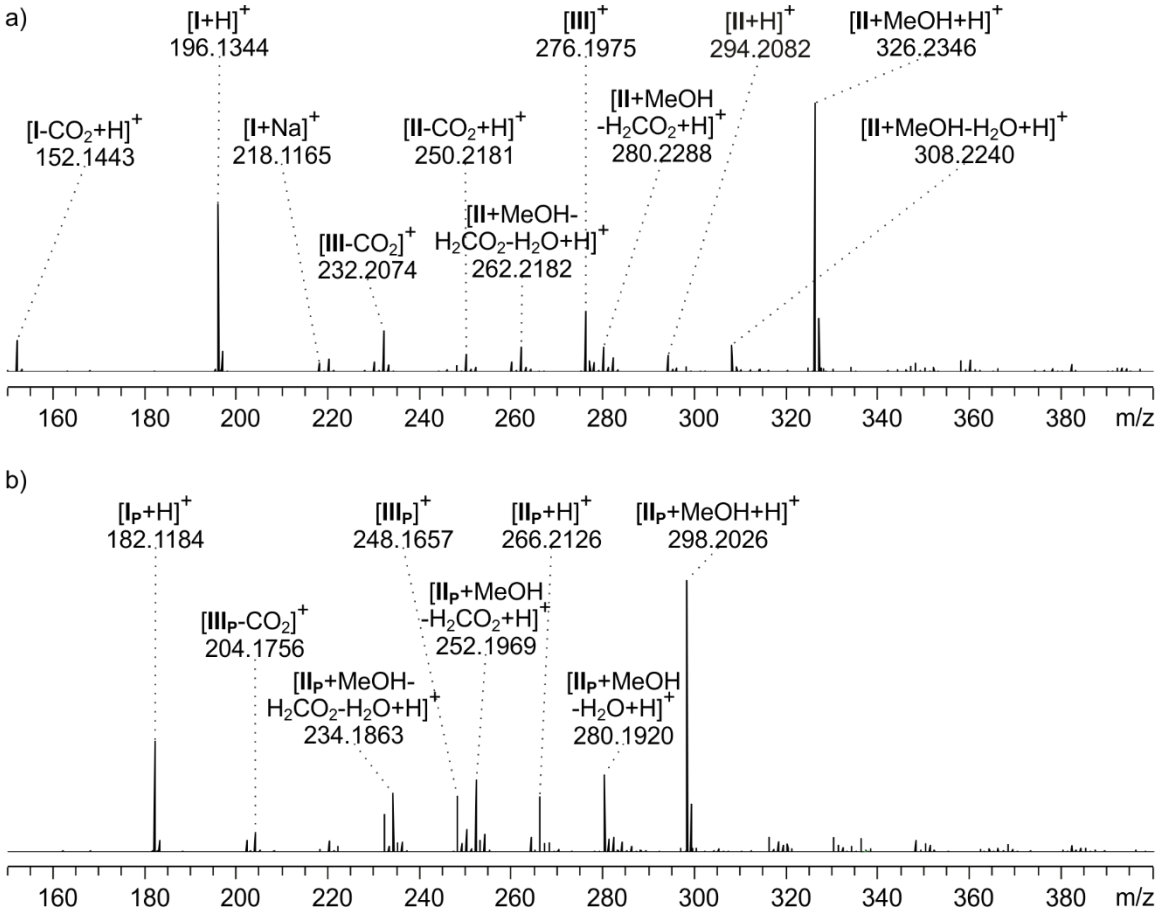

Figure 3.2.23 Orbitrap XL spectra ESI(+) after two hours reaction time for a) reaction with *trans*-2-hexenal **2**, b) reaction with *trans*-2-pentenal **10**.

The same revised catalytic cycle as for *trans*-2-hexenal **2** (Figure 3.2.10) can be set up for the reaction of *trans*-2-pentenal **10** (Figure 3.2.24).

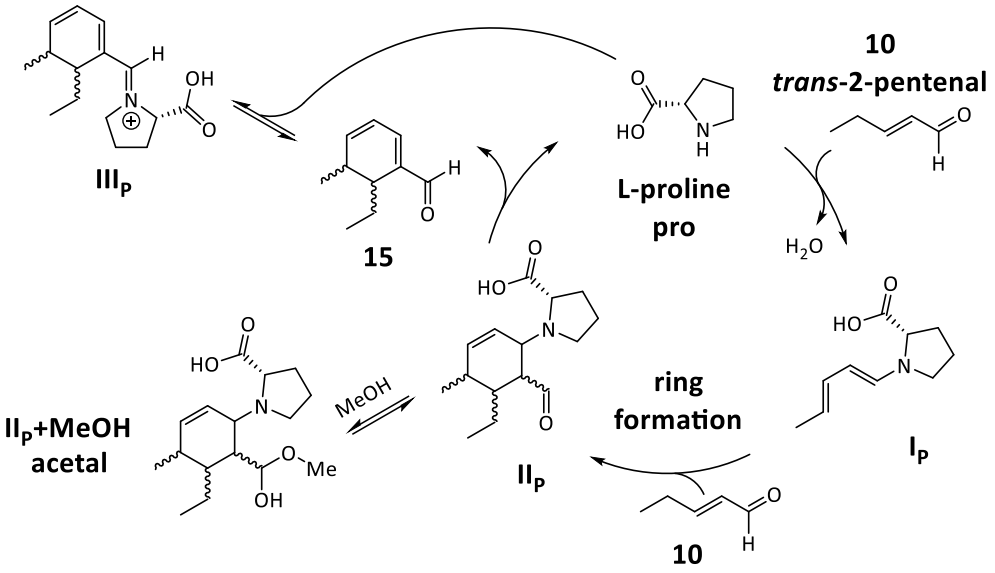

Figure 3.2.24 Revised catalytic cycle for the reaction with *trans*-2-pentenal **10**.

The MS^2 experiment of the second intermediate with methanol [**II$_P$**+MeOH+H]$^+$ (*m/z* 298) again shows the loss of H_2O and methanol (Figure 3.2.25). Thus, **II$_P$**+MeOH can too be attributed to the acetal formed from methanol and the second intermediate.

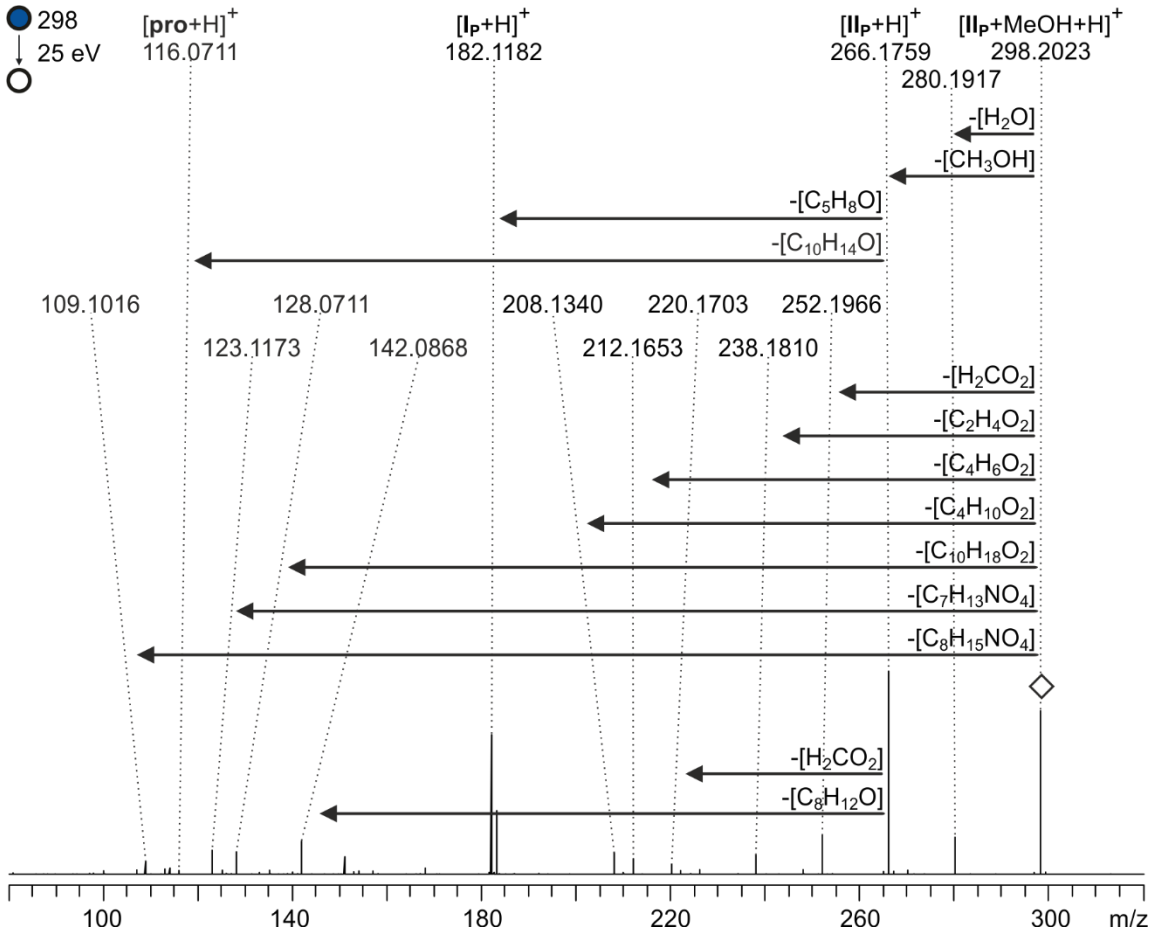

Figure 3.2.25 Orbitrap XL spectrum ESI(+) MS^2 of [**II$_P$**+MeOH+H]$^+$ *m/z* 298 25 eV.

The MS^n experiments of the first and second intermediate of the reaction with *trans*-2-pentenal **10** show the same behavior as the intermediates of the reaction with *trans*-2-hexenal **2**. The second intermediate $[\mathbf{II_P}+H]^+$ is induced to go backward to the first intermediate $[\mathbf{I_P}+H]^+$ and forward to the catalyst $[\mathbf{pro}+H]^+$ in the catalytic cycle (Figure 3.2.26 a)). The comparison of the MS^3 experiment of $[\mathbf{I_P}+H]^+$ generated from $[\mathbf{II_P}+H]^+$ with the MS^2 experiment of $[\mathbf{I_P}+H]^+$ shows that indeed the second intermediate is induced to go backward in the catalytic cycle to form the first intermediate (Figure 3.2.26 b) and c)). However only the protonated intermediates can be observed here, neutral species might not exhibit the same behavior.

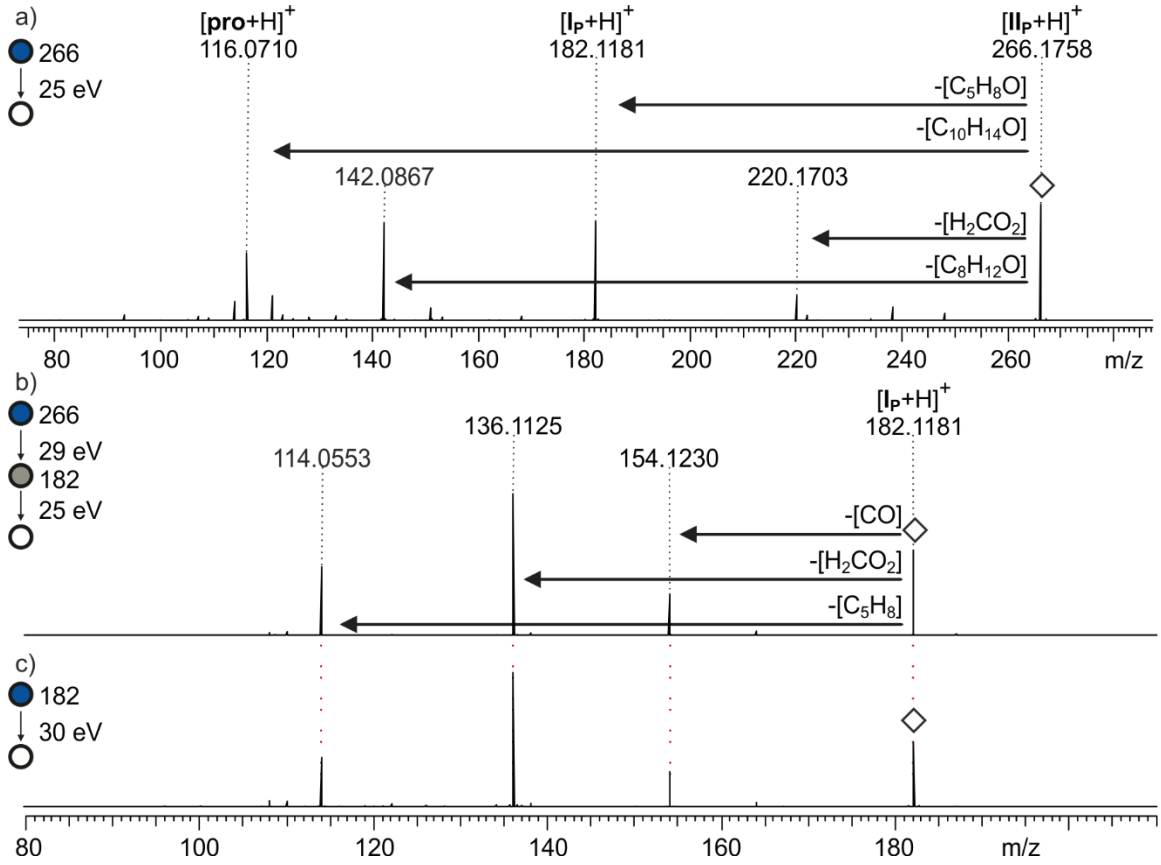

Figure 3.2.26 Orbitrap XL spectra ESI (+) a) MS^2 of $[\mathbf{II_P}+H]^+$ *m/z* 266 25 eV, b) MS^3 of $[\mathbf{II_P}+H]^+$ *m/z* 266 29 eV, $[\mathbf{I_P}+H]^+$ *m/z* 182 25 eV c) MS^2 of $[\mathbf{I_P}+H]^+$ *m/z* 182 30 eV.

With *trans*-2-pentenal **10** I also performed the experiment with the charge-tagged catalyst **1**·**Cl** to study the unprotonated charge-tagged intermediates $\mathbf{I}_{Pct}$ and $\mathbf{II}_{Pct}$ (Figure 3.2.27).

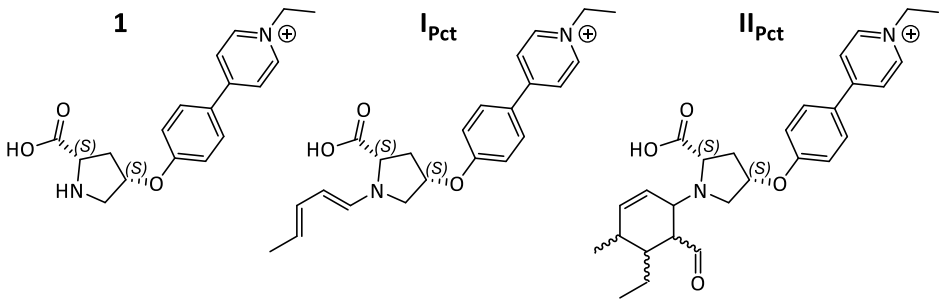

Figure 3.2.27 Charge tagged intermediates $\mathbf{I}_{Pct}$ and $\mathbf{II}_{Pct}$ of the reaction with *trans*-2-pentenal **10** with the charge-tagged catalyst **1**.

In the overview spectra of the charge-tagged reaction with *trans*-2-pentenal **10** (Figure 3.2.28), all corresponding species to the charge-tagged reaction with *trans*-2-hexenal **2** were found.

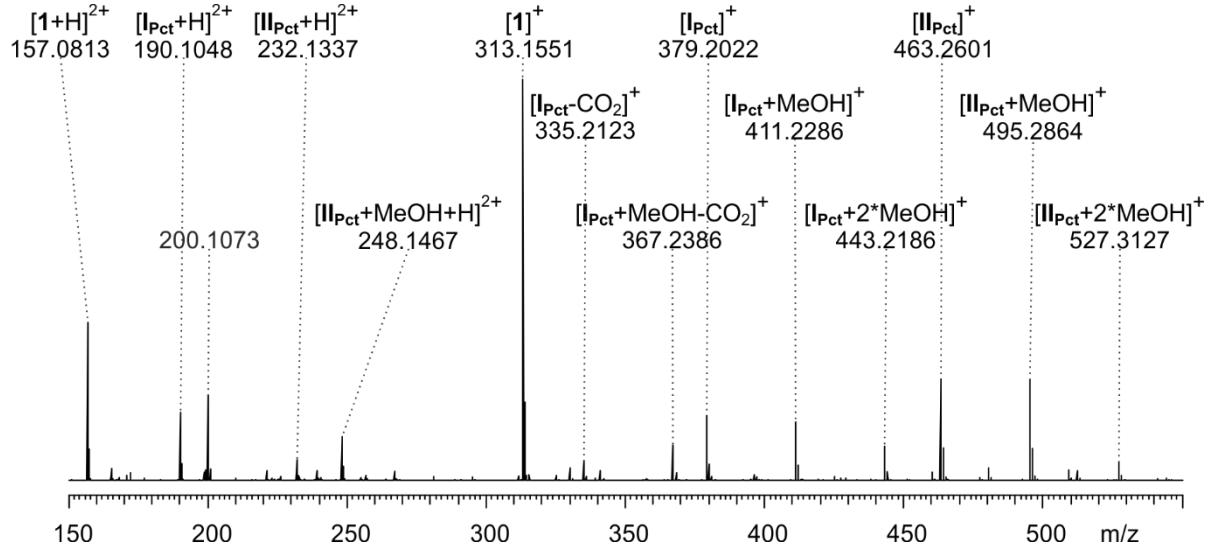

Figure 3.2.28 Orbitrap XL spectrum ESI(+)of the charge-tagged reaction of **1** and *trans*-2-pentenal **10** after 2 hours reaction time. *m/z* 200 is a known fragment of $[\mathbf{1}]^+$.

The first intermediate $[\mathbf{I}_{Pct}]^+$ is detected at *m/z* 379 and the second intermediate $[\mathbf{II}_{Pct}]^+$ at *m/z* 463. Further, the intermediates are also present as doubly charged species (*m/z* 190, 232, 248), after the loss of CO_2 (*m/z* 335, 367), and in conjunction with methanol (*m/z* 248, 367, 411, 443, 495, 527). In the experiment without the charge-tag the methanol acetal of the second intermediate was detected ($\mathbf{II}_P$+MeOH), with the charge-tag the signal for $[\mathbf{II}_{Pct}$+MeOH$]^+$ (*m/z* 495) (Figure 3.2.28) is also present. In the MS^2 experiment of $[\mathbf{II}_{Pct}$+MeOH$]^+$ *m/z* 495 only the loss of methanol and not of water was observed (Figure 3.2.29). However, 20 eV are still needed for the fragmentation, which indicates the acetal structure and not just a solvent adduct with methanol.

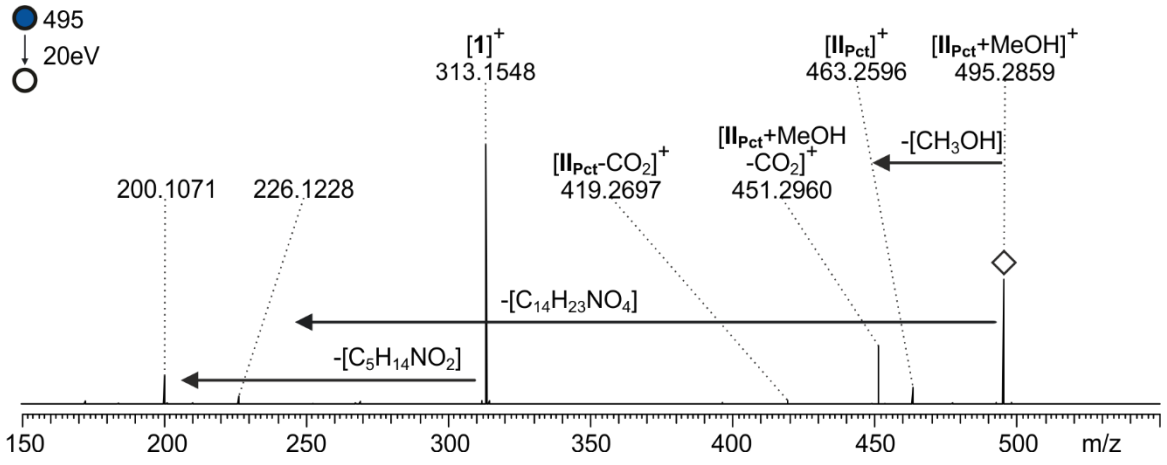

Figure 3.2.29 Orbitrap XL spectrum ESI(+) MS^2 of $[\mathbf{II}_{Pct}+MeOH]^+$ *m/z* 495 20 eV.

Figure 3.2.30 shows the MS^2 experiment of the second intermediate $[\mathbf{II}_{Pct}]^+$.(*m/z* 463). I observed similar behavior as without the charge-tag. $[\mathbf{II}_{Pct}]^+$ easily loses CO_2 and then forms the first intermediate without CO_2 $[\mathbf{I}_{Pct}\text{-}CO_2]^+$. Additionally, $[\mathbf{II}_{Pct}]^+$ forms the first intermediate $[\mathbf{I}_{Pct}]^+$, although not with high intensity and $[\mathbf{II}_{Pct}]^+$ forms the catalyst $[\mathbf{1}]^+$. So again, I can induce the second intermediate to mimic the steps of the catalytic cycle by going forward to the catalyst $[\mathbf{1}]^+$ and backward to the first intermediate ($[\mathbf{I}_{Pct}]^+$ or $[\mathbf{I}_{Pct}\text{-}CO_2]^+$). In this case, no additional proton is present, thus the behavior might reflect the behavior of a neutral molecule in solution.

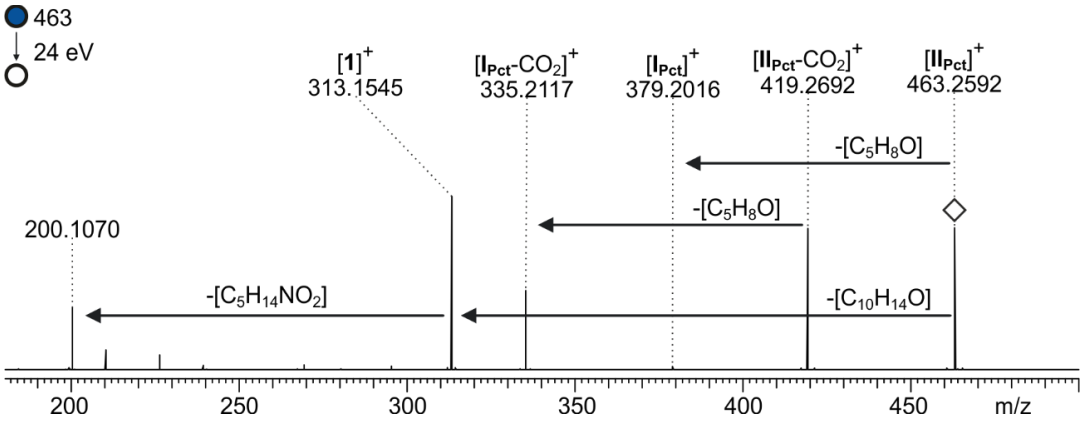

Figure 3.2.30 Orbitrap XL spectrum ESI(+) MS^2 of $[\mathbf{II}_{Pct}]^+$ *m/z* 463 24 eV.

The MS^3 experiment of the fragment after the loss of CO_2 of the second intermediate $[\mathbf{II_{Pct}}\text{-}CO_2]^+$ *m/z* 419 too is induced to go backward in the catalytic cycle towards $[\mathbf{I_{Pct}}\text{-}CO_2]^+$ (Figure 3.2.31).

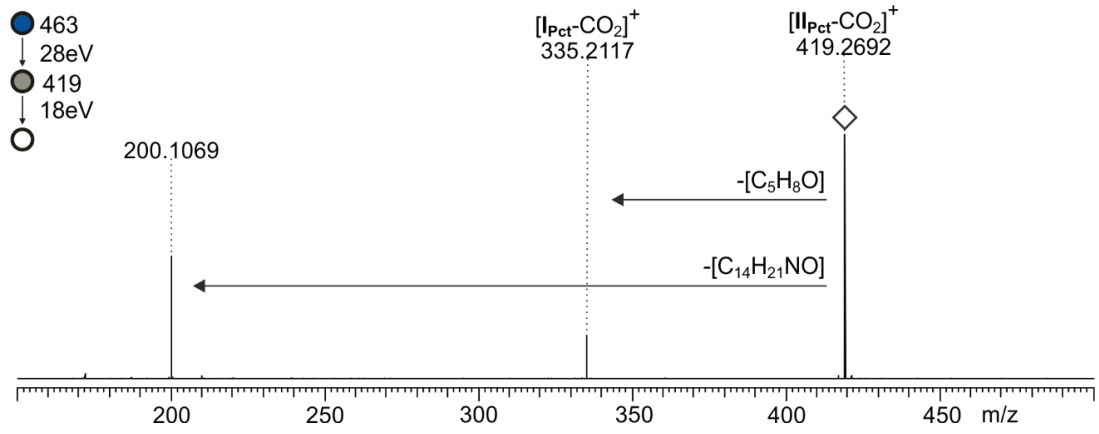

Figure 3.2.31 MS^3 of $[\mathbf{II_{Pct}}]^+$ *m/z* 463 28 eV, $[\mathbf{II_{Pct}}\text{-}CO_2]^+$ *m/z* 419 18 eV.

Figure 3.2.32 shows the MS^2 experiment of the charge-tagged first intermediate $[\mathbf{I_{Pct}}]^+$, which only loses CO_2.

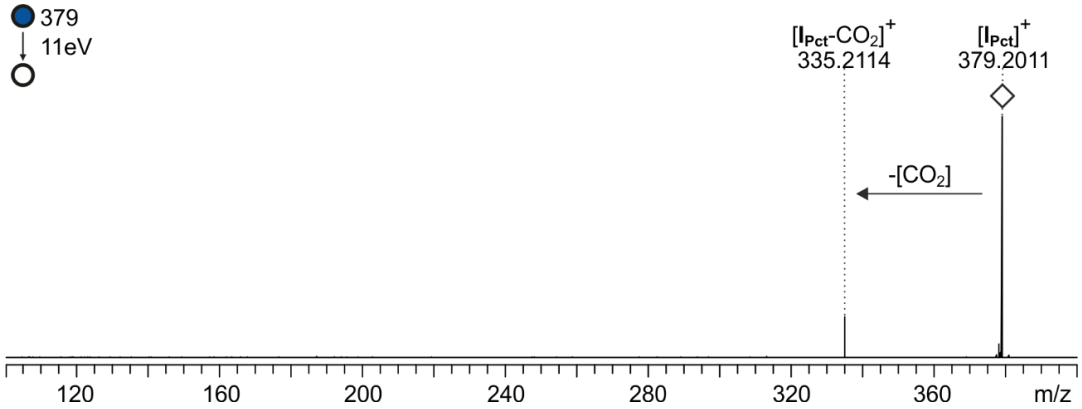

Figure 3.2.32 Orbitrap XL spectrum ESI(+) MS^2 of $[\mathbf{I_{Pct}}]^+$ *m/z* 379 11 eV.

Here too, the temporal progress of the reaction of L-proline with *trans*-2-pentenal **10** was studied. Again, I took samples out of the reaction mixture via an autosampler (set to 20 °C) in regular intervals and measured ESI spectra on the micrOTOF-Q. The absolute signal intensities of peaks pertaining to the same species were added and plotted against the reaction time (Figure 3.2.33). *Trans*-2-pentenal **10** too is neither detectable with ESI nor APCI. Therefore, I can only plot the first intermediate $\mathbf{I_P}$ (*m/z* 182, 204), the second intermediate $\mathbf{II_P}$ (*m/z* 266,288), the acetal of the second intermediate $\mathbf{II_P}$**+MeOH** (*m/z* 326), and species $\mathbf{III_P}$ (*m/z* 248). The first intermediate $\mathbf{I_P}$ starts with high intensity and slowly decays, whereas the second intermediate $\mathbf{II_P}$ starts at very low intensities, rises quickly in the first two hours, and then stays steady. The methanol acetal of the second intermediate $\mathbf{II_P}$**+MeOH** rises quickly in the first two hours and then stays steady but rises to intensities three times higher than the second intermediate $\mathbf{II_P}$. This shows that the resting state $\mathbf{II_P}$**+MeOH** is favored in the equilibrium between it

and the second intermediate **II$_P$**. Species **III$_P$** behaves similar to **II$_P$+MeOH**, namely rising quickly in the first hour and then staying steady but reaching approximately half the intensity of **II$_P$**.

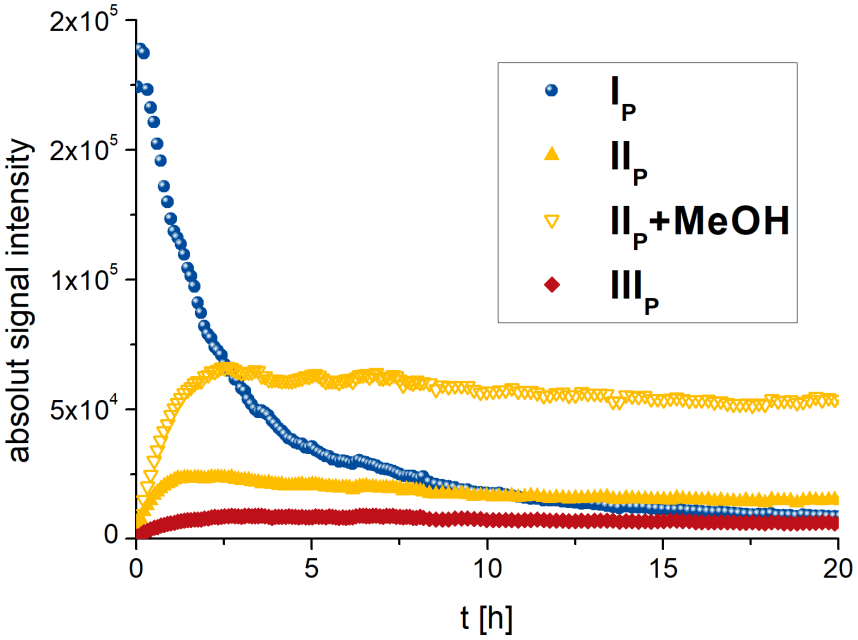

Figure 3.2.33 Temporal progress of the L-proline catalyzed reaction with *trans*-2-pentenal **10** based on micrOTOF-Q spectra. The H- and Na-adduct signals were added for plotting. **I$_P$** (*m/z* 182, 204), **II$_P$** (*m/z* 266,288), **II$_P$**+MeOH (*m/z* 298, 320), **III$_P$** (only *m/z* 248).

Because the first intermediate **I$_P$** decays while the second intermediate **II$_P$** and the acetal of the second intermediate **II$_P$+MeOH** steady over time, I here too conclude that the ring formation is faster than the liberation of the catalyst and product. Making the last step the rate-determining step of the reaction here too. In tests to speed the reaction up, I added acetic acid and pyridine to the reaction mixture in separate experiments, but no change was observed (see Figure 6.1.3 p. 126 and Figure 6.1.4 p. 126).

In comparison to the reaction with *trans*-2-hexenal **2** (Figure 3.2.21) the reaction with *trans*-2-pentenal **10** is faster, which can be seen in the quicker rising of **II$_P$** and **II$_P$**+MeOH than **II** and **II**+MeOH. The reaction with *trans*-2-pentenal **10** might be faster because the species involved might have less steric hindrance due to the shorter chain length.

3.2.3 Conclusion

I have conducted a thorough study of the L-proline catalyzed formation of cyclohexadienals from *trans*-2-hexenal and *trans*-2-pentenal by ESI MS. The results of the experiments with both aldehydes are in accordance with each other. By adding two additional species (**III** and **II+MeOH**), I revised the catalytic cycle postulated by *Griesbeck* et al.[1]. As I confirmed the two postulated intermediates (**I** and **II**), I disagree with *Bench* et al.[2] who claimed two catalyst molecules take part in the ring formation step. With MS^n experiments, I could elucidate or confirm the structure of all four species (**I**, **II**, **II+MeOH** and **III**). In particular, the second intermediate's **II** behavior in MS^n experiments was riveting; I was able to induce it in the gas phase to mimic the neighboring reaction steps going backward and forward in the catalytic cycle. With the aid of the charge-tagged proline derived catalyst **1**·**Cl**, I could study both intermediates in an unprotonated form and again mimic the catalytic steps in the gas phase, providing further evidence for the catalytic cycle. In addition, I studied the temporal progress of the reactive species and found that the liberation of the catalyst and product is the rate-determining step.

To sum up, I have revised the catalytic cycle by adding two additional species, characterized the intermediates **I** and **II** thoroughly by MS^n experiments, and have identified the rate-determining step.

3.2.4 Experimental Details

Instruments

micrOTOF-Q from *Bruker Daltonik* (Bremen) and Orbitrap XL from *Thermo Fisher Scientific* (Bremen).

With the micrOTOF-Q an *Agilent* HPLC 1200 series was used with the following modules: G1312A, G1316A, G1367B, G1330B. With the Orbitrap XL the HPLC from *Thermo Fisher Scientific* ultimate 3000 was used.

Trans-2-hexenal and L-proline

In 6.780 ml methanol 26.0 mg L-proline (0.226 mmol, 0.1 eq.) are dissolved. At 20 °C then 262 µl *trans*-2-hexenal (2.260 mmol, 1 eq.) are added. For the temporal progress study, 1.5 ml of the reaction mixture are transferred to a vial. From which the autosampler (set to 20 °C) injects 2 µl at regular intervals, with methanol as solvent, into the micrOTOF-Q spectrometer with ESI ionization. As a representative spectrum, the spectra from 1.8 min till 3.2 min are summed up. For experiments with the Orbitrap XL spectrometer, the reaction solution was prepared as described above, and 10 µl were injected with the autosampler, with acetonitrile as solvent.

Trans-2-hexenal and charge-tagged proline **1**·**Cl**

In 292 µl methanol 3.4 mg charge-tagged L-proline **1**·**Cl** (0.0097 mmol, 0.1 eq.) are dissolved. At room temperature, then 11.3 µl *trans*-2-hexenal (0.0975 mmol, 1 eq.) are added. The reaction solution is transferred to a vial. 10 µl were injected with the autosampler into the Orbitrap XL, with acetonitrile as solvent.

Trans-2-hexenal, L-proline, and acetic acid

In 6.618 ml methanol 25.4 mg L-proline (0.221 mmol, 0.1 eq.) are dissolved. 6.3 µl glacial acetic acid (0.110 mmol, 0.05 eq.) are added. At 20 °C then 256 µl *trans*-2-hexenal (2.206 mmol, 1 eq.) are added. For the temporal progress study, 1.5 ml of the reaction mixture are transferred to a vial. From which the autosampler (set to 20 °C) injects 2 µl at regular intervals, with methanol as solvent, into the micrOTOF-Q spectrometer with ESI ionization. As a representative spectrum, the spectra from 1.8 min till 3.4 min are summed up.

Trans-2-hexenal, L-proline, and pyridine

In 6.691 ml methanol 25.7 mg L-proline (0.223 mmol, 0.1 eq.) are dissolved. 9.0 µl pyridine (0.112 mmol, 0.05 eq.) are added. At 20 °C then 259 µl *trans*-2-hexenal (2.231 mmol, 1 eq.) are added. For the temporal progress study, 1.5 ml of the reaction mixture are transferred to a vial. From which the autosampler (set to 20 °C) injects 2 µl at regular intervals, with methanol as solvent, into the

micrOTOF-Q spectrometer with ESI ionization. As a representative spectrum, the spectra from 1.8 min till 3.4 min are summed up.

Trans-2-pentenal and L-proline

In 6.830 ml methanol 26.2 mg L-proline (0.228 mmol, 0.1 eq.) are dissolved. At 20 °C then 223 µl *trans*-2-pentenal (2.277 mmol, 1 eq.) are added. For the temporal progress study, 1.5 ml of the reaction mixture are transferred to a vial. From which the autosampler (set to 20 °C) injects 2 µl at regular intervals, with methanol as solvent, into the micrOTOF-Q spectrometer with ESI ionization. As a representative spectrum, the spectra from 1.8 min till 3.4 min are summed up. For experiments with the Orbitrap XL spectrometer, the reaction solution was prepared as described above, and 10 µl were injected with the autosampler, with acetonitrile as solvent.

Trans-2-pentenal and charge-tagged proline **1**·**Cl**

In 369 µl methanol 4.3 mg charge-tagged L-proline **1**·**Cl** (0.0123 mmol, 0.1 eq.) are dissolved. At room temperature, then 12.3 µl *trans*-2-pentenal (0.1233 mmol, 1 eq.) are added. The reaction solution is transferred to a vial. 10 µl were injected with the autosampler into the Orbitrap XL, with acetonitrile as solvent.

Trans-2-pentenal, L-proline, and acetic acid

In 6.887 ml methanol 26.4 mg L-proline (0.230 mmol, 0.1 eq.) are dissolved. 6.6 µl glacial acetic acid (0.115 mmol, 0.05 eq.) are added. At 20 °C then 225 µl *trans*-2-pentenal (2.296 mmol, 1 eq.) are added. For the temporal progress study, 1.5 ml of the reaction mixture are transferred to a vial. From which the autosampler (set to 20 °C) injects 2 µl at regular intervals, with methanol as solvent, into the micrOTOF-Q spectrometer with ESI ionization. As a representative spectrum, the spectra from 1.8 min till 3.4 min are summed up.

Trans-2-pentenal, L-proline, and pyridine

In 6.605 ml methanol 25.4 mg L-proline (0.220 mmol, 0.1 eq.) are dissolved. 8.9 µl pyridine (0.110 mmol, 0.05 eq.) are added. At 20 °C then 215 µl *trans*-2-pentenal (2.202 mmol, 1 eq.) are added. For the temporal progress study, 1.5 ml of the reaction mixture are transferred to a vial. From which the autosampler (set to 20 °C) injects 2 µl at regular intervals, with methanol as solvent, into the micrOTOF-Q spectrometer with ESI ionization. As a representative spectrum, the spectra from 1.8 min till 3.4 min are summed up.

3.2.5 References

[1] A. G. Griesbeck, A. de Kiff, J. M. Neudörfl, S. Sillner, *Arkivoc* **2014**, *2015*, 101.

[2] B. J. Bench, C. Liu, C. R. Evett, C. M. H. Watanabe, *J. Org. Chem.* **2006**, *71*, 9458.

[3] B.-C. Hong, M.-F. Wu, H.-C. Tseng, G.-F. Huang, C.-F. Su, J.-H. Liao, *J. Org. Chem.* **2007**, *72*, 8459.

[4] S. Bertelsen, M. Marigo, S. Brandes, P. Dinér, K. A. Jørgensen, *J. Am. Chem. Soc.* **2006**, *128*, 12973.

[5] B. Łągiewka, Ł. Albrecht, *Asian J. Org. Chem.* **2017**, *6*, 516.

[6] R. M. de Figueiredo, R. Fröhlich, M. Christmann, R. M. de Figueiredo, *Angew. Chem. Int. Ed.* **2008**, *47*, 1450.

3.3 Mechanistic studies of an L-proline-catalyzed pyridazine formation involving a Diels–Alder reaction with inverse electron demand

The results of this chapter have been published in:

A. Schnell, J. A. Willms, S. Nozinovic, M. Engeser, *Beilstein J. Org. Chem.* **2019**, *15,* 30-43.

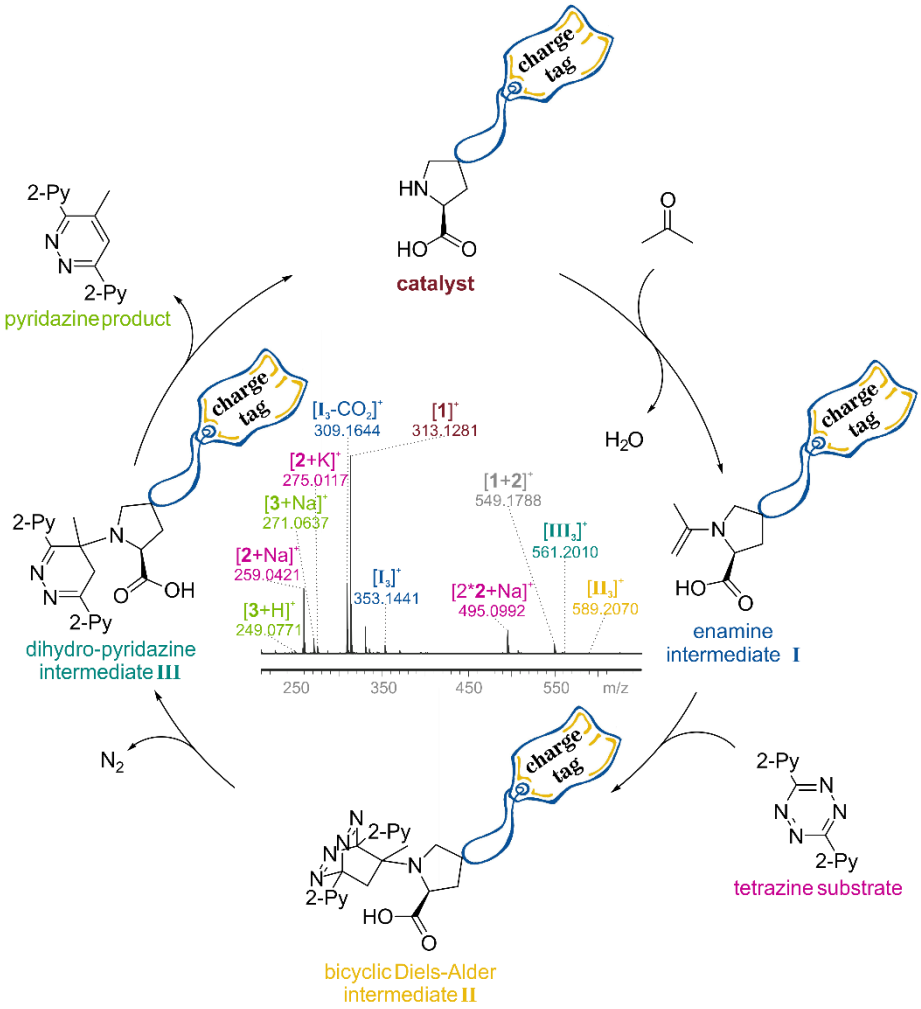

I started this project during my bachelor thesis and continued working on it during my master thesis. The synthesis of the charge tagged tetrazine and parts of the ESI MS experiments were performed during that time. Further ESI MS experiments, the NMR experiments and the writing of the publication were performed during the PhD.

3.3.1 Introduction

In this chapter, the publication "Mechanistic studies of an L-proline-catalyzed pyridazine formation involving a Diels–Alder reaction with inverse electron demand" will be presented.[1]

ESI MS was used as the primary analytical tool, as it is a suitable method for the analysis of reaction mechanisms (see chapter 2.2). The study utilized a newly synthesized charge-tagged substrate and the charge-tagged catalyst **1**·**Cl** from *Willms* et al.[2] to find elusive intermediates.

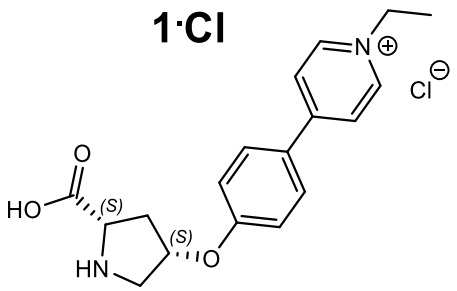

Figure 3.3.1 Charge-tagged L-proline derived catalyst published by *Willms* et al.[2].

The reaction of interest was published by *Xie* et al.[3], which is an L-proline catalyzed reaction between a ketone and a tetrazine (Figure 3.3.2). L-proline serves as organocatalyst, which facilitates this reaction by transforming the ketone into an enamine. The enamine reacts as the electron rich dienophile with the electron poor tetrazine in a *Diels-Alder* reaction with *inverse electron demand*. The final product of the reaction is a pyridazine.

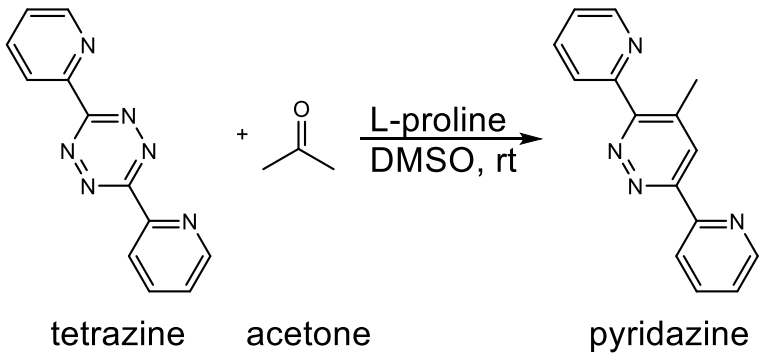

Figure 3.3.2 Reaction published by *Xie* et al.[3].

3.3.2 Facsimile of the publication

Mechanistic studies of an L-proline-catalyzed pyridazine formation involving a Diels–Alder reaction with inverse electron demand

Anne Schnell, J. Alexander Willms, S. Nozinovic and Marianne Engeser*

Full Research Paper

Open Access

Address:
University of Bonn, Kekulé-Institute of Organic Chemistry and Biochemistry, Gerhard-Domagk-Str. 1, D-53121 Bonn, Germany

Email:
Marianne Engeser* - Marianne.Engeser@uni-bonn.de

* Corresponding author

Keywords:
charge-tag; electrospray ionization; enamine organocatalysis; L-proline; reaction mechanism

Beilstein J. Org. Chem. **2019,** *15,* 30–43.
doi:10.3762/bjoc.15.3

Received: 25 August 2018
Accepted: 28 November 2018
Published: 03 January 2019

Associate Editor: J. A. Murphy

Abstract

The mechanism of an L-proline-catalyzed pyridazine formation from acetone and aryl-substituted tetrazines via a Diels–Alder reaction with inverse electron demand has been studied with NMR and with electrospray ionization mass spectrometry. A catalytic cycle with three intermediates has been proposed. An enamine derived from L-proline and acetone acts as an electron-rich dienophile in a [4 + 2] cycloaddition with the electron-poor tetrazine forming a tetraazabicyclo[2.2.2]octadiene derivative which then eliminates N_2 in a retro-Diels–Alder reaction to yield a 4,5-dihydropyridazine species. The reaction was studied in three variants: unmodified, with a charge-tagged substrate, and with a charge-tagged proline catalyst. The charge-tagging technique strongly increases the ESI response of the respective species and therefore enables to capture otherwise undetected reaction components. With the first two reaction variants, only small intensities of intermediates were found, but the temporal progress of reactants and products could be monitored very well. In experiments with the charge-tagged L-proline-derived catalyst, all three intermediates of the proposed catalytic cycle were detected and characterized by collision-induced dissociation (CID) experiments. Some of the CID pathways of intermediates mimic single steps of the proposed catalytic cycle in the gas phase. Thus, the charge-tagged catalyst proved one more time its superior effectiveness for the detection and study of reactive intermediates at low concentrations.

Introduction

Electrospray (ESI) mass spectrometry (MS) [1] is well suited for studying reaction mechanisms as it is a soft ionization method leaving most species intact [1-3]. In addition, it is a fast analytical method [3] making it possible to study transient intermediates [4-6]. Various types of reactions have been studied successfully by ESIMS ranging from Ziegler–Natta polymerization [7] and coupling reactions [8,9] to organic reactions such as the Baylis–Hillman [10-15], aldol [16-18] or Diels–Alder reac-

Beilstein J. Org. Chem. **2019,** *15,* 30–43.

tions [19,20]. An advantageous feature of high-resolution ESIMS is that each ionic species in the gas phase produces distinct signals which are unlikely to be overlaid with signals from other species [6]. As a consequence, reaction mixtures typically containing many different species can be analyzed without prior separation of the components [5,6]. As a drawback of MS, isomers typically are hard to analyze as they have the same mass and thus lead to the same signal. However, they can be distinguished in fortunate cases by more sophisticated approaches like tandem mass spectrometry [3], ion mobility mass spectrometry [21], or coupling with liquid or gas chromatography. Further, ESI signal intensities do not directly correlate to concentrations in solution, but to the ESI response of the pertaining molecules [3,22]. The ESI response is influenced by a variety of factors like chargeability and surface activity of a given analyte and also by the applied electrospray conditions [22]. If there are big differences in the ESI response between species of interest, some species might dominate the spectrum so much that species with a low ESI response are concealed [2,17]. To counteract these problems, covalently linked charge-tags can be introduced into the analyte molecules, usually in the form of alkylated amines or phosphines [5,6]. The charge-tag can be located either within the substrate [23-25] or the catalyst [18,26,27]. As a result, all species containing the charge-tag will have a similarly high ESI response [6,25] while species that are not involved in the reaction and do not carry the charge-tag will have a much lower ESI response. A charge-tag thus facilitates "fishing" [5,23,28] for reactive intermediates. We have previously used the charge-tagged L-proline derived catalyst **1**·Cl (Figure 1) in an ESIMS study of a L-proline-catalyzed aldol reaction.

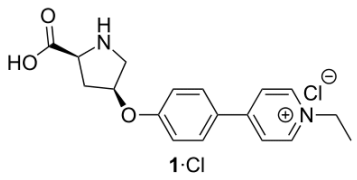

Figure 1: Charge-tagged L-proline-derived catalyst **1**·Cl [18].

Organocatalysis has become a major research field with many applications and has proven to be a valuable complementary approach to organometallic or enzymatic catalysis [29-34]. The advantages especially in comparison to organometallic catalysis lie in a lower toxicity, air sensitivity and lower costs [34]. A huge repertoire of organocatalyzed reactions have been published in recent years with high efficiencies and selectivities [29,33,35-39]. Proline as a natural amino acid is a perfect example of an organocatalyst. Both enantiomers are inexpensive and easily available. The work of List and Barbas in 2000 was groundbreaking for L-proline-catalyzed reactions [40]. They published a L-proline-catalyzed asymmetric aldol reaction and suggested that the essential catalytic step is the enamine formation between the secondary amine function of L-proline and the carbonyl substrate acetone [40]. Houk and co-worker [41] verified the mechanism with quantum mechanical calculations, thus giving rise to the "List–Houk*"* mechanism. A discussion about the role of oxazolidinones as isomeric species to enamines has been raised in the scientific community [42-47]. Tetrazines and their reactivity in Diels–Alder reactions with inverse electron demand are of interest in the field of biology [48,49]. Very recently, they have been studied by mass spectrometric means [50].

In 2008, Xie et al. [51] published an L-proline-catalyzed reaction between ketones and aryl-substituted 1,2,4,5-tetrazines which leads to functionalized pyridazines. They also postulated a mechanism (Scheme 1) for the reaction [51]. Based on the knowledge that secondary amines catalyze the formation of enamines from ketones and other carbonyl compounds [33], an initial formation of the enamine **I** seems plausible. It is an electron-rich dienophile which could undergo a [4 + 2] cycloaddition with the electron-poor aryl-substituted tetrazine **2** in a Diels–Alder reaction with inverse electron demand. The bicyclic Diels–Alder intermediate **II** then might undergo a retro-Diels–Alder reaction by eliminating dinitrogen. This leads to the dihydropyridazine intermediate **III** out of which the catalyst is released to yield the pyridazine product **3** [51].

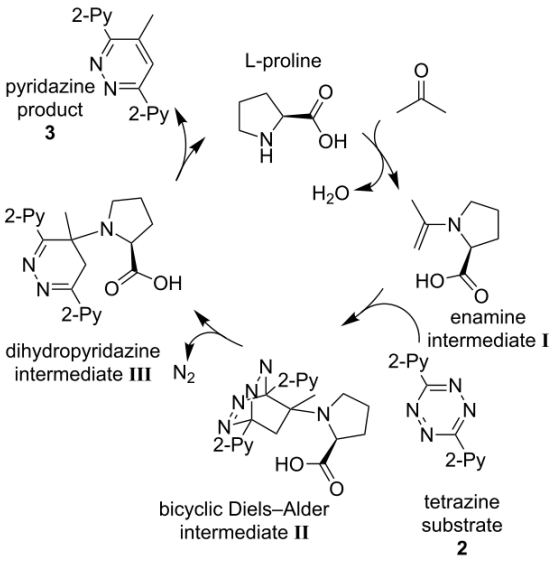

Scheme 1: Putative catalytic cycle [51] for the L-proline-catalyzed Diels–Alder reaction with inverse electron demand.

Beilstein J. Org. Chem. **2019,** *15,* 30–43.

Shihab et al. later studied a related reaction of a series of dienophiles with dimethyl 1,2,4,5-tetrazine-3,6-dicarboxylate by theoretical methods [52]. Their results are in agreement with the catalytic cycle presented in Scheme 1. However, the question is raised whether the bicyclic Diels–Alder species **II** is a real intermediate or rather a transition state of a concerted formation of the dihydropyridazine intermediate **III** directly from the enamine/dienophile **I** and the tetrazine. Thus, we decided to use NMR (nuclear magnetic resonance) spectroscopy and ESI mass spectrometry in combination with a charge-tagging strategy to get deeper insights in the presence or absence of the three intermediates by experimental means.

Results and Discussion

Synthesis

In addition to the charge-tagged proline catalyst **1**·Cl [18], the charge-tagged tetrazine substrate **4**·Br was synthesized (Scheme 2). We were inspired by the work of McIndoe and co-workers [6,25,53] who introduced and established the triphenylphosphonium charge-tag. The corresponding Diels–Alder reaction starting from this reactant yields pyridazine product **5**·Br. The first two synthetic steps (Scheme 2) towards benzenehydrazonoyl chloride **7** [54] were performed according to the protocol of Wang et al. [55]. The formation of new tetrazine compound **8** was performed in accordance to the procedure published by Liu et al. [56] and bromination to the new benzyl bromide **9** succeeded with tribromoisocyanuric acid (TBCA) as published by de Almeida et al. [57]. The final transformation of benzyl bromide **9** to triphenylphosphonium charge-tagged **4**·Br was performed with a slightly modified protocol from Vikse et al. [53].

Mechanistic studies: ^{1}H NMR experiments

^{1}H NMR experiments of reaction R1 (Scheme 3) show the temporal progress of the reaction which is easily tracked by the concentrations of substrate **2**, acetone and product **3** (Figure 2, and Figures S1 and S2 in Supporting Information File 1). How-

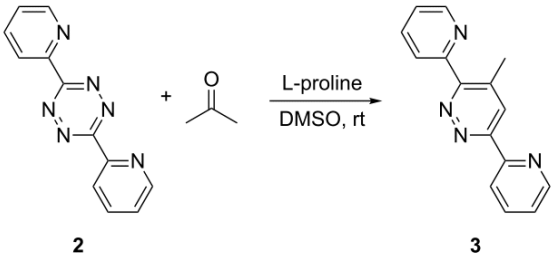

Scheme 3: Reaction R1: L-proline-catalyzed reaction between **2** and acetone.

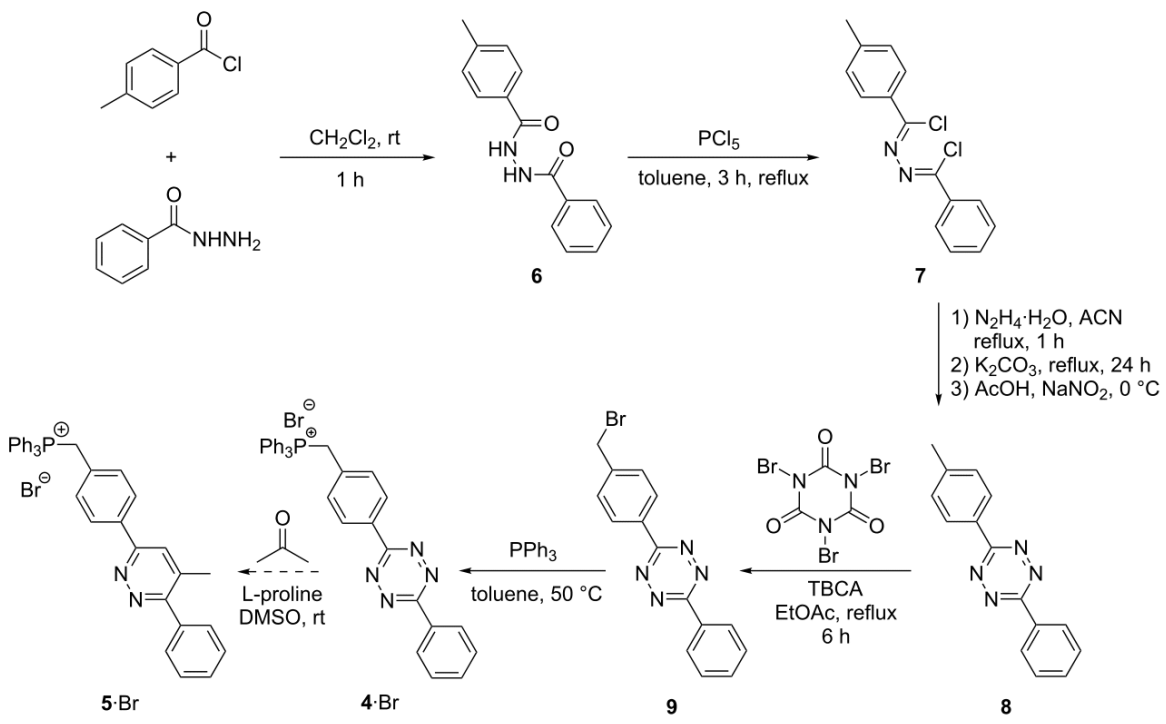

Scheme 2: Synthesis of the charge-tagged tetrazine **4**·Br as a reactant for the proline-catalyzed Diels–Alder reaction leading to **5**·Br.

Beilstein J. Org. Chem. **2019,** *15,* 30–43.

ever, no reaction intermediates could be detected either in this case or with enhanced concentrations (Figure S3, Supporting Information File 1).

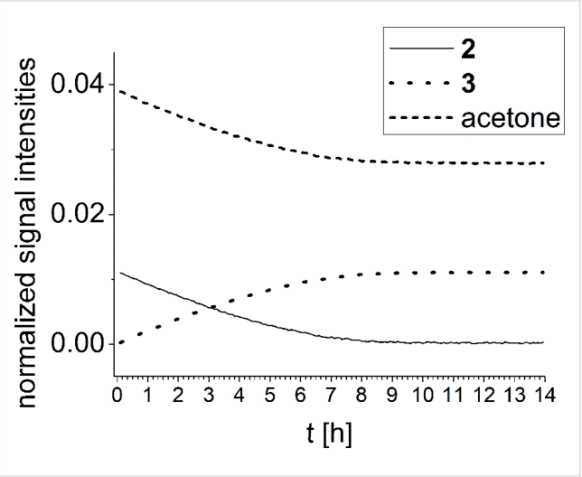

Figure 2: NMR monitoring of reaction R1 in deuterated DMSO (concentration of tetrazine 0.005 mmol/mL).

In absence of tetrazine **2**, the ^{1}H NMR spectra of a reaction mixture only containing L-proline and acetone in deuterated DMSO show an additional small signal at δ = 4.4 ppm (Figure S3, Supporting Information File 1), characteristic for an oxazolidinone (Scheme 4). In agreement with the findings from List [58] and Gschwind [46], the equilibrium concentration of the isomeric enamine is too low to be detected although this species is required as dienophile for the Diels–Alder reaction to proceed.

Mechanistic studies: ESIMS experiments

As ESIMS has a lower limit of detection than NMR, we also studied the proceeding reaction with ESIMS. In its simplest version, i.e., without charge-tagged components (R1, Scheme 3) and at a low concentration (0.005 mmol/mL of tetrazine), the temporal progress of substrate **2** and product **3** could be followed directly (Figure S5, Supporting Information File 1). Unfortunately, no reaction intermediates were detected. Using a lower amount of solvent (0.2 mmol of tetrazine in 10 mL of dimethyl sulfoxide) has the downside that not all of the substrate **2** gets dissolved initially. Product **3** is completely soluble at this concentration, so only while the substrate **2** transforms into product **3**, **2** gets fully dissolved. Small samples were taken from the reaction flask at regular intervals, diluted and immediately analyzed by ESIMS. The decay of substrate **2** (*m*/*z* 237, *m*/*z* 259, *m*/*z* 495) and the increase of product **3** (*m*/*z* 249, *m*/*z* 271) were easily observed (Figure 3a,b). Furthermore, the dihydropyridazine intermediate **III$_1$** (*m*/*z* 386) could be detected

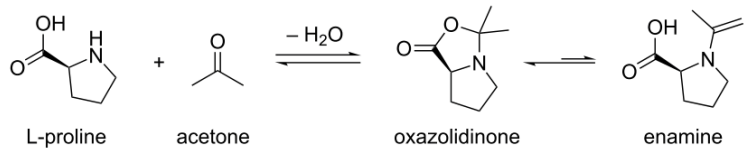

Scheme 4: Equilibrium of oxazolidinone and enamine formation.

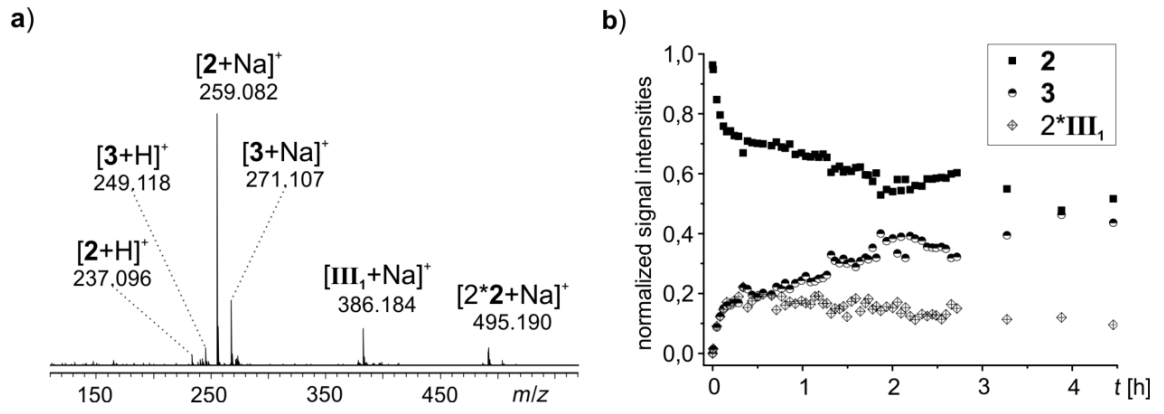

Figure 3: a) ESI mass spectrum of reaction R1 after 26 min. b) ESIMS monitoring of reaction R1. To better visualize the trend of **III$_1$**, the signal intensities of **III$_1$** have been multiplied by a factor of two.

Beilstein J. Org. Chem. **2019,** *15,* 30–43.

for the first time (Figure 3a). The intensity of $\mathbf{III_1}$ initially rises more quickly than the intensity of product **3** and declines very slowly as the reaction progresses (Figure 3b). However, no signals for the intermediates $\mathbf{I_1}$ (enamine) and $\mathbf{II_1}$ (bicyclic Diels–Alder intermediate) were found.

Intermediate $\mathbf{I_1}$ (*m*/*z* 156) has been observed before by Marquez et al. in ESIMS experiments of an aldol reaction [17]. In our case, it unfortunately does not accumulate in sufficient amounts for detection. Thus, the reaction was setup differently: instead of premixing L-proline (0.05 equiv) and tetrazine substrate **2** (1 equiv) in solution and then adding acetone (4 equiv) to start the reaction as before, now L-proline (1 equiv) and acetone (95 equiv) were mixed first. The formation of intermediate enamine $\mathbf{I_1}$ and/or the isomeric oxazolidinone was validated by the detection of a signal at *m*/*z* 156 for the protonated species in ESIMS spectra, and only then the tetrazine substrate **2** (1 equiv) was added. By this way, it was possible to detect not only substrate **2** (*m*/*z* 237, *m*/*z* 259), product **3** (*m*/*z* 249, *m*/*z* 271, *m*/*z* 287) and the proline catalyst (*m*/*z* 116, *m*/*z* 138), but also the intermediate $\mathbf{I_1}$ and/or its oxazolidinone isomer (*m*/*z* 156) and the dihydropyridazine intermediate $\mathbf{III_1}$ (*m*/*z* 386, Figure 4) in the reacting solution.

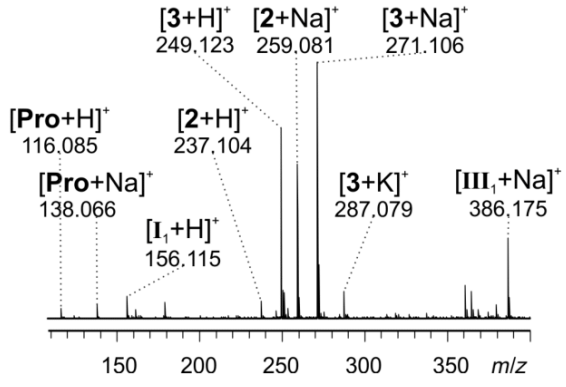

Figure 4: ESI mass spectrum of reaction R1 with preformed $\mathbf{I_1}$ 8 minutes after adding substrate **2**.

In order to enhance the ESI response of putative reactive intermediates, the reaction was performed with the charge-tagged tetrazine **4**·Br (R2, Scheme 5).

A continuous-flow setup [4,17,18] was used for fast sampling of the reaction R2 directly after its initiation. A solution of substrate **4**·Br and L-proline was mixed with acetone in a commercial PEEK microreactor mixing tee. The reacting solution was diluted with acetonitrile using a second microreactor and subsequently fed into the ESI source of the mass spectrometer. Beside a very prominent signal of the charge-tagged substrate **4**

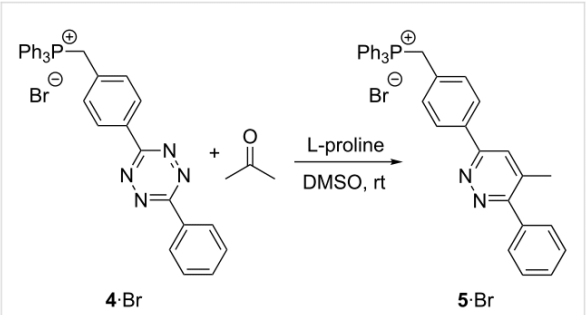

Scheme 5: Reaction R2: L-proline-catalyzed reaction between charge-tagged substrate **4**·Br and acetone. The regioselectivity has not been specified. **5**·Br could be either regioisomer (Scheme S1, Supporting Information File 1).

(*m*/*z* 509), signals corresponding to the product **5** (*m*/*z* 521, *m*/*z* 539) were observed (Figure 5). In addition, a low intensity signal for the dihydropyridazine intermediate $\mathbf{III_2}$ (*m*/*z* 636) could be found. The enamine intermediate $\mathbf{I_2}$ does not carry a charge-tag in this experiment and thus was not detected. Unfortunately, any indications for the charge-tagged bicyclic Diels–Alder intermediate $\mathbf{II_2}$ could not be found either.

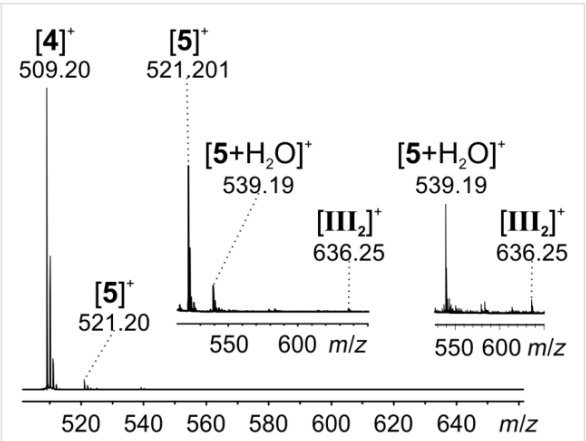

Figure 5: ESI mass spectrum of reaction R2 using a continuous-flow setup with a calculated reaction time of 86 s. The two insets show zooms into relevant parts of the spectrum.

To study the reaction R2 over a longer period of time, substrate **4**·Br, acetone and L-proline were simply mixed in a syringe and directly fed into the ESI mass spectrometer over a time span of 4 hours. The signals for substrate **4** (*m*/*z* 509) and product **5** (*m*/*z* 521, Figure 6a) were detected. Approximately 50% conversion was achieved after 4 hours at room temperature (Figure 6b). No signals corresponding to the bicyclic Diels–Alder intermediate $\mathbf{II_2}$ and the dihydropyridazine intermediate $\mathbf{III_2}$ could be detected, even though the charge-tagging strategy should have facilitated their detection. Clearly, the

Beilstein J. Org. Chem. **2019,** *15,* 30–43.

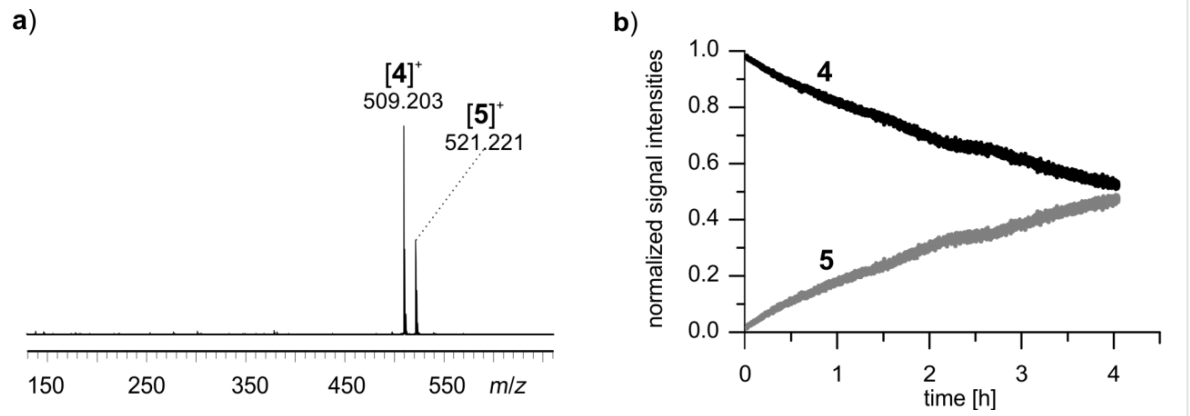

Figure 6: a) Reaction R2 after two hours (syringe setup). b) ESIMS monitoring of reaction R2. Signal intensities for substrate **4** and product **5** are depicted.

presence of high amounts of **4**·Br and **5**·Br suppressed ESI signals of other species of interest.

In contrast, less equivalents of charge-tagged species are present in the reaction solution if the charge-tag is part of the catalyst. The intermediates might not be concealed under these conditions. Therefore, substrate **2** and acetone were mixed with the charge-tagged catalyst **1**·Cl in a third variant of the reaction (R3, Scheme 6).

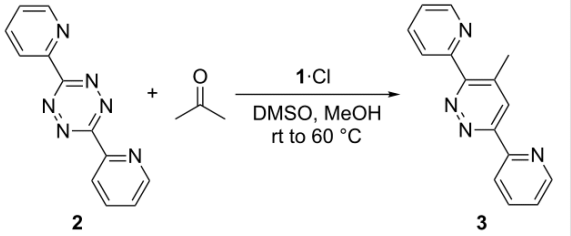

Scheme 6: Reaction R3: substrate **2**, acetone and charge-tagged catalyst **1**·Cl.

As the reaction R3 does not show conversion at room temperature, the mixture was successively heated up to 60 °C. Small samples were taken from the reaction flask at regular intervals, diluted and fed into the ESI source. Signals corresponding to tetrazine substrate **2** (*m*/*z* 259, *m*/*z* 275, *m*/*z* 495, *m*/*z* 549), pyridazine product **3** (*m*/*z* 249, *m*/*z* 271) and catalyst **1** (*m*/*z* 313, *m*/*z* 549) were observed as expected (Figure 7).

In addition, signals corresponding to all three proposed intermediates (Scheme 7) were found: intermediate $\mathbf{I_3}$ (*m*/*z* 353), dihydropyridazine intermediate $\mathbf{III_3}$ (*m*/*z* 561) and, for the first time, the most intriguing bicyclic Diels–Alder intermediate $\mathbf{II_3}$

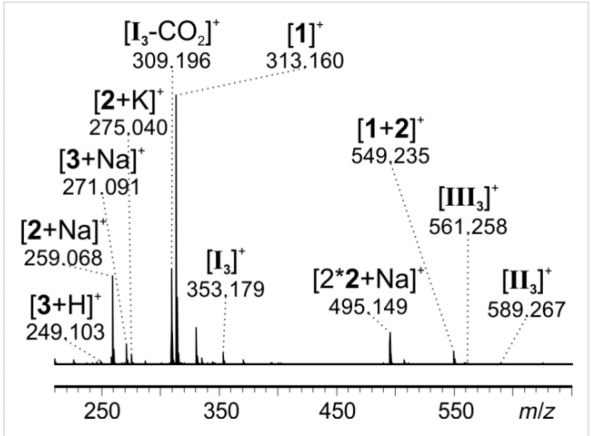

Figure 7: ESI mass spectrum of reaction R3 at 60 °C after 1.5 h.

(*m*/*z* 589). It has to be emphasized that each of these species was detected as an unmodified ion. As all intermediates are formed by reaction with the charge-tagged catalyst, they are inherently charged and do not need to be protonated during the ionization process. Ion $\mathbf{I_3}$ very easily loses CO_2 which causes the signal at *m*/*z* 309. This behavior could be confirmed by induced fragmentation experiments (see below).

Monitoring the temporal progress of reaction R3 was achieved by taking small samples at regular intervals, diluting and swiftly feeding them into the spectrometer (Figure 8). The conversion of substrate **2** to product **3** can easily be followed by the change of the respective signal intensities. The signal intensities for the intermediates stay relatively constant and are rather low for $\mathbf{II_3}$ and $\mathbf{III_3}$. The relatively high signal intensity of the intermediate $\mathbf{I_3}$ in contrast to the other two intermediates might indicate that the [4 + 2] cycloaddition between enamine intermediate $\mathbf{I_3}$ and tetrazine substrate **2** in R3 does not proceed as easily as for the

Beilstein J. Org. Chem. **2019,** *15,* 30–43.

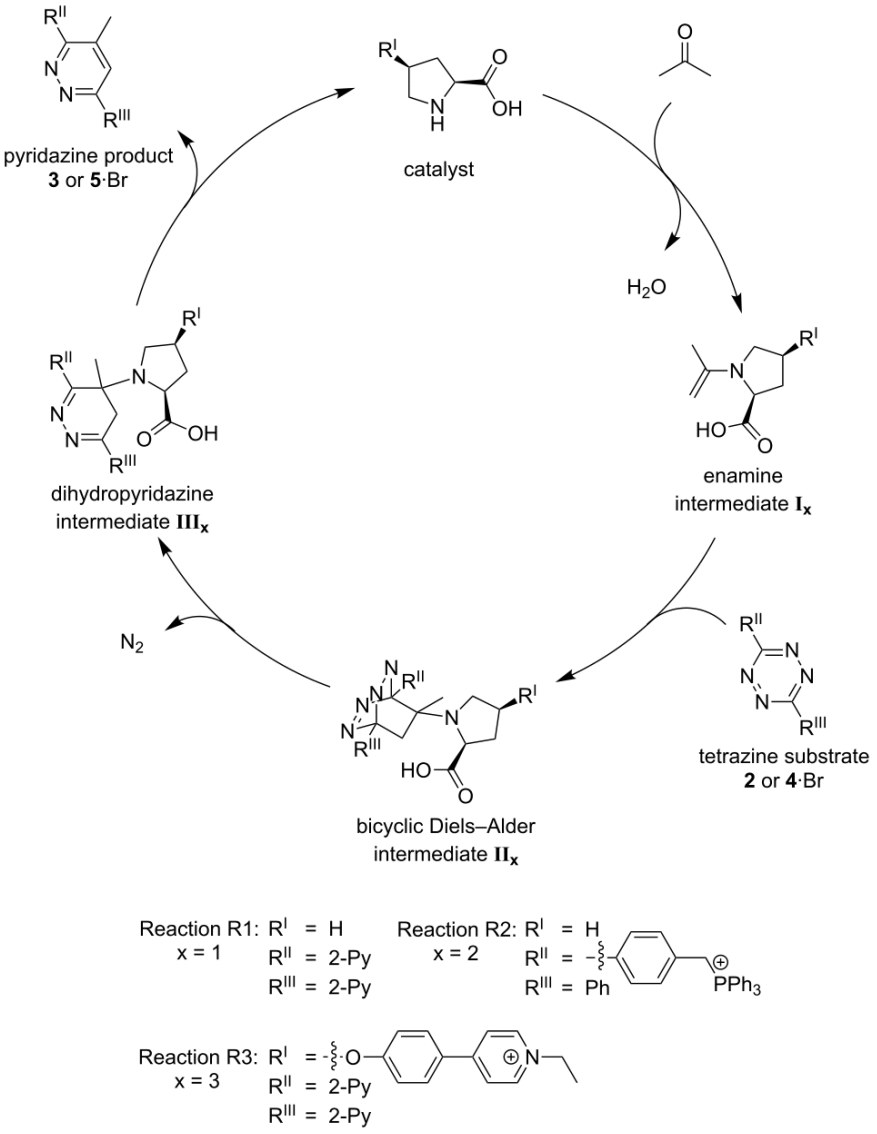

Scheme 7: General catalytic cycle for reactions R1–R3.

untagged reaction R1 discussed above. This difference in the kinetic behavior might be due to the higher steric hindrance for the [4 + 2] cycloaddition with the charge-tagged enamine intermediate $\mathbf{I_3}$ in comparison to the untagged enamine intermediate $\mathbf{I_1}$. Thus, the use of the charge-tagged catalyst was essential for the detection of the elusive, but mechanistically most interesting intermediate $\mathbf{II_3}$. However, this comes at the cost of putative changes of both the overall energy barrier of the reaction (R3 is significantly slower than R1) as well as the relative energetics of the elementary steps in the catalytic cycle (visible in the abundance ratio of intermediates).

All three intermediates could be further characterized by collision induced dissociation (CID) experiments (see below).

The signal at *m*/*z* 353 of intermediate $\mathbf{I_3}$ can correspond to three isomeric forms, i.e., enamine $[\mathbf{I_{3a}}]^+$, oxazolidinone $[\mathbf{I_{3b}}]^+$ or iminium $[\mathbf{I_{3c}}]^+$ (Figure 9). The oxazolidinone species is well known to exist in reacting solutions of L-proline-catalyzed reactions [43,45-47], but the enamine species has been detected as well [46]. The equilibrium is highly solvent-dependent. Gschwind and co-workers [46] found that for the condensation of L-proline with propanal in DMSO, 9% of the resulting

Beilstein J. Org. Chem. **2019,** *15,* 30–43.

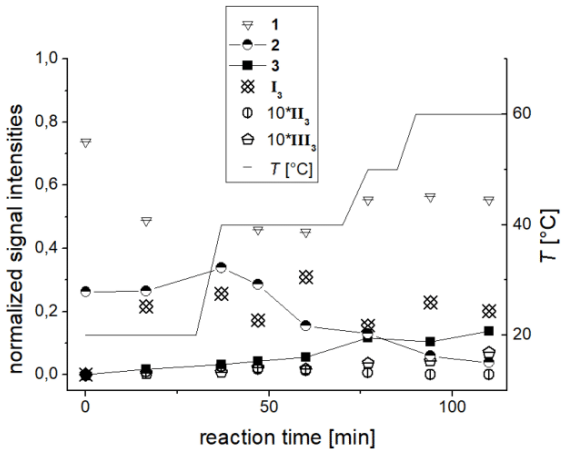

Figure 8: ESIMS monitoring of reaction R3. The plotted intensity values for each molecule are a sum of all corresponding signal intensities (i.e., $[M + H]^+$, $[M + Na]^+$, etc.). Signal intensities of $\mathbf{II}_3$ and $\mathbf{III}_3$ have been multiplied by a factor of ten for better visualization.

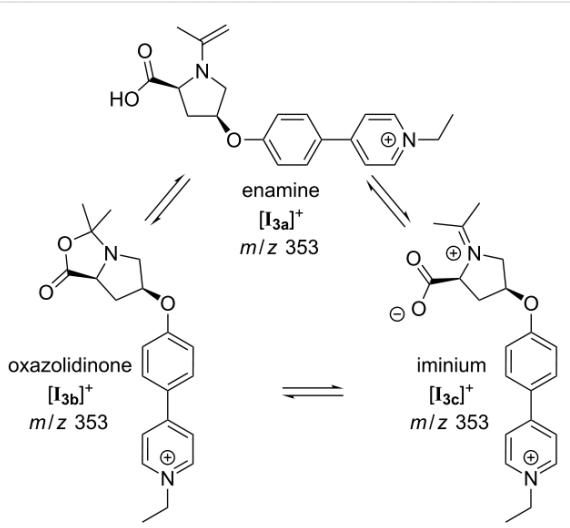

Figure 9: Isomeric forms in equilibrium: enamine $[\mathbf{I}_{3a}]^+$, oxazolidinone $[\mathbf{I}_{3b}]^+$ and iminium $[\mathbf{I}_{3c}]^+$.

species are the enamine species and 91% the two possible diastereomeric oxazolidinone species, and the oxazolidinone is the only NMR-detectable species with acetone in DMSO. As only the enamine species can act as a dienophile and not the oxazolidinone species, we here expect the presence of both isomers in the reacting solution with the oxazolidinone present in large excess. Upon CID of the mass-selected signal for $\mathbf{I}_3$ at *m*/*z* 353 (Figure 10), only elimination of CO_2 was observed. The spectra very much resemble the ones we obtained for ions with the same *m*/*z* observed when spraying acetonitrile solutions of **1**·Cl and acetone. These were characterized as the oxazolidinone species $[\mathbf{I}_{3b}]^+$ by infrared multiphoton dissociation (IRMPD) action spectroscopy in the gas phase [18,59]. The fragmentation already takes place at very low collision energies, so that some amount of fragmentation is expected to occur in the ESI source under normal ESI conditions – in accordance with the experimental observation as depicted in Figure 7.

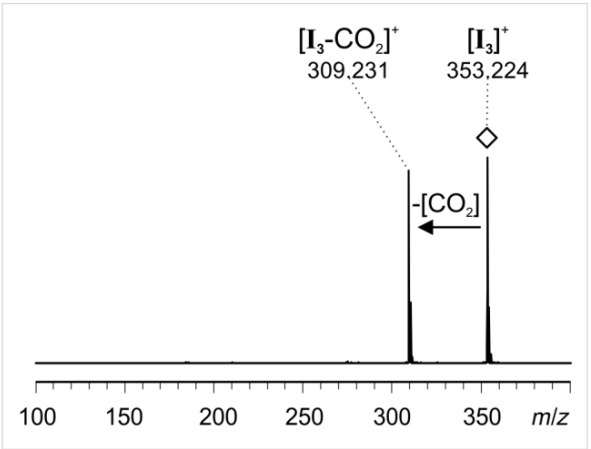

Figure 10: ESI(+) CID spectrum of mass-selected $[\mathbf{I}_3]^+$ (*m*/*z* 353); collision energy voltage 1 V.

CID of the bicyclic Diels–Alder intermediate $[\mathbf{II}_3]^+$ revealed a fascinating feature (Figure 11). $[\mathbf{II}_3]^+$ shows two competing fragmentation pathways upon collisional activation. On the one hand, it releases substrate **2** which leads back to the ion $[\mathbf{I}_3]^+$. This ion subsequently loses CO_2 as already observed in the CID experiment for $[\mathbf{I}_3]^+$ (Figure 10). The first pathway thus mimics going back one step in the catalytic cycle. On the other hand, $[\mathbf{II}_3]^+$ fragments into catalyst **1** by simultaneously cleaving off N_2 and the product **3**. The second pathway thus reflects going two steps ahead in the catalytic cycle. Such a combination of

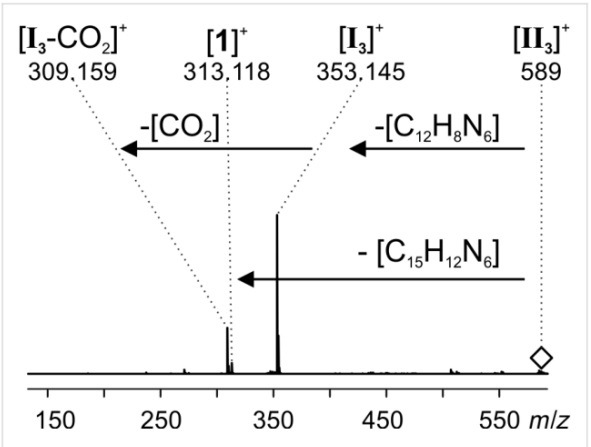

Figure 11: ESI(+) CID spectrum of mass selected $[\mathbf{II}_3]^+$ (*m*/*z* 589); collision energy voltage 5 V.

fragmentation pathways is in perfect accordance with expectations for a reaction intermediate $\mathbf{II_3}$ at this position in the catalytic cycle.

Finally, CID of the mass-selected dihydropyridazine intermediate $\mathbf{III_3}$ again leads to catalyst **1** by elimination of product **3** (Figure 12). Thus, also the last step of the catalytic cycle is viable in the gas phase which lends further support to the interpretation of the observed ions as reaction intermediates.

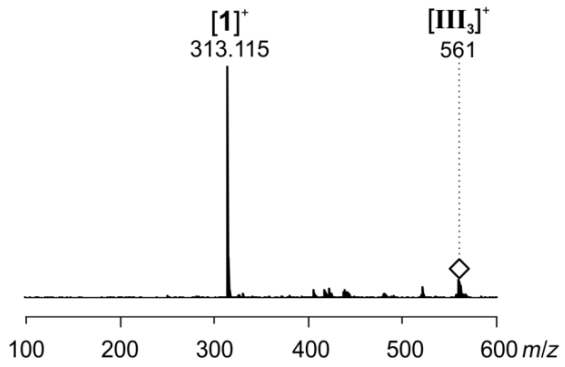

Figure 12: ESI(+) CID spectrum of mass selected $[\mathbf{III_3}]^+$ (*m/z* 561); collision energy voltage 10 V.

Conclusion

The L-proline-catalyzed reaction between acetone and 3,6-di(2-pyridyl)-1,2,4,5-tetrazine (**2**) via a Diels–Alder reaction with inverse electron demand was thoroughly studied by ^{1}H NMR and ESIMS. Without modification of the substrates, the progress of the reaction could be monitored over time, but only two out of three proposed intermediates of the postulated catalytic cycle [51] could be experimentally detected. The use of a charge-tagged reactant did not lead to better results. However, the charge-tagged proline derivative $\mathbf{1}^+$ designed for an enhanced mass spectrometric detection of low-concentrated intermediates made it possible to detect all relevant species of the reaction including the elusive Diels–Alder intermediate $\mathbf{II_3}$. The direct observation of this ion is the first experimental proof that the reaction is not concerted, but does proceed in a stepwise manner. The three intermediates could be further characterized by collision-induced dissociation in the gas phase. The observed fragmentation pathways mimic the neighboring steps in the catalytic cycle and thus give further support for the intermediate nature of the detected species.

Experimental

ESIMS and NMR experiments

All ESIMS experiments were conducted with a micrOTOF-Q mass spectrometer from Bruker Daltonik. Before each measurement, the settings were tuned for high signal intensities. The parameters were adjusted accordingly for each measurement within the following ranges or were constant: end plate offset: −500 V, capillary voltage: −5000 V to −3000 V, nebulizer gas: 1–4 bar, dry gas: 1–3 L/min, dry temperature: 200 °C, collision energy: 1–8 eV, collision RF: 120–155 Vpp, transfer time: 134 µs, pre pulse storage: 8–10 µs, funnel 1 RF: 150–200 Vpp, funnel 2 RF: 150–200 Vpp, hexapole RF: 150 Vpp, ISCID energy: 0 eV, quadrupole ion energy: 1–6 eV. The mass calibration in the MS^2 spectra was unfortunately slightly shifted. The measured *m/z* values are about 35 mDa too high (Figure 10) and about 40 mDa too low (Figure 11 and Figure 12). PEEK tubes with an inner diameter of 0.127 mm and PEEK microreactors (swept volume: 2.2 µL) were used. Airtight glass syringes (250 µL and 5 mL) from Hamilton and syringe pumps (single and double) from Cole Parmer were used.

All kinetic ^{1}H NMR experiments were conducted with a Bruker Avance III HD Ascend 700 MHz spectrometer equipped with a 5 mm QCI H-P/C/N cryoprobe with Z-gradient coils. The sample was shimmed before the first measurement. Then, spectra were measured with only one scan in defined intervals without ejecting the sample tube from the instrument.

Reaction R1 (acetone, untagged substrate, L-proline, rt)

Experiment 1 NMR

A solution of L-proline in deuterated dimethyl sulfoxide (1.206 mL, 0.58 mmol/L, 0.0007 mmol, 0.05 equiv) was added to commercially available 3,6-di(2-pyridyl)-1,2,4,5-tetrazine (**2**, 3.3 mg, 0.014 mmol, 1.0 equiv). Additional 1.764 mL of deuterated dimethyl sulfoxide were added. The concentration was chosen sufficiently low to ensure that all components were fully dissolved at room temperature. A solution of acetone in deuterated dimethyl sulfoxide solution was added last (41 µL, 1.4 mmol/mL, 0.057 mmol, 4 equiv) to start the reaction. The first spectrum was measured 6:14 minutes after the start of the reaction. Then spectra were measured in intervals of 5 minutes at room temperature. The plotted signal intensities were normalized to the dimethyl sulfoxide solvent peak.

Experiment 2 ESIMS

Commercially available 3,6-di(2-pyridyl)-1,2,4,5-tetrazine (**2**, 50 mg, 0.20 mmol, 1.0 equiv) and L-proline (1.2 mg, 0.01 mmol, 0.05 equiv) were mixed in 10 mL dimethyl sulfoxide. Acetone (63 µL, 0.8 mmol, 4 equiv) was added last. In regular intervals, samples of 1 µL were taken directly from the reaction mixture and immediately diluted in 0.5 mL acetonitrile. The diluted samples were fed into the mass spectrometer in a timely manner with a flow rate of 300 µL/h.

Beilstein J. Org. Chem. **2019,** *15,* 30–43.

Experiment 3 ESIMS (enamine preformation)

L-proline (1.2 mg, 0.01 mmol, 1.0 equiv) and acetone (72 µL, 0.97 mmol, 95 equiv) were mixed in 5 mL dimethyl sulfoxide and stirred at room temperature for 10 min. The preformation of enamine $\mathbf{I_1}$ was validated with ESIMS. Afterwards, commercially available 3,6-di(2-pyridyl)-1,2,4,5-tetrazine (**2**, 2.4 mg, 0.01 mmol, 1.0 equiv) was added. In regular intervals, samples of 20 µL were taken directly from the reaction mixture and immediately diluted in 0.5 mL acetonitrile. The diluted samples were fed into the mass spectrometer in a timely manner with a flow rate of 200 µL/h.

Reaction R2 (acetone, charge-tagged substrate, L-proline, rt) ESIMS

A 0.4 mmol/L stock solution of **4**·Br in dimethyl sulfoxide was prepared (stock solution ss_1), as well as a 0.001 mmol/L stock solution of L-proline in dimethyl sulfoxide/acetone 1:1 (stock solution ss_2).

Continuous flow setup

A continuous flow setup [4,17,18] was used for the experiment. A schematic depiction of the setup can be found in Scheme S2, Supporting Information File 1. An airtight syringe s_1 was loaded with stock solution ss_1 and syringe s_2 was loaded with stock solution ss_2. By using a double syringe pump, the contents of s_1 and s_2 were pumped via PEEK tubes with a flow rate f_A = 75 µL/h into microreactor m_A, where they were mixed. From microreactor m_A the combined solutions flowed towards microreactor m_B where they were diluted with DMSO, which was injected with flow rate f_B = 150 µL/h. The outlet of microreactor m_B was directly fed into the spectrometer with an effective flow rate of $f_B + 2 \times f_A$ = 300 µL/h. The theoretical reaction time was calculated. Further details on the calculation can be found in Supporting Information File 1.

Syringe setup

1 mL (0.0004 mmol, 1 equiv of **4**·Br) of stock solution ss_1 was mixed with 2 mL dimethyl sulfoxide and 1 mL of stock solution ss_2, which contained 0.001 mmol, 4 equiv of L-proline and 0.5 mL of acetone.

A 5 mL syringe was charged with the combined solution and fed it into the ESI source of the mass spectrometer over a period of 4 h with a flow rate of 400 µL/h, while spectra were taken continuously.

Reaction R3 (acetone, untagged substrate, charge-tagged catalyst, rt to 60 °C) ESIMS

Commercially available 3,6-di(2-pyridyl)-1,2,4,5-tetrazine (**2**, 19 mg, 0.08 mmol, 1 equiv) and **1**·Cl (6 mg, 0.02 mmol, 0.2 equiv) were mixed in 1.13 mL dimethyl sulfoxide and 0.2 mL methanol. Acetone (600 µL, 3.87 mmol, 50 equiv) was added last. During the experiment the temperature was slowly raised from room temperature up to 60 °C (see temperature curve in Figure 7 and Figure S3, Supporting Information File 1). In regular intervals, samples of 2 µL were taken directly from the reaction mixture and immediately diluted with 0.5 mL of a (1:1) mixture of methanol and acetonitrile. The diluted samples were fed into the ESI source of the mass spectrometer in a timely manner with a flow rate of 300 µL/h.

A CID experiment of **1** has been performed (Figure S1, Supporting Information File 1).

Synthesis

All ratios given are volume ratios unless stated otherwise. Commercially available chemicals were used without prior purification. Solvents (cyclohexane, dichloromethane, ethyl acetate) were dried with standardized methods. Inert gas atmosphere reactions were performed under argon using standard Schlenk techniques and oven-dried glassware prior to use. Thin-layer chromatography was performed with TLC plates form Merck (aluminum sheets silica gel 60 F_{254}) and detection was performed by fluorescent light λ = 245 nm and λ = 366 nm. Purification of products by column chromatography was done on silica gel 60, 40–63 µm from Merck. For ^{1}H and ^{13}C NMR analysis a Bruker Avance I 400 MHz instrument was used with 400 MHz for ^{1}H spectra, 162 MHz for ^{31}P spectra and 101 MHz for ^{13}C spectra or a Bruker Avance I 500 MHz instrument was used with 500 MHz for ^{1}H spectra and with 126 MHz for ^{13}C spectra. The allocation of NMR signals was accomplished with H,H-COSY, HMBC or HSQC spectra. Deuterated solvents chloroform-d_1 and DMSO-d_6 were obtained from Deutero GmbH and the remaining non-deuterated solvent signals were used as internal standards as references for the ^{1}H shifts and ^{13}C shifts which are all reported on the δ [ppm] scale. UV–vis spectra were measured on a Lambda 18 instrument from Perkin Elmer and fluorescence spectra were measured on a LS50B instrument from Perkin Elmer. All EI spectra were measured on a MAT 95 XL instrument from Thermo Finnigan and ESI spectra of synthesized compounds were measured with either the micrOTOF-Q instrument from Bruker Daltonik GmbH or with an Orbitrap XL instrument from Thermo Fisher Scientific.

Charge-tagged catalyst (**1**·Cl)

The charge-tagged catalyst **1**·Cl was synthesized according to the protocol of Willms et al. [18].

1-Benzoyl-2-*p*-toluoylhydrazide (**6**)

Under argon atmosphere benzhydrazide (0.09 g, 0.64 mmol, 1.0 equiv) was dissolved in dichloromethane (6.5 mL) and

within 40 min *p*-toluoyl chloride (0.11 g, 0.71 mmol, 1.1 equiv) in dichloromethane (1.3 mL) was added dropwise under constant stirring. A colorless solid precipitated. The suspension was stirred for 1 h at room temperature. The solid was filtered off and washed with dichloromethane (10 mL) and dried in vacuo. 0.12 g of raw product were obtained and purified via column chromatography (ethyl acetate/cyclohexane 4:1, R_f = 0.91). 0.10 g of colorless solid were obtained. The protocol has been adapted from Wang et al. [55]. Yield: 0.10 g (0.39 mmol, 83%), ^{1}H NMR (400 MHz, DMSO-d_6, 298 K) δ [ppm] 10.46 (s, 2H, H-7, H-8), 7.96–7.93 (m, 2H, H-11), 7.85 (pd, 2H, H-4), 7.62–7.57 (m, 1H, H-13), 7.55–7.50 (m, 2H, H-12), 7.33 (pd, 2H, H-3), 2.38 (s, 3H, H-1); ^{13}C{^{1}H} NMR (101 MHz, DMSO-d_6, 298 K) δ [ppm] 165.9 (C-9), 165.8 (C-6), 141.9 (C-2), 132.6 (C-13), 131.8 (C-10), 129.8 (C-5), 129.0 (C-3), 128.5 (C-12), 127.51 (C-4), 127.47 (C-11), 21.1 (C-1). The numbering of the atoms in the molecule can be found in Supporting Information File 1. The allocation of signals has been done with HMBC and HSQC spectra. HRESIMS(+) *m/z*: [M + Na]$^+$ calcd for $C_{15}H_{14}N_2O_2Na$, 277.0947; found, 277.0981.

N-(Chloro(phenyl)methylene)-4-methylbenzohydrazonoyl chloride (**7**)

Under argon atmosphere **6** (1.00 g, 7.34 mmol, 1.0 equiv) was dissolved in toluene (50 mL) and phosphorous pentachloride (8.05 g, 36.72 mmol, 5.0 equiv) was added. The mixture was stirred at reflux conditions for 3 h. The solvent was distilled of in vacuo at 40 °C. The raw product (0.65 g) was purified via column chromatography (cyclohexane/dichloromethane, 100:1, R_f = 0.23). A yellow solid was obtained (0.48 g). The protocol has been adapted from Wang et al. [55]. Yield: 0.48 g (1.65 mmol, 48%), ^{1}H NMR (400 MHz, $CDCl_3$, 298 K) δ [ppm] 8.17–8.14 (m, 2H, H-9), 8.04 (pd, 2H, H-4), 7.56–7.52 (m, 1H, H-11), 7.51–7.46 (m, 2H, H-10), 7.29 (pd, 2H, H-3), 2.44 (s, 3H, H-1); ^{13}C{^{1}H} NMR (101 MHz, $CDCl_3$, 298 K) δ [ppm] 144.6 (C-7), 144.3 (C-6), 142.6 (C-2), 133.9 (C-8), 131.9 (C-11), 131.1 (C-5), 129.4 (C-3), 128.69 (C-4, C-9), 128.65 (C-10), 21.7 (C-1). The numbering of the atoms in the molecule can be found in Supporting Information File 1. The allocation of signals has been done with HMBC and HSQC spectra; EIMS (70 eV) *m/z* (%): 290.0 (69) [M]$^{+\bullet}$, 255.0 (69) [M − Cl]$^+$, 152.0 (100) [M − C_8H_7Cl]$^{+\bullet}$, 138.0 (47), 117.0 (38), 103.0 (39), 91.0 (42) [C_7H_7]$^+$, 77.0 (39)) [C_6H_5]$^+$.

3-(4-Methylphenyl)-6-phenyl-1,2,4,5-tetrazine (**8**)

7 (434 mg, 1.66 mmol, 1 equiv) was dissolved in 11 mL acetonitrile and hydrazine (98 µL, 1.66 mmol, 1 equiv) was added. The mixture was refluxed for 1 h behind a blast shield. Then potassium carbonate (412 mg, 3.31 mmol, 2 equiv) was added and the mixture was refluxed for another 24 h. Hydrazine (587 µL, 9.93 mmol, 6 equiv) was added again and the mixture was refluxed for 1 h. When the mixture had cooled to room temperature 10 mL of dichloromethane were added. The organic layer was washed with brine and dried over magnesium sulfate. The solvents were evaporated and the remaining solid was dissolved in 4.4 mL acetic acid at 0 °C. The mixture was stirred while a solution of sodium nitrite (839 mg, 12.17 mmol, 7.4 equiv) in 1 mL of deionized water was added dropwise. The mixture was stirred for another 3 h, after the solution of sodium nitrite had been added. 55 mL dichloromethane were added and the organic layer was washed twice with saturated sodium hydrogen carbonate solution and dried over magnesium sulfate. The solvents were evaporated and 340 mg of a pink raw product were purified with column chromatography (cyclohexane/dichloromethane 7:3, R_f = 0.41). 193 mg of a pink solid were obtained. Yield: 193 mg (0.78 mmol, 52%), ^{1}H NMR (400 MHz, $CDCl_3$, 298 K) δ [ppm] 8.66–8.62 (m, 2H, H-9), 8.54 (pd, 2H, H-4), 7.66–7.58 (m, 3H, H-10 and H-11), 7.42 (pd, 2H, H-3), 2.48 (s, 3H, H-1); ^{13}C{^{1}H} NMR (101 MHz, $CDCl_3$, 298 K) δ [ppm] 164.1 (C-6), 163.9 (C-7), 143.6 (C-2), 132.7 (C-11), 132.0 (C-8), 130.2 (C-3), 129.4 (C-10), 129.2 (C-5), 128.1 (C-4), 128.0 (C-9), 21.9 (C-1). The numbering of the atoms in the molecule can be found in Supporting Information File 1. The allocation of NMR signals was accomplished with H,H-COSY, HMBC and HSQC spectra; HREIMS: [M]$^{+\bullet}$ calcd for $C_{15}H_{12}N_4$, 248.1062; found, 248.1059.

3-(4-Bromomethylphenyl)-6-phenyl-1,2,4,5-tetrazine (**9**)

9 was prepared in a slight modification of the protocol used by de Almeida et al. [57]. **8** (76 mg, 0.31 mmol, 1 equiv) and TBCA (tribromoisocyanuric acid, 336 mg, 0.92 mmol, 3 equiv) were refluxed in 3 mL ethyl acetate for six hours. The precipitated cyanuric acid was filtered off over Celite®. The solvent was evaporated and 102 mg of a pink raw product was obtained. The raw product was purified via column chromatography (cyclohexane/ethyl acetate, 10:0.25, R_f = 0.1) and 45 mg of a pink product were obtained. Yield: 45 mg (0.14 mmol, 45%), ^{1}H NMR (500 MHz, $CDCl_3$, 298 K) δ [ppm] 8.67–8.63 (m, 4H, H-4, H-9), 7.67–7.60 (m, 5H, H-3, H-11, H-10), 4.58 (s, 2H, H-1); ^{13}C{^{1}H} NMR 126 MHz, $CDCl_3$, 298 K) δ [ppm] 164.1 and 163.7 (C-6, C-7)*, 142.6 (C-2), 132.9 (C-11), 131.9 and 131.9 (C-5, C-8)*, 130.1 (C-3), 129.5 (C-10), 128.5 and 128.2 (C-4, C-9)*, 32.5 (C-1). The numbering of the atoms in the molecule can be found in Supporting Information File 1. *The two signals can only be allocated to either two carbon atoms. The allocation of NMR signals was accomplished with H,H-COSY, HMBC and HSQC spectra. UV–vis: 307.5 nm global maximum, 224.5 nm local maximum, 549 nm local maximum. Fluorescence (excitation 307 nm): 358.5 nm global maximum, 610.5 local maximum. HREIMS: [M]$^{+\bullet}$ calcd for $C_{15}H_{11}BrN_4$, 326.0167; found, 326.0165; EIMS *m/z* (%): 326.0 (3%) [M]$^{+\bullet}$,

247.1 (4%) $[M - Br]^+$, 116.0 (100%) $[M - C_7H_5BrN_3]^+$, 103.0 (36%), 76.0 (7%).

TBCA preparation

The synthesis of tribromoisocyanuric acid was conducted according to the procedure of de Almeida et al. [57]. A solution of OXONE® (14.29 g, 46.49 mmol, 3 equiv, ingredients see below) in 186 mL deionized water was added dropwise to a 0 °C cold stirred solution of cyanuric acid (2.00 g, 15.50 mmol, 1 equiv), sodium hydroxide (1.86 g, 46.49 mmol, 3 equiv), sodium carbonate (2.46 g, 23.24 mmol, 1.5 equiv) and potassium bromide (5.53 g, 46.49 mmol, 3 equiv) in 223 mL deionized water within 2 h. The solution was stirred at room temperature for 24 h. The precipitated white solid was filtered off and washed with cold deionized water. TBCA was directly used for the synthesis of **9** without further treatment.

Triphenyl[4-(6-phenyl-1,2,4,5-tetrazin-3-yl)benzyl]-phosphonium bromide (**4**·Br)

4·Br was prepared in a slight modification of the protocol published by Vikse et al. [53]. Under argon atmosphere **9** (40 mg, 0.12 mmol, 1 equiv) and triphenylphosphane (67 mg, 0.18 mmol, 1.5 equiv) were mixed in 0.47 mL toluene and stirred at 50 °C for 24 h. Dichloromethane (15 mL) was added and the organic layer was washed six times with a 2:1 mixture of deionized water/methanol (6 × 40 mL). The aqueous layer was evaporated to yield 17 mg of a light pink solid. The ^{1}H NMR, ^{31}P NMR and ESIMS spectra show an impurity of triphenylphosphine oxide in the product, which does not interfere with the ESIMS experiment in which **4**·Br was used as the charge-tagged substrate. Yield: 17 mg (0.03 mmol, ≈27% including impurity), ^{1}H NMR (400 MHz, $CDCl_3$, 298 K) δ [ppm] 8.54–8.52 (m, 2H, H-4), 8.26–8.24 (m, 2H, H-9), 7.88–7.84 (m, 6H, H-14), 7.78–7.75 (m, 3H, H-16), 7.69–7.58 (m, 9H, 6H of the 9H correlate to H-15, rest correlates to impurity of $POPh_3$), 7.55–7.52 (m, 2H, H-3), 7.48–7.45 (m, 1H, H-11), 7.40–7.37 (m, 2H, H-10), 5.85 (d, 2H, H-1); ^{13}C{^{1}H} NMR (126 MHz, $CDCl_3$, 298 K) δ [ppm] 164.0 (C-6), 163.6 (C-7), 135.1 or 135.1 (C 13), 134.8 (C-14), 134.7 (C-16), 132.8 or 132.8 or 132.8 (C-5 and C-8), 130.4 or 130.3 (C-15), 129.4 (C-3), 128.7 (C-10), 128.6 (C-11), 128.1 (C-4), 128.1 (C-9), 128.1, 118.3 (C-2), 117.6 (C-2), 31.0 or 30.6 (C-1). Signals not allocated to **4**·Br: 132.9, 132.7, 132.3, 132.2, 132.1, 131.7, 131.7, 131.6; ^{31}P{^{1}H} NMR (162 MHz, $CDCl_3$, 298 K) δ [ppm] 29.22 (triphenylphosphine oxide), 23.72 (P-12). The numbering of the atoms in the molecule can be found in Supporting Information File 1. The allocation of NMR signals was accomplished with H,H-COSY, HMBC and HSQC spectra. UV–vis: local maximum ≈240 nm, local maximum ≈300 nm, local maximum 548.5 nm. Fluorescence (excitation 302 nm): 368.0 nm global maximum. HRESIMS: $[M]^+$ calcd for $C_{33}H_{26}N_4P^+$, 509.1890; found, 509.1884. ESI-CID (Figure S4, Supporting Information File 1).

Supporting Information

Supporting Information File 1

Additional material.
[https://www.beilstein-journals.org/bjoc/content/supplementary/1860-5397-15-3-S1.pdf]

Acknowledgements

Financial support by the DFG (SFB 813) is gratefully acknowledged.

ORCID® iDs

Marianne Engeser - https://orcid.org/0000-0001-6987-4126

References

1. Fenn, J. B. *Angew. Chem., Int. Ed.* **2003,** *42,* 3871–3894. doi:10.1002/anie.200300605
2. Cole, R. B. *Electrospray ionization mass spectrometry. Fundamentals, instrumentation, and applications;* Wiley: New York, NY, 1997.
3. Gross, J. H. *Mass spectrometry. A textbook;* Springer: Berlin, 2004. *with tables;* 1. ed, corr. 2. print.
4. Santos, L. S.; Knaack, L.; Metzger, J. O. *Int. J. Mass Spectrom.* **2005,** *246,* 84–104. doi:10.1016/j.ijms.2005.08.016
5. Schröder, D. *Acc. Chem. Res.* **2012,** *45,* 1521–1532. doi:10.1021/ar3000426
6. Yunker, L. P. E.; Stoddard, R. L.; McIndoe, J. S. *J. Mass Spectrom.* **2014,** *49,* 1–8. doi:10.1002/jms.3303
7. Santos, L. S.; Metzger, J. O. *Angew. Chem., Int. Ed.* **2006,** *45,* 977–981. doi:10.1002/anie.200503307
8. Aliprantis, A. O.; Canary, J. W. *J. Am. Chem. Soc.* **1994,** *116,* 6985–6986. doi:10.1021/ja00094a083
9. Yan, X.; Sokol, E.; Li, X.; Li, G.; Xu, S.; Cooks, R. G. *Angew. Chem., Int. Ed.* **2014,** *53,* 5931–5935. doi:10.1002/anie.201310493
10. Santos, L. S.; Pavam, C. H.; Almeida, W. P.; Coelho, F.; Eberlin, M. N. *Angew. Chem., Int. Ed.* **2004,** *43,* 4430–4433. doi:10.1002/anie.200460059
11. Amarante, G. W.; Benassi, M.; Milagre, H. M. S.; Braga, A. A. C.; Maseras, F.; Eberlin, M. N.; Coelho, F. *Chem. – Eur. J.* **2009,** *15,* 12460–12469. doi:10.1002/chem.200900966
12. Amarante, G. W.; Benassi, M.; Pascoal, R. N.; Eberlin, M. N.; Coelho, F. *Tetrahedron* **2010,** *66,* 4370–4376. doi:10.1016/j.tet.2010.04.018
13. Regiani, T.; Santos, V. G.; Godoi, M. N.; Vaz, B. G.; Eberlin, M. N.; Coelho, F. *Chem. Commun.* **2011,** *47,* 6593–6595. doi:10.1039/c1cc10678c
14. Rodrigues, T. S.; Silva, V. H. C.; Lalli, P. M.; de Oliveira, H. C. B.; da Silva, W. A.; Coelho, F.; Eberlin, M. N.; Neto, B. A. D. *J. Org. Chem.* **2014,** *79,* 5239–5248. doi:10.1021/jo500799j
15. Galaverna, R.; Camilo, N. S.; Godoi, M. N.; Coelho, F.; Eberlin, M. N. *J. Org. Chem.* **2016,** *81,* 1089–1098. doi:10.1021/acs.joc.5b02651

16. Guillena, G.; Hita, M. d. C.; Nájera, C.; Viózquez, S. F. *J. Org. Chem.* **2008,** *73,* 5933–5943. doi:10.1021/jo800773q
17. Marquez, C.; Metzger, J. O. *Chem. Commun.* **2006,** 1539–1541. doi:10.1039/b518288c
18. Willms, J. A.; Beel, R.; Schmidt, M. L.; Mundt, C.; Engeser, M. *Beilstein J. Org. Chem.* **2014,** *10,* 2027–2037. doi:10.3762/bjoc.10.211
19. Fürmeier, S.; Metzger, J. O. *J. Am. Chem. Soc.* **2004,** *126,* 14485–14492. doi:10.1021/ja046157z
20. Teichert, A.; Pfaltz, A. *Angew. Chem., Int. Ed.* **2008,** *47,* 3360–3362. doi:10.1002/anie.200705082
21. Harvey, D. J.; Watanabe, Y.; Allen, J. D.; Rudd, P.; Pagel, K.; Crispin, M.; Struwe, W. B. *J. Am. Soc. Mass Spectrom.* **2018,** *29,* 1250–1261. doi:10.1007/s13361-018-1930-1
22. Cech, N. B.; Enke, C. G. *Mass Spectrom. Rev.* **2001,** *20,* 362–387. doi:10.1002/mas.10008
23. Adlhart, C.; Chen, P. *Helv. Chim. Acta* **2000,** *83,* 2192–2196. doi:10.1002/1522-2675(20000906)83:9<2192::aid-hlca2192>3.0.co;2-g
24. Schade, M. A.; Fleckenstein, J. E.; Knochel, P.; Koszinowski, K. *J. Org. Chem.* **2010,** *75,* 6848–6857. doi:10.1021/jo101337a
25. Luo, J.; Oliver, A. G.; McIndoe, J. S. *Dalton Trans.* **2013,** *42,* 11312–11318. doi:10.1039/c3dt51212f
26. Beierlein, C. H.; Breit, B.; Paz Schmidt, R. A.; Plattner, D. A. *Organometallics* **2010,** *29,* 2521–2532. doi:10.1021/om100131t
27. Polyansky, D. E.; Muckerman, J. T.; Rochford, J.; Zong, R.; Thummel, R. P.; Fujita, E. *J. Am. Chem. Soc.* **2011,** *133,* 14649–14665. doi:10.1021/ja203249e
28. Iacobucci, C.; Reale, S.; De Angelis, F. *Angew. Chem., Int. Ed.* **2016,** *55,* 2980–2993. doi:10.1002/anie.201507088
29. Dalko, P. I.; Moisan, L. *Angew. Chem., Int. Ed.* **2001,** *40,* 3726–3748. doi:10.1002/1521-3773(20011015)40:20<3726::aid-anie3726>3.0.co;2-d
30. Dalko, P. I. *Enantioselective Organocatalysis;* Wiley-VCH Verlag GmbH & Co. KGaA: Weinheim, Germany, 2007.
31. Berkessel, A.; Gröger, H. *Asymmetric Organocatalysis // Reduction of Carbonyl Compounds;* Wiley-VCH Verlag GmbH & Co. KGaA: Weinheim, Germany, 2005.
32. Melchiorre, P.; Marigo, M.; Carlone, A.; Bartoli, G. *Angew. Chem., Int. Ed.* **2008,** *47,* 6138–6171. doi:10.1002/anie.200705523
33. Dalko, P. I.; Moisan, L. *Angew. Chem., Int. Ed.* **2004,** *43,* 5138–5175. doi:10.1002/anie.200400650
34. MacMillan, D. W. C. *Nature* **2008,** *455,* 304–308. doi:10.1038/nature07367
35. Fiorani, G.; Guo, W.; Kleij, A. W. *Green Chem.* **2015,** *17,* 1375–1389. doi:10.1039/c4gc01959h
36. Govender, T.; Arvidsson, P. I.; Maguire, G. E. M.; Kruger, H. G.; Naicker, T. *Chem. Rev.* **2016,** *116,* 9375–9437. doi:10.1021/acs.chemrev.6b00156
37. Aursnes, M.; Tungen, J. E.; Hansen, T. V. *J. Org. Chem.* **2016,** *81,* 8287–8295. doi:10.1021/acs.joc.6b01375
38. Nájera, C.; Yus, M. *Tetrahedron Lett.* **2015,** *56,* 2623–2633. doi:10.1016/j.tetlet.2015.03.099
39. Candy, M.; Durand, T.; Galano, J.-M.; Oger, C. *Eur. J. Org. Chem.* **2016,** 5813–5816. doi:10.1002/ejoc.201601301
40. List, B.; Lerner, R. A.; Barbas, C. F. *J. Am. Chem. Soc.* **2000,** *122,* 2395–2396. doi:10.1021/ja994280y
41. Clemente, F. R.; Houk, K. N. *Angew. Chem., Int. Ed.* **2004,** *43,* 5766–5768. doi:10.1002/anie.200460916
42. Seebach, D.; Beck, A. K.; Badine, D. M.; Limbach, M.; Eschenmoser, A.; Treasurywala, A. M.; Hobi, R.; Prikoszovich, W.; Linder, B. *Helv. Chim. Acta* **2007,** *90,* 425–471. doi:10.1002/hlca.200790050
43. Bock, D. A.; Lehmann, C. W.; List, B. *Proc. Natl. Acad. Sci. U. S. A.* **2010,** *107,* 20636–20641. doi:10.1073/pnas.1006509107
44. Sharma, A. K.; Sunoj, R. B. *Angew. Chem., Int. Ed.* **2010,** *49,* 6373–6377. doi:10.1002/anie.201001588
45. Kanzian, T.; Lakhdar, S.; Mayr, H. *Angew. Chem., Int. Ed.* **2010,** *49,* 9526–9529. doi:10.1002/anie.201004344
46. Schmid, M. B.; Zeitler, K.; Gschwind, R. M. *Angew. Chem., Int. Ed.* **2010,** *49,* 4997–5003. doi:10.1002/anie.200906629
47. Haindl, M. H.; Hioe, J.; Gschwind, R. M. *J. Am. Chem. Soc.* **2015,** *137,* 12835–12842. doi:10.1021/jacs.5b03420
48. Eggert, F.; Kulikov, K.; Domnick, C.; Leifels, P.; Kath-Schorr, S. *Methods* **2017,** *120,* 17–27. doi:10.1016/j.ymeth.2017.04.021
49. Erdmann, R. S.; Takakura, H.; Thompson, A. D.; Rivera-Molina, F.; Allgeyer, E. S.; Bewersdorf, J.; Toomre, D.; Schepartz, A. *Angew. Chem., Int. Ed.* **2014,** *53,* 10242–10246. doi:10.1002/anie.201403349
50. van Geenen, F. A. M. G.; Franssen, M. C. R.; Zuilhof, H.; Nielen, M. W. F. *Anal. Chem.* **2018,** *90,* 10409–10416. doi:10.1021/acs.analchem.8b02290
51. Xie, H.; Zu, L.; Oueis, H. R.; Li, H.; Wang, J.; Wang, W. *Org. Lett.* **2008,** *10,* 1923–1926. doi:10.1021/ol800417q
52. Shihab, M. S. *Arabian J. Sci. Eng.* **2012,** *37,* 75–90. doi:10.1007/s13369-011-0167-0
53. Vikse, K. L.; Ahmadi, Z.; Manning, C. C.; Harrington, D. A.; McIndoe, J. S. *Angew. Chem., Int. Ed.* **2011,** *50,* 8304–8306. doi:10.1002/anie.201102630
54. Gautun, O.; Carlsen, P. *Molecules* **2001,** *6,* 969–978. doi:10.3390/61200969
55. Wang, D.; Chen, W.; Zheng, Y.; Dai, C.; Wang, L.; Wang, B. *Heterocycl. Commun.* **2013,** *19,* 171–177. doi:10.1515/hc-2013-0072
56. Liu, D. S.; Tangpeerachaikul, A.; Selvaraj, R.; Taylor, M. T.; Fox, J. M.; Ting, A. Y. *J. Am. Chem. Soc.* **2012,** *134,* 792–795. doi:10.1021/ja209325n
57. de Almeida, L. S.; Esteves, P. M.; de Mattos, M. C. S. *Tetrahedron Lett.* **2015,** *56,* 6843–6845. doi:10.1016/j.tetlet.2015.10.081
58. List, B.; Hoang, L.; Martin, H. J. *Proc. Natl. Acad. Sci. U. S. A.* **2004,** *101,* 5839–5842. doi:10.1073/pnas.0307979101
59. Willms, J. A.; Vidic, J.; Barthelmes, J.; Steinmetz, V.; Bredow,, T.; Maître, P.; Engeser, M. *Phys. Chem. Chem. Phys.* **2018**. manuscript submitted.

Beilstein J. Org. Chem. **2019,** *15,* 30–43.

3.3.3 Summary

With ^{1}H-NMR and ESI MS, the L-proline catalyzed reaction between acetone and a tetrazine via a *Diels-Alder* reaction with *inverse electron demand* was thoroughly studied. In the reaction without modified reactants, the temporal progress of the reaction could be monitored over time, however only two of the three postulated intermediates could be detected experimentally. Utilizing the charge-tagged tetrazine did not yield better results. The use of the charge-tagged catalyst facilitated the detection of all three postulated intermediates including the elusive Diels-Alder intermediate $\mathbf{II_3}$. The detection of this intermediate is the first experimental proof that the reaction proceeds in a stepwise manner and is not concerted. All three intermediates were studied with collision-induced dissociation experiments in the gas phase, which characterized them further. It was possible to mimic the intermediates' neighboring steps in the catalytic cycle, giving further support for their intermediate nature.

3.3.4 References

[1] A. Schnell, J. A. Willms, S. Nozinovic, M. Engeser, *Beilstein J. Org. Chem.* **2019**, *15*, 30.

[2] J. A. Willms, R. Beel, M. L. Schmidt, C. Mundt, M. Engeser, *Beilstein J. Org. Chem.* **2014**, *10*, 2027.

[3] H. Xie, L. Zu, H. R. Oueis, H. Li, J. Wang, W. Wang, *Org. Lett.* **2008**, *10*, 1923.

4 Mass spectrometric analysis of fossils

4.1 HPLC-ESI MS analysis of pigments in dinosaur egg shells

4.1.1 Introduction

Biliverdin (BV) and protoporphyrin IX (PP) are the color pigments of interest in this study (Figure 4.1.1). PP consists of the porphyrin ring, a tetrapyrrole macrocycle, and two carboxylic acid groups. BV is structurally related to PP by being the open-chain version of PP. PP has a brown color, which e.g. is responsible for the brown color in brown chicken eggs[1] (Figure 4.1.1 e)). BB has a blue color, which is the blue color in emu eggs (Figure 4.1.1b)). Both PP and BV are degradation product of heme[2], which becomes apparent in bruising, as BV is the reason why bruises appear blue underneath the skin.[3]

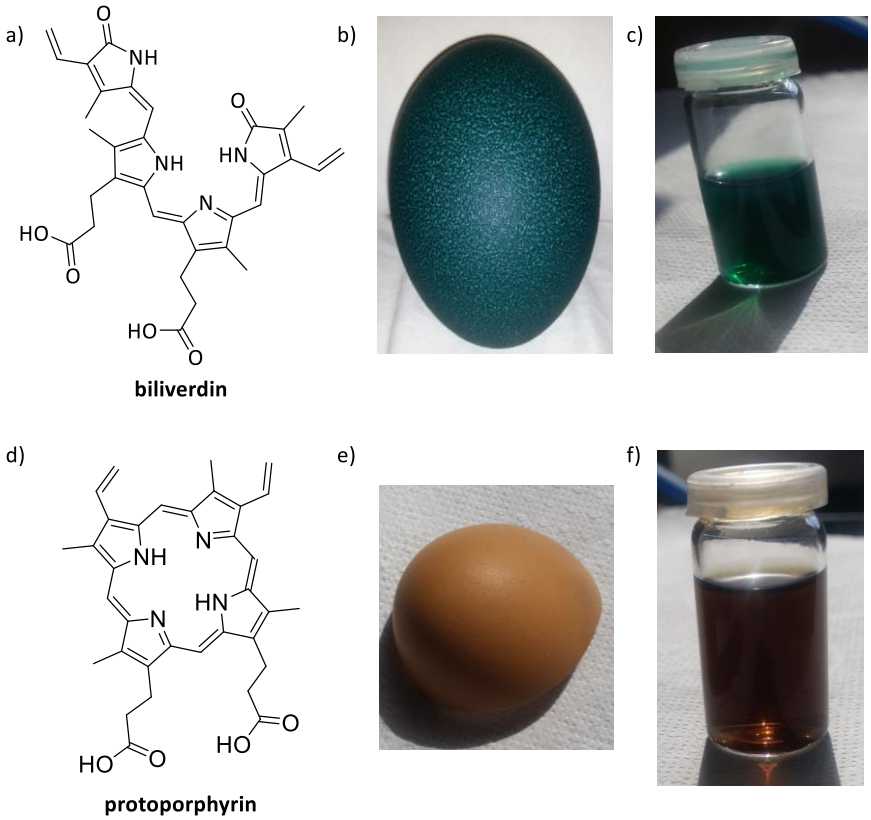

Figure 4.1.1 a) chemical structure of biliverdin, b) emu egg, c) biliverdin standard solution, d) chemical structure of protoporphyrin, e) brown chicken egg and f) protoporphyrin IX standard solution.

Both compounds are known to be the color pigments responsible for the coloration of bird egg shells.[4] Bird egg shell colors range from no color white (e.g. ostrich, white chicken egg) to the intensely colored emu and chicken egg shells with different maculation patterns, i.e. spots or streaks in between.[5–7] The coloration of egg shells is of scientific interest because it correlates with different ecological behaviors. One main benefit of coloration is the camouflaging aspect, which brings protection to the egg clutches against predators, while the parent birds leave the nest vulnerable due to e.g. food foraging.[5,7,8] The ostrich has white eggs because it does not need camouflaging coloration of its eggs as it is well able to

defend its clutches.[5,7] Crocodiles, birds' closest modern relatives, too have white egg shells, because they protect their reproductive investment by burying their eggs underground, making camouflaging coloration unnecessary.[9,10] Further, coloration of bird egg shells depends on nesting sites, as in open nesting camouflage is needed and eggs are colored, whereas in cavity and cave-breeding birds egg shell coloration is reduced.[8,10,11] The color of bird eggs can also protect against parasitic brooding, which would commonly be described as the "cuckoo phenomenon".[8,12–14] Through discrimination of the eggs color, the parasitic egg/"cuckoos egg" can be identified and ejected from the nest.[8,12–14]

HPLC-ESI MS is a suitable analytical method for the analysis of BV and PP as it is able to dissect and even quantify complex biological mixtures. It was used to study PP and BV in various sample types: rat liver extracts[15], urine[16,17], blood[16–18], feces[16,17,19], bacteria cultures[20], meat[21] or fish[22]. The method was also employed to study different extant bird egg shells.[6,8,13,23,24–27] *Igic* et al.[25] and *Verdes* et al.[24] not only studied BV and PP in extant birds but found BV and PP in subfossil eggshells from the extinct moa of New Zealand, which are approximately 500 years old. As samples for HPLC-ESI MS are liquid, the egg shells need to be extracted. Different extraction procedures have been published, but all are based on the dissolution of the shell's main component calcium carbonate and the subsequent dissolving of the color pigment in an organic solvent. An older procedure includes sulfuric acid and methanol, which results in the intentional methylation of BV and PP.[8,25,27] The methylation was necessary in early publications as the non-methylated compounds could not be separated[6]. However, the method is harsh, might result in the loss of pigments altogether and the separation of the non-methylated pigments is now possible.[6] Thus, a newer softer extraction procedure based on EDTA (ethylenediaminetetraacetic acid) was published[6,24], and a hydrochloric acid (HCl) based extraction method without methylation too[26]. The acids dissolve the carbonate of the calcium carbonate, whereas EDTA is a chelating ligand for the calcium ions.[28]

4.1.2 Preliminary work of *Wiemann* et al.[10]

Wiemann et al.[10] hypothesized that in the eggshells of bird-like non-avian Oviraptorosauria (Figure 4.1.1), BV and PP could have been present. This hypothesis is based on the following: birds evolved from dinosaurs so common traits are likely and already known, e.g. dinosaurs like birds laid eggs.[29,30] Further in open nesting birds coloration of the eggs is often observed.[5,7,8] Although dinosaurs, in general, buried their eggs, evidence indicates that Oviraptorosauria exhibited open nesting behavior.[29,30] Thus, *Wiemann* et al.[10] searched for BV and PP in three different 65 million years old oviraptorid (*Macroolithus yaotunensis*) eggs from three different provinces in China (Henan, Jiangxi and Guangdong, Figure 4.1.3, Figure 4.1.4), as to be able to draw conclusions about the nesting behavior of the Oviraptorosauria.[10]

Figure 4.1.2 Artist's reconstruction of a brooding oviraptor over a clutch of eggs. (Courtesy of Michael B. H. (https://commons.wikimedia.org/wiki/File:Nesting_Nemegtomaia.jpg))[31].

Figure 4.1.3 Geographical map of China with the capital Beijing marked with a red star and the three provinces in which the oviraptorid eggs were found highlighted in red. Figure was adapted from *Wiemann* et al.[10].

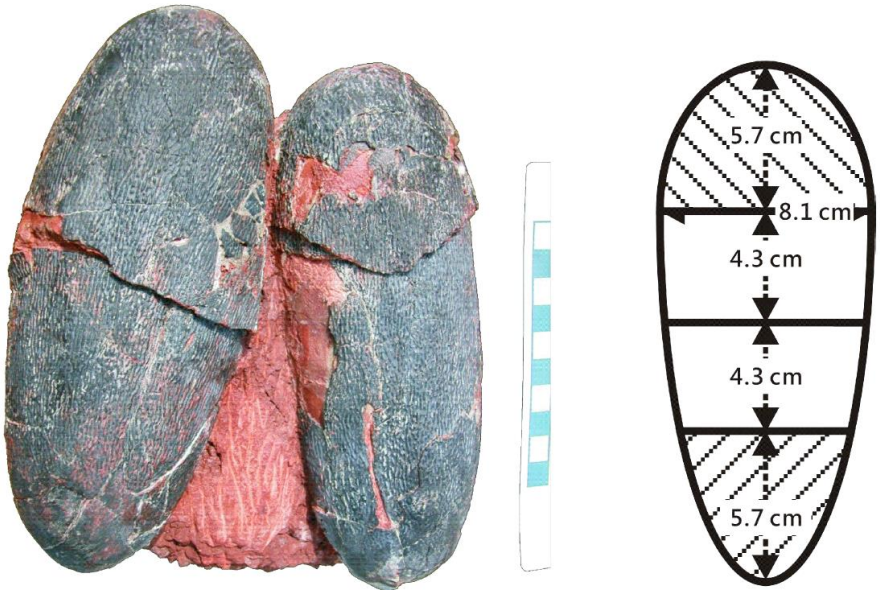

Figure 4.1.4 Two oviraptorid *Heyuannia* eggs from the Chinese province of Jiangxi. Scale bar equals 10 cm. Figure was adapted from *Wiemann* et al.[10].

Wiemann et al.[10] did find BV and PP in all three specimens, and in combination with studies of oviraptorid clutch arrangements[32], they conclude that the oviraptorid eggs were likely laid in overlapping circles. They suggest a partially open nesting behavior, with the eggs partially exposed sticking out of the nesting material, due to the coloring of the eggs.[10] They infer that the nesting material was likely colored similarly to the eggs for camouflage purposes.[10]

4.1.2.1 Experimental details from Wiemann et al.[10]

Wiemann et al.[10] used the EDTA based extraction procedure, which is described as follows and will be referred to as extraction procedure No. 1 over the course of this work:

The egg shell fragment (180-562 mg) is placed in an Eppendorf tube and admixed with 500 µl EDTA solution (100 mg/ml), which was adjusted to a pH value of 7.2. The fragment was incubated for 5 min and then transferred to a fresh Eppendorf tube, while the solution was discarded. The sample was again incubated in EDTA solution for 5 min, during which the tubes were vortexed three times for 1 min. They claim that carbon dioxide was produced as effervescence was observed, and thus the vortexing was performed with the lid of the tubes open. The tubes were centrifuged for 1 min at 15000 g. The supernatant was collected in a separate tube, and EDTA was added to the remaining solid. The previous steps were repeated two more times. To the remaining solid 1 ml of acetonitrile/acetic acid (4:1, v/v) was added for 10 min incubation. How long the sample was vortexed during the 10 min incubation time is not described consistently in the publication and its supporting information. The tube was centrifuged for 2 min at 15000 g, and the supernatant is the pigment

extract, which was stored in a dark environment at 4 °C no longer than 24 h before they were analyzed by HPLC-ESI MS. They identified BV and PP through the HPLC-ESI MS measurements by comparing the chromatogram and MS peaks with those of commercial standards. How the HPLC-ESI MS measurements were quantified is not mentioned, but presumably through external quantification with commercial standards. This yields numbers for amounts of BV and PP in the dissolution layer, which will be interpreted as the measured sample solution. Based on these amounts, *Wiemann* et al.[10] performed an experiment-empirical correction, to draw conclusions for the amounts originally present in the eggs. However, in order to compare my measurements with their results, only the amounts quantified in the HPLC-ESI MS experiment are relevant. These can be found in a table in the supporting information of *Wiemann* et al.[10], which is given in Figure 4.1.5 below. However, *Wiemann* et al.[10] seem to have made a mistake in using the unit [nmol] because the given amounts in a dissolution layer for the reported values are in the range of 10^{-11}-10^{-9}. If the unit [nmol] were correct, amounts of 10^{-20}-10^{-18} mol would have been detected, which is far beyond the detection limit of the used mass spectrometer described in the experiment. Thus, a more reasonable unit for the reported values is [mol].

Eggshell Specimen	Mass of Fragment [g]	Amount of PP in one dissolution layer [nmol]	Amount of BV in one dissolution layer [nmol]
Dromaius novaehollandiae	0.187	$\sim 8.0\times10^{-11}$	$\sim 4.1\times10^{-9}$
Heyuannia huangi (Henan)	0.463	$\sim 2.7\times10^{-10}$	$\sim 2.3\times10^{-10}$
Heyuannia huangi (Jiangxi)	0.368	$\sim 1.4\times10^{-10}$	$\sim 6.8\times10^{-11}$
Heyuannia huangi (Guangdong)	0.289	$\sim 9.0\times10^{-11}$	$\sim 2.3\times10^{-11}$

Figure 4.1.5 Table from *Wiemann* et al.[10] (SI, p. 8, Table 1), with seemingly wrong unit of [nmol]. The more likely unit is [mol].

This gives when dividing the detected amount through the 1 ml sample volume the concentrations given in Table 4.1.1 with values between 0.023 nmol/ml and 0.27 nmol/ml for BV and PP for the different oviraptorid eggshells.

Eggshell Specimen	Mass of Fragment [g]	Concentration of PP [nmol/ml]	Concentration of BV [nmol/ml]
Dromaius novaehollandiae (emu)	0.187	0.08	4.1
Heyuannia huangi (Henan)	0.463	0.27	0.23
Heyuannia huangi (Jiangxi)	0.368	0.14	0.068
Heyuannia huangi (Guangdong)	0.289	0.09	0.023

Table 4.1.1 Interpretation of results from *Wiemann* et al.[10].

4.1.3 Goal and motivation

Wiemann et al.[10] detected BV and PP in the three different oviraptorid egg shells. The goal for my studies was to build on the findings from *Wiemann* et al.[10]. Optimizing the methodology was one goal, e.g. ensuring reproducibility of the method and possibly reducing the sample amount needed. With the optimized method, the analysis should be expanded to the vast collection of the Goldfuß museum of the Steinmann-Institute for Geology, Mineralogy and Paleontology (University of Bonn) in collaboration with Prof. *M. Sander*.

4.1.4 Results

To test the EDTA based extraction method (No. 1) from *Wiemann* et al.[10], I extracted emu and brown chicken egg shell. The HPLC-ESI MS measurements of the extraction solutions were performed on our micrOTOF-Q mass spectrometer (overview about all used instruments in Table 6.3.1 p. 145 and extraction methods in Table 6.3.2 p. 145). For these measurements, a solvent system based on water and methanol with 0.05 % trifluoroacetic acid (TFA) (solvent system 1) was used (a full overview of all used solvent systems can be seen in Table 6.3.3 p. 146). For all measurements a reverse phase C18 column was used. The extracted ion chromatogram (EIC) for the protonated BV ($[M+H]^+$) is at *m/z* 583.25 and for the protonated PP ($[M+H]^+$) at *m/z* 563.26. The EICs can be seen in Figure 4.1.6 a) for the emu egg, b) for the chicken egg, and in c) for a solution of commercially available standards of BV and PP. As can be seen in the EICs of the standard solution Figure 4.1.6 c) BV has a retention time of 11.5 min and PP of 14.5 min. As the peaks in the EICs for BV and PP of the egg shells have the same retention time as the standard's EICs, the identification of BV and PP in the emu and chicken egg shells respectively, can be made. All measurements are listed with a measurement No., the sample ID, mass of the egg shell, extraction method, solvent system, and used instrument in Table 6.3.4 (p. 149). The emu egg measurement is measurement ***1***, and the chicken egg measurement is measurement ***2***.

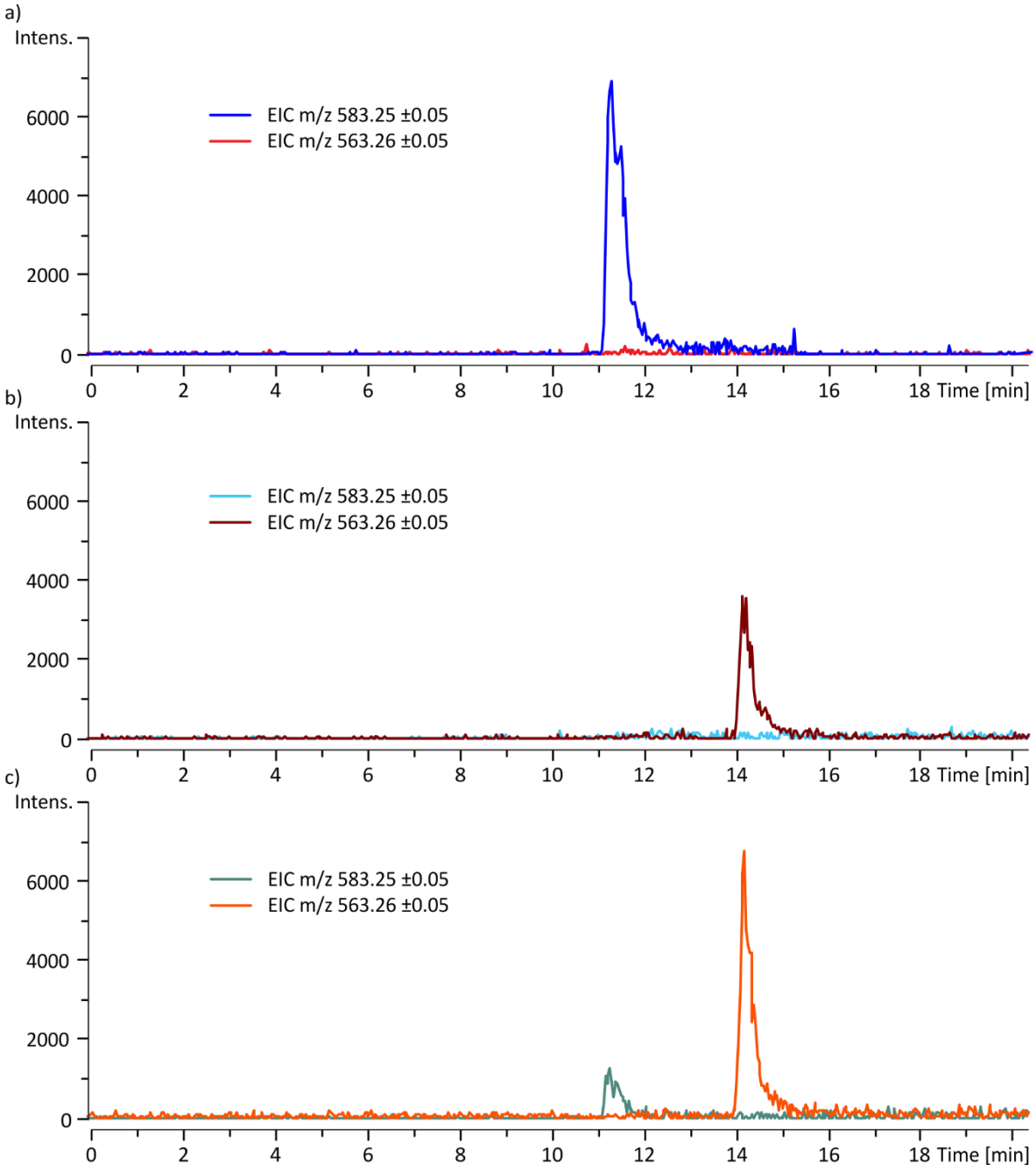

Figure 4.1.6 a) Emu egg measurement ***1***, b) chicken egg measurement ***2*** and c) measurement ***3*** of commercially available standards of BV and PP.

It is also possible to detect BV and PP within the same sample. For this, pulverized emu and chicken egg were mixed and the mixture was extracted with the EDTA method (No. 1). The peaks of BV and PP are well separated at 11.5 min and 14.5 min in measurement ***4*** (Figure 4.1.7).

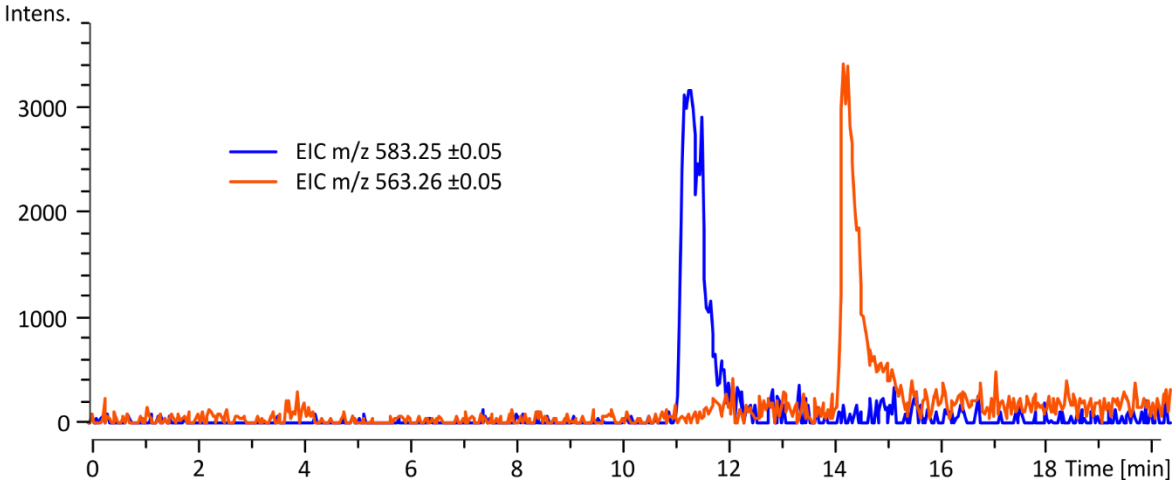

Figure 4.1.7 EICs of *m/z* 583 and *m/z* 563 for measurement ***4*** of a mixture of emu and chicken egg.

I analyzed the organic layer of the extraction procedure, which yield the results shown above, but in addition also the EDTA solution, which is put aside in the extraction procedure (see Table 6.3.2 p. 145). Neither BV nor PP was detectable in the EDTA solution.

The group of Prof. *M. Sander* supplied samples of the same three localities as *Wiemann* et al.[10] studied. I will use the sample IDs used in the *Sander* group, which is E131 for the samples from the Henan province, E132 for Jiangxi, and E082 for Guangdong. A full list of all analyzed specimens can be found in Table 6.3.5 (p. 150). With the EDTA extraction method (No. 1) used by *Wiemann* et al.[10] I extracted all three samples at least twice, but could not detect BV or PP (measurements No. ***5***-***11***) in any of them in measurements at the micrOTOF-Q.

With serial dilutions of the standard compounds, I was able to determine the detection limit of the micrOTOF-Q. By measuring the serial dilutions, i.e. different samples with different concentrations, it is possible to generate calibration curves for BV (Figure 4.1.8) and PP (Figure 4.1.9) (for details on the calibration see chapter 6.3.1 p. 151). Measurements for the calibration curves were always done directly before or after the sample measurements, with the same solvent system and MS acquisition as the samples. The lowest concentration that yielded reasonable intensity was 0.054 nmol/ml for BV and 0.056 nmol/ml for PP, which constitutes the detection limit for BV and PP and sensitivity of the micrOTOF-Q. The results from *Wiemann* et al.[10] in Table 4.1.1 show the concentrations for BV and PP between 0.023 nmol/ml and 0.27 nmol/ml for BV and PP for the different oviraptorid eggshells. Thus, the sensitivity of the micrOTOF-Q is not ideal, but at least in the samples with higher concentrations

of BV and PP according to *Wiemann* et al.[10] BV and PP should have been detected with the micrOTOF-Q.

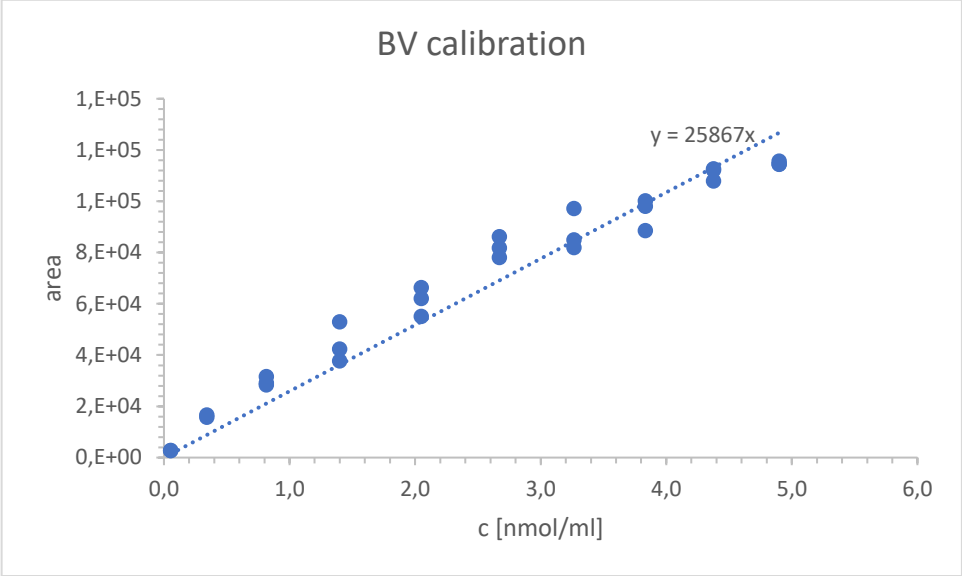

Figure 4.1.8 Calibration curve of BV for measurements ***1***, ***2***, ***4***, ***12-14***.

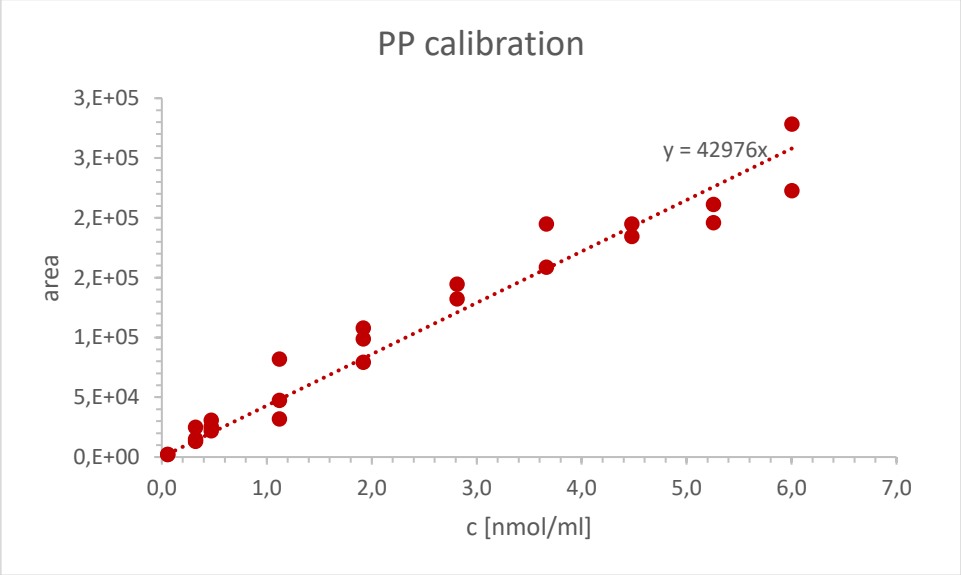

Figure 4.1.9 Calibration curve of PP for measurements ***1***, ***2***, ***4***, ***12-14***.

In order to achieve higher concentrations through extraction, I tested the HCl based extraction method (extraction method No. 2, see Table 6.3.2 p. 145) published by *Moreno* et al.[26]. In Figure 4.1.10 the already seen measurements ***1***, ***2***, and ***4*** based on EDTA extraction (No. 1) (Figure 4.1.6 and Figure 4.1.7) are compared with measurements ***12-14*** of HCl extractions (No.2) of the same amount of egg shells.

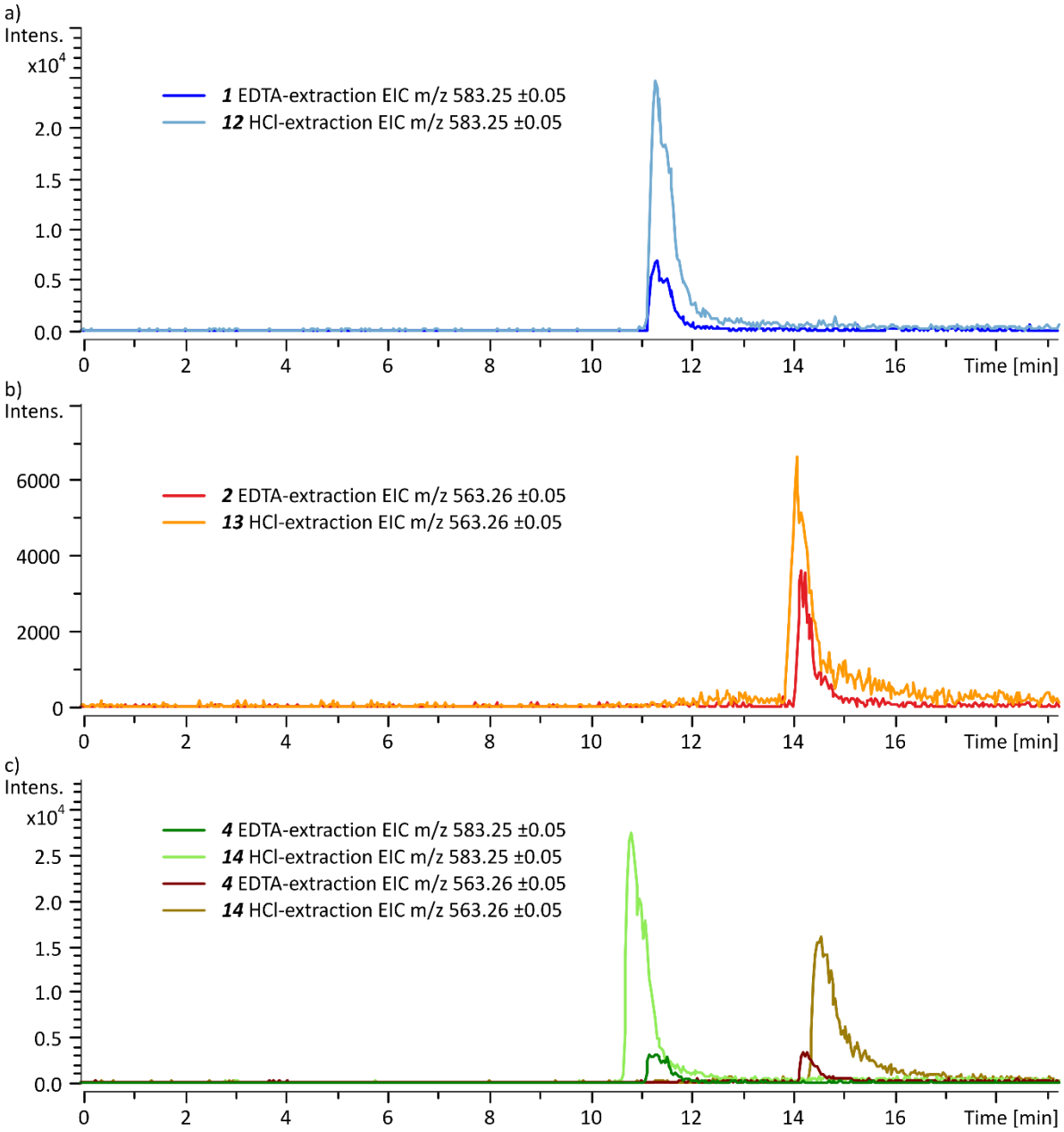

Figure 4.1.10 a) EIC *m/z* 583 of measurement ***1*** (EDTA extraction) and ***12*** (HCl-extraction) of emu egg, b) EIC *m/z* 563 of measurement ***2*** (EDTA extraction) and ***13*** (HCl-extraction) of chicken egg, c) EICs *m/z* 583 and *m/z* 563 of measurement ***4*** (EDTA extraction) and ***14*** (HCl-extraction) of emu and chicken egg mixture.

Through external quantification with the calibration curves shown in Figure 4.1.8 and Figure 4.1.9 the concentrations of BV and PP in the extraction solutions could be determined (see Table 4.1.2).

Extraction method	Measurement No.	c(BV) [nmol/ml]	c(PP) [nmol/ml]
EDTA (No. 1)	***1***	7.13	/
HCl (No. 2)	***12***	27.80	/
EDTA (No. 1)	***2***	/	1.52
HCl (No. 2)	***13***	/	4.07
EDTA (No. 1)	***4***	4.23	9.97
HCl (No. 2)	***14***	29.69	16.92

Table 4.1.2 Concentrations of BV and PP in measurements ***1***, ***2***, ***4*** and ***12***-***14***.

For PP the HCl extraction method (No. 2) is 1.7-2.7 times more efficient and for BV even 3.9-7.0 times more (Table 4.1.2).

Thus, I extracted the three different oviraptorid samples (E131, E132, and E082) with the HCl extraction method (No. 2), but still I was not able to detect BV or PP in any of them (measurements ***15***-***20***).

Further, the group of Prof. *M. Sander* provided me with additional egg shell samples from different dinosaurs like sauropods, oviraptor egg shells from other locations than the ones from *Wiemann* et al.[10], and subfossil moa egg shells (see Table 6.3.5 p. 150). I extracted all samples with the EDTA (No. 1) and HCl extraction method (No. 2) (measurements ***21***-***38***) but did not find BV or PP in any of them.

As the search for BV and PP was unsuccessful with the micrOTOF-Q, I wanted to perform measurements on a more sensitive mass spectrometer. Kindly the group of Prof. *U. Karst* from the university of Münster granted me access to their timsTOF flex. However, I needed to change my solvent system, as contamination with TFA needed to be avoided. Thus, I tested solvent system 2, which is based on water and methanol with 0.1 % acetic acid (see Table 6.3.3 p. 146), on the micrOTOF-Q. As can be seen in Figure 4.1.11 with solvent system 2 the separation of BV and PP, with retention times of 11 min and 17 min respectively, is sufficient. Further, external quantification shows here too the higher efficiency of the HCl extraction method (No. 2) over the EDTA extraction method (No. 1) (see Table 4.1.3) (calibration curves Figure 6.3.1 p. 151 and Figure 6.3.2 p. 152).

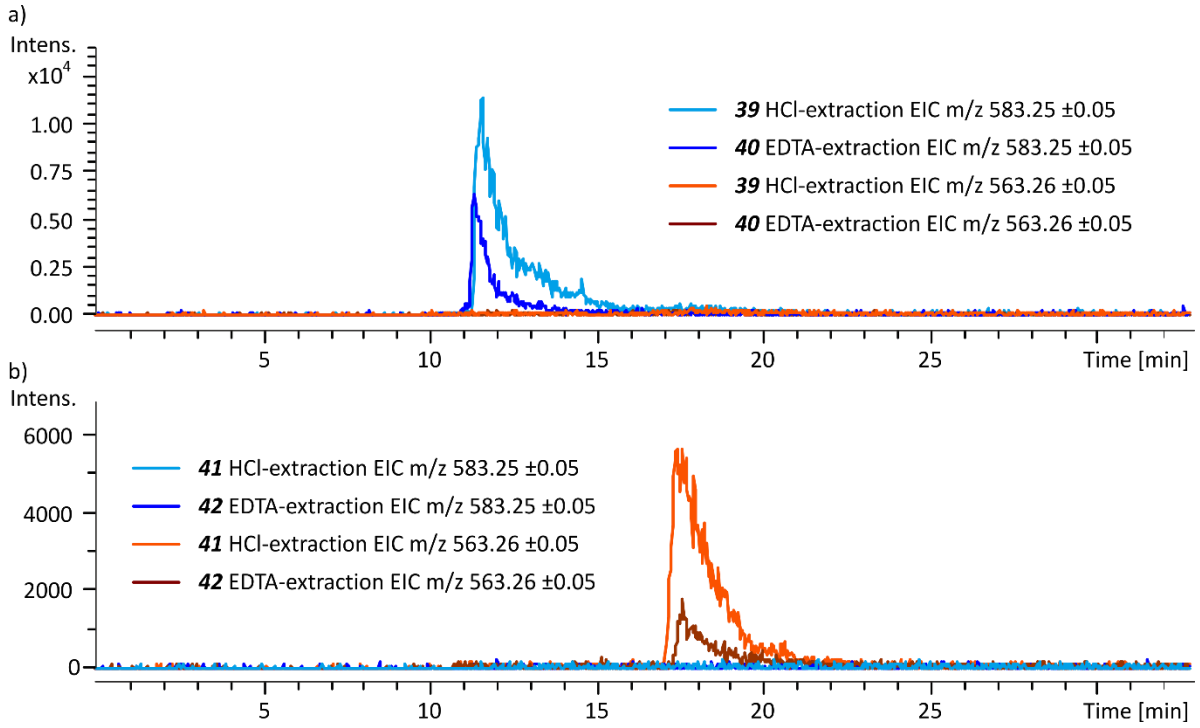

Figure 4.1.11 a) Measurements of emu egg shell extracted with HCl (extraction method No. 2) ***39*** and EDTA (extraction method No. 1) ***40***, b) measurements of chicken egg shell extracted with HCl (extraction method No. 2) ***41*** and EDTA (extraction method No. 1) ***42*** . Measurements were performed with solvent system 2, with water and methanol with 0.1 % acetic acid.

Extraction method	Measurement No.	c(BV) [nmol/ml]	c(PP) [nmol/ml]
HCl (No. 2)	***39***	17.01	/
EDTA (No. 1)	***40***	5.66	/
HCl (No. 2)	***41***	/	0.79
EDTA (No. 1)	***42***	/	0.17

Table 4.1.3 Concentrations of BV and PP in measurements ***39-42***.

The higher sensitivity of the timsTOF flex in Münster was immediately apparent when measuring the serial dilution of the commercial standards, as the sample with the lowest concentration of BV (0.016 nmol/ml) and PP (0.017 nmol/ml) still gave intensities of 10^4 (see Figure 4.1.12 a) measurement ***43***). Due to the higher sensitivity however, it became apparent that the solvent system 2 was not ideal, because the issue of carry-over arose. I.e., after the run of a sample the next run, which is always a blank measurement, still showed BV and PP and so a false positive for the following measurement could not be ruled out. This occurred for the EDTA extraction (No. 1) of the oviraptorid egg shells E082 and E132 (measurements ***44*** and ***45***). The EDTA extraction (No. 1) of the oviraptorid egg shell E131 (measurement ***46***) and the HCl extractions (No. 2) of E131 and E132 (measurements ***47*** and ***48***) had clean blank measurements before and thus could be reliably interpreted.

In the EDTA extraction (No. 1) of the oviraptorid egg shell E131 (measurement ***46***), I was able to detect PP for the first time in a fossil sample (see Figure 4.1.12 b)). The chromatogram peak does not show a high intensity, but nonetheless through quantification I determined the concentration of PP at 0.0019 nmol/ml (calibration curve in Figure 6.3.3 p. 152). BV was not detectable. In the HCl extraction (No. 2) of E131 (measurement ***48***) and E132 (measurement ***47***), neither BV nor PP could be detected. As only the EDTA extraction (No. 1) of E131 and not the HCl extraction (No. 2) showed PP, I formed the tentative hypothesis that the milder EDTA extraction (No. 1) might be the more suitable extraction method for the oviraptorid egg shells. However, before I was able to form this tentative hypothesis, I extracted egg shells from a subfossil moa egg and an ostrich egg from the Miocene with the HCl extraction (No. 2) but did not find either PP or BV (measurements ***49*** and ***50***).

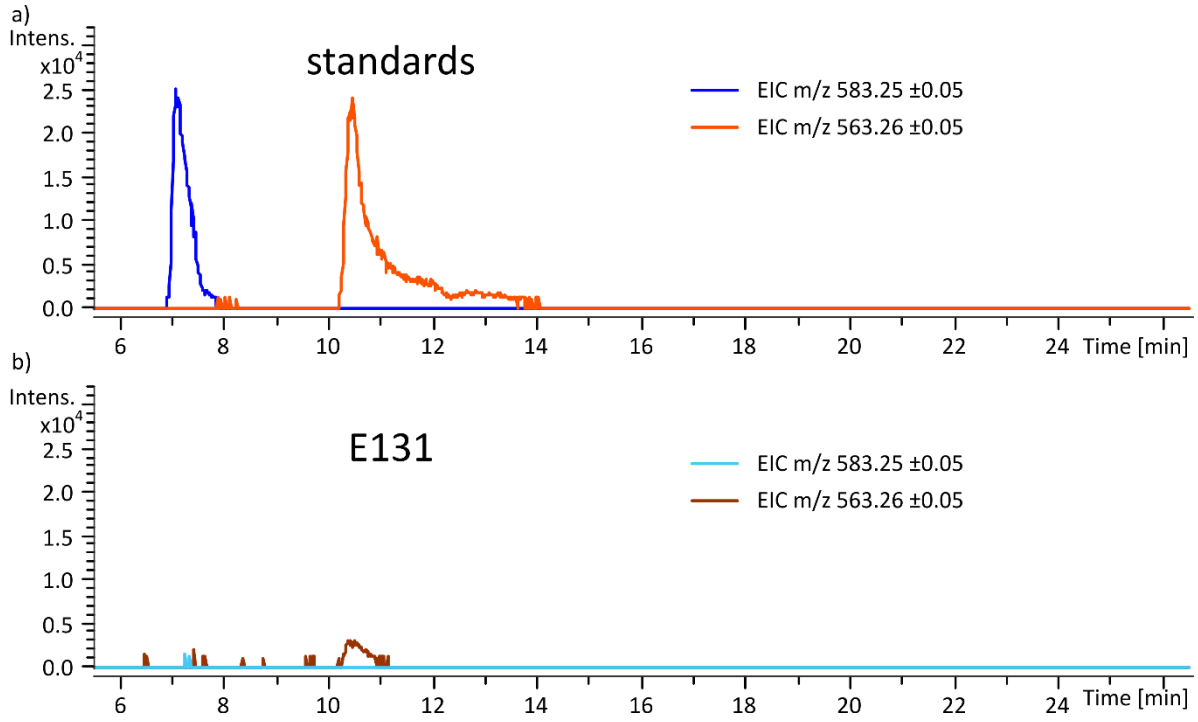

Figure 4.1.12 a) Measurement ***43*** of commercially available standards BV (0.016 nmol/ml) and PP (0.017 nmol/ml), b) measurement ***46*** of oviraptorid egg shell E131 with EDTA extraction method (No. 1).

As only PP was found with the timsTOF flex, an even more sensitive mass spectrometer was sought out. I was granted measuring time at the Qtrap instrument in the group of Prof. *P. Dörmann* of the biology department at the University of Bonn. However only limited measurement time was available, thus only initial measurements were possible. The Qtrap utilizes multiple reaction monitoring (MRM) to gain very high sensitivity (see chapter 1.3.3).

In the MRM for BV the ion pair of *m/z* 583 and *m/z* 297 was chosen and for PP the ion pair of *m/z* 563 and *m/z* 504. They were determined beforehand with MS^2 experiments on the micrOTOF-Q (Figure 4.1.13).

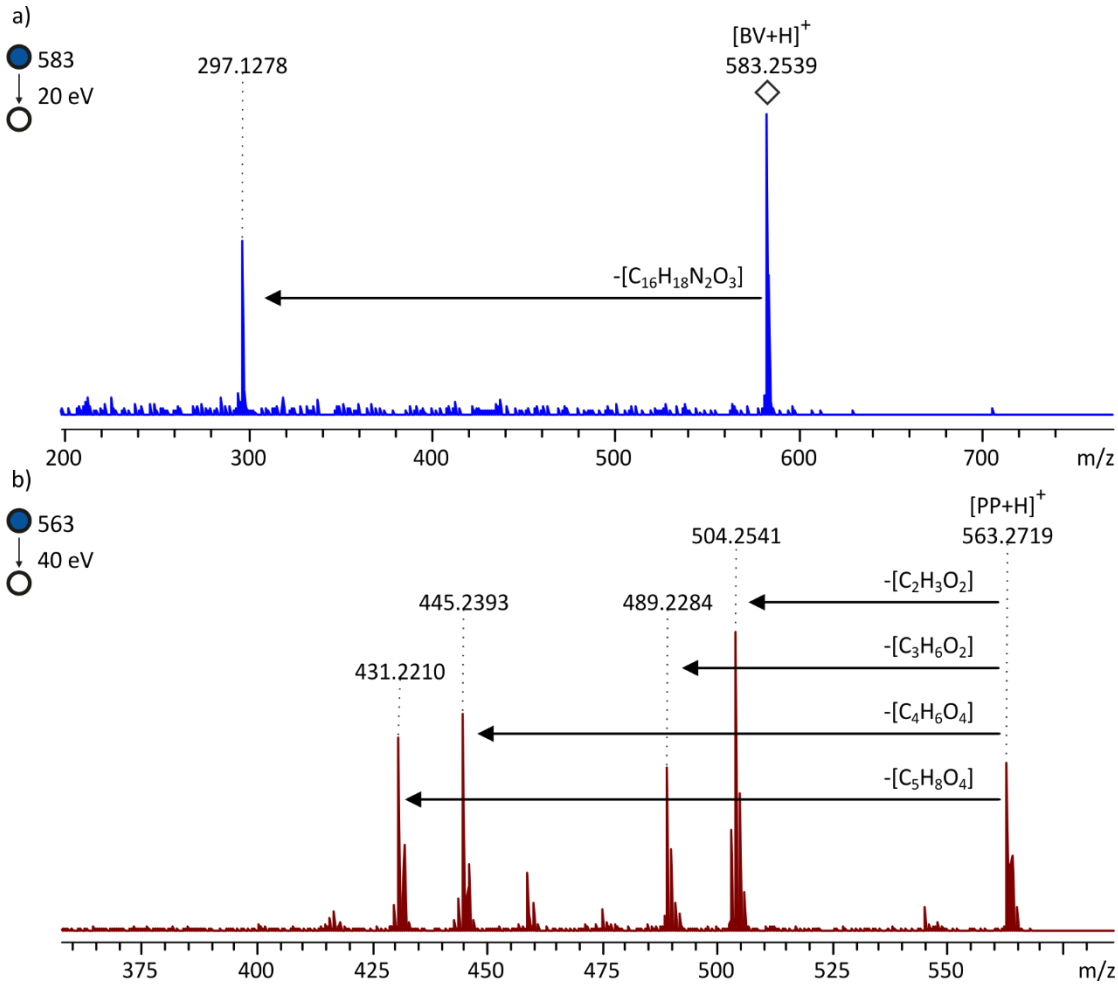

Figure 4.1.13 ESI(+) micrOTOF-Q measurement a) MS^2 of $[BV+H]^+$ *m/z* 583 20 eV, b) MS^2 of $[PP+H]^+$ *m/z* 563 40 eV.

The first measurements at the Qtrap still showed the issue of carry-over, although several flushing runs were set in between runs, making the measurements of extraction solutions meaningless. Nonetheless, the instrument showed its high sensitivity by being able to show concentrations as low as 0.0017 nmol/ml for both BV and PP (measurement ***51***, Figure 4.1.14).

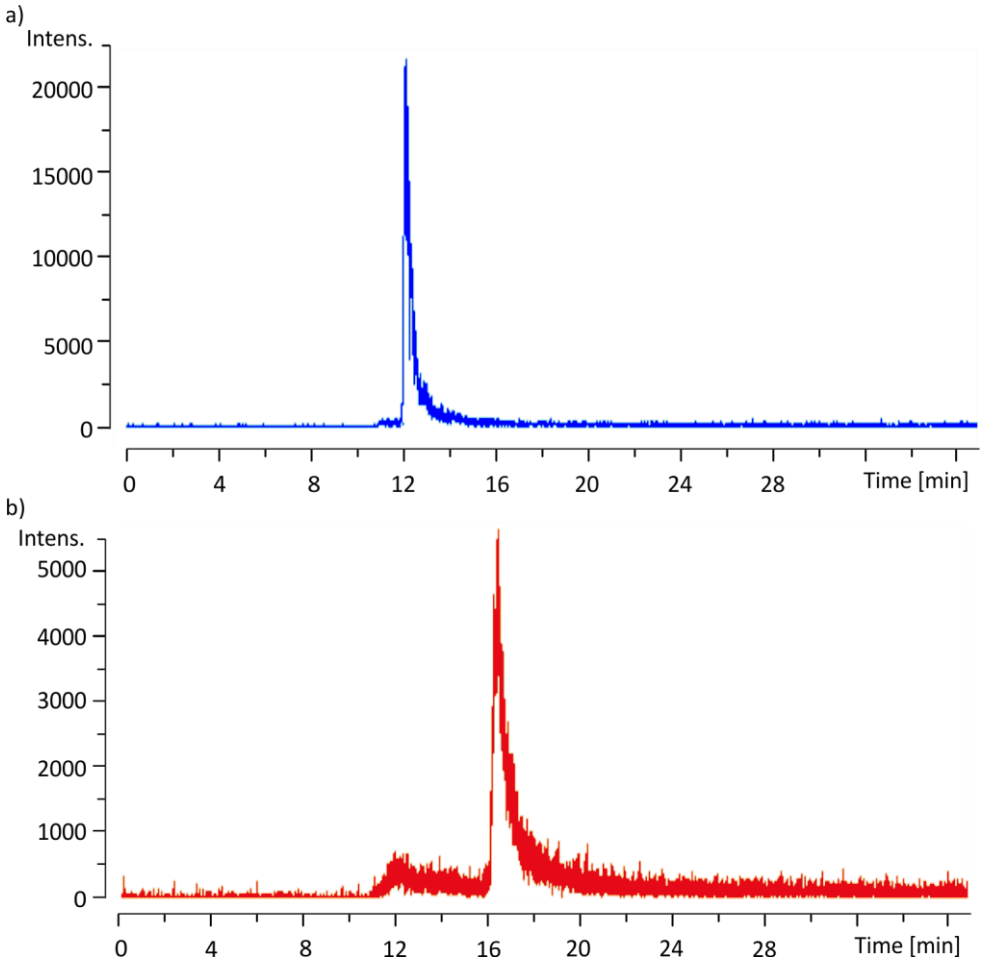

Figure 4.1.14 Measurement ***51*** of standard compounds BV (0.0017 nmol/ml) and PP (0.0017 nmol/ml) a) EIC of the ion pair *m/z* 583 to *m/z* 297, b) EIC of the ion pair *m/z* 563 to *m/z* 504.

With a new solvent system 3 (methanol 0.1 % acetic acid, isocratic Table 6.3.3 p. 146), the issue of carry-over was eliminated, and EDTA extraction (No. 1) solutions of E131 and E132 (measurements ***52*** and ***53***) could be analyzed. The measurements had clean blank runs before and thus can be interpreted. PP was found in both samples, and no BV in either (see Figure 4.1.15). PP has a retention time of 5 min as can be seen from the measurement of the standard compound in Figure 4.1.15 c). In both measurements of the samples Figure 4.1.15 a) and b) smaller peaks at 4.3 min can be observed, which might be an isomeric structure to PP or PP which passed the column in a differently charged state, but got ionized in the same way as the standard compound.

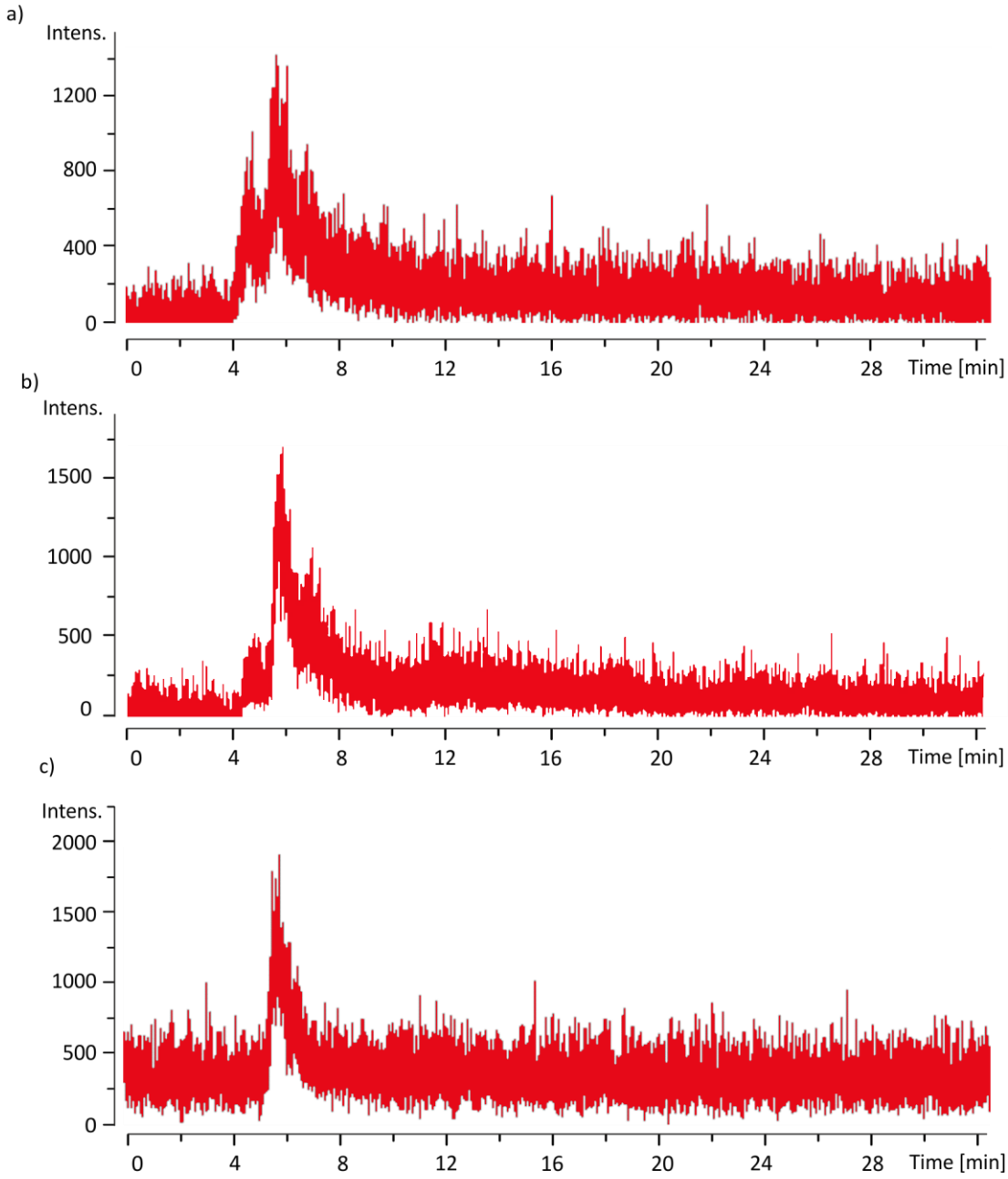

Figure 4.1.15 EICs of the ion pair *m/z* 563 to *m/z* 504 for a) measurement ***52*** E131 extracted with EDTA (No. 1), b) measurement ***53*** E132 extracted with EDTA (No. 1) c) measurement ***54*** of standard compound PP (0.00086 nmol/ml).

Through quantification, the concentrations of the extraction solutions could be determined (Table 4.1.4, calibration curve Figure 6.3.4 p. 153). Unfortunately, no measurement time was available yet for the analysis of the egg shell E082.

Extraction method	Measurement No.	Sample ID	c(BV) [nmol/ml]	c(PP) [nmol/ml]
EDTA (No. 1)	***52***	E131	/	0.00138
EDTA (No. 1)	***53***	E132	/	0.00157

Table 4.1.4 Concentration of PP in measurements ***52*** and ***53***.

For additional measurements, I was given the opportunity in Münster at the timsTOF flex again. Due to spiking experiments which will be discussed in chapter 4.1.4.1, the HCl extraction seemed more promising. Thus, I modified the HCl extraction method (No. 2) by using only half the acetonitrile in the extraction process to gain higher concentrations resulting in HCl extraction method (No. 3) (see Table 6.3.2 p. 145). With the HCl extraction method (No. 3), I extracted all three oviraptorid egg shells (E082, E131 and E132, measurements ***55***-***57***) and for the first time in a fossil sample I was able to detect BV. In E132 (measurement ***57***) I was able to quantify 0.0576 nmol/ml BV and no PP (Figure 4.1.16, calibration curve Figure 6.3.7 p. 154). The retention time of BV in the sample is at 3.5 min (Figure 4.1.16 a)) whereas in the measurement of the standard compound BV has a retention time of 3 min (Figure 4.1.16 b)). This shift likely occurred due to the different pH levels in the sample and standard solution. In the other two measurements ***55*** and ***56*** of E082 and E131 neither BV nor PP were detected.

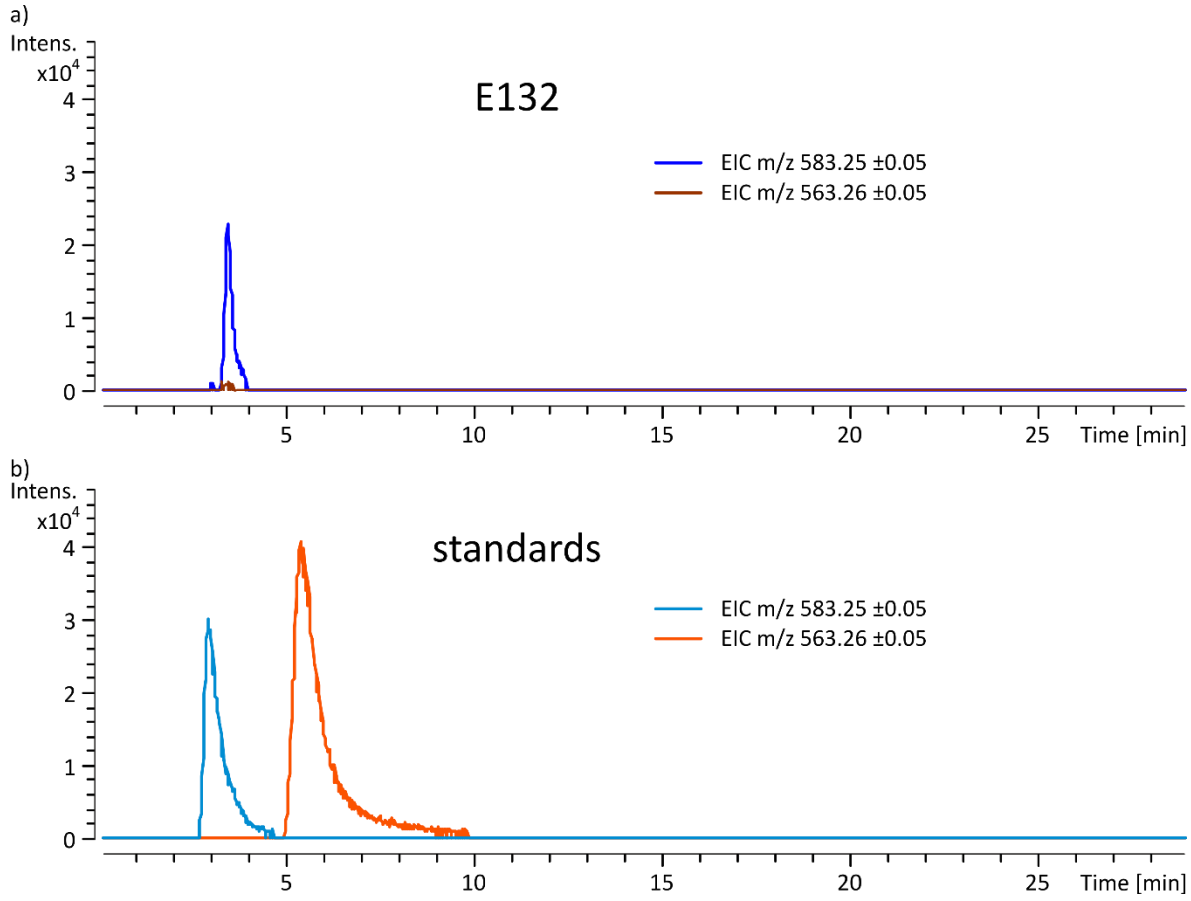

Figure 4.1.16 a) Measurement ***57*** of E132 with HCl extraction method (No. 3), b) measurement ***58*** of commercially available standards of BV (0.13 nmol/ml) and PP (0.12 nmol/ml).

BV and PP can also form complexes with iron (Fe^{2+}), calcium (Ca^{2+}) or zinc (Zn^{2+})[6], but none were detected in any measurement. Also, no derivate resulting from double or mono methylation or ethylation of PP or BV was detected in any measurement.

However, degradation products of BV and PP namely different dialkyl-substituted maleimides **1** and **2** (Figure 4.1.17) were detected.[33]

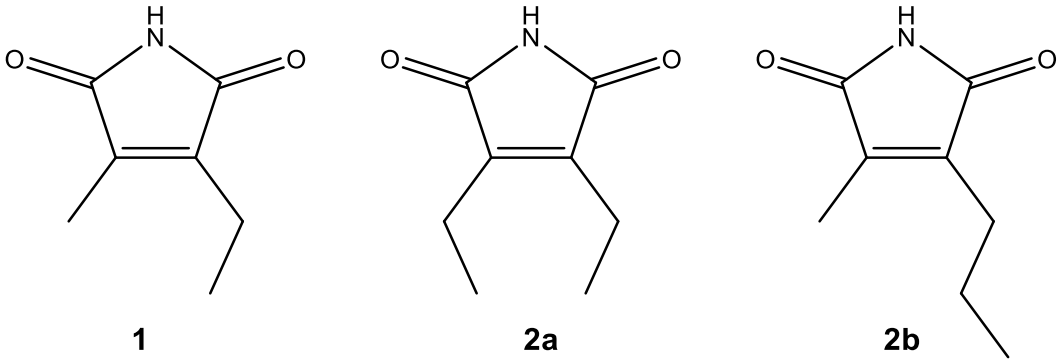

Figure 4.1.17 Degradation products of BV and PP dialkyl-substituted maleimides **1** and the isomers **2a** and **2b**.[33]

The dialkyl-substituted maleimides were detected in the samples extracted with HCl (No. 2) of the oviraptorid egg shell E131 (measurements ***15***, ***18*** and ***20***), the ostrich egg shell sample from the Miocene (measurement ***37***) and the sauropod egg shell (measurement ***31***), but not in the EDTA extraction (No. 1) of these samples (measurements ***8***, ***9***, ***32*** and ***38***). The maleimides were detected as *m/z* 140 [**1**+H]$^+$ and *m/z* 154 [**2**+H]$^+$ and their derivatives that have been hydrogenated twice (*m/z* 142 [$\mathbf{1H_2}$+H]$^+$and *m/z* 156 [$\mathbf{2H_2}$+H]$^+$) and four times (*m/z* 144 [$\mathbf{1H_4}$+H]$^+$and *m/z* 158 [$\mathbf{2H_4}$+H]$^+$) (Figure 4.1.18). In measurements of emu and chicken egg shells, in neither the HCl extraction nor the EDTA extraction solution maleimides were detected (measurements ***1***, ***2***, ***4***, ***12***, ***13*** and ***14***). Thus, it can be concluded, that the maleimides do not arise through degradation of BV or PP during the HCl extraction process.

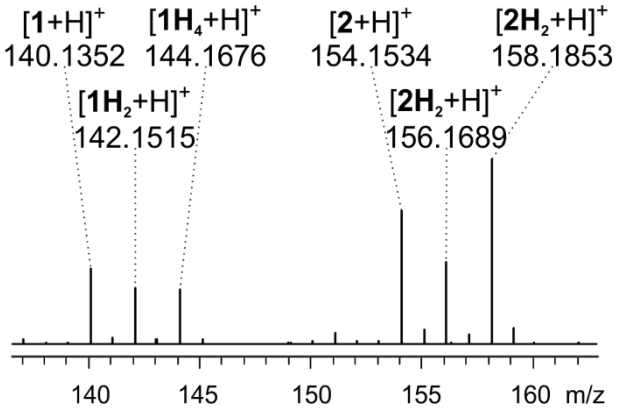

Figure 4.1.18 MicrOTOF-Q ESI (+) MS spectrum at retention time 11.5 min of measurement ***15*** of oviraptorid egg shell E131 with HCl extraction method No. 2.

4.1.4.1 Spiking experiments

As the results were still inconclusive, I decided to study the extraction methods and their efficiency. For this, I developed the following spiking experiment. For a spiking experiment it is necessary to create a sample with a known concentration of the compound of interest. Then this sample gets extracted and quantified to gain information on the efficiency of the extraction method.

To generate samples with a known concentration of BV and PP, I mixed the commercially available solid standard compounds of BV and PP with powdered white chicken egg shell, which does not contain either BV or PP, and performed a solid-state serial dilution (see Figure 4.1.19). I used white chicken egg shell, due to the hypothesis that it could mimic the original egg shell best.

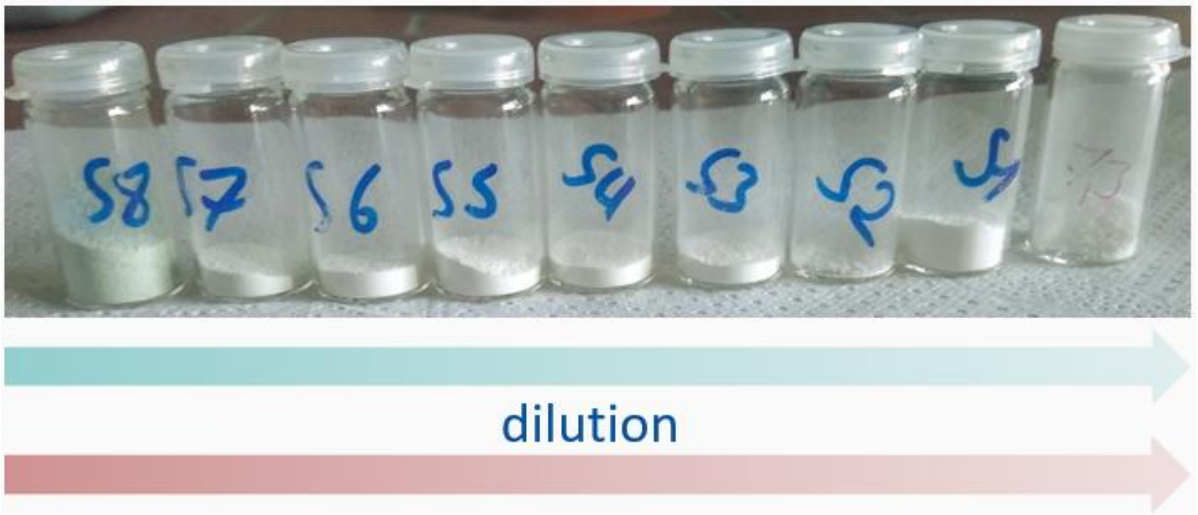

Figure 4.1.19 Solid state serial dilution of BV and PP mixed into white chicken egg shell powder.

As our micrOTOF-Q was out of order, I was kindly granted access to the micrOTOF-Q III of the pharmacy department of the university of Bonn. There I was able to perform the first spiking experiment, i.e. measure and quantify the extraction solutions of the spiking samples gained with the EDTA extraction method (No. 1) (measurements ***59***-***64***) and HCl extraction method (No. 2) (measurements ***65***-***70***, calibration curves Figure 6.3.5 p. 153 and Figure 6.3.6 p. 154).

The results will be visualized with the extraction ratio, which is the quantified concentration in the extraction solution divided by the concentration if 100 % of BV or PP would have been extracted:

$$extraction\ ratio = \frac{quantified\ concentration}{100\ \%\ extraction\ concentration} \qquad \textbf{Equation 4.1.1}$$

So, the extraction ratio should range between 0 for no extraction and 1 for full extraction. The extraction ratio is then plotted against the concentration of the different spiking samples. For the EDTA extraction method (No. 1) this is shown for BV in Figure 4.1.20 and PP in Figure 4.1.21.

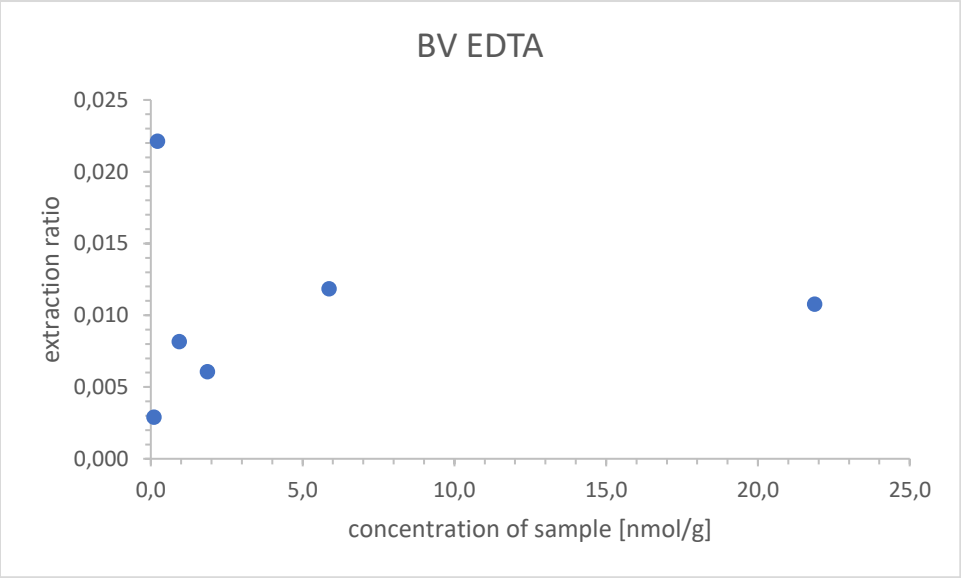

Figure 4.1.20 Extraction ratio plotted against concentration of spiking sample for BV with EDTA extraction method (No. 1), spiking experiment 1.

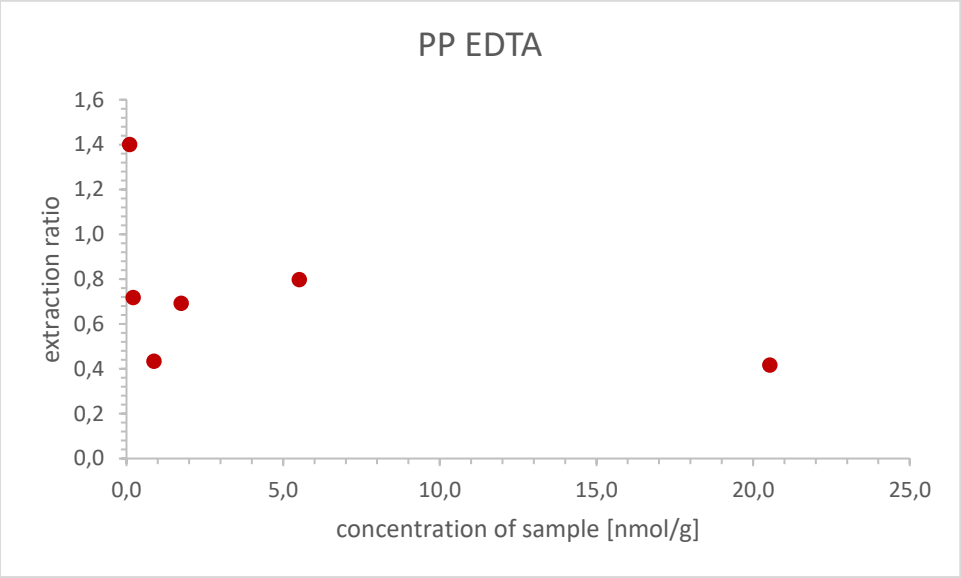

Figure 4.1.21 Extraction ratio plotted against concentration of spiking sample for PP with EDTA extraction method (No. 1), spiking experiment 1.

For BV the extraction ratio is extremely low, between 0.003 and 0.022 (Figure 4.1.20). For PP the extraction ratio lies between 0.417 and 0.719 for the higher concentrations, which are typical values for an extraction ration, and at an impossible 1.4 for the lowest concentration (Figure 4.1.21). This tendency of a high values for low concentrations is also found for BV (Figure 4.1.20).

Here too, I analyzed the organic layer of the extraction method, which yields the results shown above, but in addition also the EDTA solution, which is put aside in the extraction procedure (see Table 6.3.2 p. 145). I did not detect either BV or PP in the EDTA solution.

With the HCl extraction method (No. 2) the extraction ratio for BV lies between 0.218 and 0.827 (Figure 4.1.22). For PP the extraction ratio lies between 0.688 and 0.975 for the three higher concentrations and between impossible 1.705 and 11.583 for the three lower concentrations (Figure 4.1.23).

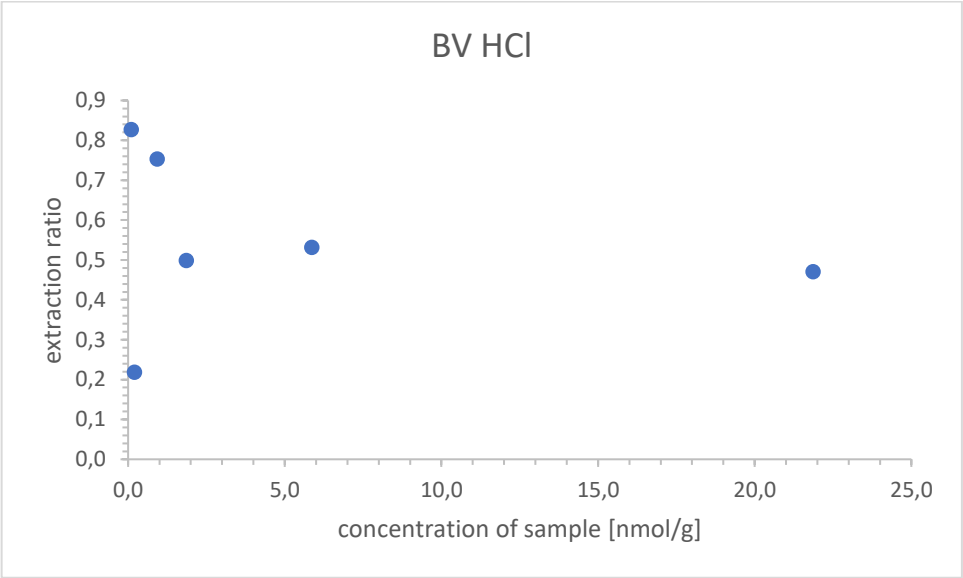

Figure 4.1.22 Extraction ratio plotted against concentration of spiking sample for BV with HCl extraction method (No. 2), spiking experiment 1.

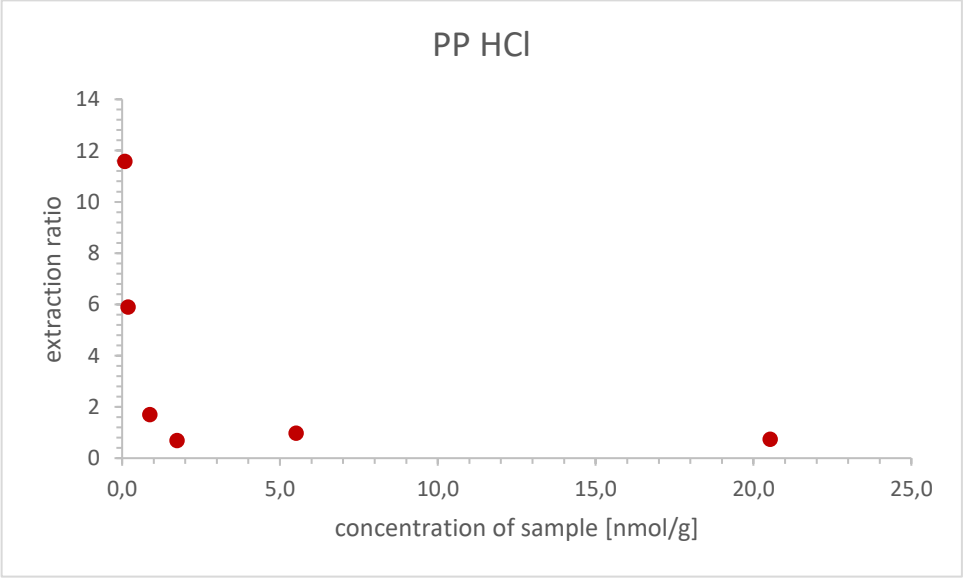

Figure 4.1.23 Extraction ratio plotted against concentration of spiking sample for PP with HCl extraction method (No. 2), spiking experiment 1.

The conclusion can be drawn that the EDTA extraction method (No. 1) is unsuitable for the extraction of BV from egg shells, whereas the HCl extraction method (No. 2) seems promising. However, the high extraction ratios of PP for low concentrations are impossible, so the spiking experiment needed to be repeated.

As the micrOTOF-Q III was not working, I was fortunately able to perform the spiking experiment 2 with the timsTOF flex in Münster. The spiking experiment 2 was set up in the same way as spiking experiment 1, except HCl extraction method No. 3 and not No. 2 was used (measurements ***71***-***75***, calibration curves Figure 6.3.7 p. 154 and Figure 6.3.8 p. 155).

For BV the extraction ratio lies between 0.009 and 0.651 again with higher values for lower concentrations (Figure 4.1.24). For PP the extraction ratios are impossibly high between 1.396 and 6.895 for lower concentrations, while for higher concentrations the extraction ratio is below 1 at 0.661 and 0.768 (Figure 4.1.25), similar to the results of the spiking experiment 1.

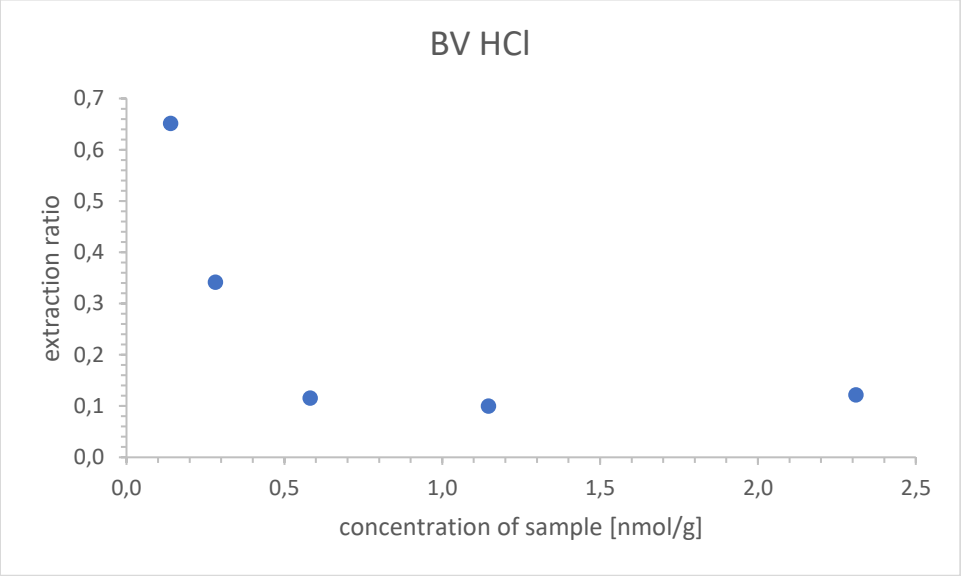

Figure 4.1.24 Extraction ratio plotted against concentration of spiking sample for BV with HCl extraction method (No. 3), spiking experiment 2.

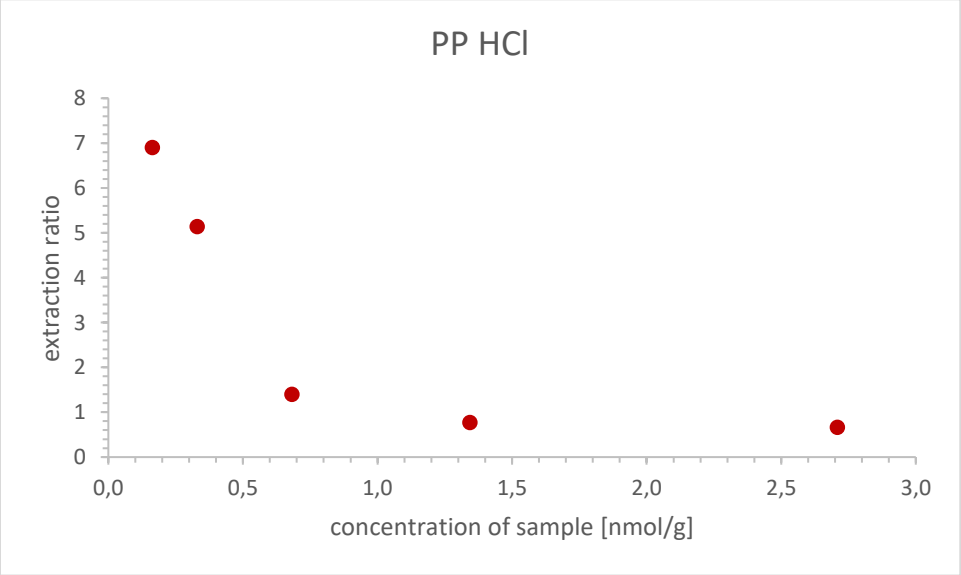

Figure 4.1.25 Extraction ratio plotted against concentration of spiking sample for PP with HCl extraction method (No. 3), spiking experiment 2.

As these results for PP seem so unreasonable, I hypothesized that the performed quantification might be incorrect making the extraction ratios impossible. For the quantification, I measured serial dilutions of standard compounds. As BV and PP are not available or very expensive in their pure form, for BV I used biliverdin hydrochloride and for PP the disodium salt of PP as a standard compound. To protonate the PP disodium salt, I used methanol with 0.1 % acetic acid to dissolve the standard and to enhance solubility I added dimethyl sulfoxide (DMSO). For a detailed description of the preparation of the standard serial dilutions, see chapter 6.3.1 (p. 151). Although the solutions are already acidic with 0.1 % of acetic acid, it is still possible that the detection of the compounds varies with different pH levels in the sample. Further, different solvents might have an effect, as the quantification solutions are based in methanol and the samples are based on acetonitrile.

Measurements were performed on the micrOTOF-Q III. As to test the influence of the solvent of the sample, three different solvents were prepared: acetonitrile with 0.1 % acetic acid, methanol with 0.1 % acetic acid, and "special acetonitrile". The "special acetonitrile" was generated through extracting white chicken egg with extraction method No. 3. Thus, the "special acetonitrile" mimics the solvent of the samples prepared with HCl extraction method No. 3. To these three different solvents, standard solutions were added. The first standard solutions were prepared, as the standard solutions for all previous calibration curves (see chapter 6.3.1 p. 151), by dissolving the standards in a mixture of methanol with 0.1 % acetic acid and dimethyl sulfoxide (DMSO) and diluting the solution with methanol with 0.1 % acetic acid. In the last dilution step, the three different solvents described above were used and two levels of concentration were generated (see Table 4.1.5) and measured (measurements ***76***-***81***).

Measurement No.	Solvent	c(BV) [nmol/ml]	c(PP) [nmol/ml]
76	"special acetonitrile"	0.16	0.16
77	acetonitrile 0.1 % acetic acid	0.16	0.16
78	methanol 0.1 % acetic acid	0.16	0.16
79	"special acetonitrile"	0.31	0.32
80	acetonitrile 0.1 % acetic acid	0.31	0.32
81	methanol 0.1 % acetic acid	0.31	0.32

Table 4.1.5 Measurements ***76***-***81***, with solvents and generated concentrations.

For PP the chromatograms for the three different solvents and the two different concentrations are shown in Figure 4.1.26. For the lower concentration, the sample's intensity in the "special acetonitrile" is higher than for acetonitrile and methanol with 0.1 % acetic acid, which have approximately the same intensity (Figure 4.1.26 a)). The same trend, although not as pronounced, is observed for the higher concentration (Figure 4.1.26 b)).

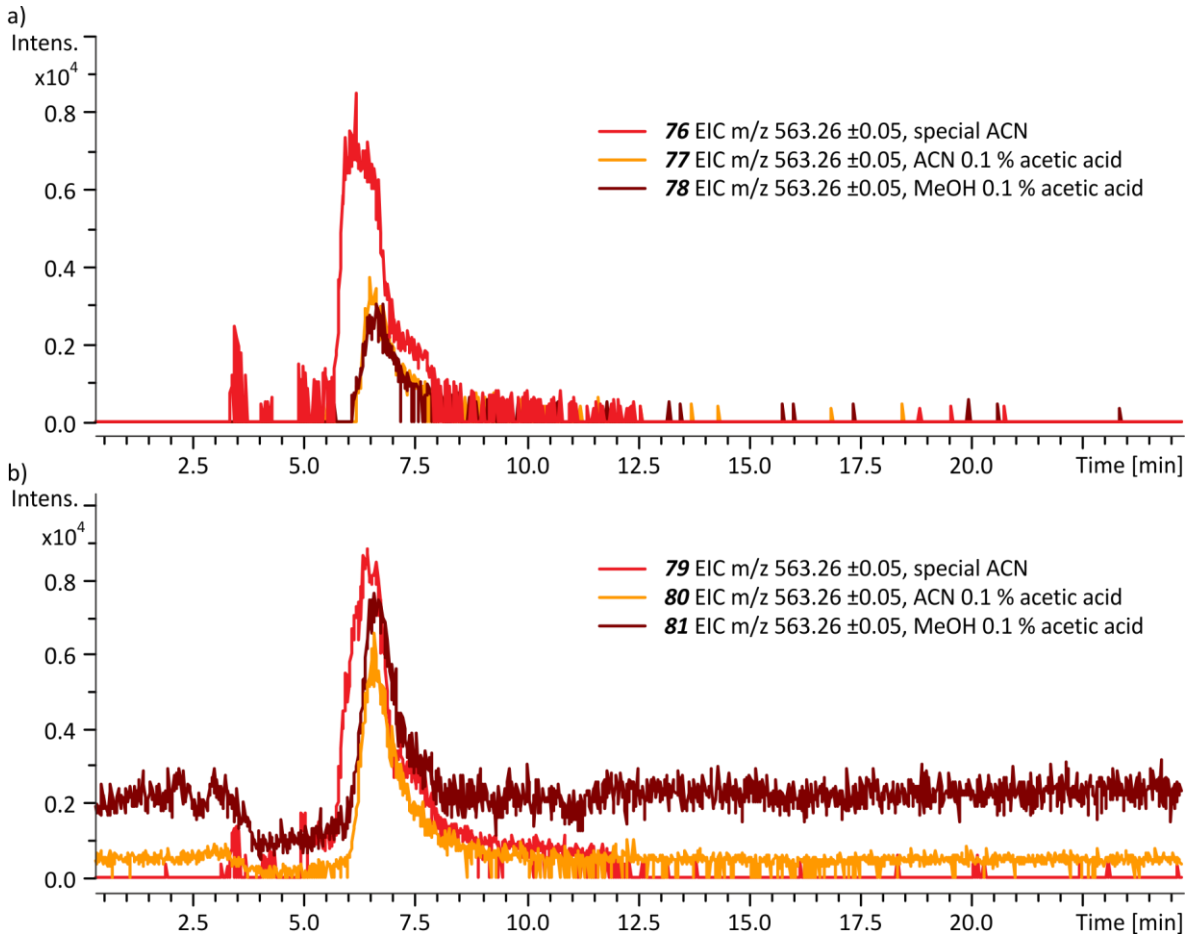

Figure 4.1.26 EICs *m/z* 563 of a) measurements ***76***-***78*** (lower concentration), b) measurements ***79***-***81*** (higher concentration).

The opposite trend is observed for BV; for both with the lower and higher concentration, BV is nearly undetectable in the "special acetonitrile" (Figure 4.1.27). The samples in acetonitrile with 0.1 % acetic acid show slightly higher intensities of BV than the samples in methanol with 0.1 % acetic acid.

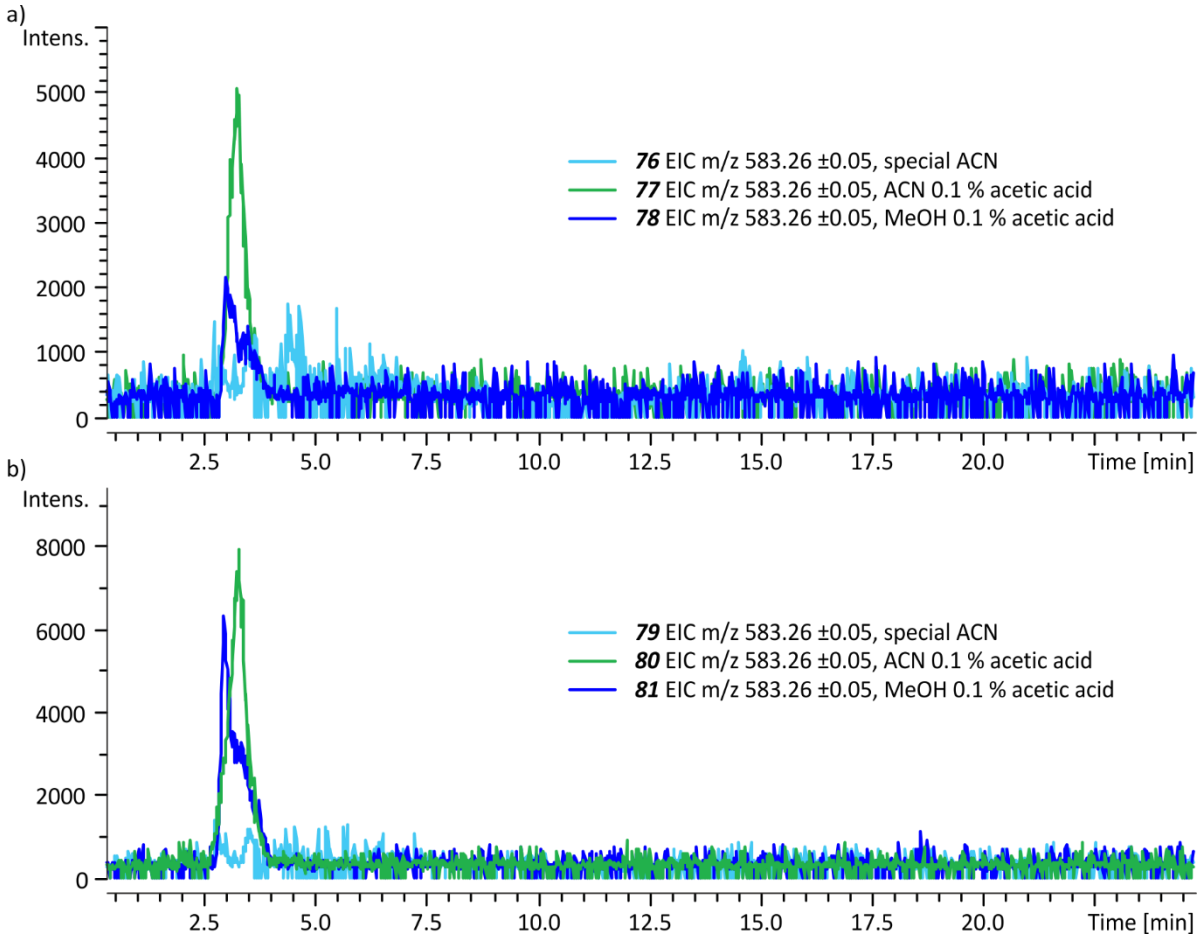

Figure 4.1.27 EICs *m/z* 583 of a) measurements ***76***-***78*** (lower concentration), b) measurements ***79***-***81*** (higher concentration).

In a second set of measurements, 3 N HCl was added to the first solution after dissolving the standards. Then again two levels of concentration in the three different solvents (see Table 4.1.6) were generated and measured (measurements ***82***-***87***).

Measurement No.	Solvent	c(BV) [nmol/ml]	c(PP) [nmol/ml]
82	"special acetonitrile"	0.17	0.16
83	acetonitrile 0.1 % acetic acid	0.17	0.16
84	methanol 0.1 % acetic acid	0.17	0.16
85	"special acetonitrile"	0.34	0.32
86	acetonitrile 0.1 % acetic acid	0.34	0.32
87	methanol 0.1 % acetic acid	0.34	0.32

Table 4.1.6 Measurements ***82***-***87***, with solvents and concentrations.

Adding HCl to the standard solution brings an even higher intensity for PP in the “special acetonitrile” compared to the other two solvents than before (Figure 4.1.28). But this time, the effect is more pronounced for the higher concentration (Figure 4.1.28 b)) than the lower concentration (Figure 4.1.28 a)), although still considerable for the lower concentration.

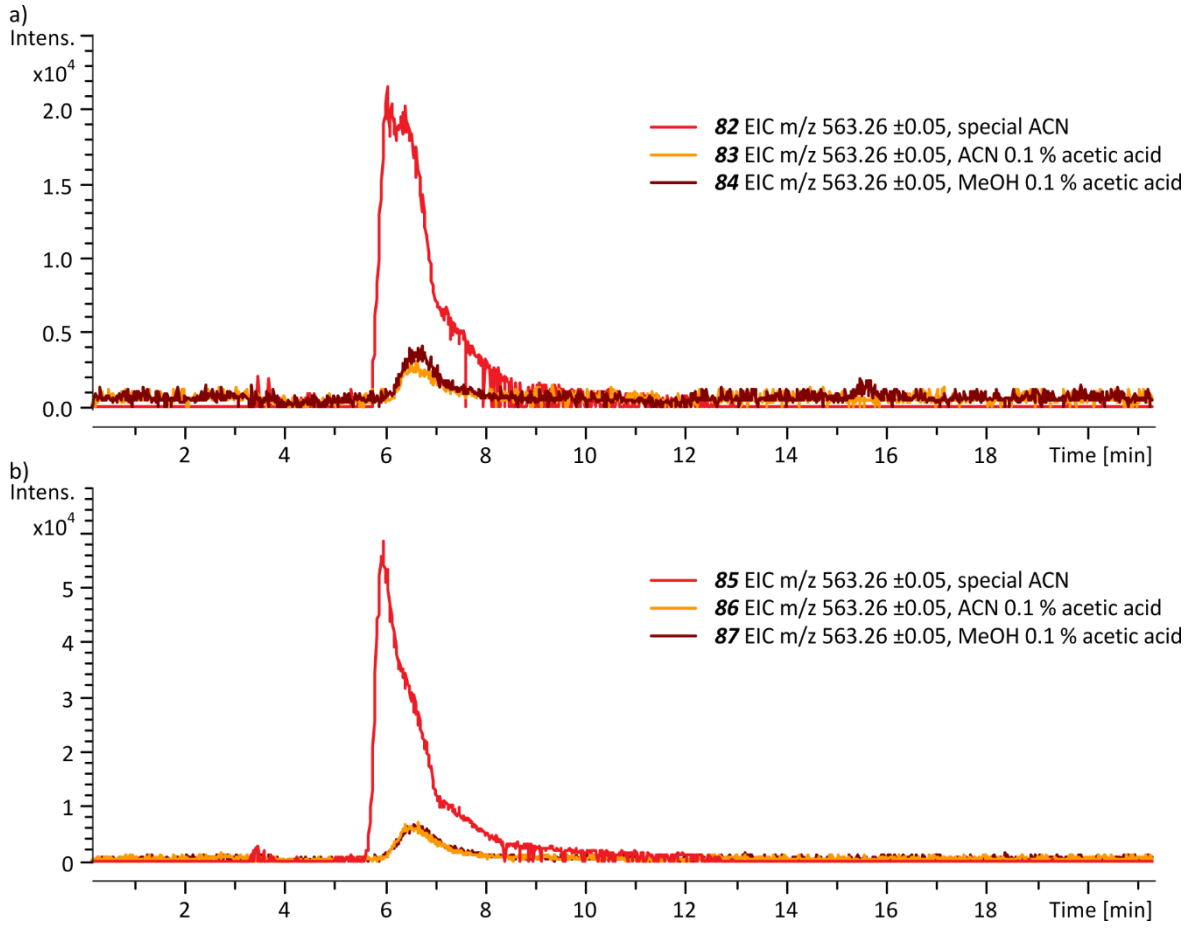

Figure 4.1.28 EICs *m/z* 563 of a) measurements ***82-84*** (lower concentration), b) measurements ***85-87*** (higher concentration). The sample solutions were prepared with additional HCl in the initial standard solution.

BV is still not detectable in the “special acetonitrile”, and in the acetonitrile and methanol with 0.1 % acetic acid, the intensities are approximately similar (Figure 4.1.29).

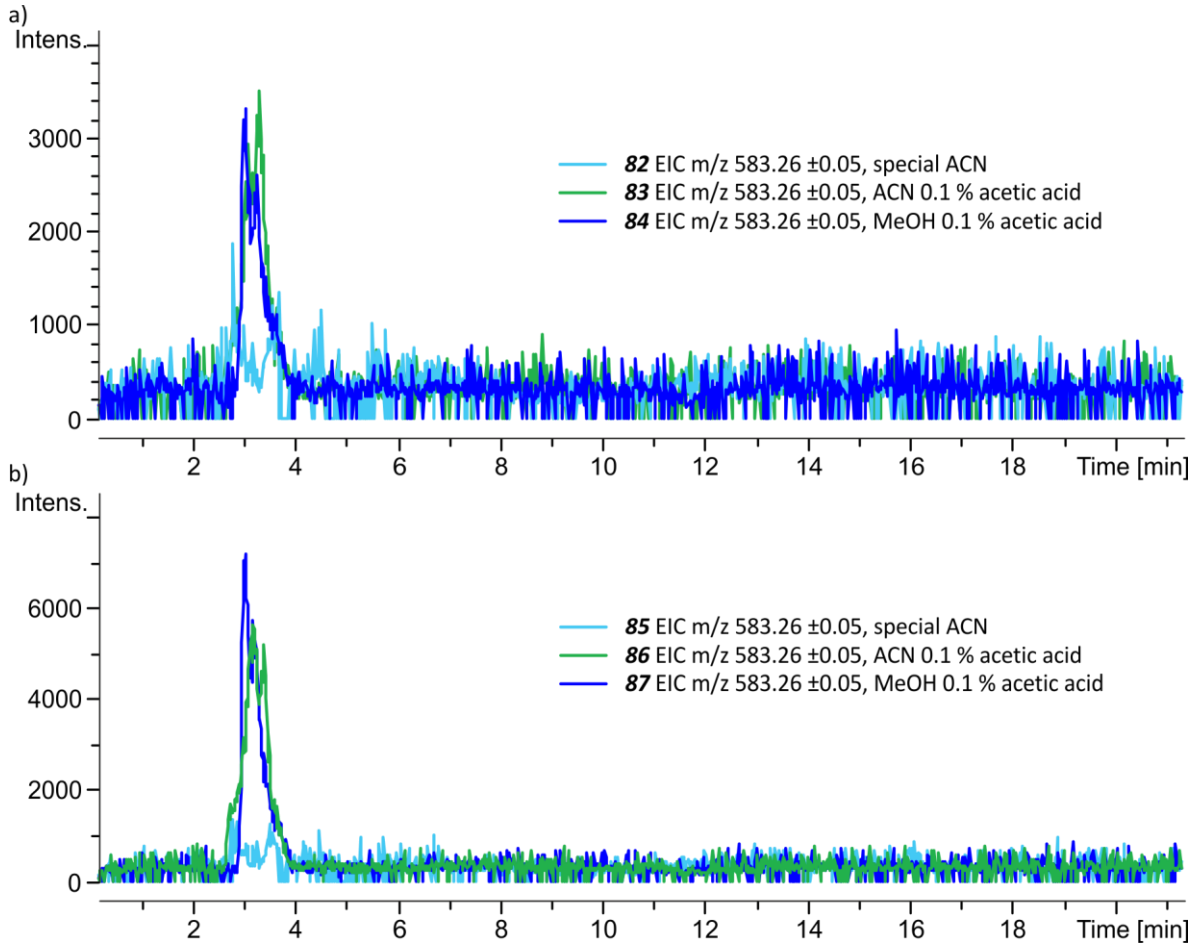

Figure 4.1.29 EICs *m/z* 583 of a) measurements ***82***-***84*** (lower concentration), b) measurements ***85***-***87*** (higher concentration). The sample solutions were prepared with additional HCl in the initial standard solution.

Figure 4.1.30 shows the comparison of PP in the lower and higher concentrations of the standard solutions without and with added hydrochloric acid in the “special acetonitrile”. It becomes apparent that the addition of the hydrochloric enhances the detection of PP in the “special acetonitrile” even further than just the “special acetonitrile”.

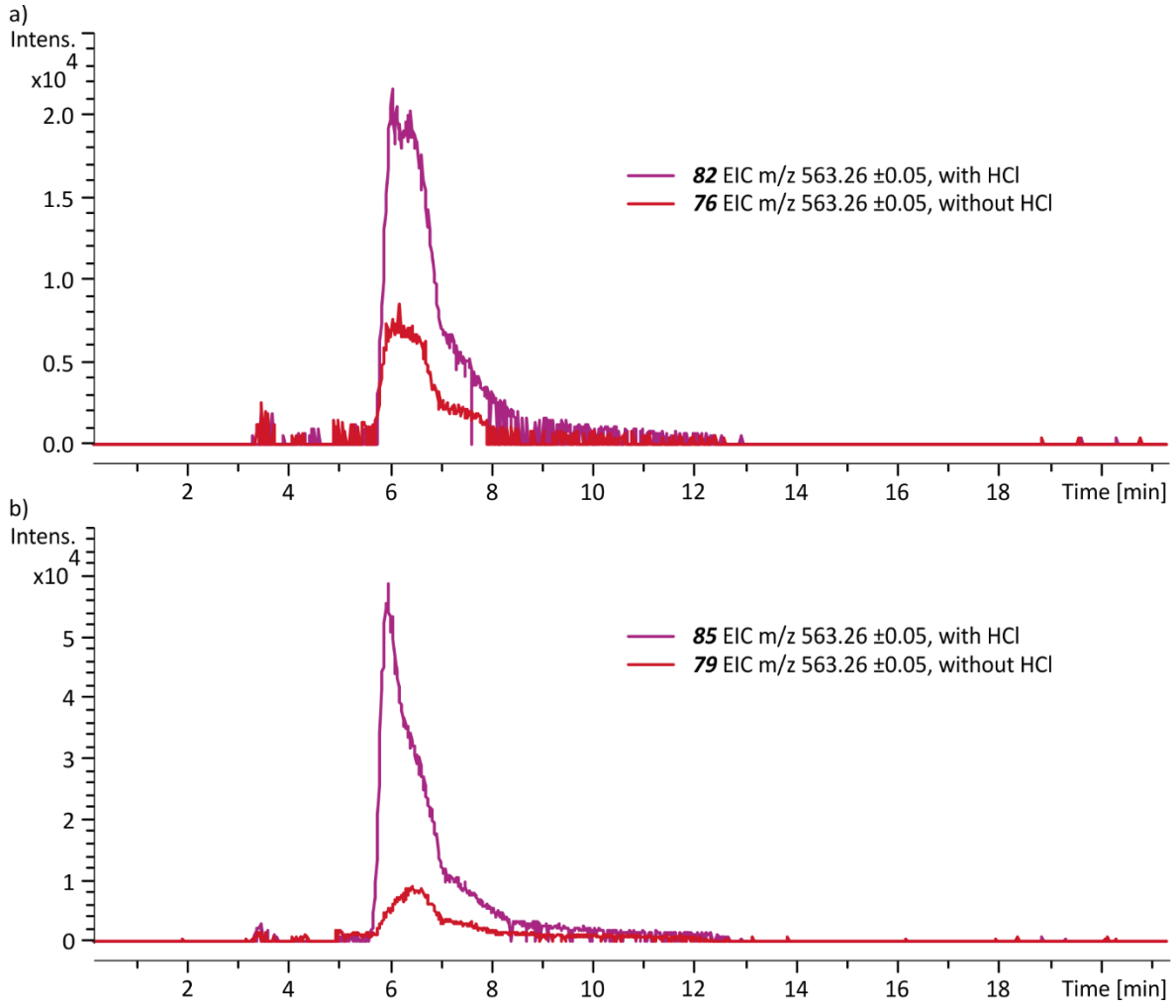

Figure 4.1.30 EICs *m/z* 563 of a) measurements of lower concentrations with ***82*** and without ***76*** added HCl to the initial standard solution, b) measurements of higher concentrations with ***85*** and without ***79*** added HCl to the initial standard solution.

From these tests, it is evident that the quantification of PP of HCl extractions cannot be based on the quantification methods used so far. If the sample solutions have been prepared with HCl and the calibration solutions without, an overestimation of the sample solutions concentration occurs. However, in none of the HCl extractions of the oviraptorid egg shells PP has been detected. Nevertheless, these findings might help explain the impossibly high extraction ratios for PP in the spiking experiments 1 and 2. It might be possible, that in the concentration frame of PP in the spiking experiments, PP in “special acetonitrile” does not exhibit a linear relationship between detectability and the actual concentration. This might lead to the overestimation of extraction ratios for low concentrations in the spiking experiments. The “special acetonitrile” enhances the detection of PP so much presumably due to a higher concentration of calcium chloride or a well-suited pH level. The calcium chloride is generated through neutralization of the shell’s calcium carbonate with the hydrochloric acid.

However, the results for BV not being detectable in the “special acetonitrile” do not fit to the extraction ratios for BV found for the HCl extraction methods (No. 2 and No. 3) in spiking experiments 1 and 2 and the comparison of the EDTA and HCl extraction methods (No.1 and No. 2) on emu and chicken eggs (Figure 4.1.10). The spiking experiments 1 and 2 have shown BV is detectable with reasonable extraction ratios between 0.009 and 0.827 and the HCl extraction method No. 2 proved to be more efficient on the emu egg. Thus, the solvent tests will need to be repeated to determine why this discrepancy occurred.

Based on the spiking experiments 1 and 2 HCl based extraction methods are more promising. As the extraction ratios of BV for the EDTA based extraction method were so low, BV apparently needs to be extracted with HCl. However, based on the observed solvent effect, quantification of BV is difficult. For PP both EDTA and HCl based extraction methods are suitable, but quantification is difficult, due to solvent effects. However, tests with buffer systems should be performed in the future. With a buffer a defined pH level could be ensured and possibly an optimal pH level for the detection of PP and BV could be determined. PP and BV might have different optimal pH levels and thus the analysis might need to be performed separately.

4.1.5 Discussion/conclusion

Table 4.1.7 shows an overview of the measurements done at the more sensitive instruments timsTOF flex and Qtrap for the three oviraptorid egg shells *Wiemann* et al.[10] studied and the results from *Wiemann* et al.[10].

Instrument	Extraction method	Pigment	Sample ID		
			E082	E131	E132
timsTOF flex	EDTA No. 1	BV	***44*** not detectable	***46*** not detectable	***45*** false positive
		PP	***44*** false positive	***46*** 0.0019 nmol/ml	***45*** false positive
	HCl No. 2	BV	not measured	***48*** not detectable	***47*** not detectable
		PP	not measured	***48*** not detectable	***47*** not detectable
	HCl No. 3	BV	***55*** not detectable	***56*** not detectable	***57*** 0.057 nmol/ml
		PP	***55*** not detectable	***56*** not detectable	***57*** not detectable
Qtrap	EDTA No. 1	BV	not measured	***52*** not detectable	***53*** not detectable
		PP	not measured	***52*** 0.00138 nmol/ml	***53*** 0.00157 nmol/ml
Wiemann et al.[10]	EDTA No. 1	BV	0.023 nmol/ml	0.23 nmol/ml	0.068 nmol/ml
		PP	0.09 nmol/ml	0.27 nmol/ml	0.14 nmol/ml

Table 4.1.7 Overview of oviraptorid egg shell measurements at the timsTOF flex and Qtrap and results from *Wiemann* et al.[10].

Based on these results (Table 4.1.7), it seems like the samples, although from the same locality, are not all the same, i.e. not all the specimens can be treated as one sample type. When comparing the measurements ***46*** and ***48***, the EDTA extraction (No. 1) vs. the HCl extraction (No. 2), of E131, PP is only detected in the EDTA extraction and not in the HCl extraction. Although based on the spiking experiments, PP should be detectable in both. Further, it is curious as to why the measurements of E132 ***47*** and ***57*** not both show BV. Both were extracted with HCl extraction, but ***47*** with extraction

No. 2 and ***57*** with No 3. However, for ***47*** about double the amount of egg shell was used compared to ***57***, so in this case extraction method No. 2 and No. 3 should be comparable. Thus, it seems like although samples stem from the same locality, no reliable similarity in BV and PP preservation occurs. This might be due to different geological histories for the different specimens, or it might be due to maculation of the egg shells. I.e., the egg might have had a pigment-based pattern, and thus, the concentrations of pigments would fluctuated between different egg shell fragments. To overcome this issue, it would be necessary to analyze a large number of samples.

In regard to the findings of *Wiemann* et al.[10], I was not able to reproduce the results. I could only detect PP and BV at much lower concentrations and not in all three oviraptorid egg shells. The lower concentrations might be due to underestimation of my measurements, but as *Wiemann* et al.[10] omitted to describe their quantification procedure, no comparison can be made. Measurements of the HCl extractions of the oviraptorid egg shells on the Qtrap have not been performed yet, but they shall be performed in the future and the results should be promising. The detection of BV is likely, as the HCl based extraction method (No. 3) is suitable for BV extraction and with the Qtraps high sensitivity it was possible to detect PP in two samples extracted with EDTA. BV was not detected in these samples, which fits to the findings of spiking experiment 1 that the EDTA extraction method is not suitable for BV.

Further, I could not detect BV and PP in any other fossilized specimens, but most of these analyses were performed at the less sensitive instrument micrOTOF-Q and thus should be repeated at the more sensitive instrument Qtrap. Fortunately, a new Qtrap instrument will be available soon at the pharmacy department of the university of Bonn and measurement time was already granted.

4.1.6 References

[1] T. K. With, *Biochem. J.* **1974**, *137*, 596.2-598.

[2] M. D. Maines, *Curr. Protoc. Toxicol.* **2001**, *Chapter 9*, Unit 9.1.

[3] V. K. Hughes, P. S. Ellis, T. Burt, N. E. I. Langlois, *J. Clin. Pathol.* **2004**, *57*, 355.

[4] G. Y. Kennedy, H. G. Vevers, *Comp. Biochem. Physiol. B* **1976**, *55*, 117.

[5] R. M. Kilner, *Biol. Rev Camb. Philos. Soc.* **2006**, *81*, 383.

[6] A. Gorchein, C. K. Lim, P. Cassey, *Biomed. Chromatogr.* **2009**, *23*, 602.

[7] N. H. Sparks, *Avian Biol. Res.* **2011**, *4*, 162.

[8] P. Cassey, Thomas, Gavin H., Portugal, Steven J., Maurer, Golo, M. E. Hauber, T. Grim, P. G. LOVELL, I. Miksik, *Biol. J. Linn. Soc.* **2012**, *106*, 657.

[9] a) P. A. Leighton, J. A. Horrocks, D. L. Kramer, *Behav. Ecol.* **2009**, *20*, 1299; b) M. Packard, R. Seymour, S. Sumida, K. Martin, *Amniote Origins, chapter 8*, Elsevier Science, **1997**.

[10] J. Wiemann, T.-R. Yang, P. N. Sander, M. Schneider, M. Engeser, S. Kath-Schorr, C. E. Müller, P. M. Sander, *PeerJ* **2017**, *5*.

[11] W. C. Hewitson, *British oology*, Published for the author by C. Empson, Newcastle upon Tyne, **1833**.

[12] A. Newton, R. Lydekker, C. S. Roy, R. W. Shufeldt, *A dictionary of birds*, A. and C. Black, London, **1896**.

[13] M. E. Hauber, M. Dainson, D. T. Baldassarre, M. Hossain, M. Holford, C. Riehl, *J. Avian. Biol.* **2018**, *49*, e01776.

[14] I. J. Øien, A. Moksnes, E. Røskaft, *Behav. Ecol.* **1995**, *6*, 166.

[15] M. Niittynen, J. T. Tuomisto, S. Auriola, R. Pohjanvirta, P. Syrjälä, U. Simanainen, M. Viluksela, J. Tuomisto, *Toxicol. Sci.* **2003**, *71*, 112.

[16] M. Danton, C. K. Lim, *Biomed. Chromatogr.* **2006**, *20*, 612.

[17] P. Macours, F. Cotton, *Clin. Chem. Lab. Med.* **2006**, *44*, 1433.

[18] E. Rossi, P. Garcia-Webb, *Biomed. Chromatogr.* **1986**, *1*, 163.

[19] a) C. Taylor, L. K. Duffy, F. G. Plumley, R. T. Bowyer, *Environ. Res.* **2000**, *84*, 56; b) R. Mateo, G. Castells, A. J. Green, C. Godoy, C. Cristòfol, *J. Chromatogr. B* **2004**, *810*, 305.

[20] D. Chen, J. D. Brown, Y. Kawasaki, J. Bommer, J. Y. Takemoto, *BMC Biotech.* **2012**, *12*, 89.

[21] a) J.-I. Wakamatsu, H. Odagiri, T. Nishimura, A. Hattori, *Meat Sci.* **2009**, *82*, 139; b) J.-I. Wakamatsu, J. Okui, N. Hayashi, T. Nishimura, A. Hattori, *Meat Sci.* **2007**, *77*, 580.

[22] F. Jüttner, M. Stiesch, W. Ternes, *Eur. Food Res. Technol.* **2013**, *236*, 943.

[23] a) M. E. Hauber, A. L. Bond, A.-L. Kouwenberg, G. J. Robertson, E. S. Hansen, M. Holford, M. Dainson, A. Luro, J. Dale, *J. R. Soc. Interface* **2019**, *16*, 20190115; b) R. Zhao, G. Y. Xu, Z. Z. Liu, J. Y. Li, N. Yang, *Poult. Sci.* **2006**, *85*, 546.

[24] A. Verdes, W. Cho, M. Hossain, P. L. R. Brennan, D. Hanley, T. GRIM, M. E. Hauber, M. Holford, *PloS one* **2015**, *10*, e0143545.

[25] B. Igic, D. R. Greenwood, D. J. Palmer, P. Cassey, B. J. Gill, T. Grim, P. L. R. Brennan, S. M. Bassett, P. F. Battley, M. E. Hauber, *Chemoecology* **2010**, *20*, 43.

[26] J. Moreno, E. Lobato, J. Morales, S. Merino, G. Tomás, J. La Martínez-de Puente, J. J. Sanz, R. Mateo, J. J. Soler, *Behav. Ecol.* **2006**, *17*, 651.

[27] I. Mikšík, V. Holáň, Z. Deyl, *Comp. Biochem. Physiol. B* **1996**, *113*, 607.

[28] E. Schweda, *Jander/Blasius, Anorganische Chemie II. Quantitative Analyse und Präparate*, Hirzel, S., Verlag, Stuttgart, **2016**.

[29] D. J. Varricchio, F. D. Jackson, *J. Vertebr. Paleontol.* **2004**, *24*, 931.

[30] M. A. Norell, J. M. Clark, L. M. Chiappe, D. Dashzeveg, *Nature* **1995**, *378*, 774.

[31] Michael B. H., "Nesting Nemegtomaia", can be found under https://commons.wikimedia.org/wiki/File:Nesting_Nemegtomaia.jpg.

[32] a) M. Huh, B. S. Kim, Y. Woo, D. J. Simon, I. S. Paik, H. J. Kim, *Hist. Biol.* **2014**, *26*, 218; b) H. Pu, D. K. Zelenitsky, J. Lü, P. J. Currie, K. Carpenter, L. Xu, E. B. Koppelhus, S. Jia, Le Xiao, H. Chuang et al., *Nat. Commun.* **2017**, 14952.

[33] A. D. Kinghorn, H. Falk, S. Gibbons, J. Kobayashi, *Progress in the Chemistry of Organic Natural Products 104*, Springer International Publishing, Cham, **2017**.

4.2 Mass spectrometric analysis of fossilized wood

4.2.1 Introduction

The fossil specimen studied here was found embedded in the silty sandstones of the Late Jurassic Morrison Formation in Six Mile Draw (North East Utah, USA). It is a woody tree trunk from a *gymnosperm coniferous Araucariaceae*. The fossilized specimen first drew our attention because it is varicolored: macroscopic examination reveals three different domains, which can be distinguished by the intensity of their coloration – dark, medium, and light (Figure 4.2.1).

Figure 4.2.1 Plane-polarized light microscopic picture of specimen. Left to right dark, medium and light domain.

In palaeobotanical fossilization, silicification is a highly relevant process through which internal tissues in plants are preserved.[1] In silicification fluid fronts with dissolved silicates penetrate the specimen, and over time the silicate precipitates, preserving the underlying structure.[1] Through the preservation, information is gained about the life history and evolution of land plants and their anatomy.[1]

The plant division of *coniferous gymnosperms* includes many commonly known conifer trees like pine, cypress, cedar, hemlock, larch, spruce, and redwood.[2] Wood is comprised of three main components next to water: cellulose, hemicelluloses, and lignin.[3] Cellulose is the most abundant natural organic polymer (Figure 4.2.2).[4,5] It is a polysaccharide comprised of D-glucose building blocks, with degrees of polymerization of e.g. 300 and 1700 for wood pulp and 800-10000 for cotton and other plant fibers.[4]

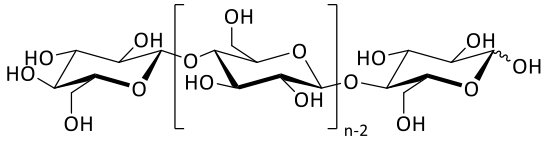

Figure 4.2.2 Structure of cellulose (n = degree of polymerization).

Lignin is a polymer that gives structural support and provides rigidity and compressive strength to wood.[6] The polymer forms through oxidative coupling of three different monolignols, the lignin

monomers.[2,7] They have the basic structure of *p*-hydroxy-cinnamyl alcohol, which is also called *p*-coumarylalcohol (see Figure 4.2.3).[2,7] The other two have one or two additional methoxy groups at the aromatic ring and are called coniferyl- and sinapylalcohol (see Figure 4.2.3).[2,7] In conifer trees, lignin is made up primarily from the *p*-coumaryl- and coniferylalcohol forming the lignin units of *p*-hydroxyphenyl (H) and guaiacyl (G) respectively.[2] Mass spectrometric studies of extant wood show lignin monomers, dimers, and trimers.[8,9]

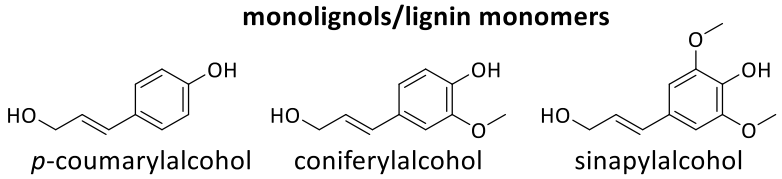

Figure 4.2.3 Monolignols *p*-coumaryl-, coniferyl- and sinapylalcohol.

To transport or store monolignols within the plant, monolignol glucosides are used in the lignification process. [10–13] In a monolignol glucoside, the monolignol forms a glycosidic bond with a glucose. Coniferin is one possible monolignol glucoside, where a glucose molecule is bound to a coniferylalcohol (see Figure 4.2.4).[10,14]

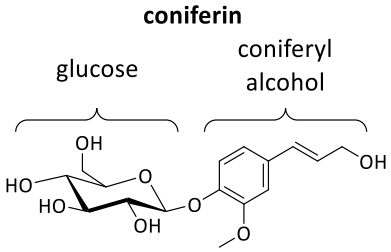

Figure 4.2.4 Coniferin: a monolignol glucoside made from the subunits glucose and coniferylalcohol.

To the best of my knowledge, only one previous mass spectrometric study was performed on silicified wood. In 1978 *Sigleo*[15] studied a specimen of black silicified wood with Pyrolysis-GC-MS, finding phenolic compounds, which are indicative of degraded lignin.

Within our study, several different analytical methods were used by different cooperation partners. I will briefly summarize the results of polarized light microscopy, electron probe micro analysis (EPMA), Fourier-transform infrared (FTIR) spectroscopy, and Raman spectroscopy from my cooperation partners in chapter 4.2.2. In detail, I will present the results of the MALDI MS experiments performed by myself in chapter 4.2.3.

4.2.2 Analyses performed by cooperation partners

Polarized light microscopy shows that the anatomical structure of the wood is well preserved in the darkest regions, and toward lighter domains its microscopic visibility decreases. Further, a fibrous microstructure can be seen, and that the sample consists of chalcedony (α-quartz).

With Raman spectroscopy the silica/carbon ratio in the different domains were studied, by comparing the intensity of the α-quartz band (465 cm^{-1}) with the carbon G_L-band (≈1600 cm^{-1}). As expected from the visual inspection, the intensity of the carbon G_L-band increases with the darkening of the color of the wood, which means higher carbon concentration in darker wood. Additionally, from the full width at half-maximum of the D1-band, the peak temperature the sample experienced could be determined to be 100 ± 6 °C.

FTIR analysis of a demineralized sample of the dark wood show guaiacyl ring vibrations of lignin.

With EPMA (electron probe micro analysis) trace element distribution mappings were performed. Calcium and sulfur were found to highlight the wood anatomy, i.e. the cell walls (Figure 4.2.5). However, the two trace elements show the anatomy in different ways. For the sulfur trace element distribution higher intensities are found in the cell walls of the darkest domain. The distribution of calcium shows a more complex pattern; medium intensity is found in the medium colored domain and a thin band with high intensity can be found in the dark domain directly neighboring the medium domain.

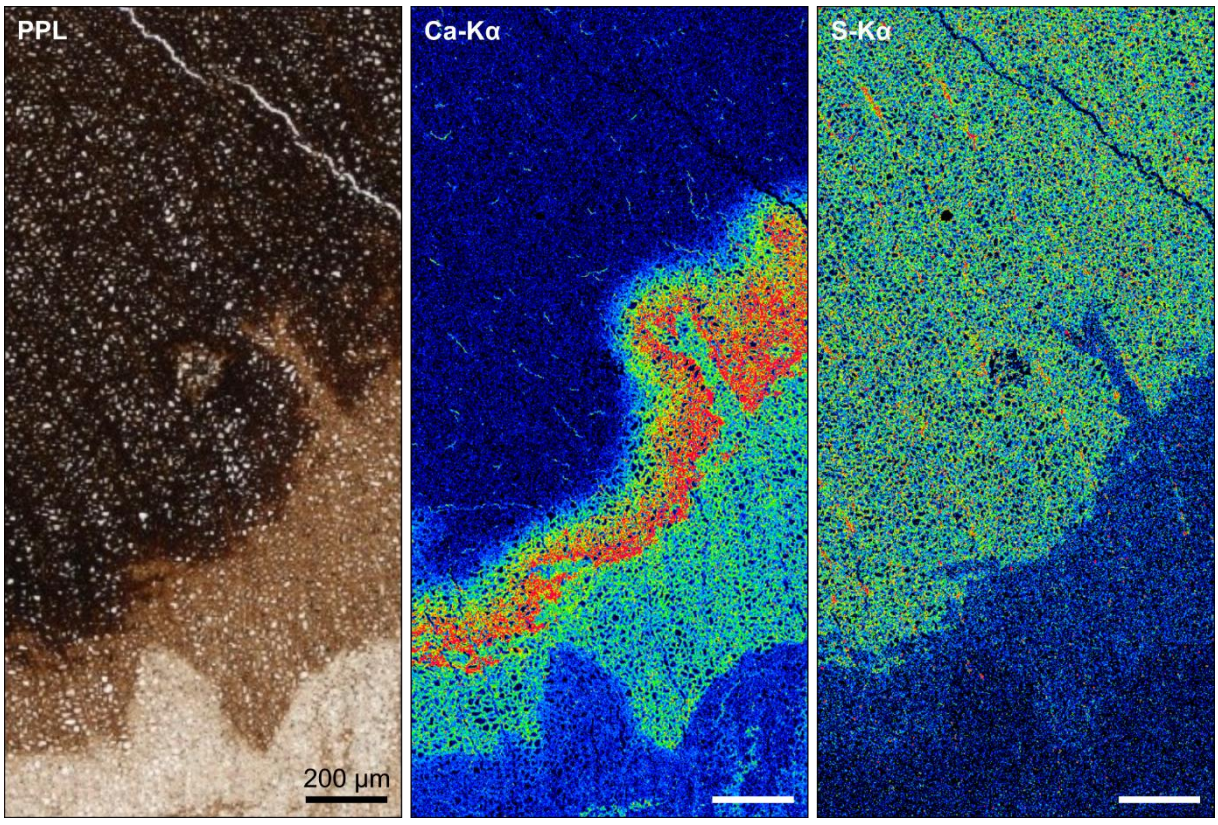

Figure 4.2.5 Plane-polarized light microscopic picture, calcium and sulfur EPMA mapping.

4.2.3 MALDI MS

The MALDI MS experiments' objective on the varicolored sample of fossilized wood is to see if the differences in color between the domains are also reflected in differences in the MALDI spectra. An additional goal is to determine if it is possible to detect preserved organic compounds of wood in this 150 million-year-old specimen of a conifer tree.

In the field of modern plant biology, MALDI MS [16] and spatially-resolved MALDI imaging[17,18] are well-established methods. However, samples of modern plant biology are not fossilized. MALDI analysis usually requires the sample to be either soluble in an organic solvent or, in the case of MALDI imaging, a thin section of soft tissue. The fossilized wood sample is not soft, neither is it soluble in an organic solvent. Thus, the sample preparation method needed to be modified in order to record MALDI MS spectra.

4.2.3.1 Sample preparation

Different methods of sample preparation and a series of typical MALDI matrices were tested[17,19]. The following suspension preparation proved to yield meaningful MALDI MS spectra. The sample was a fine powder, which was obtained through drilling into each domain of the specimen. The matrix 2,4,6-trihydroxyacetophenone (THAP) was dissolved in dimethylformamide (DMF). In this solution the sample powder was suspended and then transferred to a ground stainless-steel MALDI target plate. The suspension was spread out as evenly and thin as possible and dried at room temperature before measurement. The measurement was performed on an *ultrafleXtreme* MALDI-time of flight (TOF) instrument from *Bruker Daltonik*. The laser intensities needed to be relatively high in order to obtain reasonable signal intensities.

4.2.3.2 Results and interpretation of results

I performed measurements of samples from the light, medium, and dark domains, and further of powder gained from desilicifying the dark domain with hydrofluoric acid (HF) extraction. Figure 4.2.6 shows these MALDI spectra of the domains a) light, b) medium, c) dark, d) dark HF, and e) blank measurement of only THAP and DMF. Differences are obvious between the different domains.

A neutral molecule **1** with a mass of 342.12 Da can be inferred from the three signals *m/z* 343, *m/z* 365, and *m/z* 381, which stem from the protonated molecule [**1**+H]$^+$ and from adducts with sodium and potassium ions ([**1**+Na]$^+$, [**1**+K]$^+$). Another neutral molecule **2** with a mass of 358.06 Da might be responsible for the three signals *m/z* 359, *m/z* 381, and *m/z* 397. However, severe superposition with other signals (see annotation Figure 4.2.6) does not allow for a definite conclusion for **2**. As many as four other molecular compounds **3**-**6** could be detected as well. The signals for the matrix THAP are annotated with a ***** and shown in an inset of e) blank. A few of the annotated signals are found in the

blank measurement too (Figure 4.2.6 e) and Figure 6.4.1 p. 156). However, the intensities of these signals are significantly higher in the spectra of the samples than in the blank measurement.

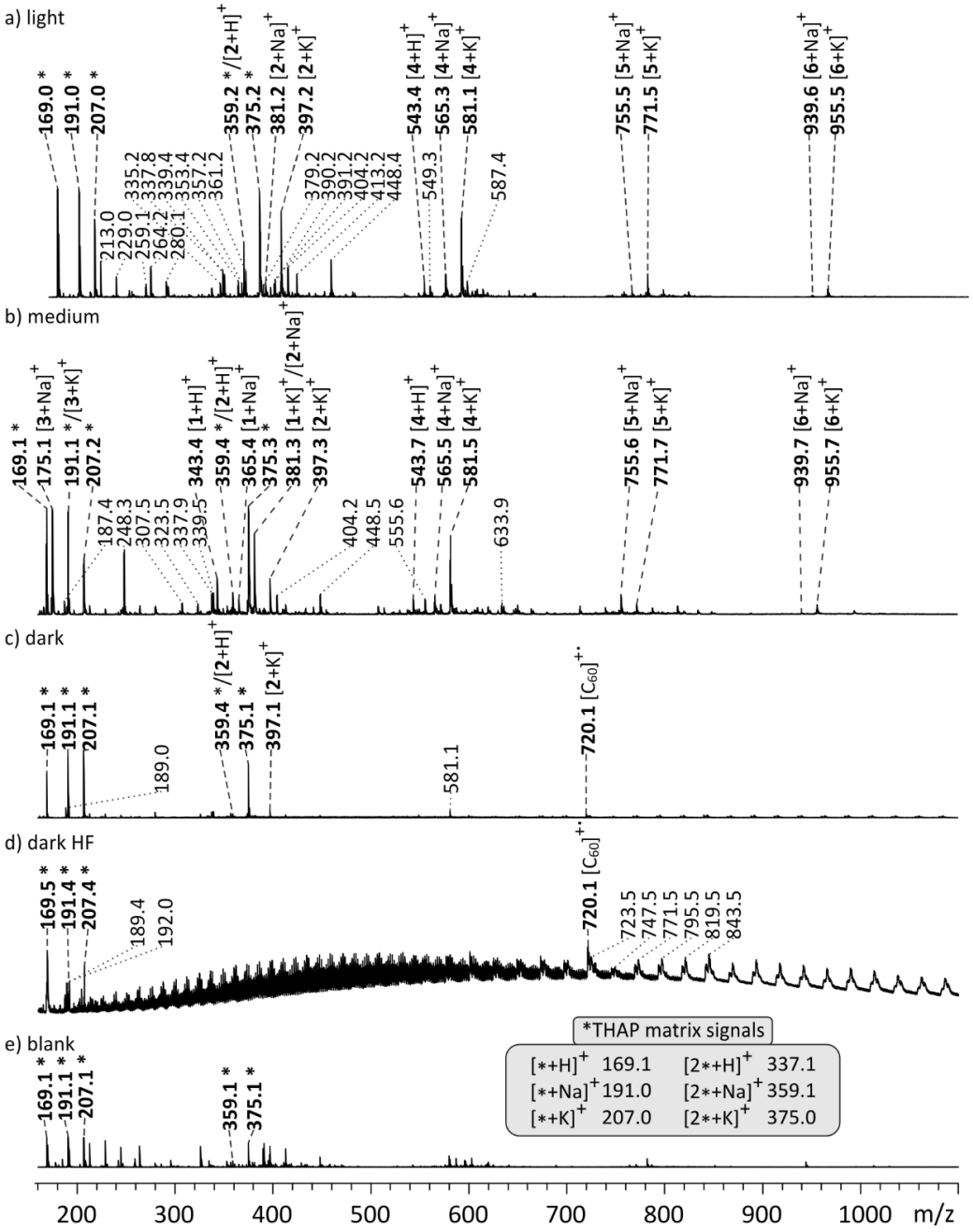

Figure 4.2.6 MALDI mass spectra (matrix THAP) of the domains a) light, b) medium, c) dark d) dark after HF extraction, and e) blank measurement. All peaks are annotated, which have a relative intensity above 10 %. In **Figure 6.4.1** p. 156 the blank spectrum e) is fully annotated. The signals were assigned after the spectra of the mass region up to *m/z* 400 were recalibrated and the peaks compared to the exact mass of the compounds. This can be seen in **Table 6.4.1** p. 157. In non-bold additional signals without assignment are annotated. Due to superposition the following signals are assigned to multiple species: *m/z* 381 to both [**1**+K]$^+$ and [**2**+Na]$^+$, *m/z* 191 to both [THAP+Na]$^+$ and [**3**+K]$^+$ in medium spectra b), as throughout the spectra potassium adducts are abundant and in medium spectrum b) *m/z* 175 [**3**+Na]$^+$ has a high intensity. Mainly [2*THAP+Na]$^+$ and minor amounts of [**2**+H]$^+$ might be assigned to *m/z* 359.

1 is mainly detected in the medium domain (Figure 4.2.6 b)) and corresponds well to the presence of basic building blocks of wood. Either a hexose disaccharide like cellobiose[20] **1a** or coniferin [10,14,21] **1b** (Figure 4.2.7) can be assigned to **1**. The measured mass value fits to both compounds within the experiment's mass accuracy (Table 6.4.1 p. 157). As mentioned above, coniferin **1b** is a monolignol glucoside, which takes part in the lignification process[10–12], as the monolignols' storage and transport form[13]. Hexose disaccharides can be a vast number of isomers of different combinations of sugars, which need special mass spectrometric means to be distinguished from one another.[22] However, our interpretation of the hexose disaccharide as cellobiose is likely. Because one main component of wood is cellulose[3] (Figure 4.2.2) and as cellobiose consists of two glucose molecules[20], cellobiose could be described as a degradation product of cellulose: cellulose with a degree of polymerization of two (Figure 4.2.7).

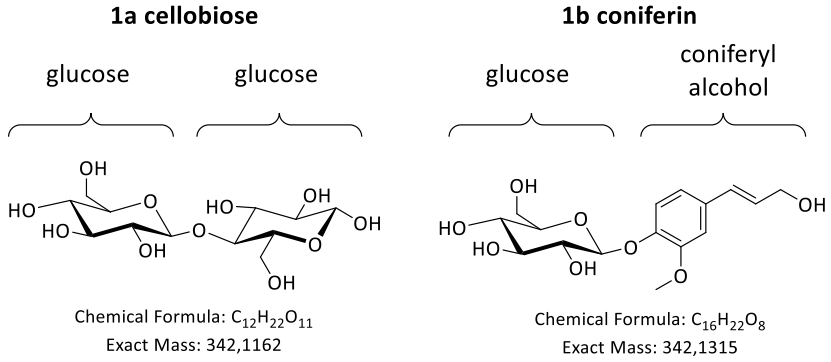

Figure 4.2.7 1a Cellobiose and **1b** coniferin.

Coniferin and cellobiose are not isomeric structures as they have different elemental compositions. Thus, they could be distinguished from one another with an accurate mass determination. However, within the MALDI experiment it was not possible to achieve a sufficient resolution and mass accuracy. Unfortunately, this is due to the uneven suspension sample preparation, which none the less was the best way to gain MALDI spectra at all. To gain higher mass accuracy, I attempted ESI and APCI MS (atmospheric pressure chemical ionization) measurements on the Orbitrap XL instrument with high resolving power. A liquid sample form is needed for ESI or APCI measurements. Thus, I extracted the sample powders with DMF in an ultrasonic bath. Neither in the ESI nor the APCI spectra **1** or **2** were detected. Apparently, the high intensity laser during the MALDI process is necessary to liberate the compounds from the solid sample powder. Therefore, I have to conclude that I am detecting either or both coniferin and cellobiose without being able to distinguish between them.

As mentioned above lignin is another basic building block of wood[6,23]; a polymer based on three different monomers/monolignols: *p*-coumaryl-, coniferyl- and sinapylalcohol (Figure 4.2.8).[6,23] Typically, remaining soluble monomers and oligomers can be detected in mass spectra of lignin-containing samples [8,9,23,24], such as lignin dimers of two monolignols. Molecule **2** might be assigned to

such a monolignol dimer of an elemental composition $C_{20}H_{22}O_6$ with a mass of 358.14 Da. Two isomeric structures are possible for **2**: a dimer based on two coniferylalcohols **2a** or a dimer based on a *p*-coumaryl- and a sinapylalcohol **2b** (Figure 4.2.8). In conifers, coniferylalcohol is the most abundant monolignol[2,14], as the name suggests. Thus, assigning **2** to the isomer **2a** in a sample of fossilized wood from a conifer tree seems reasonable. Further, this fits to the FTIR results of lignin guaicyl units, which are made up of the coniferylalcohol monolignol.

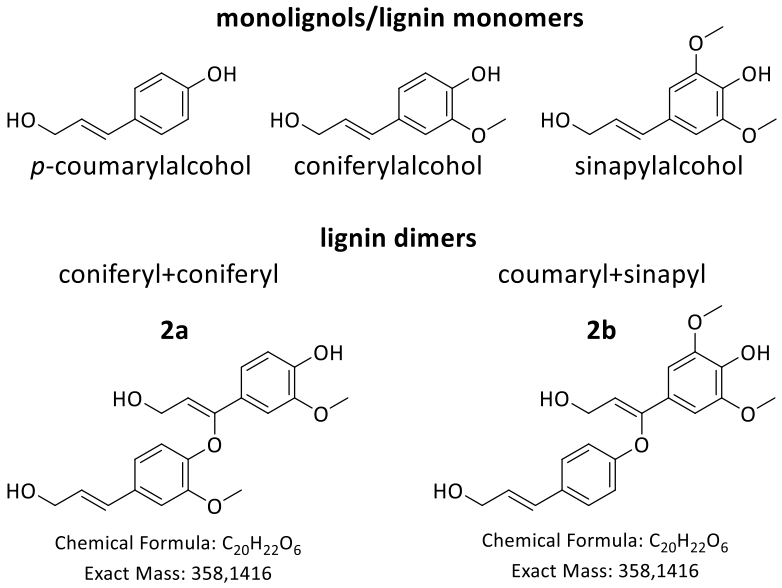

Figure 4.2.8 Monolignols/lignin monomers, *p*-coumaryl- coniferyl- and sinapylalcohol, and lignin dimers **2a** and **2b**.

When looking at the higher *m/z* values of the dark spectra c) in Figure 4.2.6, a regular pattern can be seen, although not as strong as the pattern in the dark HF spectra d) in Figure 4.2.6. In Figure 4.2.9 the mass range of *m/z* 640-2050 is shown. The pattern of signal groups 24 Da apart is apparent in dark b), dark HF c), and graphite d), which was used as reference material. Also, in all three spectra the C_{60}-fullerene signal at *m/z* 720 can be seen. Due to the similarity of the spectra from dark b) and graphite d) (Figure 4.2.9), it could be concluded that graphite or another form of elemental carbon is contained in the dark domain. When measuring the dark domain with Raman, no graphite but amorphous carbon was detected. As the only difference between graphite and amorphous carbon is the level of organization in the solid state, it is not surprising that the measurements of their gas-phase ions with MALDI are very similar. Thus, the presence of amorphous carbon in the dark domain is fully supported by the MALDI results. This explains the dark coloration, as amorphous carbon is black and is only found in the dark domain and not in the medium or light domain.

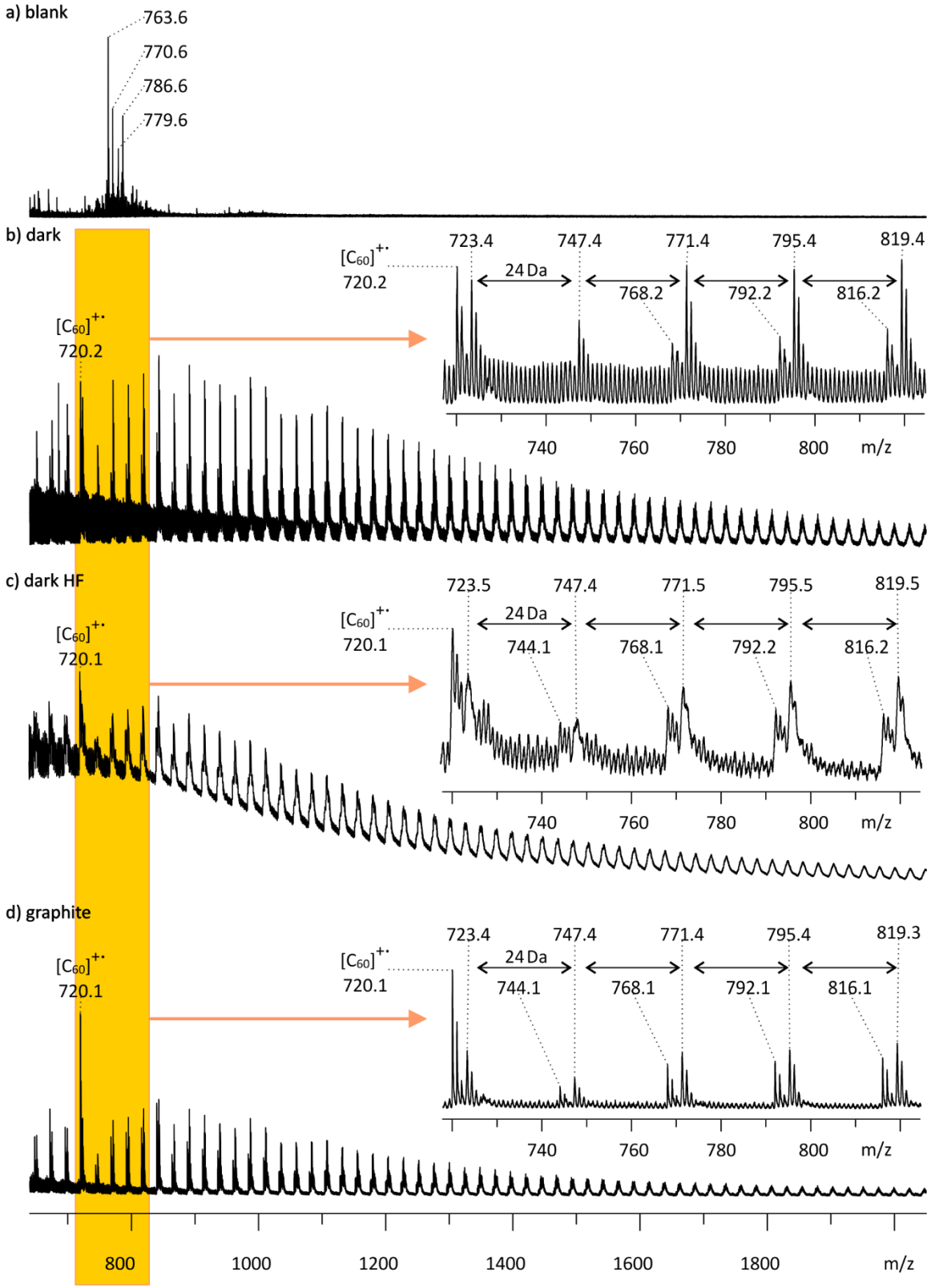

Figure 4.2.9 MALDI mass spectra (matrix THAP) *m/z* 640-2050 of a) blank (DMF and THAP), b) dark domain including zoom into *m/z* range 720-820, c) HF treated dark domain including zoom into *m/z* range 720-820 and d) graphite including zoom into *m/z* range 720-820. The graphite sample was prepared with the rubbing method described in the experimental details chapter 4.2.5.

Treatment of the dark sample powder with HF removed silicate very effectively, but organic substances were also removed. In the dark HF spectrum Figure 4.2.6 d) and Figure 4.2.9 c) only the signals for carbon can be detected, whereas in all other samples organic substances can be found; especially in the light and medium domains. Although, the organic substances could be present in similar amounts in the untreated dark domain because suppression effects could have occurred. Suppression effects caused by easily ionizable substances are a known phenomenon in MALDI measurements of complex mixtures.[17]

4.2.3.3 Conclusion MALDI MS experiments

With the MALDI MS experiments, I was able to identify organic compounds in a silicified 150 million-years-old specimen of coniferous wood and assign these compounds to specifically colored domains. Typical building blocks of wood, like lignin, cellobiose and coniferin have been detected, which agrees well with the results from FTIR measurements. In addition, the MALDI MS experiments show carbon in the dark domain, which is in agreement with Raman mappings.

4.2.4 Conclusion

Based on optical microscopy, Raman spectroscopy, and EPMA trace element mapping of calcium, at least three silicification episodes can be distinguished. Calcium represents a primary constituent that was present throughout the cell walls before the silicification episodes and thus serves as an indicator for the silicification events. Firstly, the entire specimen underwent the initial silicification in which primary organic material is impregnated by dissolved silica,[1] which reduces cell wall degradation. Nano- and micropores are generated through the selective decomposition of cell wall constituents and provide fluid pathways that allow further removal of organic substance during subsequent silicification cycles. This initial silicification event resulted in an optically dark appearance of the sample. This is documented by the decreasing carbon abundance in Raman mappings, and the detection of amorphous carbon in only the dark domain with MALDI MS. The medium colored domain is formed through decoloration in the second silicification event. Even further decoloration during the third silicification event forms the light domain. Importantly, these domains coincide with a successive loss of the calcium concentration.

The dark domain seems to represent the least altered wood substance and is where most organic matter was expected. However, the MALDI MS experiments only detect a high carbon concentration in the darkest domain, which contrasts with the more distinct signals from the medium and light domains. Likely, the organic substances found in the medium and light domains are also present in the dark domain, but the dark domain's spectra are likely affected by suppression effects, which might conceal the organic substances.

The overprint intensity (changes during fossilization) in the first three silicification episodes can be seen by the decreasing organic matter removal. This process is followed by a reduction of the fluid-accessible pore space by newly precipitated silica. The last chemical overprint of the wood sample is characterized by sulfur enrichment in the darkest domain and preservation of a thin calcium-rich band. The sulfur enrichment in the dark domain likely results from the sulfur bonding to the accessible remaining organic matter. The limited fluid pathways and organic matter abundance lead to a relative sulfur-rich dark domain compared to the more extensively leached medium and light domains. The silicification process ends with fracturing across all previously silicified domains and the final infilling of cracks with wall-lining chalcedony. Using high-resolution analytical methods, insight could be gained into the silicification process across several stages and preservation of organic compounds of the varicolored fossil wood specimen.

4.2.5 Experimental details

Sample powder generation

The sample powder was generated through drilling into the different domains with a diamond drill.

HF extraction

Powders from sawn and crushed dark domains of the silicified wood samples were demineralized with 40% hydrofluoric acid (HF) and subsequently washed with cold 6N HCl and distilled water by centrifugation.

Two different sample preparation methods for the MALDI MS experiments were used: the first using suspension and the second a solvent-free rubbing method. Different matrices were tested DHB (2,5-dihydroxybenzoic acid), HCCA (*alpha*-cyano-4-hydroxycinnamic acid) and THAP (2,4,6-trihydroxyacetophenone). THAP yielded the best results.

Sample preparation method with suspension used for light, medium, dark and dark HF measurements:

Approx. 0.6 mg of the sample powder was placed in an Eppendorf tube. 2.5 mg of the matrix 2’,4’,6’-trihydroxyacetophenone (THAP) was dissolved in dimethylformamide (DMF, 67.5 µl). With an Eppendorf pipette 0.5 µl of the matrix solution were added to the sample powder in the Eppendorf tube. With the Eppendorf pipette the suspension of matrix solution was sucked into the Eppendorf

pipette tip and ejected onto the MALDI target. With the pipette tip the mixture was spread as evenly as possible.

Sample preparation with rubbing used for graphite sample:

In a ratio of 1:10 the sample and 2',4',6'-Trihydroxyacetophenone (THAP) were added in a mortar and mixed with the pestle. The solid mixture was placed onto the MALDI target. With the flat side of a plastic spatula the mixture is rubbed into the MALDI targets surface. The MALDI target has furrows on its surface, as it is brushed steel. Loose solid was scraped of the MALDI targets surface with the edge of the spatula. The sample and matrix mixture is thus deposited in the furrows of the MALDI target.

Sample preparation for blank measurement:

2.5 mg of the matrix 2',4',6'-Trihydroxyacetophenone (THAP) was dissolved in dimethylformamide (DMF, 67.5 µl). This matrix solution (0.5 µl) is transferred to the MALDI target.

Sample preparation for ESI- and APCI-MS measurements:

100 µl of DMF were added to 1.5 mg of sample powder in an Eppendorf vial. For one hour the vial was placed in an ultrasonic bath. Then the vial was centrifuged. 70 µl of the resulting supernatant were mixed with 70 µl acetonitrile. This mixture was analyzed by ESI- and APCI-MS on an *Orbitrap* instrument.

Instruments

The *ultrafleXtreme* TOF/TOF MALDI mass spectrometer from *Bruker Daltonik,* Bremen was used for the MALDI measurements. The internal calibration was based on the matrix peaks *m/z* 169.050, 191.032 and 375.048. Unfortunately, I was not able to achieve a high resolution and mass accuracy in the MALDI experiments. This is due to the inevitably uneven solid-state sample preparation.

ESI and APCI measurements were performed with an Orbitrap XL from *Thermo Fisher Scientific,* Bremen.

4.2.6 References

[1] M. Liesegang, C. T. Gee, *Palaeontology* **2020**, *63*, 651.

[2] A. Wagner, L. Donaldson, J. Ralph in *Advances in Botanical Research* (Eds.: A. Wagner, L. Dondaldson, J. J. R. Ralph), Elsevier, **2012**, pp. 37–76.

[3] E. Sjöström, *Wood Chemistry*, Elsevier, **1993**.

[4] D. Klemm, B. Heublein, H.-P. Fink, A. Bohn, *Angew. Chem. Int. Ed.* **2005**, *44*, 3358.

[5] R. Zhbankov, S. Firsov, D. Buslov, N. Nikonenko, M. Marchewka, H. Ratajczak, *J. Mol. Struct.* **2002**, *614*, 117.

[6] R. Whetten, R. Sederoff, *Plant Cell* **1995**, *7*, 1001.

[7] J. Ralph, K. Lundquist, G. Brunow, F. Lu, H. Kim, P. F. Schatz, J. M. Marita, R. D. Hatfield, S. A. Ralph, J. H. Christensen et al., *Phytochem. Rev.* **2004**, *3*, 29.

[8] E. Kiyota, P. Mazzafera, A. C. H. F. Sawaya, *Anal. Chem.* **2012**, *84*, 7015.

[9] K. Saito, T. Kato, H. Takamori, T. Kishimoto, K. Fukushima, *Biomacromolecules* **2005**, *6*, 2688.

[10] A. Yoshinaga, H. Kamitakahara, K. Takabe, *Tree Physiol.* **2016**, *36*, 643.

[11] K. Freudenberg, J. M. Harkin, *Phytochemistry* **1963**, *2*, 189.

[12] K. Freudenberg, J. Torres-Serres, *Ann.* **1967**, *703*, 225.

[13] N. Terashima, C. Ko, Y. Matsushita, U. Westermark, *Holzforschung* **2016**, *70*, 801.

[14] M. Kaneda, K. H. Rensing, J. C. T. Wong, B. Banno, S. D. Mansfield, A. L. Samuels, *Plant Physiol.* **2008**, *147*, 1750.

[15] A. C. Sigleo, *Geochim. Cosmochim. Acta* **1978**, *42*, 1397.

[16] a) D. Sturtevant, Y.-J. Lee, K. D. Chapman, *Curr. Opin. Biotechnol.* **2016**, *37*, 53; b) S. Kaspar, M. Peukert, A. Svatos, A. Matros, H.-P. Mock, *Proteomics* **2011**, *11*, 1840; c) M. Monagas, J. E. Quintanilla-López, C. Gómez-Cordovés, B. Bartolomé, R. Lebrón-Aguilar, *J. Pharm. Biomed. Anal.* **2010**, *51*, 358; d) M. Peukert, A. Matros, G. Lattanzio, S. Kaspar, J. Abadía, H.-P. Mock, *New Phytol.* **2012**, *193*, 806.

[17] F. Hillenkamp, J. Peter-Katalinić (Eds.) *MALDI MS. A practical guide to instrumentation, methods and applications*, Wiley - VCH, Weinheim, **2009**.

[18] E. R. van Amstalden Hove, D. F. Smith, R. M. A. Heeren, *J. Chromatogr. A* **2010**, *1217*, 3946.

[19] D. S. Kosyakov, N. V. Ul'yanovskii, E. A. Sorokina, N. S. Gorbova, *J. Anal. Chem.* **2014**, *69*, 1344.

[20] S. Ren, L. Zhang, Z. Cheng, Y. Guo, *J. Am. Soc. Mass Spectrom.* **2005**, *16*, 333.

[21] D. Aoki, Y. Hanaya, T. Akita, Y. Matsushita, M. Yoshida, K. Kuroda, S. Yagami, R. Takama, K. Fukushima, *Sci. Rep.* **2016**, *6*, 31525.

[22] a) K. Pagel, D. J. Harvey, *Anal. Chem.* **2013**, *85*, 5138; b) J. Hofmann, K. Pagel, *Angew. Chem. Int. Ed.* **2017**, *56*, 8342.

[23] P. Araújo, M. S. Ferreira, D. N. de Oliveira, L. Pereira, A. C. H. F. Sawaya, R. R. Catharino, P. Mazzafera, *Anal. Chem.* **2014**, *86*, 3415.

[24] K. Saito, T. Kato, Y. Tsuji, K. Fukushima, *Biomacromolecules* **2005**, *6*, 678.

5 Conclusion

With ESI MS I extensively and successfully studied two L-proline catalyzed reactions. For the first reaction of α,β-unsaturated aldehydes I was able to revise the catalytic cycle by adding two additional species. I performed MS^n experiments on the postulated intermediates and could induce them to mimic their catalytic steps in the gas phase. Thereby, I confirmed the catalytic cycle and the detected ions as intermediates. Through the study of the temporal progress of the reaction, I found the rate-determining step.

In the second L-proline catalyzed reaction of acetone with a tetrazine, three intermediates were postulated. Without charge-tagging, I only found two of the three intermediates. However, when utilizing the charge-tagged L-proline derived catalyst, I could detect the elusive third intermediate. Through this first experimental detection, I could prove that the reaction occurs in a stepwise manner via this elusive intermediate and not in one concerted step from the first to the third intermediate.

The search for two pigments in dinosaur egg shells by HPLC-ESI MS proved to be challenging. I could only reproduce the project's preliminary work in parts, as the pigments were only detected sparingly. Further work on the project is needed, but future steps can build on the insights I could gain so far.

The study on a varicolored specimen of silicified wood with MALDI MS was successful. Amorphous carbon could be detected, which explains the differently colored domains. Fascinatingly, I could further detect organic compounds, like lignin, cellobiose and coniferin, which are basic building blocks of wood.

This work has shown that mass spectrometry is a useful tool for different scientific problems like studying reaction mechanisms to find elusive intermediates or detecting compounds in millions of year-old fossils.

6 Appendix

6.1 Additional material for chapter 3.2

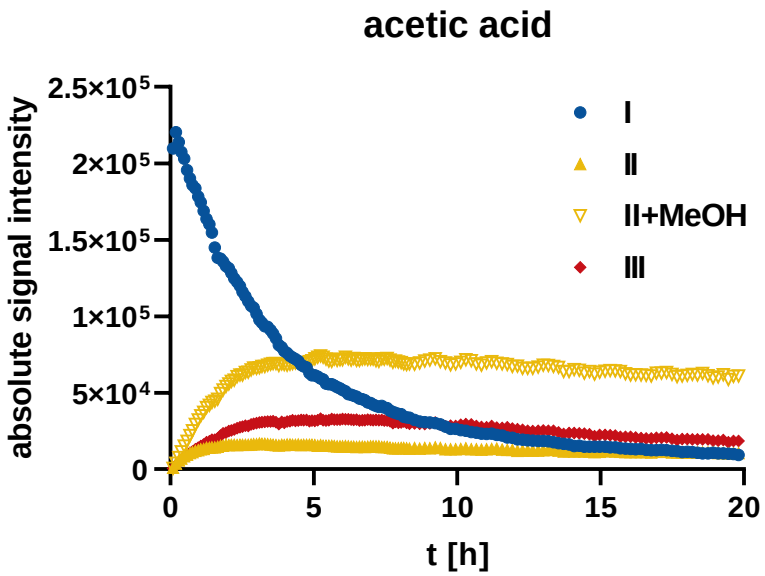

Figure 6.1.1 Temporal progress of the L-proline catalyzed reaction with *trans*-2-hexenal **2** with acetic acid based on micrOTOF-Q spectra. The H and Na-adduct signals were added for plotting. **I** (*m/z* 196, 218), **II** (*m/z* 294,316), **II**+MeOH (*m/z* 326, 348), **III** (only *m/z* 276).

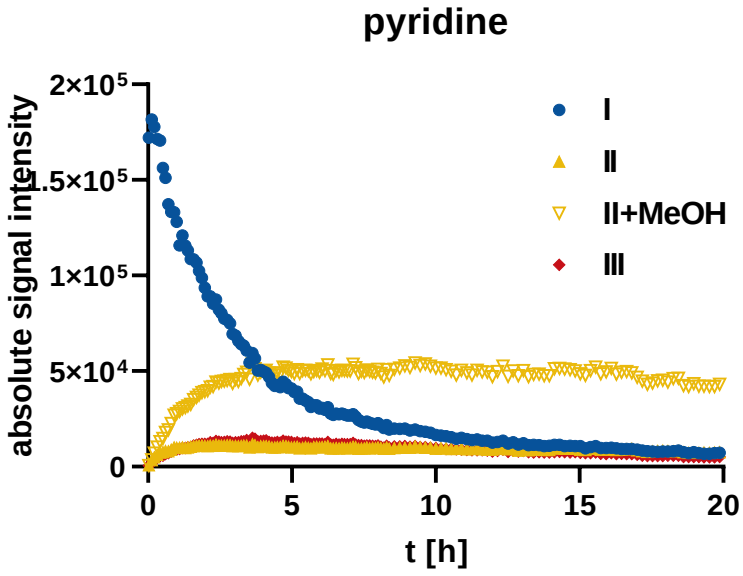

Figure 6.1.2 Temporal progress of the L-proline catalyzed reaction with *trans*-2-hexenal **2** with pyridine based on micrOTOF-Q spectra. The H and Na-adduct signals were added for plotting. **I** (*m/z* 196, 218), **II** (*m/z* 294,316), **II**+MeOH (*m/z* 326, 348), **III** (only *m/z* 276).

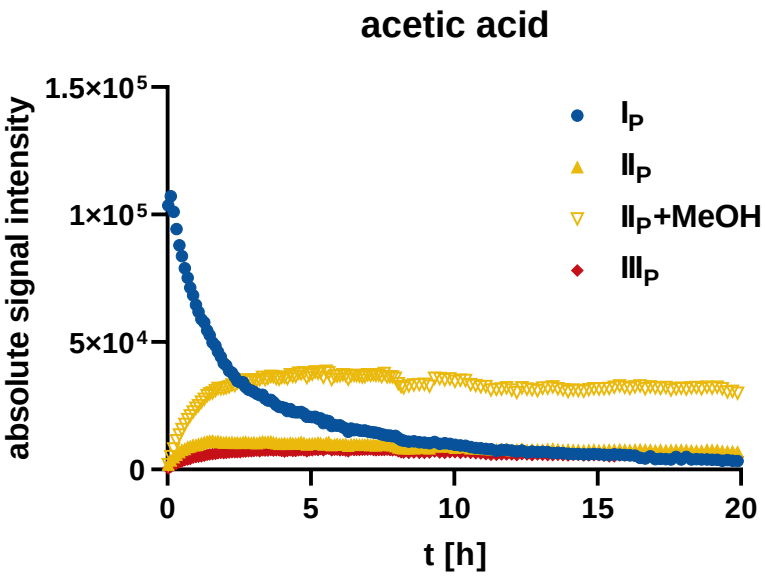

Figure 6.1.3 Temporal progress of the L-proline catalyzed reaction with *trans*-2-pentenal **10** with acetic acid based on micrOTOF-Q spectra. The H- and Na-adduct signals were added for plotting. **I**$_P$ (*m/z* 182, 204), **II**$_P$ (*m/z* 266,288), **II**$_P$+MeOH (*m/z* 298, 320), **III**$_P$ (only *m/z* 248).

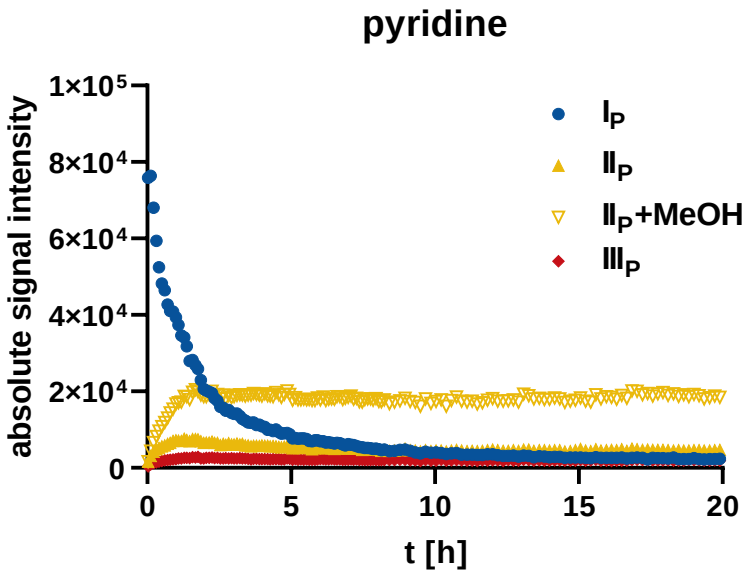

Figure 6.1.4 Temporal progress of the L-proline catalyzed reaction with *trans*-2-pentenal **10** with pyridine based on micrOTOF-Q spectra. The H- and Na-adduct signals were added for plotting. **I**$_P$ (*m/z* 182, 204), **II**$_P$ (*m/z* 266,288), **II**$_P$+MeOH (*m/z* 298, 320), **III**$_P$ (only *m/z* 248).

6.2 Additional material for chapter 3.3

BEILSTEIN JOURNAL OF ORGANIC CHEMISTRY

Supporting Information

for

Mechanistic studies of an L-proline-catalyzed pyridazine formation involving a Diels–Alder reaction with inverse electron demand

Anne Schnell, J. Alexander Willms, S. Nozinovic and Marianne Engeser

Beilstein J. Org. Chem. **2019,** *15,* 30–43. doi:10.3762/bjoc.15.3

Additional material

Table of Contents:

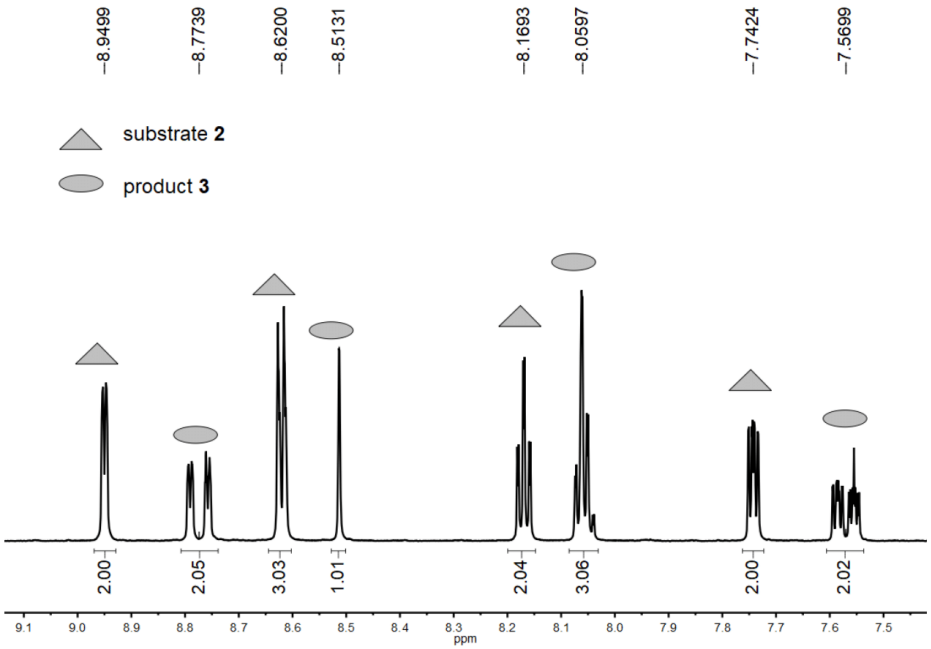

Figure S1: ^{1}H NMR spectrum (aromatic region) during the NMR experiment of reaction R1 with low concentration (concentration of tetrazine 0.005 mmol/mL) after 3 h and 50% conversion.

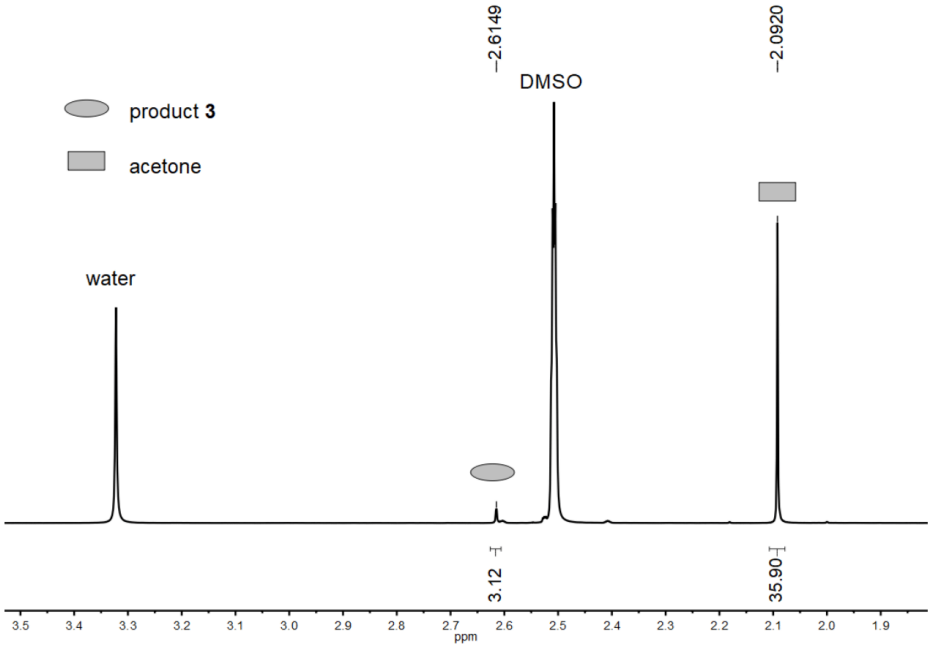

Figure S2: ^{1}H NMR spectrum (aliphatic region) during the NMR experiment of reaction R1 with low concentration (concentration of tetrazine 0.005 mmol/mL) after 3 h and 50% conversion.

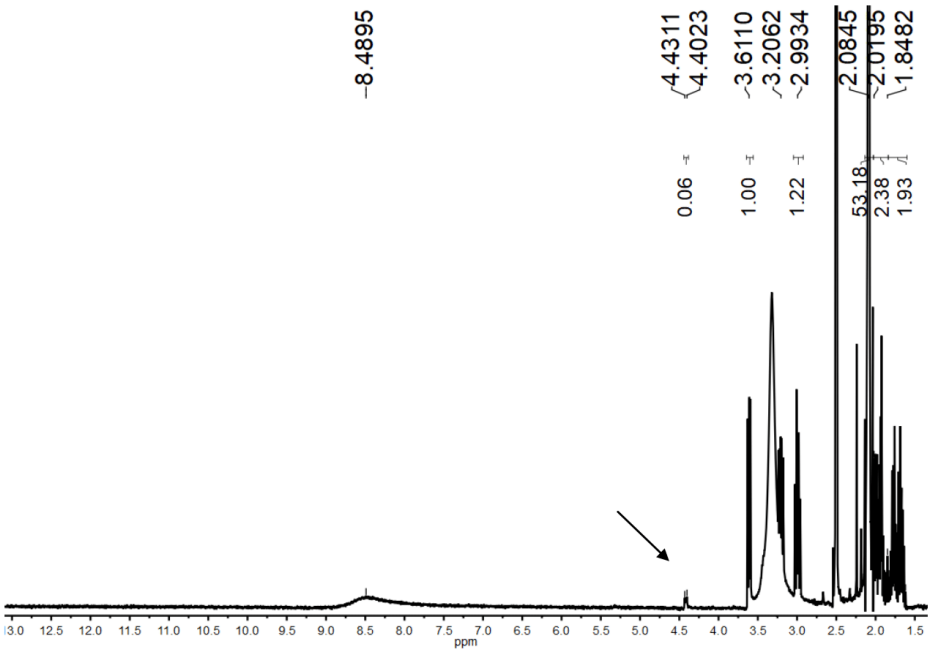

Figure S3: ^{1}H NMR spectrum of the reaction mixture in absence of tetrazine, i.e., a mixture of acetone (1 equiv) and L-proline (0.01 equiv) in deuterated dimethyl sulfoxide. The arrow points at the signal at 4.4 ppm which is the significant signal for the oxazolidinone as published by List [1] and Gschwind [2]. The spectrum was measured with a Bruker Avance I 400 MHz NMR spectrometer.

NMR study of reaction R1 at higher concentrations:

Commercially available 3,6-di-2-pyridyl-1,2,4,5-tetrazine **2** (28.3 mg, 0.12 mmol, 1.0 equiv) and L-proline (0.69 mg, 0.006 mmol, 0.05 equiv) were mixed in 3.6 mL of deuterated dimethyl sulfoxide. 0.5 mL of this mixture were transferred to the NMR sample tube. To start the reaction, a solution of acetone in deuterated dimethyl sulfoxide was added (50 µL, 9.6 mmol/ml, 0.48 mmol, 4 equiv). The first spectrum was measured 3 minutes after the start of the reaction. Subsequent spectra were measured in regular intervals of 1 minute at rt.

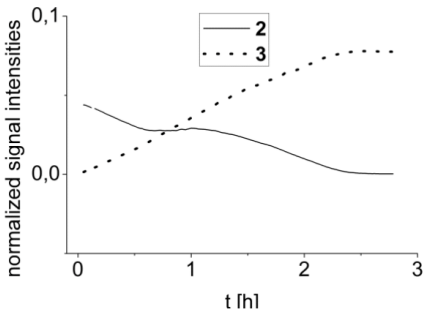

Figure S4: NMR study of reaction R1 at higher concentrations (concentration of tetrazine 0.033 mmol/mL). Product **3** is completely soluble at the given concentration, whereas substrate **2** is only partially dissolved. While substrate **2** transforms into the product **3**, more of substrate **2** gets dissolved until full conversion is reached.

ESIMS study of reaction R1 at lower concentrations:

A solution of L-proline in dimethyl sulfoxide (1.353 mL, 0.76 mmol/L, 0.001 mmol, 0.05 equiv) is added to commercially available 3,6-di-2-pyridyl-1,2,4,5-tetrazine **2** (4.86 mg, 0.02 mmol, 1.0 equiv). Additional 3.02 mL of dimethyl sulfoxide were added. A solution of acetone in dimethyl sulfoxide was added last (37 µL, 1.1 mmol/mL, 0.08 mmol, 4 equiv). The first spectrum was measured 2:20 minutes after the start of the reaction, subsequent measurements were recorded in intervals of 7.5 min.

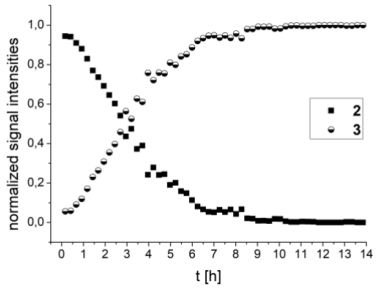

Figure S5: Temporal progress of reaction R1 at low concentrations (0.005 mmol/mL of tetrazine) in ESIMS experiment.

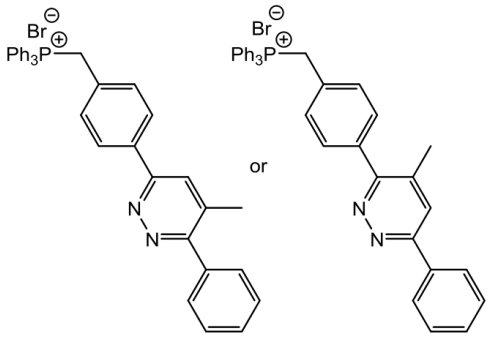

Scheme S1: Two possible regioisomers of **5**·Br in reaction R2.

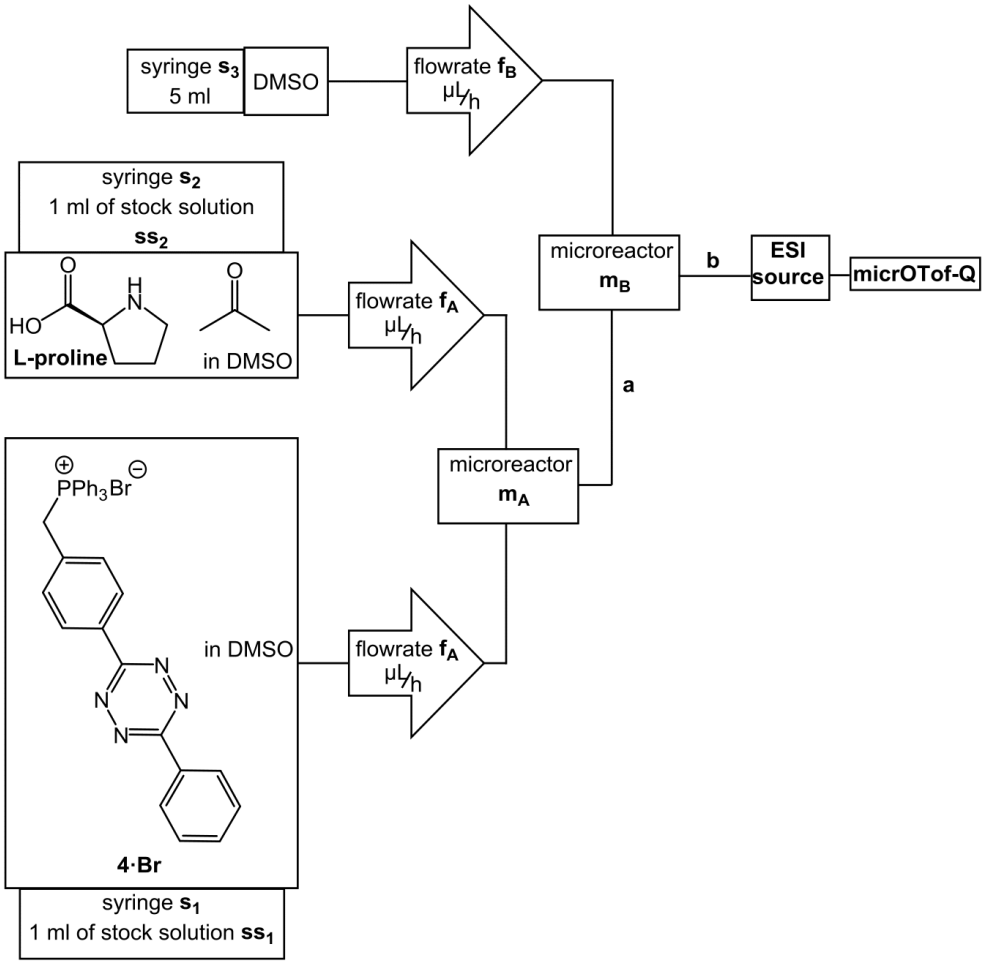

Scheme S2: A schematic depiction of the continuous flow setup for reaction R2.

The theoretical reaction time for the continuous flow setup was calculated by considering the experimental flow rates f_A (150 µL/h) and f_B (300 µL/h). The flowrate in tube a is assumed to be $2*f_A$ = 300 µL/h = f_B. Further, the swept volume (V_{swept} =2.2 µL) in the microreactors, the dimensions of the connecting PEEK tubes (length: a = 357 mm, b = 110 mm; diameter d = 0.127 mm) and the volume of the ESI needle (V_{needle} = 0.0069115 µL) is needed. Furthermore, the assumption was made that because the

microreactor m_b dilutes the reaction mixture by half, the reaction rate decreases according to the behavior of a bimolecular reaction, namely resulting in a fourth of the original reaction rate. The volumina V_a and V_b are defined as

$$V_a = a * \left(\frac{d}{2}\right)^2 * \pi + V_{swept}$$

$$V_b = b * \left(\frac{d}{2}\right)^2 * \pi + V_{swept} + V_{needle}$$

and in combination with the flowrates the reaction time can be calculated.

$$t = \frac{V_a}{2 * f_a} + \frac{V_b}{2 * f_b} * 0.25 = \frac{a * \left(\frac{d}{2}\right)^2 * \pi + V_{swept}}{2 * f_a} + \frac{b * \left(\frac{d}{2}\right)^2 * \pi + V_{swept} + V_{needle}}{2 * f_b} * 0{,}25$$

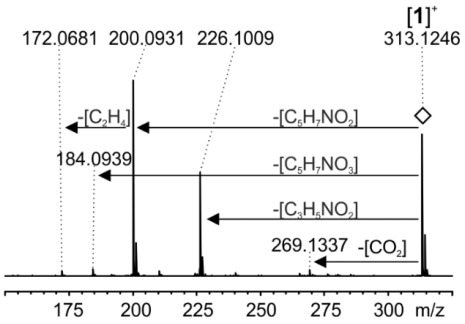

Figure S6: ESI(+) CID spectrum of mass selected [**1**]$^+$ (*m*/*z* 313); collisional energy voltage 15 V.

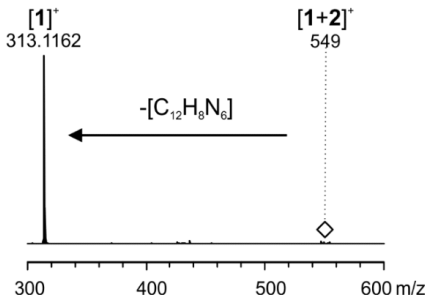

Figure S7: ESI(+) CID spectrum of the mass selected non-covalent adduct [**1**+**2**]$^+$ (*m*/*z* 549); collisional energy voltage 1 V.

Synthesis

Depiction of synthetic products including the numbering used for the NMR signal allocation.

1-Benzoyl-2-*p*-toluoylhydrazide (6)

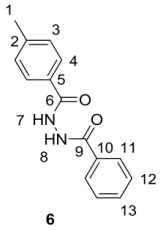

6

***N*-(Chlor(phenyl)methylene)-4-methylbenzohydrazonoyl chloride (7)**

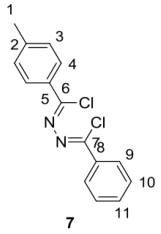

7

3-(4-Methylphenyl)-6-phenyl-1,2,4,5-tetrazine (8)

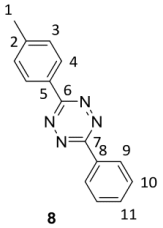

8

3-(4-Bromomethylphenyl)-6-phenyl-1,2,4,5-tetrazine (9)

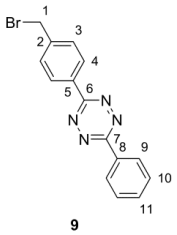

9

3-(4-Triphenylphosphoniummethylphenyl)-6-phenyl-1,2,4,5-tetrazine (4·Br)

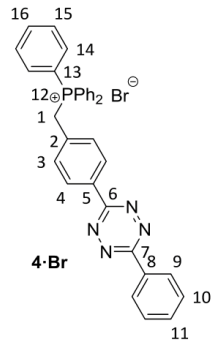

4·Br

Accurate mass determination with Orbitrap XL

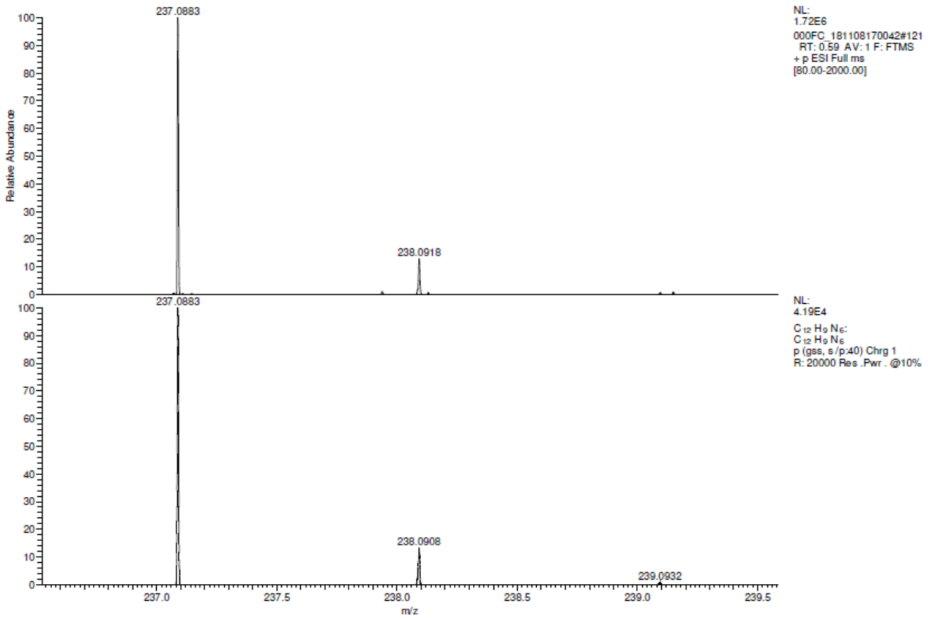

Figure S8: Accurate mass determination with Orbitrap XL of substrate **2** ([**2**+H]$^+$).

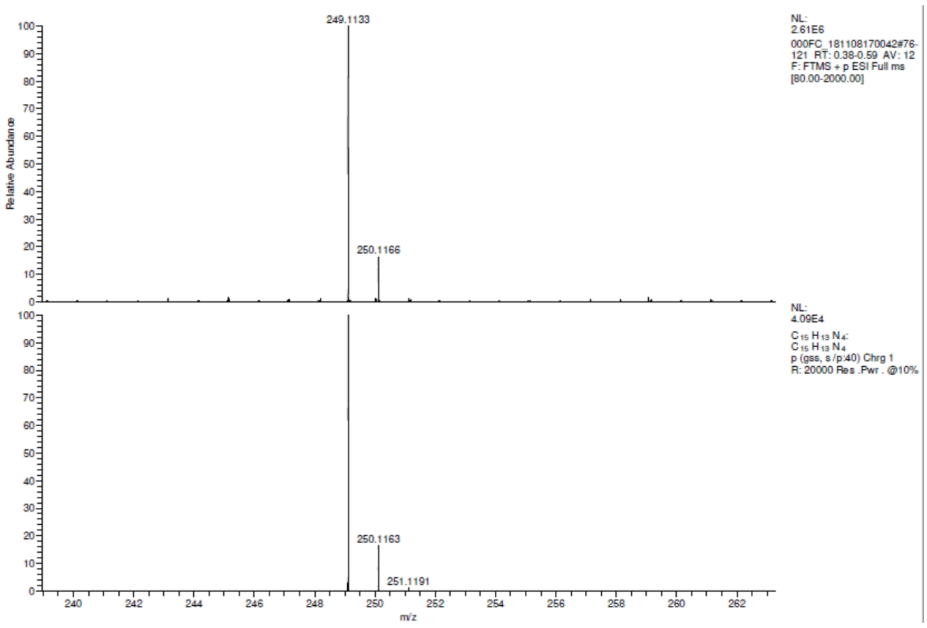

Figure S9: Accurate mass determination with Orbitrap XL of product **3** ([**3**+H]$^+$).

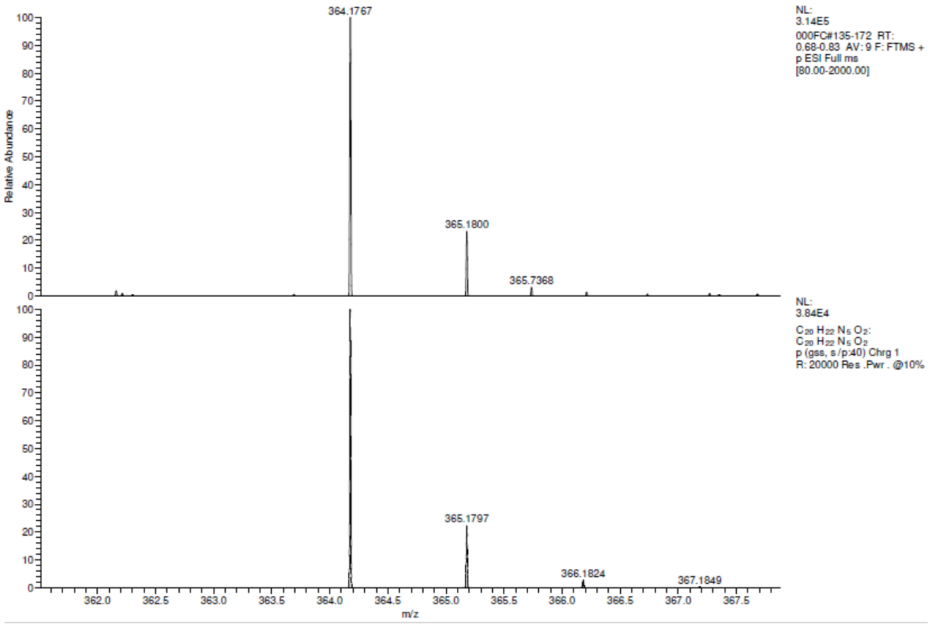

Figure S10 Accurate mass determination with Orbitrap XL of intermediate $\mathbf{III_1}$ ($[\mathbf{III_1}+H]^+$).

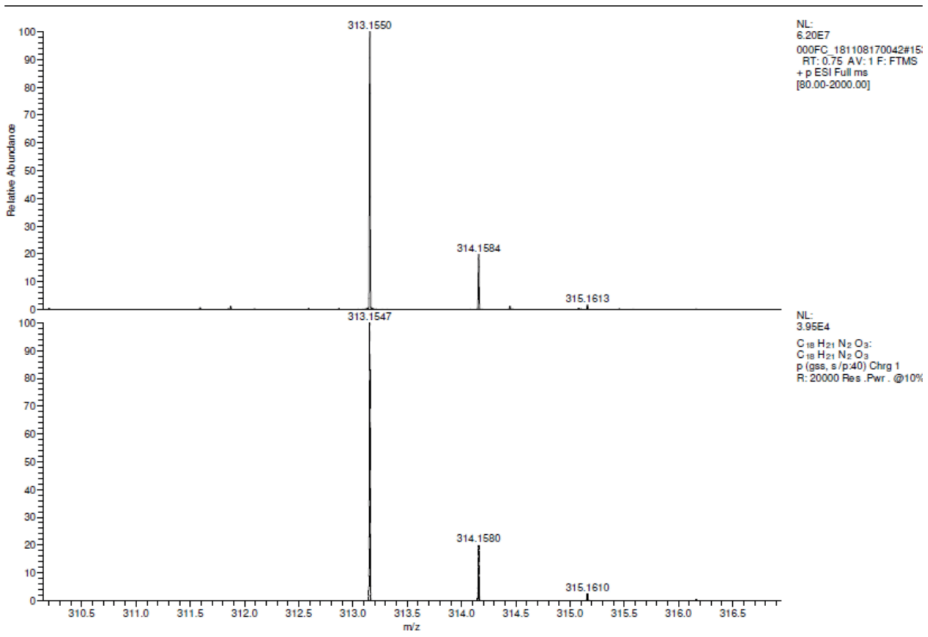

Figure S11: Accurate mass determination with Orbitrap XL of charge tagged catalyst **1** ([**1**]$^+$).

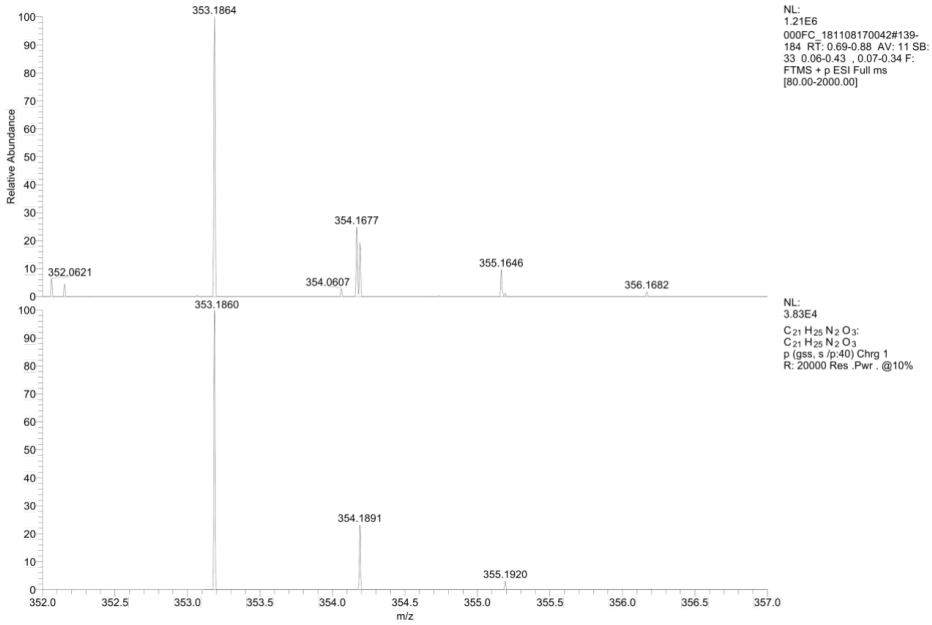

Figure S12 Accurate mass determination with Orbitrap XL of intermediate $\mathbf{I_3}$ ($[\mathbf{I_3}]^+$).

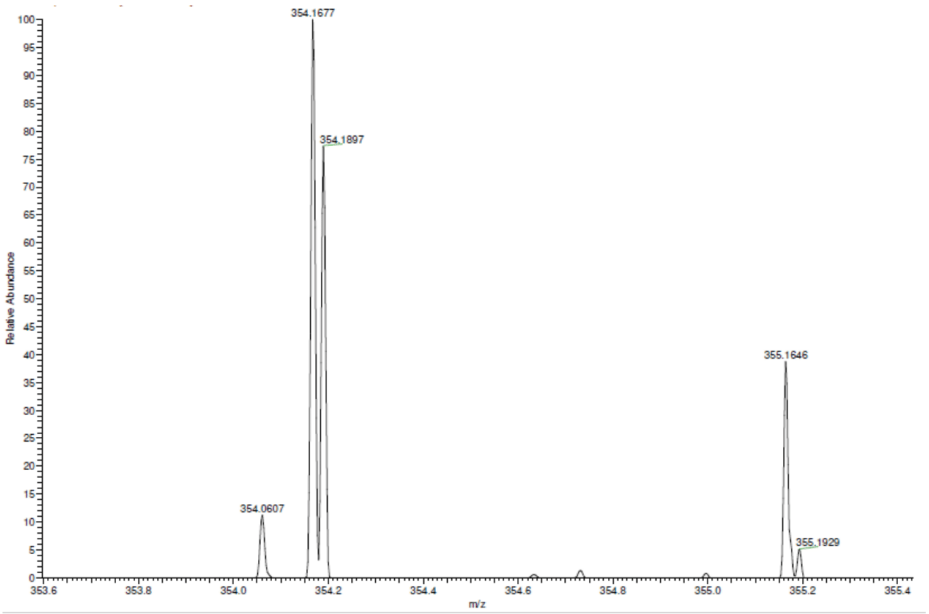

Figure S13 Zoom into ^{13}C peak of $\mathbf{I_3}$ ($[\mathbf{I_3}]^+$).

References

[1] List, B.; Hoang, L.; Martin, H. J. *Proc. Natl. Acad. Sci. U. S. A.* **2004,** *101,* 5839–5842. doi:10.1073/pnas.0307979101

[2] Schmid, M. B.; Zeitler, K.; Gschwind, R. M. *Angew. Chem., Int. Ed.* **2010,** *49,* 4997–5003. doi:10.1002/anie.200906629

6.3 Additional material for chapter 4.1

Instrument	Company	department	City
micrOTOF-Q	Bruker Daltonik Bremen	Chemistry department	University of Bonn
timsTOF flex	Bruker Daltonik Bremen	Chemistry department	University of Münster
Qtrap	Sciex	Biology department	University of Bonn
micrOTOF-Q III	Bruker Daltonik Bremen	Pharmacy department	University of Bonn

Table 6.3.1 List of all instruments used in this study and to which department they belong.

No.	Extraction method	Reference	Detailed procedure
1	EDTA extraction	*Wiemann* et al.[1]	See below
2	HCl extraction	*Moreno* et al.[2]	See below
3	HCl extraction	Modified from *Moreno* et al.[2]	See below

Table 6.3.2 List of all used extraction methods.

Extraction method No. 1:

Wiemann et al.[1] extracted egg shell fragments, whereas I pulverized the egg shell fragment in an achat mortar before extraction.

The sample powder is placed in an Eppendorf tube and admixed with 500 µl EDTA solution (100 mg/ml), which was adjusted to a pH of 7.2, no effervescence was observed by me. The solid is incubated for 5 min and centrifuged for 3 min at 14000 U/min. The supernatant is collected in a separate tube. The sample is again incubated in EDTA solution for 5 min, during which the tubes are vortexed for 3 min. The tubes are centrifuged for 3 min at 14000 U/min. The supernatant is collected in a separate tube and EDTA is added to the remaining solid. The previous steps are repeated two more times. To the remaining solid 1 ml of acetonitrile/acetic acid (4:1, v/v) are added for 10 min incubation. The sample is vortexed for 5 min during the 10 min incubation. The tube is centrifuged for3 min at 14000 U/min and the supernatant is then transferred to an LC-vial with inlet with a glass pipette. When extracting an emu egg the supernatant has a pale blue color otherwise it is colorless. The measurement is performed within 12 hours.

Extraction method No. 2:

The sample is pulverized in achat mortar. The pulverized sample is placed in a 2.0 ml Eppendorf tube. 0,6 ml ACN are added to the sample. Slowly 0,5 ml 3N HCl are added. Immediate effervescence occurs, so the Eppendorf tube is not closed and the HCl is added slowly. When effervescence stops, the Eppendorf tube is vortexed for 20 s and then centrifuged for 3 min at 14000U/min. Then phase separation occurs with the organic phase on top of the watery phase, with the remaining solids on the bottom. When extracting an emu egg the organic phase has a blue color otherwise it is colorless. Carefully with a glass pipette the organic phase is transferred into an LC-vial with an inlet and the measurement is performed within 12 hours.

Extraction method No. 3:

The sample is pulverized in achat mortar. The pulverized sample is placed in a 2.0 ml Eppendorf tube. 0,3 ml ACN are added to the sample. Slowly 0,5 ml 3N HCl are added. Immediate effervescence occurs, so the Eppendorf tube is not closed and the HCl is added slowly. When effervescence stops, the Eppendorf tube is vortexed for 20 s and then centrifuged for 3 min at 14000U/min. Then phase separation occurs with the organic phase on top of the watery phase, with the remaining solids on the bottom. When extracting an emu egg the organic phase has a blue color otherwise it is colorless. Carefully with a glass pipette the organic phase is transferred into an LC-vial with an inlet and the measurement was performed within 12 hours.

Solvent system No.	Solvents	Gradient
1	Solvent A:	Flow rate 0.15 ml/min
	Water +0.05 % trifluoroacetic acid	0 min: A 95 %, B 5 %
	Solvent B:	2 min: A 0 %, B 100 %
	methanol 0.05 % trifluoroacetic acid	30 min: A 95 %, B 5 %
		End 45 min
2	Solvent A:	Flow rate 0.15 ml/min
	Water +0.1 % acetic acid	0 min: A 95 %, B 5 %
	Solvent B:	2 min: A 0 %, B 100 %
	methanol 0.1 % acetic acid	30 min: A 95 %, B 5 %
		End 45 min
3	Solvent A: methanol 0.1 % acetic acid	Flow rate 0.15 ml/min
		Isocratic, i.e. only solvent A
		End 30 min

Table 6.3.3 List of all used solvent systems.

A Knauer, Eurospher II C18 reverse phase, 150*2 mm column and a Eurospher II C18 reverse phase, 5*4.6 mm precolumn were used for all measurements.

Measurement No.	Sample ID	Mass of egg shell [mg]	Extraction method No.	Solvent system	Instrument
1	Emu	401.4	1	1	micrOTOF-Q
2	Chicken	399.7	1	1	micrOTOF-Q
3	Standards BV and PP	c(BV)= 0.96 nmol/ml c(PP)= 1.7 nmol/ml		1	micrOTOF-Q
4	Emu Chicken	Emu: 202.7 Chicken: 202.8	1	1	micrOTOF-Q
5	E131	383.8	1	1	micrOTOF-Q
6	E132	379.9	1	1	micrOTOF-Q
7	E082	382.2	1	1	micrOTOF-Q
8	E131	453.8	1	1	micrOTOF-Q
9	E131	767.5	1	1	micrOTOF-Q
10	E082	749.6	1	1	micrOTOF-Q
11	E132	643.3	1	1	micrOTOF-Q
12	Emu	400.9	2	1	micrOTOF-Q
13	Chicken	400.8	2	1	micrOTOF-Q
14	Emu Chicken	Emu: 202.0 Chicken: 202.9	2	1	micrOTOF-Q
15	E131	472.0	2	1	micrOTOF-Q
16	E132	379.5	2	1	micrOTOF-Q
17	E082	381.8	2	1	micrOTOF-Q
18	E131	383.7	2	1	micrOTOF-Q
19	E082	749.5	2	1	micrOTOF-Q
20	E131	453.9	2	1	micrOTOF-Q
21	E061	358.9	2	1	micrOTOF-Q
22	E061	359.7	1	1	micrOTOF-Q
23	E062	399.8	2	1	micrOTOF-Q
24	E062	399.3	1	1	micrOTOF-Q
25	E074	349.2	2	1	micrOTOF-Q
26	E074	349.0	1	1	micrOTOF-Q
27	E137	424.1	2	1	micrOTOF-Q
28	E137	423.5	1	1	micrOTOF-Q
29	YS2016_6	360.8	2	1	micrOTOF-Q
30	YS2016_6	360.3	1	1	micrOTOF-Q
31	ESauro	518.0	2	1	micrOTOF-Q
32	ESauro	517.8	1	1	micrOTOF-Q
33	YS2016_2	360.8	2	1	micrOTOF-Q
34	YS2016_2	360.3	1	1	micrOTOF-Q
35	Moa	428.2	2	1	micrOTOF-Q
36	Moa	428.2	1	1	micrOTOF-Q
37	Ostrich miocene	406.0	2	1	micrOTOF-Q
38	Ostrich miocene	407.9	1	1	micrOTOF-Q
39	Emu	199.7	2	2	micrOTOF-Q

40	Emu	199.8	1	2	micrOTOF-Q
41	Chicken	199.9	2	2	micrOTOF-Q
42	Chicken	199.7	1	2	micrOTOF-Q
43	Standards BV and PP	c(BV)= 0.0167 nmol/ml c(PP)= 0.0171 nmol/ml		2	timsTOF flex
44	E082	336.5	1	2	timsTOF flex
45	E132	763.5	1	2	timsTOF flex
46	E131	757.5	1	2	timsTOF flex
47	E132	747.8	2	2	timsTOF flex
48	E131	747.8	2	2	timsTOF flex
49	Moa	702.5	2	2	timsTOF flex
50	Ostrich miocene	654.5	2	2	timsTOF flex
51	Standards BV and PP	c(BV)= 0.0017 nmol/ml c(PP)= 0.0017 nmol/ml		2	Qtrap
52	E131	710.5	1	3	Qtrap
53	E132	745.4	1	3	Qtrap
54	Standards BV and PP	c(BV)= 0.00083 nmol/ml c(PP)= 0.00086 nmol/ml		3	Qtrap
55	E082	416.0	3	3	timsTOF flex
56	E131	424.0	3	3	timsTOF flex
57	E132	401.0	3	3	timsTOF flex
58	Standards BV and PP	c(BV)= 0.13 nmol/ml c(PP)= 0.12 nmol/ml		3	timsTOF flex
59	BV: 0.10 nmol/g PP: 0.09 nmol/g	400.0	1	3	micrOTOF-Q III
60	BV: 0.21 nmol/g PP: 0.20 nmol/g	400.0	1	3	micrOTOF-Q III
61	BV: 0.94 nmol/g PP: 0.88 nmol/g	400.7	1	3	micrOTOF-Q III
62	BV: 1.86 nmol/g PP: 1.75 nmol/g	400.6	1	3	micrOTOF-Q III
63	BV: 5.87 nmol/g PP: 5.51 nmol/g	400.0	1	3	micrOTOF-Q III
64	BV: 21.86 nmol/g PP: 20.53 nmol/g	400.4	1	3	micrOTOF-Q III
65	BV: 0.10 nmol/g PP: 0.09 nmol/g	400.0	2	3	micrOTOF-Q III
66	BV: 0.21 nmol/g PP: 0.20 nmol/g	400.0	2	3	micrOTOF-Q III
67	BV: 0.94 nmol/g PP: 0.88 nmol/g	400.7	2	3	micrOTOF-Q III
68	BV: 1.86 nmol/g PP: 1.75 nmol/g	400.6	2	3	micrOTOF-Q III

69	BV: 5.87 nmol/g PP: 5.51 nmol/g	400.0	2	3	micrOTOF-Q III
70	BV: 21.86 nmol/g PP: 20.53 nmol/g	400.4	2	3	micrOTOF-Q III
71	BV: 0.14 nmol/g PP: 0.16 nmol/g	399.2	3	3	timsTOF flex
72	BV: 0.28 nmol/g PP: 0.33 nmol/g	401.2	3	3	timsTOF flex
73	BV: 0.58 nmol/g PP: 0.68 nmol/g	399.1	3	3	timsTOF flex
74	BV: 1.15 nmol/g PP: 1.34 nmol/g	400.0	3	3	timsTOF flex
75	BV: 2.31 nmol/g PP: 2.71 nmol/g	401.3	3	3	timsTOF flex
76	Solvent: “special ACN”	c(BV)= 0.16 nmol/ml c(PP)= 0.16 nmol/ml	No added HCl	3	micrOTOF-Q III
77	Solvent: ACN 0.1 % acetic acid	c(BV)= 0.16 nmol/ml c(PP)= 0.16 nmol/ml	No added HCl	3	micrOTOF-Q III
78	Solvent: MeOH 0.1 % acetic acid	c(BV)= 0.16 nmol/ml c(PP)= 0.16 nmol/ml	No added HCl	3	micrOTOF-Q III
79	Solvent: “special ACN"	c(BV)= 0.31 nmol/ml c(PP)= 0.32 nmol/ml	No added HCl	3	micrOTOF-Q III
80	Solvent: ACN 0.1 % acetic acid	c(BV)= 0.31 nmol/ml c(PP)= 0.32 nmol/ml	No added HCl	3	micrOTOF-Q III
81	Solvent: MeOH 0.1 % acetic acid	c(BV)= 0.31 nmol/ml c(PP)= 0.32 nmol/ml	No added HCl	3	micrOTOF-Q III
82	Solvent: “special ACN"	c(BV)= 0.17 nmol/ml c(PP)= 0.16 nmol/ml	added HCl	3	micrOTOF-Q III
83	Solvent: ACN 0.1 % acetic acid	c(BV)= 0.17 nmol/ml c(PP)= 0.16 nmol/ml	added HCl	3	micrOTOF-Q III
84	Solvent: MeOH 0.1 % acetic acid	c(BV)= 0.17 nmol/ml c(PP)= 0.16 nmol/ml	added HCl	3	micrOTOF-Q III
85	Solvent: “special ACN"	c(BV)= 0.34 nmol/ml c(PP)= 0.32 nmol/ml	added HCl	3	micrOTOF-Q III
86	Solvent: ACN 0.1 % acetic acid	c(BV)= 0.34 nmol/ml c(PP)= 0.32 nmol/ml	added HCl	3	micrOTOF-Q III
87	Solvent: MeOH 0.1 % acetic acid	c(BV)= 0.34 nmol/ml c(PP)= 0.32 nmol/ml	added HCl	3	micrOTOF-Q III

Table 6.3.4 List of all HPLC-ESI MS measurements of PP and BV.

Number	Location	Country	Species
E082	Nanxiong Basin, Guangdong Province	China (Institute of Geosciences, University of Bonn)	Oviraptorid
E131	Liguanqiao Basin, Henan Province	China (Institute of Geosciences, University of Bonn)	Oviraptorid
E132	Hongcheng Basin, Jiangxi Province	China (Institute of Geosciences, University of Bonn)	Oviraptorid
DE137	Laiyang, Shandong Province	China (Institute of Geosciences, University of Bonn)	possibly hadrosaurid
Moa-E1	New Zealand	New Zealand (private collection)	*Dinornis novaezealandiae*
ESauro	Roques Hautes, Aix-en-Provence	France	Sauropods
E61	Nanxiong Basin, Guangdong Province	China (Institute of Geosciences, University of Bonn)	Oviraptorid
E62	Nanxiong Basin, Guangdong Province	China (Institute of Geosciences, University of Bonn)	Oviraptorid
E74	Nanxiong Basin, Guangdong Province	China (Institute of Geosciences, University of Bonn)	Oviraptorid
YS2016/2	Nanxiong Basin, Guangdong Province	China	Oviraptorid
YS2016/6	Nanxiong Basin, Guangdong Province	China	Oviraptorid
Ostrich	Hezheng Biota, Gansu Province	China	Ostrich from the Miocene

Table 6.3.5 List of all analyzed fossilized specimens.

6.3.1 Preparation of standard solutions and calibration curves

The two standard compounds biliverdin hydrochloride and disodium protoporphyrin IX are dissolved separately.

About 1.5 mg of biliverdin hydrochloride are weighed in a 50 ml glass vial and the exact weight is noted. 9 ml of methanol with 0.1 % acetic acid and 1 ml of DMSO are added. The vial is placed in an ultrasonic bath for 10 min. The solution is diluted approx. 1:9 (v:v), which is then diluted approx. 1:5 (v:v). From this solution aliquots between 15 µl and 175 µl are added to 1 ml of methanol with 0.1 % acetic acid. This way solutions of different levels of concentration are generated.

About 1.5 mg of disodium protoporphyrin IX are weighed in a 50 ml glass vial and the exact weight is noted. 36 ml of methanol with 0.1 % acetic acid and 4 ml of DMSO are added. The vial is placed in an ultrasonic bath for 10 min. The solution is diluted approx. 1:9 (v:v). From this solution aliquots between 15 µl and 175 µl are added to 1 ml of methanol with 0.1 % acetic acid. This way solutions of different levels of concentration are generated.

Then the BV and PP solutions are combined, by e.g. mixing 500 µl of the lowest concentration of BV with 500 µl of the lowest concentration of PP. Thus, samples with both BV and PP at different levels of concentrations are generated.

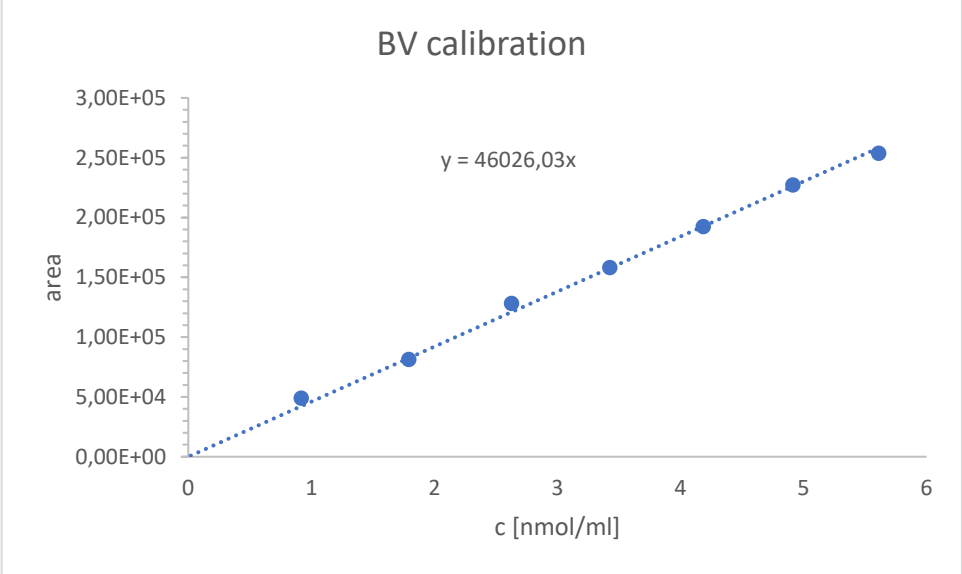

Figure 6.3.1 Calibration curve of BV for measurements ***39*** and ***40***.

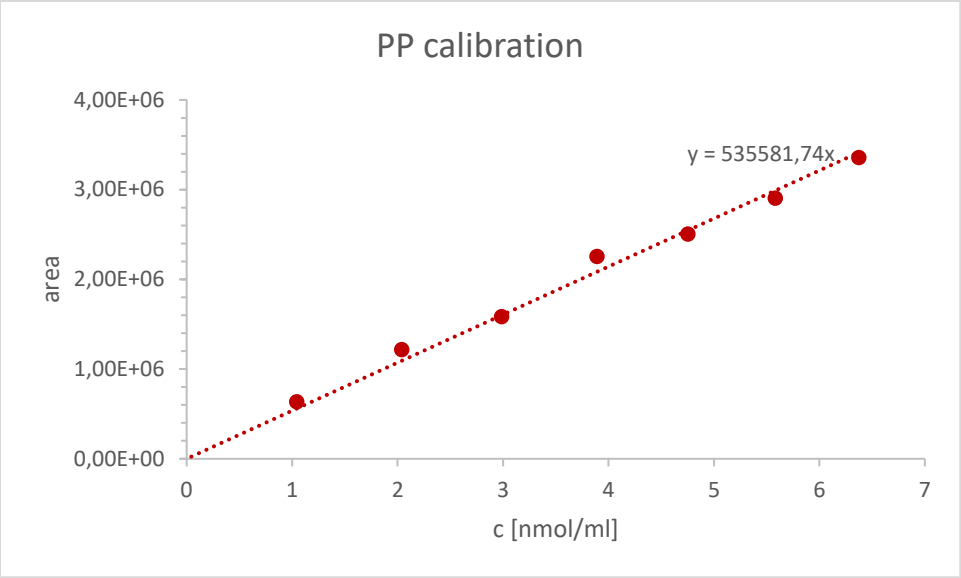

Figure 6.3.2 Calibration curve of PP for measurements ***41*** and ***42***.

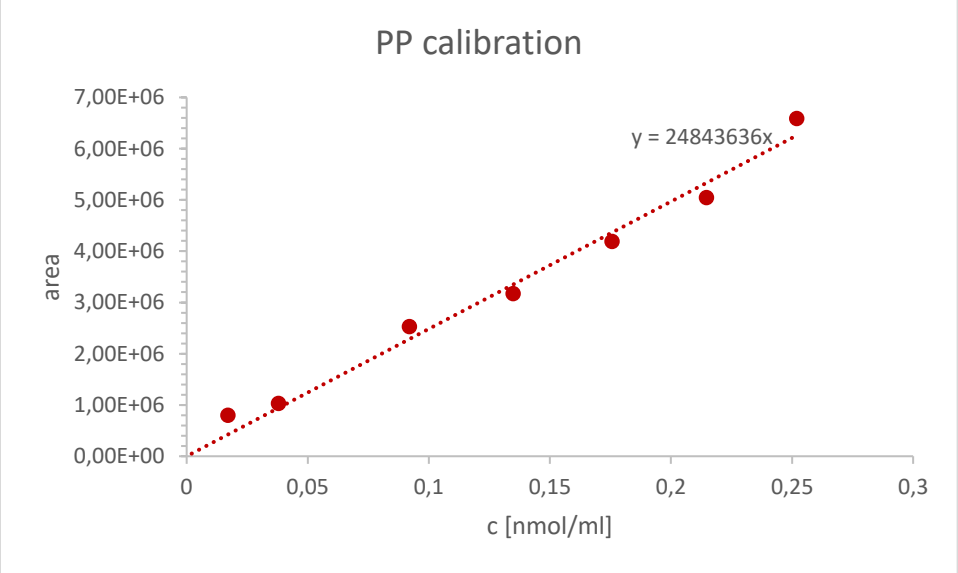

Figure 6.3.3 Calibration curve of PP for measurement ***46***.

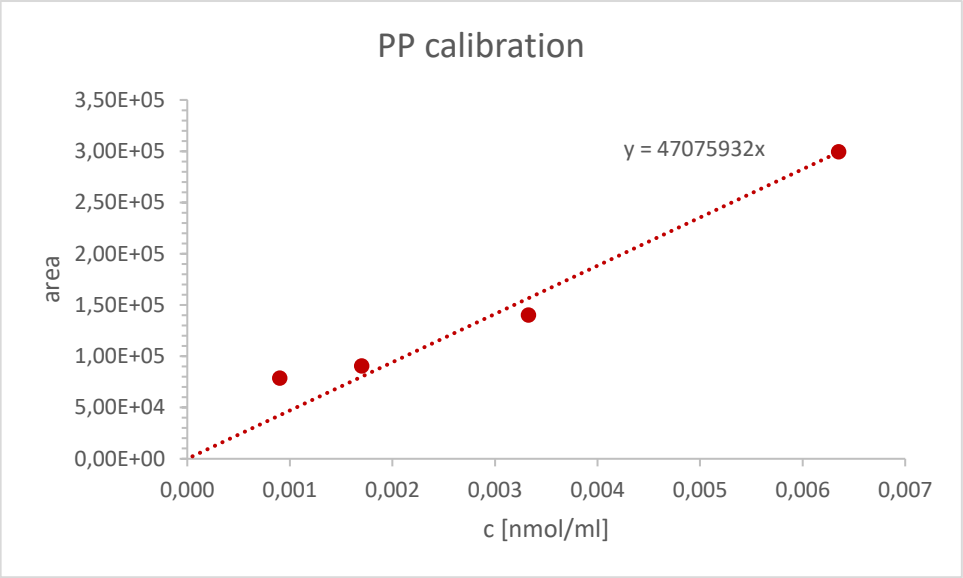

Figure 6.3.4 Calibration curve of PP for measurements ***52*** and ***53***.

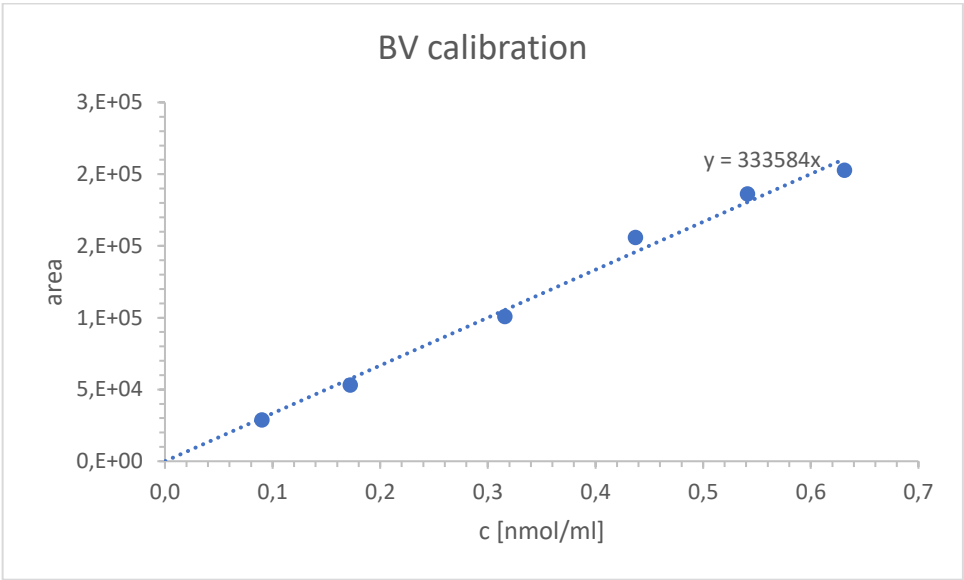

Figure 6.3.5 Calibration curve of BV for spiking experiment 1 measurements ***59***-***70***.

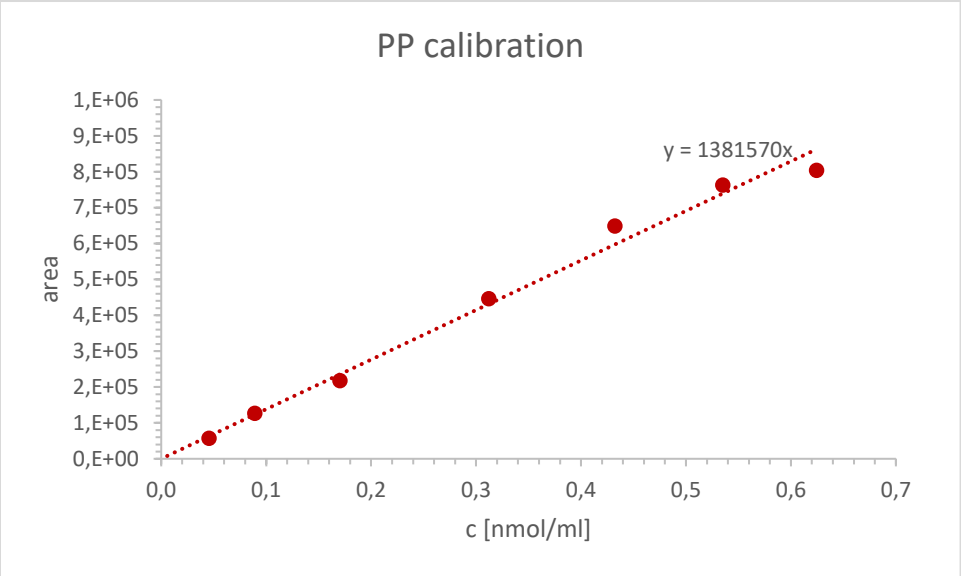

Figure 6.3.6 Calibration curve of PP for spiking experiment 1 measurements ***59-70*.**

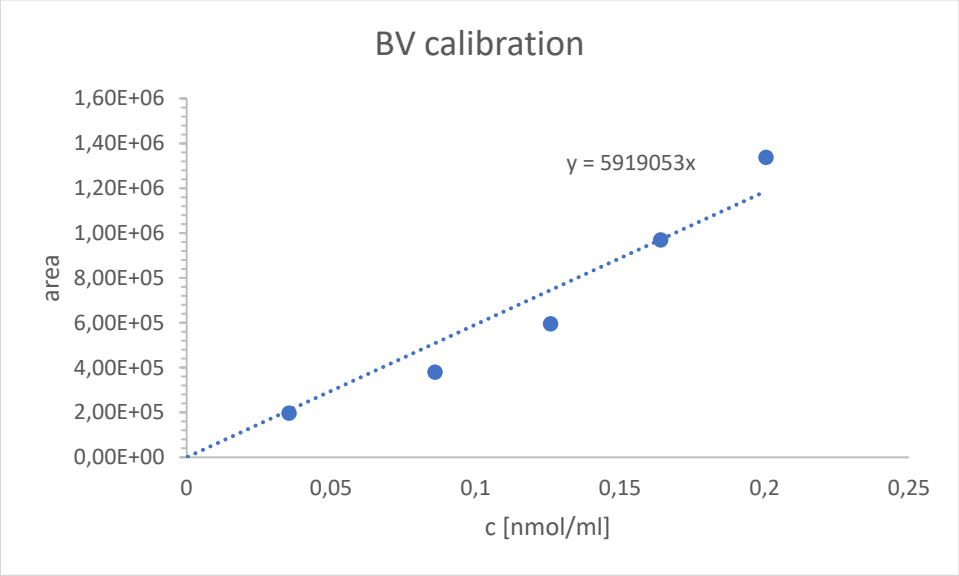

Figure 6.3.7 Calibration curve of BV for spiking experiment 2 measurements ***57*** and ***71-55***.

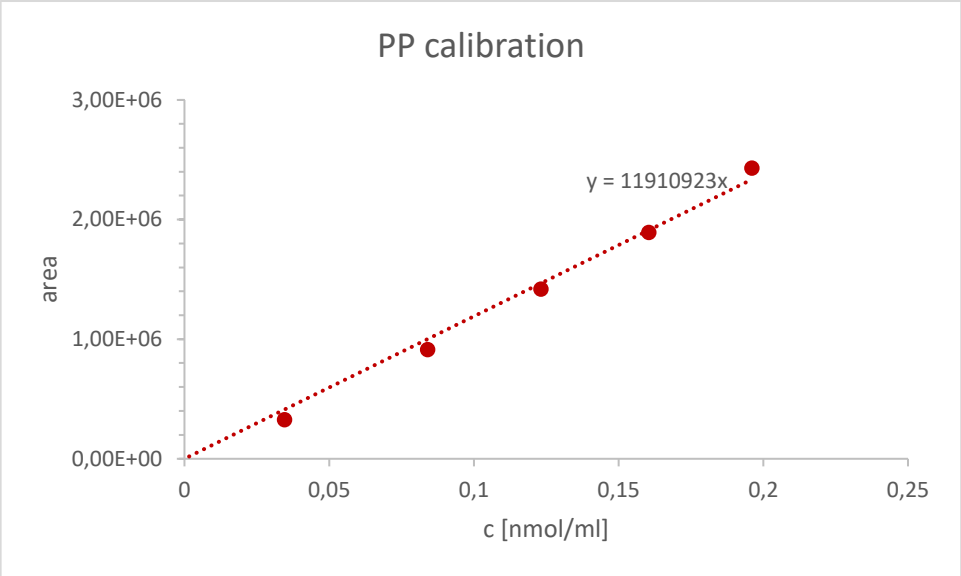

Figure 6.3.8 Calibration curve of PP for spiking experiment 2 measurements ***71*-*55***.

6.3.2 References

[1] J. Wiemann, T.-R. Yang, P. N. Sander, M. Schneider, M. Engeser, S. Kath-Schorr, C. E. Müller, P. M. Sander, *PeerJ* **2017**, *5*.

[2] J. Moreno, E. Lobato, J. Morales, S. Merino, G. Tomás, J. La Martínez-de Puente, J. J. Sanz, R. Mateo, J. J. Soler, *Behav. Ecol.* **2006**, *17*, 651.

6.4 Additional material for chapter 4.2

a) blank *m/z* 500-1100

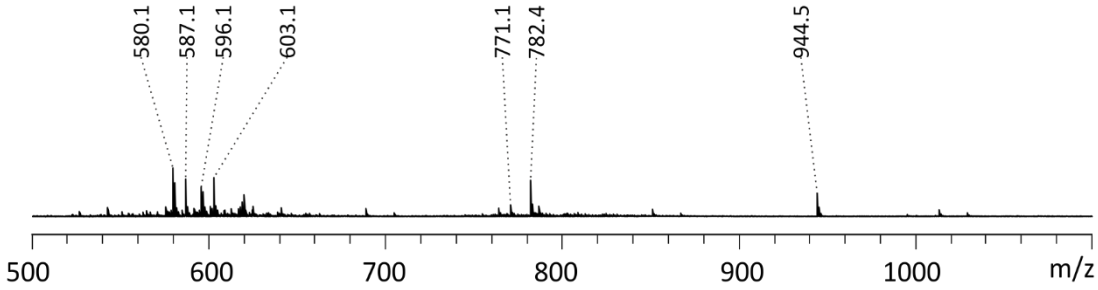

b) blank *m/z* 160-500

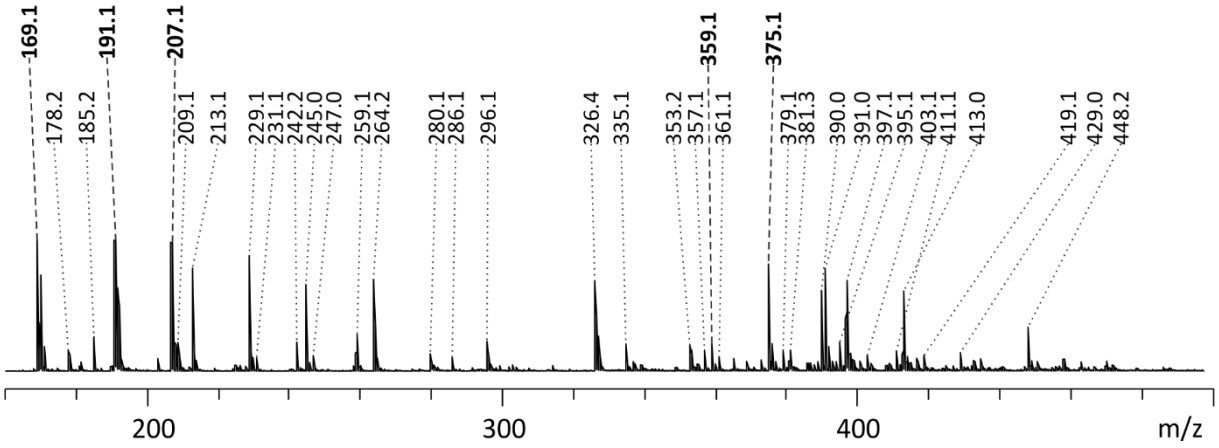

Figure 6.4.1 Blank spectrum (e) **Figure 4.2.6**) fully annotated in two parts a) *m/z* 500-1100 and b) *m/z* 160-500.

recalibrated *m/z* values of measurements		light		359,069			381,075	397,023
		medium	343,14	359,088	365,14	375,048	381,038	397,017
		dark		359,067				397,018
		blank	343,325	359,095	365,295	375,047	381,057	397,023
in medium	**1a** coniferin	calculated mass of [M+X]+	343,139		365,121		381,095	
	1b cellobiose	calculated mass of [M+X]+	343,124		365,106		381,080	
in light, medium, dark	**2** lignin dimer	calculated mass of [M+X]+		359,149			381,131	397,105
	THAP matrix	calculated mass of [2*THAP+Na]+		359,074				
Δ recalibrated *m/z* values - calculated *m/z* values	**1a** coniferin	medium	0,001		0,019		-0,057	
		blank	0,186		0,174		-0,038	
	1b cellobiose	medium	0,016		0,034		-0,042	
		blank	0,201		0,189		-0,023	
	2 lignin dimer	light		-0,080			-0,056	-0,082
		medium		-0,061			-0,093	-0,088
		dark		-0,082				-0,087
		blank		-0,054			-0,074	-0,082
	THAP matrix	light		-0,005				
		medium		0,014				
		dark		-0,007				
		blank		0,021				

Table 6.4.1 The spectra of **Figure 4.2.6** have been recalibrated to the matrix peaks *m/z* 169.050, 191.032 and 375.048. The recalibrated *m/z* values of relevant peaks for the assignment of **1** and **2** of the different measurements (light, medium, dark and blank) are listed on top. In the middle the calculated *m/z* values for the different compounds (1a, 1b, 2 and THAP) are listed. On the bottom the difference between the recalibrated *m/z* values (left) and the calculated *m/z* values (middle) are listed.